学位論文

Theoretical Study on Efimov Physics in Ultracold Atoms

(冷却原子気体におけるEfimov状態の物理の理論的研究)

平成25年12月　博士（理学）申請

東京大学大学院理学系研究科

物理学専攻

遠藤　晋平

Abstract

The Efimov states are three-body bound states, which appear universally when the s-wave scattering length between the particles is resonantly large. Since the Efimov states and their characteristic discrete scale invariance have recently been observed in ultracold atoms, the Efimov states and their associated few-body phenomena have attracted widening interest both theoretically and experimentally. In this thesis, I theoretically study the Efimov physics and related phenomena, focusing on the following three topics:

(i) Universal three-body physics for a mass-imbalanced Fermi system (Chapter 3).

For a system of two identical spinless (i.e., spin-polarized) fermions and one distinguishable particle which interact via a short-range potential with a large s-wave scattering length, two classes of universal three-body bound states have been known to appear in different regimes of the mass ratio: the Efimov trimers and the Kartavtsev-Malykh trimers, which feature the discrete and continuous scale invariance, respectively. I have found the third class of universal three-body bound states, which I call the "crossover trimers". The crossover trimers show neither the discrete nor continuous scale invariance. I have identified the regions of these three classes of trimers as a function of the mass ratio and the s-wave scattering length, and shown that the Kartavtsev-Malykh trimers and the Efimov trimers can continuously transform into each other via the crossover trimers as the mass ratio and the s-wave scattering length are varied.

Owing to the presence of the crossover trimers, the Kartavtsev-Malykh trimers dissociate into a particle and a dimer when the s-wave scattering length is varied, inducing resonances in the particle-dimer scattering. I have calculated the elastic particle-dimer scattering lengths in arbitrary angular-momentum channels, and shown that the particle-dimer resonances indeed occur. From the resonance positions, I have found accurate values of the critical mass ratios at which the Kartavtsev-Malykh trimers in the higher angular-momentum channels appear.

(ii) Universal three-body parameter (Chapter 4).

In the Efimov physics, the three-body parameter fixes the short-range three-body phase and hence the scale of the energy spectrum. Until quite recently, it has been widely held that the three-body parameter should depend on the short-range part of the inter-atomic potential, and hence vary almost randomly between different atomic species and hyperfine states. However, mounting evidence in recent experiments suggests otherwise. While some theoretical studies have succeeded in reproducing the universal behavior in the three-body parameter, the underlying physical mechanism has remained unclear and controversial. In this thesis, I elucidate the physical origin of the universal three-body parameter. I propose that a non-adiabatic deformation of the three-body wave function induced by a universal two-body correlation results in a universal three-body repulsion, which prevents three particles from coming close and renders the three-body parameter universal. This mechanism is verified by reproducing the universal three-body repulsion with a simple model wave function.

The mechanism found here suggests that the three-body parameter would also be universal for non-van der Waals types of potentials. For various classes of deep two-body potentials, it is shown that the effective range is the relevant length scale to characterize the two-body correlation and sets the three-body parameter. Depending on the shape of the two-body correlation, there

exist two classes in which the value of the three-body parameter is universally determined. One class corresponds to short-range two-body potentials decaying as a power law, relevant to atomic interactions, for which the universal pair correlation behaves smoothly. The other corresponds to deep two-body potentials decaying exponentially, relevant to nuclear systems, for which the universal pair correlation shows discontinuity.

(iii) Effective interaction between heavy particles immersed in a Fermi sea of light fermions (Chapter 5).

For a system of two heavy particles resonantly interacting with one light fermion, the Efimov states generally appear. Recently, it has been shown numerically that the formation of the Efimov states is suppressed when the number of light fermions is increased so that they form a Fermi sea. I show that this is also true in the case of N heavy particles. To be more specific, I consider N heavy particles immersed in a Fermi sea of light, spinless (i.e., spin-polarized) fermions, and study the interaction between the heavy particles induced by the surrounding light fermions at zero temperature. With the Born-Oppenheimer method, I have analytically shown that the induced interaction vanishes for any N in the limit of high light-fermion density. The induced interaction vanishes even in the unitarity regime. This suggests that the formation of the Efimov states and their associated N-body bound states is suppressed in the presence of the dense Fermi sea. I have ascribed the vanishing induced interaction to the screening effect in the neutral Fermi system.

Acknowledgment

I would like to express my deepest gratitude to my supervisor Prof. Masahito Ueda. He has provided me with the great opportunity to enjoy my Ph. D research in his group, and he has been the best teacher. All the research presented in this thesis would have been impossible without his patient guidance, continuing encouragement, and valuable discussion.

Dr. Pascal Naidon has been one of the most important collaborators. He is the person who had motivated me to start studying the Efimov physics in ultracold atoms. His continuing interest, encouragement, and valuable discussion on the Efimov physics for this three years have been one of the most important support I had.

I am also greatly indebted to many other colleagues and researchers. I am grateful to Prof. Yusuke Nishida for discussion and insightful comments on the Efimov physics and the polaron physics in ultracold atoms. I appreciate Dr. Shuta Nakajima for teaching me experimental details of his research on the Efimov states and for valuable discussion. I acknowledge Mr. Issei Yoshimoto for valuable discussion on the renormalization group analysis of the Efimov states and for our recent collaboration on the three-body physics for a mass imbalanced Fermi system. I am grateful to Mr. Kohei Kato for insightful discussions on a bosonic mixture of Rb and K atoms. I would like to thank Dr. Naoyuki Sakumichi and Mr. Yusuke Horinouchi for continuing interest in my research and inspiring discussion on various fundamental topics in physics. I thank Prof. Shunsuke Furukawa, Dr. Yu Watanabe, and Prof. Yuki Kawaguchi for all their assistance, especially for keeping the computer I have been using and for their assistance in numerical calculations. I appreciate Ms. Lumi Oshima, Ms. Yumiko Wada, and Ms. Kimiko Kowashi for all their assistance, especially in dealing with paperwork on travel expenses and research funds. I would like to thank all the members of Prof. Masahito Ueda group and the colleagues in the condensed matter theory group in the Department of Physics, the University of Tokyo for my exciting life as a Ph. D student.

I appreciate all members of the thesis committee, Prof. Tetsuo Hatsuda, Prof. Shin Inouye, Prof. Yusuke Kato, Prof. Naoki Kawashima, and Prof. Susumu Shimoura, for carefully reviewing this thesis and for numerous insightful comments.

The research presented in this thesis would have been impossible without financial supports from the Japanese Society for the Promotion of Science (JSPS). The research has been supported by the JSPS Research Fellowships for Young Scientists DC1 (Grant No. 237049), and the Institutional Program for Young Researcher Overseas Visits.

Finally, I would like to express my gratitude to my parents and my wife Takako for their love, patience, and warm encouragement.

Publication List

Publications relevant to this thesis

(i) Shimpei Endo, Pascal Naidon, and Masahito Ueda, Few-Body Systems, **51**, 207 (2011)
"Universal physics of 2+1 particles with non-zero angular momentum."

(ii) Shimpei Endo, Pascal Naidon, and Masahito Ueda, Phys. Rev. A **86**, 062703 (2012)
"Crossover trimers connecting continuous and discrete scaling regimes"

(iii) Pascal Naidon, Shimpei Endo, and Masahito Ueda, arXiv:1208.3912 (2012)
"Physical Origin of the Universal Three-body Parameter in Atomic Efimov Physics"

(vi) Shimpei Endo, and Masahito Ueda, arXiv:1309.7797 (2013)
"Perfect screening of the inter-polaronic interaction"

(v) Pascal Naidon, Shimpei Endo, and Masahito Ueda, to be published in Phys. Rev. Lett.
"Microscopic Origin and Universality Classes of the Efimov Three-body Parameter"

Publications irrelevant to this thesis

(vi) Shimpei Endo, Takashi Oka, and Hideo Aoki, Phys. Rev. B **81**, 113104 (2010)
"Tight-binding photonic bands in metallophotonic waveguide networks and flat bands in kagome lattices."

(vii) Chuan-zhou Zhu, Shimpei Endo, Pascal Naidon, and Peng Zhang,
Few-Body Systems **54**, 1921 (2013)
"Scattering and bound states of two polaritons in an array of coupled cavities"

Contents

Chapter 1

Introduction

1.1 Efimov states

In 1970, Vitaly Efimov found a new class of three-body bound states, which are now called the Efimov states [1, 2]. He considered non-relativistic three identical bosons in three spatial dimensions, where the three particles interact with each other via a short-ranged attractive interaction. He fine-tuned the strength of the attractive interaction such that a two-body bound state is about to appear in the s-wave channel, so that a resonant scattering occurs and the s-wave scattering length between the particles gets divergently large. By analytically solving the three-body problem under these conditions, he found that an infinite number of three-body bound states appear. The most remarkable feature of these three-body bound states is that their properties are the same after a scaling transformation: assume that you have found one of the three-body bound states. Then, all the other three-body bound states can be obtained by a proper scale transformation. For example, the wave functions and the binding energies of the n-th and $(n+1)$-th three-body bound states are related to each other as $\Psi_{n+1}(r_i) = \Psi_n(r_i e^{-\pi/s_0})$, and $E_{n+1} = e^{-2\pi/s_0} E_n$, where $e^{\pi/s_0} = 22.7\ldots$ ($s_0 = 1.0024\ldots$) is the universal scaling factor.

The Efimov states are universal three-body bound states that appear in any system when the inter-particle interaction is short-ranged and resonant. The Efimov states have been sought in various systems for more than 30 years. Originally, Efimov investigated the possibility of the Efimov states for three-body systems of nucleons[§] (i.e., protons and neutrons), since the nuclear force is short-ranged and the scattering lengths between the nucleons is relatively larger than the range of the nuclear force [1, 2]. The Efimov physics has also been discussed in the context of neutron rich nuclei [3, 4, 5]. For some nuclei containing much larger number of neutrons than typical stable nuclei, such as ^{6}He [4] and ^{11}Li [4, 6], their radii have been found to be much larger than those for typical nuclei, and the neutron's wave function extends to a long distance. Such nuclei are called halo nuclei, and it is argued that these halo nuclei are closely related to the Efimov states. The Efimov states have also been studied in the atomic and molecular physics [7, 8, 9, 10]. For ^{4}He atoms, there exists a weakly bound two-body bound states of ^{4}He atoms and the scattering length between the two ^{4}He atoms is very large [11, 12, 13, 14]. A three-body problem of three ^{4}He atoms

[§] He also considered the possibility of the Efimov states for ^{12}C, which can be regarded as a three-body system of α particles.

has been studied theoretically, and it has been suggested that there are two three-body bound states, one of which is rather weakly bound and has an Efimov character [8, 9, 10].

However, the Efimov states have eluded experimental investigations for a long time. The main difficulty is the necessity for *truly* resonant interactions. The interaction between particles is resonant only when it is, by coincidence or for some reasons, fine-tuned such that a bound state is about to appear/disappear. Unfortunately, such fine-tuned systems are quite rare in Nature. Furthermore, it turns out that one needs a fine-tuning with extreme precision to observe more than one three-body bound state. In his original work [1], Efimov estimated the number of the Efimov states to be

$$N \approx \frac{1}{\pi} \log \frac{|a|}{r_0}, \tag{1.1}$$

where a is the s-wave scattering length, and r_0 is the range of the inter-particle interaction. From this estimate, one can see that the scattering length must be extremely large to observe several Efimov energy levels: $N \geq 2$ corresponds to $|a|/r_0 \gtrsim 500$, and $N \geq 3$ corresponds to $|a|/r_0 \gtrsim 10^4$. In all the examples shown above, however, the scattering length is only moderately large $|a|/r_0 \sim 5 - 20$, and it is impossible to observe more than one three-body bound state. This has made it difficult to study Efimov physics experimentally in these systems

A major breakthrough has occurred recently in the field of ultracold atoms. Advanced cooling techniques such as the laser cooling [15, 16, 17, 18] and the evaporative cooling [19, 20] developed in the 1970s to 1990s have enabled one to prepare neutral atoms at extremely low temperatures $T \sim 1 - 100$ nK. At such ultracold temperatures, the interaction between the atoms is dominated by the s-wave scattering channel, which is characterized by the s-wave scattering length a. In 1998, the s-wave scattering length has been found to be controllable by applying an external magnetic field [21]. This technique is called the Feshbach resonance [22, 23]. Since its first experimental realization, it has been the standard tool and widely used in the field of ultracold atoms (see Ref. [24] for a review of the Feshbach resonance). The unique feature of the Feshbach resonance is that one can prepare a system with a desired value of the interaction strength in experiments with extreme precision. In Fig. 1.1, the s-wave scattering length between ^{7}Li atoms is shown as a function of the external magnetic field. One can clearly see that the s-wave scattering length changes dramatically as the strength of the magnetic field is varied. By precisely controlling the external magnetic field, the s-wave scattering length can be changed by several orders of magnitude. With the Feshbach resonance, one can experimentally study few-body and many-body physics by continuously varying the inter-atomic interaction from the weakly interacting limit $a \to 0$ up to the strongly interacting limit $a \to \pm\infty$. This is in marked contrast with other systems, where the interactions between particles is generally set by Nature and one has little control over it.

The Feshbach resonance has enabled the observation of the elusive Efimov states. In 2006, the first signature of the Efimov states has been observed in ultracold atoms by a team of the Innsbruck University [27]. In a subsequent experiment [28], two adjacent Efimov states have been observed. As shown previously, the s-wave scattering length should be extremely large $|a|/r_0 \gtrsim 500$ to achieve this, but such an extreme fine-tuning is possible with the Feshbach resonance. In this experiment, the discrete scale invariance has been confirmed and the universal scaling factor has been found to be 25 ± 4 [28], which is consistent with the theoretically predicted value $e^{\pi/s_0} = 22.7\ldots$.

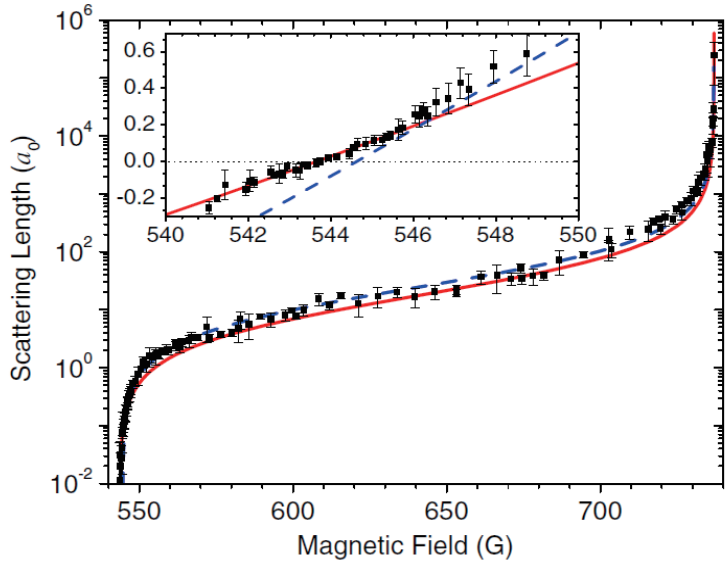

Figure 1.1: Feshbach resonance observed for ^{7}Li atoms [25]. The s-wave scattering length a is shown in the atomic unit a_0 as a function of the external magnetic field. The s-wave scattering length is varied by seven orders of magnitude in the vicinity of the resonance. The red solid curve and the blue dashed curve are the coupled-channel calculation and the Feshbach resonance fit in Eq. (2.15), respectively. The inset is a blowup around the zero-crossing $a \approx 0$. The scattering length is estimated from a BEC size measurement [25], which is affected by beyond mean-field effects and anharmonic contributions to a trapping potential at large scattering length. In Ref. [26], a new measurement with less systematic uncertainties has been done by the same group. [Figure reprinted with permission from S. E. Pollack *et al.*, Phys. Rev. Lett. **102**, 090402 (2009). Copyright © (2009) by The American Physical Society.]

1.2 Efimov physics as a universal few-body phenomenon

Although the Efimov physics has eluded experimental investigations for more than 30 years, it is a universal phenomenon and, in principle, it can appear in various physical systems. For non-relativistic three identical bosons interacting via short-ranged two-body interactions, the Efimov states appear when the following two conditions are satisfied:

- The inter-particle interaction is short-ranged, so that the s-wave interaction is dominant at low energy.
- The s-wave scattering length between the particles is divergently large $|a| \gg r_0$, where r_0 is the range of the interaction.

Historically, the possibility of the Efimov states has been studied in various systems, such as the halo states of the neutron rich nuclei, ^{4}He clusters, and ultracold atoms. In all these systems, the two conditions are, to some extent, satisfied.

These conditions for the appearance of the Efimov states can be used as a guideline to search for the Efimov states in novel systems. If one wants to know whether the Efimov states can appear

for a given system, one can first check the above two conditions. If they are satisfied, it is very likely that the Efimov states appear. In 2013, it has been theoretically predicted that the Efimov states can appear in a quantum spin system [29, 30]. This new finding can be interpreted in the above framework: in a quantum spin system described by the ferromagnetic Heisenberg model, the low energy excitations are magnons. They behave as bosonic quasi-particles and their low-energy dispersion is the same as that for non-relativistic free particles in the vacuum $\varepsilon_k \propto k^2$. Therefore, their scattering problem can be treated in a manner similar to that of non-relativistic identical bosons in the vacuum. In real quantum spin systems in solids, there are often some anisotropies[§] which can induce a short-ranged magnon-magnon interaction. If this magnon-magnon interaction is such that the resonance of the magnon-magnon scattering occurs, the above two conditions are satisfied at low energy and the Efimov states appear.

It is notable that the general features of the Efimov states in various systems are the same. If one virtually changes the Hamiltonians of the halo nuclei, quantum spin systems, ^{4}He, or ultracold atoms, and fine-tunes the s-wave scattering length to be $1/a = 0$ in these systems, the Efimov states appear in all these systems. The scaling factors for the Efimov states in these systems are exactly the same $e^{\pi/s_0} = 22.7\ldots$, and their low-energy properties are also quantitatively the same. This seems to be quite remarkable, since the Hamiltonians of these systems are totally different: the interactions between the nucleons and nuclei are the Yukawa interaction $-e^{-\kappa r}/r$ at long distance, while they are the on-site or nearest-neighbor interactions for a quantum spin system, and they are the van der Waals interaction $-C_6/r^6$ at long distance for ^{4}He atoms and for typical neutral atoms. Furthermore, the energy scales of these systems differ significantly. The energy scales of the Efimov states in the nuclear system and the ultracold atoms are $E \sim 1$ MeV and $E \sim 1\ \mu$K, respectively. They are different by more than 15 orders of magnitude. In spite of these tremendous differences, the emergent Efimov states behave in the same manner.

In other words, the Efimov physics is a universal few-body phenomenon. Here, the word "universal" means that seemingly different systems behave in the same fashion and they can be described by a single unifying theory. The most famous example of the universal phenomena may be the universality class in the theory of phase transitions. A magnetic phase transition and a liquid-gas phase transition seems at first sight to be totally distinct phenomena, but they belong to the same universality class and can be understood in a unified manner close to the critical temperature. Similarly, the Efimov states in all the above examples can be described by a unifying theory, the zero-range Efimov theory (see Sec. 2.2 for more details), as long as we are interested in their low energy behavior close to resonance.

The analogy with the universality in the theory of phase transitions is rather helpful in understanding why such a universal few-body phenomenon can appear in the resonantly interacting three-body system. One similarity between the Efimov physics and the phase transition is that in both cases, one is concerned about their low-energy (i.e., long-distance) behavior. This allows us to significantly decrease the number of relevant parameters and characterize the system in a simple manner. In the case of the phase transitions, this procedure is known as a "coarse graining"; if one observes the system at a large length scale, all the microscopic details of the complicated Hamiltonian are averaged out, and one is left with a simple low-energy effective field theory which

[§]In Ref. [29], the anisotropic Heisenberg model with the single-ion anisotropy term has been studied.

contains only a few parameters. In the case of the few-body problem at low energy, a similar simplification and reduction of variables occur. When one considers a two-body scattering problem at low-energy and focuses on its long-range behavior, the role of the inter-atomic interaction is merely to alter the asymptotic phase shift. At low energy, the asymptotic phase shift can be characterized by a single parameter, the s-wave scattering length. Thus, the low-energy two-body physics can be characterized by the s-wave scattering length, and all the other details of the inter-particle potential is unimportant in discussing low-energy properties. Similarly, in the three-body problem, it turns out that there are only two relevant parameters to characterize the system at low energy, the s-wave scattering length and the three-body parameter (see Sec. 2.1 for more details about the universality in the two-body and three-body physics).

Another similarity is the presence of a divergently large length scale. Close to the critical point of the second order phase transitions, the correlation length becomes divergently large. On the other hand, the s-wave scattering length is divergently large when the Efimov states appear. In the vicinity of the critical point of the second order phase transitions, systems become scale invariant due to the divergent correlation length, and the renormalization group method turns out to be a powerful tool in analyzing the critical phenomena. Similarly, the scale invariance and the renormalization group method are essential for studying the Efimov states [31, 32]. One spectacular difference is that the scale invariance in the Efimov physics is discrete, while for the phase transitions it is continuous. In the renormalization group language, the Efimov physics corresponds to the limit-cycle solution [31], while the fixed-point solutions are playing essential roles in the theory of the phase transitions. While the fixed-point solutions are rather common in Nature, in his pioneering studies of the renormalization group studies [33, 34], K. G. Wilson pointed out that, in principle, there can be limit-cycle solutions for the renormalization group trajectory. The limit-cycle solutions are quite rare in Nature. Some mathematical models have been proposed which shows the limit cycle [35, 36, 37], but the Efimov physics is the only example where the renormalization group limit cycle in a quantum-mechanical system has clearly been observed.

The universality of the Efimov states can, in turn, be used as a criterion to judge whether a three-body bound state can be called as an Efimov state. The Efimov states have several characteristic features: they are weakly bound three-body bound states, whose spatial size is much larger than the range of the interaction; they appear when the inter-particle scattering length is divergently large. If a given thee-body bound state shows these properties, it is a good hint that it is the Efimov state, but these criteria seem to be too vague and far from conclusive. Rather, the clearest signature of the Efimov state would be the universal scaling factor $e^{\pi/s_0} = 22.7\ldots$. In ultracold atoms, the discrete scale invariance has been confirmed in experiments and the observed scaling factor 25 ± 4 [28] was in excellent agreement with the universal prediction $e^{\pi/s_0} = 22.7\ldots$. These are the smoking-gun experiments to conclude that the Efimov physics is indeed being observed in ultracold atoms.

1.3 Further development of the Efimov physics

Since Efimov studied a resonantly interacting three-body system of identical bosons, various kinds of other resonantly interacting few-body systems have been theoretically investigated in subsequent studies. It has gradually become clear that what Efimov found in 1970 is just a small

fraction of broad classes of exotic few-body phenomena in resonantly interacting systems at low energy. In this section, I will introduce some important generalizations of Efimov's scenario and recent progresses in the field of Efimov physics in ultracold atoms. There are many important developments, but here I only present those which are relevant to this thesis, and briefly summarize how this thesis is related to them.

(i) Efimov physics in various types of three-body systems (Chapter 3)

In his first papers, Efimov considered a three-body system of identical bosons [1, 2], but he subsequently extended his idea to three-body systems with different statistics of particles [38]. For example, for a system of two identical bosons (B) and one distinguishable particle (A), both with no internal degree of freedom, three-body bound states of B-B-A and A-A-B appear when the interaction between A and B particles is resonant. In the case of three distinguishable particles, three-body bound states generally appear when more than one of the two-body interaction is resonant [38, 39, 40]. In all these cases, properties of the three-body bound states are mostly the same as those of identical bosons: they are weakly bound three-body bound states and show the discrete scale invariance. The only notable difference is that the value of the scaling factor is different from that of three identical bosons of 22.7, but the other features mostly remain the same. Thus, the Efimov physics is not something unique to a system of three identical bosons, but is a more general phenomenon.

For a three-body system with identical fermions, the three-body states become more exotic. One of the main work of this thesis (Chap. 3) deals with this fermionic three-body physics. For identical fermions, the Pauli exclusion principle dictates that the relative orbital angular momentum between the identical fermions must be nonzero. The system then acquires an additional centrifugal repulsion. The centrifugal repulsion tends to suppress the formation of three-body bound states, and there is a competition between the Efimov physics and the centrifugal repulsion. If the centrifugal repulsion is strong enough, there is no three-body bound state, while the Efimov states appear when the centrifugal repulsion is negligibly small. Since the centrifugal repulsion is inversely proportional to the mass of the fermions, the presence or absence of the Efimov states strongly depends on the mass of the fermions. In one of his pioneering studies, Efimov considered a three-body system of two identical fermions (F) and one distinguishable particle (A) [38]. He found that the Efimov states of F-F-A can appear when the mass of the fermions is much larger than that of the other particle, while the Efimov states disappear when the mass of the fermions is comparable to that of the other particle. Thus, the masses of the particles are essential parameters determining the presence or absence of the Efimov states. If one can vary them, one can control the presence or absence of the Efimov states. This is in marked contrast with the bosonic three-body systems, in which the Efimov states appear for any mass ratio.

As one can see from these examples, the Efimov physics is not a unique phenomenon restricted to a system of three identical bosons, but it is more general. The Efimov states can instead appear for various kinds of resonantly interacting three-body systems. This is another reason why the Efimov states are called "universal" three-body bound states.

In ultracold atoms, these three-body systems with different statistics of particles can also be ex-

plored experimentally. For a neutral atom, its internal state is characterized by the hyperfine states. Since ultracold atoms are prepared to be fairly dilute, the spin exchange processes are typically so slow that the hyperfine states of the atoms can be regarded as well-defined internal states[§]. Since the internal degree of freedom is frozen, the hyperfine states can be used as a "label" to distinguish particles, so that atoms in different hyperfine states can be effectively regarded as "different" particles. Thus, in ultracold atoms, we typically deal with bosons or fermions with no internal degree of freedom, and throughout this thesis, I also consider particles with no internal degree of freedom. Since the hyperfine states of the atoms can be controlled by microwaves, three-body physics for desired statistics of particles can be explored in ultracold atoms. By preparing ^{7}Li atoms in the same hyperfine states, for example, the Efimov states for three identical bosons have been observed [26, 44, 45, 46, 47]. The Efimov states for three distinguishable particles have also been realized by preparing ^{6}Li atoms in three different hyperfine states [48, 49, 50, 51, 52, 53, 54]. Another way to control the statistics of the particles is to prepare a mixture of totally different atomic species or isotopes. For example, in 2009, it has been reported that the Efimov states have been observed in a bosonic mixture of ^{87}Rb and ^{41}K atoms [55]. These atoms behave as bosons, since their total numbers of the protons, neutrons and electrons are even. The Efimov states of ^{87}Rb-^{87}Rb-^{41}K and ^{87}Rb-^{41}K-^{41}K have been claimed to be observed by performing the inter-species Feshbach resonance, i.e., the Feshbach resonance between ^{87}Rb and ^{41}K atoms. Atomic species such as ^{6}Li, ^{40}K, and ^{173}Yb, on the other hand, behave as fermionic atoms, since their total numbers of the protons, neutrons and electrons are odd. Atomic mixtures with these fermionic atoms have been realized, such as ^{40}K-^{6}Li [56], and ^{173}Yb-^{6}Li [57, 58]. A mass-imbalanced fermionic mixture under resonant interaction has been achieved recently [56], and there has been growing experimental interest in its few-body and many-body behaviors.

The fermionic few-body problem has also attracted theoretical interest recently. While the Efimov states in the fermionic three-body system has been found in 1973 [38], there are major theoretical breakthroughs in the late 2000's [59]. In 2007, Kartavtsev and Malykh pointed out that in addition to the Efimov states, a new class of universal three-body bound states can exist in the resonantly interacting fermionic three-body system [59]. These novel three-body bound states are called the Kartavtsev-Malykh states, and they show fairly distinct features from the Efimov states. While the Efimov states show the discrete scale invariance, the Kartavtsev-Malykh states show a continuous scale invariance. Furthermore, the Kartavtsev-Malykh states are expected to be much more stable than the Efimov states [59, 60]. These two different types of universal three-body bound states appear or disappear depending on the masses of the particles and the s-wave scattering length. In previous work, these two universal three-body bound states have been studied separately, and it has not been known for what values of the parameters the Efimov states and Kartavtsev-Malykh states can exist, and how these two types of trimers change into each other as the masses and the s-wave scattering length are varied. One of the main work of this thesis is to reveal a "phase diagram" of the fermionic three-body system. In the first half of Chap. 3 of this thesis, the fermionic three-body problem is investigated for the whole parameter space of the mass ratio

[§]In some special cases, the spin exchange process is significant, and one must deals with spinors [41, 42]. While the interplay of the Efimov effect and the spinors has recently been studied theoretically in Ref. [43], I do not deal with such cases throughout this thesis.

and the s-wave scattering length. I have found that the Efimov states featuring the discrete scale invariance can continuously transform into the Kartavtsev-Malykh trimers featuring the continuous scale invariance as the mass ratio and the s-wave scattering length are varied. In between these two types of universal trimers, I have found the third class of universal three-body bound states, which I call the "crossover trimers". The crossover trimers show neither the discrete nor continuous scale invariance, but still behave and exist universally between the Kartavtsev-Malykh and the Efimov regimes. I have identified the regions of these three classes of trimers as a function of the mass ratio and the s-wave scattering length.

I have also found that the Kartavtsev-Malykh trimers dissociate into a particle and a dimer when the s-wave scattering length is varied, inducing resonances in the particle-dimer scattering. I have calculated the binding energies of trimers and the elastic particle-dimer scattering lengths in arbitrary angular-momentum channels, and shown that the particle-dimer resonances indeed occur. From the resonance positions, I have found accurate values of the critical mass ratios at which the Kartavtsev-Malykh trimers in the higher angular-momentum channels appear, which have been calculated only in an approximate manner in the previous study [61].

In 2013, a mass-imbalanced fermionic mixture of ^{40}K-^{6}Li has been realized at the Innsbruck University, and a precursor of the Kartavtsev-Malykh states has been observed [62]. On the other hand, the Kyoto University group has realized a highly mass-imbalanced mixture of ^{173}Yb-^{6}Li in 2011 [57]. In 2012, the magnetically controlled Feshbach resonance has been observed between Yb atoms by transferring atoms into a metastable excited state [63], and it is expected that with the same technique one may perform the magnetically controlled Feshbach resonant between Yb and Li atoms [64]. For such a highly mass-imbalanced fermionic mixture, the Efimov states are expected to appear at unitarity. The work in Chap. 3 would be helpful for these experimental investigations of few-body and many-body physics in the mass-imbalanced Fermi systems.

(ii) Universal three-body parameter (Chapter 4)

The most important feature of the Efimov states is, as mentioned earlier, the discrete scale invariance. At the resonant point where the s-wave scattering length diverges, the binding energies of the adjacent Efimov trimers are related to each other as $E_{n+1} = e^{-2\pi/s_0} E_n$. Here, the discrete scale invariance only fixes the ratio between the binding energies, and it does not determine their absolute values. Once the binding energy of one of the Efimov trimers is known, the binding energies of all the other Efimov trimers can be obtained by performing the discrete scale transformation[§]. Thus, one parameter is necessary and sufficient to determine the binding energies of the Efimov states. This parameter is called the three-body parameter. Once the three-body parameter is set, the energy spectra of the Efimov states are uniquely determined. It turns out that the three-body parameter is essential not only for the energy spectra, but also for various properties of the Efimov states, such as the three-body wave function, or an atomic loss (see Secs. 2.2.2 and 2.2.4 for more details). In all these physical quantities, the three-body parameter appears explicitly. Thus, the three-body parameter is a crucial quantity for the Efimov states.

[§]In fact, finite-range corrections can deteriorate, to some extent, the discrete scale invariance of the tightly bound Efimov trimers, especially the ground Efimov trimer, but here I neglect it for the sake of simplicity. See the discussions on the finite-range corrections in Sec. 2.2.2 for more details.

In ultracold atoms, one can prepare various atomic species under resonant conditions. So far, the Efimov states have been observed for ^{7}Li [26, 44, 45, 46, 47, 65], ^{39}K [28, 66], ^{85}Rb [67], and ^{133}Cs [27, 68, 69] atoms by using Feshbach resonances. By comparing the observed three-body parameters of all of these experiments, it has been found in 2011 that the three-body parameters expressed in units of the van der Waals length agree excellently for all these atomic species. Furthermore, the three-body parameter for excited-state ^{4}He atoms has also been measured in 2012 [70], and it has turned out to be consistent with that of alkalis.

These observations have surprised researchers working on the Efimov physics in ultracold atoms. While the long-range part of the inter-atomic interaction shares the same van der Waals form $-C_6/r^6$, the short-range part is rather complicated. The short-range part of the interaction depends on the details of electronic configurations of the atoms, and it can vary significantly between different atoms and hyperfine states. It has long been believed that this short-range part of the interaction would significantly affect the few-body behavior. Indeed, this is true for two-body physics. The s-wave scattering lengths for various atomic species and hyperfine states have been measured experimentally, and their values have been found to vary almost randomly between different atomic species and hyperfine states. There is no systematic law to relate the s-wave scattering lengths for different atomic species. It has long been believed that the same reasoning should apply to three-body physics: it has been widely believed that there is no systematic law to relate three-body parameters for different atomic species and hyperfine states. In addition to the short-range part of the two-body interaction, it has been suggested that an atomic species dependent three-body force present at short range can also significantly affect the three-body parameter, rendering it non-universal [71]. The experimental finding was, however, in a baffling contradiction to this conventional belief. Recently, this universality of the three-body parameter has been regarded as one of the most important issue in the Efimov physics in ultracold atoms.

Since the universal behavior of the three-body parameter has been found experimentally in 2011, people have started investigating when and why the three-body parameter should be universal. Some theoretical studies [72, 73, 74, 75] have confirmed that the three-body parameter should be universal as experimentally found, and they obtain the three-body parameters consistent with experiments. Furthermore, in Ref. [10], the three-body parameter has been numerically calculated for three ^{4}He atoms, and it turns out to be consistent with those observed in ultracold atoms.

In spite of these progresses in the numerical calculations, the physical mechanism behind the universal three-body parameter has remained unclear and controversial (see Sec. 2.4.2 for more details). It is therefore of great interest and importance to reveal what is the physical origin of the universal three-body parameter. This issue is addressed in Chap. 4, and clear answers to these questions are presented. To be more precise, I elucidate the physical origin of the universality in the three-body parameter as follows:

- For a deep two-body potential or a two-body potential with a hard-core repulsion at short distance, the probability of two particles coming close is suppressed in a universal manner.
- This universal suppression of probability induces an abrupt deformation of the three-body wave function as the hyper-radius is varied.
- This abrupt deformation of the wave function results in a strong non-adiabatic repulsion,

which explains the appearance of the universal three-body repulsion reported in Ref. [73]. Since three particles cannot come close due to the universal three-body repulsion, three-body physics is solely determined by the long-range van der Waals part, and is insensitive to atomic species dependent short-range part.

This mechanism is verified by reproducing the universal three-body repulsion with a simple model wave function. It is also shown that the three-body parameter becomes universal even for non van der Waals types of deep two-body potentials. Two classes of two-body potentials are identified, for which the three-body parameter has a universal value in units of their effective range. One class corresponds to short-range two-body potentials decaying as a power law, relevant to atomic interactions, for which the two-body probability is suppressed smoothly at short distance. The other corresponds to deep two-body potentials decaying exponentially, relevant to nuclear systems, for which the two-body probability decays abruptly at short distance. These findings may stimulate further investigation of the three-body parameter of the Efimov physics in many fields of physics, such as ultracold atoms, ^{4}He [8, 9, 10], nuclear physics [3, 4, 5], quantum spin systems [29, 30], and possibly polyexcitons in solids [76].

(iii) Efimov physics for more than three particles (Chapter 5)

Soon after the Efimov states have been found theoretically in 1970, people have started investigating what happens if the number of particles is further increased. Does a four-body bound state exist? If so, does it show a discrete scale invariance? What about five-body, six-body, and N-body bound states?

For resonantly interacting N identical bosons, these questions have been answered to some extent both experimentally and theoretically. It has been theoretically shown that there appear four-body bound states [77, 78, 79, 80], five-body bound states [81, 82, 83], ..., and N-body bound states at least up to $N \approx 10 - 40$ [84, 85]. These N-body clusters seem to behave universally in the resonantly interacting regime[§]. They seem to show the discrete scale invariance with the same scaling factor as the three-body system $e^{\pi/s_0} = 22.7\ldots$, which has been checked numerically for $N \lesssim 5-6$ [78, 80, 86, 87]. Recently, signatures of the universal four-body bound states [26, 45, 68, 88] and five-body bound states [89] have been observed experimentally, and they are in excellent agreement with theoretical predictions [77, 78, 80, 81].

For fermionic few-body systems, not much work has been carried out compared with the bosonic ones. Experimentally, three-body bound states with two identical fermions, the Efimov states, Kartavtsev-Malykh states, and crossover states, have not been observed yet, let alone four-body, five-body bound states. Theoretically, the three-body bound states have been studied recently and most of their properties are understood, as studied in Chap. 3. Fermionic four-body physics has also been studied recently: four-body bound states of the Efimov characters [90, 91]

[§]There still remains a controversy over the number of parameters needed to universally characterize these N-body bound states. For four-body bound states, some studies suggest that the s-wave scattering length and the three-body parameter are enough [77, 78, 79], while others point out the importance of an additional four-body parameter [79]. The number of the relevant parameters for N-body bound states are thus still under debate, but it is generally believed that N-body bound states can be universally characterized by only a few parameters, which should be less than N.

and Kartavtsev-Malykh characters [92] have been found in 2009 and 2012, respectively. The relation between these four-body bound states and three-body states still remains an open question, and merits further study. Furthermore, there is still little knowledge on the fermionic five-body physics and six-body physics [93].

These investigations of N-body clusters for $N \geq 3$ can be viewed as a "bottom-up" approach to bridge the gap between the few-body and many-body physics. The Efimov physics discussed above corresponds to strongly interacting N-body systems at small N: $N = 3, 4, 5....$ It is of great interest to know whether they may approach the thermodynamic limit as N gets large, and if they do, what kinds of many-body phases may appear.

There is an alternative approach to connect the few-body and many-body physics. Recently, few-body problems have been studied in the presence of some many-body backgrounds [94, 95, 96, 97, 98, 99, 100, 101]. In Ref. [94], for example, resonantly interacting (N+1+1)-body problem is considered with $N \gg 1$, in which one of the three components is degenerate and forms a Fermi sea. This system corresponds to a three-body problem in the presence of a many-body fermionic environment, and its effect on the Efimov physics has been studied. Similar few-body systems immersed in many-body backgrounds have been studied recently for both fermionic [94, 95, 96, 97, 98] and bosonic backgrounds [99, 100]. These systems correspond to (N+1+1)-body systems or (N+2)-body systems in the limit of $N \to +\infty$.

For a fermionic environment, it has been suggested numerically that the Fermi sea tends to suppress the Efimov effect for (N+1+1)-body [94] and (N+2)-body systems [97]. While these studies have shown this numerically in the case of two particles immersed in the Fermi sea, in Chap. 5, I show it analytically in the case of an arbitrary number of particles immersed in the Fermi sea. To be more specific, I study a system of N_H heavy particles immersed in the Fermi sea of N_L light, spinless (i.e., spin-polarized) fermions ($N_H \ll N_L$) and the interaction between the heavy particles induced by the light fermions under the Born-Oppenheimer approximation in Chap. 5. This system is closely related to the three-body physics of two identical spinless fermions (A) plus another distinguishable particle (B) studied in Chap. 3, and a four-body system of three identical fermions plus another distinguishable particle studied in Refs. [90, 91, 92]. The fermionic three-body (A-A-B) and four-body (A-A-A-B) bound states appear only when the fermionic A particle is much heavier than the B particle. The highly mass-imbalanced Fermi system studied in Chap. 5 corresponds to a system where there are so many fermionic B particles that they are forming a Fermi sea, and a few A particles are immersed in a Fermi sea of B particles. In Chap. 5, I analytically show that the induced interaction between the heavy particles acquires an additional repulsion due to the presence of the Fermi sea, and the interaction completely vanishes in the limit of high light-fermion density. This suggests that the formation of the Efimov states and their associated N-body bound states is suppressed for any N in the presence of a dense Fermi sea. The origin of this vanishing induced interaction is ascribed to the screening effect in the neutral Fermi system, which is also discussed in Chap. 5.

The few-body problems in the presence of many-body backgrounds can be interpreted as polaron problems once one regards the heavy particles as "impurities". In the (N+1)-system where N particles with $N \gg 1$ interact with the minority particle, the minority particle will form a dressed quasi-particle state. This dressed state is called a polaron. In ultracold atoms, the polaron state has

been realized in 2011 [102] by preparing a two-component mixture of fermionic atoms with an extreme population imbalance. The polaron physics has been actively studied in ultracold atoms both experimentally [56, 103, 104] and theoretically [105, 106, 107, 108] (for a review of the polaron physics in ultracold atoms, the readers may refer to Refs. [108] and [109]). The (N+1+1)-body systems or (N+2)-body systems corresponds to two-polaron problems: when two particles are immersed in the N-body environment, they form two polarons, which interact with each other via an induced interaction mediated by the surrounding environment of the N particles. Thus, the few-body studies in the presence of many-body backgrounds bring together the Efimov physics at large N and the polaron physics.

The few-body systems immersed in many-body backgrounds are natural systems in terms of ultracold atom experiments: few-body physics is typically studied in a system where many particles ($N \sim 10^4 - 10^6$) are prepared in a trap and the Feshbach resonance is utilized to make the scattering length large[§]. If the s-wave scattering length becomes comparable or much larger than the inter-particle spacing, the effect of the many-body background should be taken into account. It is notable that such a system has recently been studied in experiments as a "unitary Bose gas" [113, 114]. The s-wave scattering length in this system is much larger than the inter-particle spacing, and the atomic loss rate, which is closely related with the Efimov effect, has been observed to be suppressed by the presence of the many-body background. Further investigations of the unitary Bose gas experiments and possibly analogous experiments in mass-imbalanced Fermi systems, are expected to go hand in hand with theoretical studies which cover both few-body and many-body physics and cross their boundary.

1.4 Organization of this thesis

This thesis is organized as follows (the flowchart of this thesis is shown in Fig. 1.2). In Chap. 2, I review the Efimov physics in ultracold atoms. In Sec. 2.1, I introduce the universality of few-body physics at low energy. I then introduce one of the most important tool to investigate low-energy few-body systems, the boundary condition method, namely the zero-range model. By using this method, in Sec. 2.2, the Efimov physics for resonantly interacting three identical bosons is explained. In Sec. 2.2.2, I introduce experimental methods to investigate the Efimov states. In Sec. 2.3, I review the three-body physics with fermions. I will show how the Pauli exclusion principle between the identical fermions competes with the Efimov effect, and the role of the masses of the particles. Two types of universal three-body bound states, the Efimov states [38] and Kartavtsev-Malykh states [59], are introduced, together with their basic features. In Sec. 2.4, recent development in experimental and theoretical studies on the three-body parameter of the Efimov states in ultracold atoms is reviewed.

In Chap. 3, I study the three-body system of two identical fermions (i.e., fermions in the same internal state) resonantly interacting with another distinguishable particle. In this system, two classes of universal three-body bound states have been known to appear in different regimes of the mass

[§]In some specially designed systems, few-body systems have been prepared in a small trap under a deterministic control of the particle number and the interaction strength [110, 111, 112].

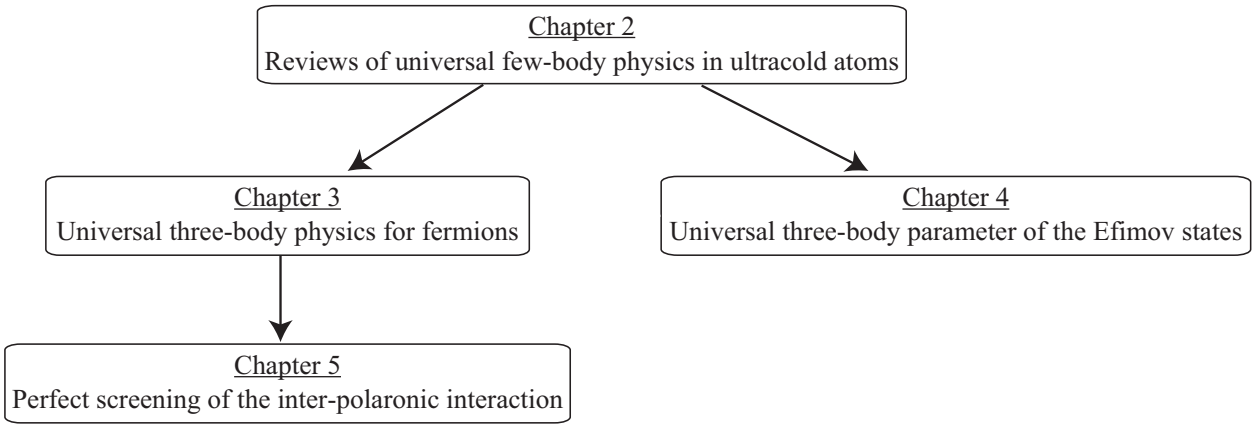

Figure 1.2: The flowchart of this thesis. Chapter 2 is devoted to reviews of previous studies which are relevant to this thesis. The main results of this thesis are shown in Chapters 3, 4, and 5.

ratio: the Efimov trimers and the Kartavtsev-Malykh trimers. I show that there exists the third class of universal three-body bound states, which I call the "crossover trimers". While the Efimov trimers and the Kartavtsev-Malykh trimers show the discrete and continuous scale invariance, the crossover trimers show neither of them. I have identified the regions of these three classes of trimers as a function of the mass ratio and the s-wave scattering length. I also show that the Kartavtsev-Malykh trimers and the Efimov trimers can continuously transform into each other via the crossover trimers as the mass ratio and the s-wave scattering length are varied. I have also found that the trimers dissociate into a particle and a dimer as the s-wave scattering length is varied, inducing particle-dimer resonances. I have also calculated the binding energies of trimers and the elastic particle-dimer scattering lengths in arbitrary angular-momentum channels. I show that the particle-dimer resonances occur at the points where the trimers dissociate into a particle and a dimer. From the resonance positions, I have found accurate values of the critical mass ratios at which the Kartavtsev-Malykh trimers in higher angular-momentum channels appear.

In Chap. 4, I address the physical origin of the universal three-body parameter. I explain in Sec. 4.1 when and why the three-body parameter should be universal, and show that a non-adiabatic deformation of the three-body wave function is the key to the universal three-body parameter. Based on the physical mechanism elucidated in Sec. 4.2, I show that the three-body parameter becomes universal even for non van der Waals types of deep two-body potentials. I identify two classes of two-body potentials for which the three-body parameter has a universal value in units of their effective range. One class corresponds to short-range two-body potentials decaying as a power law, for which the two-body probability is suppressed smoothly at short distance. The other corresponds to deep two-body potentials decaying exponentially, for which the two-body probability decays abruptly at short distance.

In Chap. 5, I study the induced interaction between N heavy particles immersed in the Fermi sea of the light spinless (i.e., spin-polarized) fermions at zero temperature. This induced interaction is essential to know how the Efimov states are affected by the many-body fermionic background. With the Born-Oppenheimer method, I show that the Efimov effect is generally suppressed by the Fermi

sea for an arbitrary number of heavy particles by proving that the effective interaction between the heavy particles vanishes in the limit of dense fermionic environment $k_F \to +\infty$. The origin of the vanishing effective interaction is ascribed to the screening effect in the neutral Fermi system.

In Chap. 6, I conclude this thesis and discuss future prospects.

Chapter 2

Reviews of universal few-body physics in ultracold atoms

In this chapter, I review few-body physics in ultracold atoms. In Sec. 2.1.1, universal properties of low-energy two-body systems are explained, and a basic mechanism of the Feshbach resonance is introduced. In Sec. 2.1.2, the three-body parameter is introduced. Some remarks on controversial N-body parameters for $N \geq 4$ are also presented. In Sec. 2.2, the Efimov physics for three identical bosons is reviewed. Qualitative descriptions are presented in Sec. 2.2.1, followed by more quantitative ones in Sec. 2.2.2. Finite-range effects are also discussed. In Sec. 2.2.4, experimental methods to observe the Efimov states in ultracold atoms are reviewed. In Sec. 2.3, fermionic three-body systems are reviewed. An essential role of the mass ratio in this system is discussed in Sec. 2.3.1. The Efimov states and the Kartavtsev-Malykh states in the fermionic three-body system with mass imbalance are introduced in Secs. 2.3.1 and 2.3.2, respectively. In Sec. 2.4, the universality of the three-body parameter is reviewed. A short history on this issue is presented in Sec. 2.4.1, followed by recent theoretical developments in Sec. 2.4.2. For more detailed reviews of the Efimov physics, the readers are referred to Refs. [32, 115]. Experimental studies of the Efimov physics in ultracold atoms are reviewed in Refs. [69, 116].

2.1 Universality of the few-body and many-body physics at low energy

For non-relativistic, quantum-mechanical few-body systems, their Hamiltonians determine all properties of the systems. If two systems have different microscopic Hamiltonians, one naturally expects that these systems will behave differently. At low energy, however, two physically different Hamiltonians can indeed show the same behavior. In other words, a low-energy quantum system exhibits universal properties. The universality allows us to replace a complicated potential in the original Hamiltonian with a simpler pseudo-potential properly constructed to show the same low-energy behavior. This dramatically reduces the difficulty in solving few-body and many-body problems: we no longer have to deal with complicated inter-particle potentials, but rather we can adopt a simple pseudo-potential. In ultracold atoms, the temperature of the system is so low that the

universality holds fairly well. Therefore, the pseudo-potential method turns out to be a powerful tool and is widely used in theoretical studies on ultracold atoms.

In addition to such simplification in the theoretical description, the universality has another important implication. As will be explained in this section, two-body and three-body systems at low energy are generally characterized by a few parameters, such as the s-wave scattering length, the effective range, and the three-body parameter. The universality dictates that any system must behave in the same manner at low energy as long as values of these relevant parameters are the same. In other words, physically different systems, such as ultracold atoms, ^{4}He clusters, bound states of magnons, or particles moving in a periodic lattice, can show the same behavior at low energy. This suggests that by studying few-body and many-body physics in ultracold atoms, one can gain insights into various kinds of low-energy systems. Theoretical and experimental studies on ultracold atoms are therefore not only relevant for researchers in this field, but are important for many other different fields in physics and thus concern general interest. Even for systems where their energy scale is not so small and the low-energy approach is inadequate, knowledge on the low-energy, dilute limit is a fundamental step toward understanding physical behaviors at higher energy, or denser systems.

In this section, I present a short review of the universality of systems in which particles interact via short-range potentials. For a two-body system, the universality can be seen most clearly, so I start introducing the universality for two particles in Sec. 2.1.1. It turns out that a low-energy two-body system can be universally characterized by just two parameters, namely the s-wave scattering length, and the effective range. Furthermore, as will be explained in Sec. 2.1.1, the effective range is irrelevant in the vicinity of a broad Feshbach resonance. For such a case, a single parameter, the s-wave scattering length, uniquely characterizes low-energy properties of the two-body system. The s-wave scattering length can be controlled experimentally by applying an external magnetic field. Its mechanism will also be briefly explained. In Sec. 2.1.2, the universality is extended to three-body systems, and the three-body parameter is introduced. The introduction of the three-body parameter is closely related to the Thomas collapse [117], which is a precursor of the Efimov effect. I will explain when and why the three-body parameter is necessary. While the universality of two-body and three-body systems is largely understood, there still remains some controversies on the universality for more than three particles. Some remarks on this issue will be presented. For a more detailed review of the universality of a few-body system at low energy, the readers are referred to Ref. [32].

2.1.1 Low-energy two-body physics

S-wave scattering length and the effective range

Let us consider the non-relativistic Schrödinger equation of two particles interacting via a central potential $V(\boldsymbol{r}) = V(r)$. The center-of-mass motion and the relative motion can be separated. The relative motion obeys the following Schrödinger equation

$$\left[-\frac{\hbar^2}{2\mu_{12}}\nabla_{\boldsymbol{r}}^2 + V(r)\right]\psi(\boldsymbol{r}) = E\psi(\boldsymbol{r}), \tag{2.1}$$

where $\boldsymbol{r} = \boldsymbol{r_1} - \boldsymbol{r_2}$ is the relative coordinate vector between the two particles, and $\mu_{12} = \dfrac{m_1 m_2}{m_1 + m_2}$ is the reduced mass.

For a central potential, the angular momentum is a good quantum number, so that the Schrödinger equation can be separated into independent partial waves. The scattering amplitude in the ℓ-th partial-wave channel is related to the ℓ-th wave phase shift $\delta_\ell(k)$ as [118]

$$f_\ell(k) = \frac{1}{k \cot \delta_\ell(k) - ik}. \tag{2.2}$$

For a short-range potential which decays rapidly at large inter-particle separation, a low-energy expansion of the phase shift can be performed, giving

$$k^{2\ell+1} \cot \delta_\ell(k) = \text{Const.} + O(k^2). \tag{2.3}$$

This suggests $f_\ell(k) \propto k^{2\ell}$ at low energy, so that the higher-partial-wave channels become irrelevant [118].

On the other hand, an inter-atomic interaction between neutral atoms is governed by the van der Waals potential $-C_6/r^6$ at large inter-particle separation. This potential is not a genuine short-range potential since it decays slowly, but still similar low-energy expansions can be made [118, 119, 120]:

$$k \cot \delta_{\ell=0}(k) = -\frac{1}{a} + \frac{r_{\text{eff}}}{2} k^2 + O(k^3), \tag{2.4}$$

$$k^3 \cot \delta_{\ell=1}(k) = -\frac{1}{v_p} + r_P^{(1)} k + O(k^2), \tag{2.5}$$

$$k^4 \cot \delta_\ell(k) = r_\ell^{(0)} + O(k) \ \ (\ell \geq 2). \tag{2.6}$$

For a van der Waals type of potential, the van der Waals length[§]

$$r_{\text{vdW}} \equiv \frac{1}{2} \left(\frac{2\mu_{12} C_6}{\hbar^2} \right)^{\frac{1}{4}} \tag{2.7}$$

sets an important length scale. All the higher partial-wave coefficients are of the order of the van der Waals length if there is no accidental resonance: $|v_p| \sim r_{\text{vdW}}^3$, $|r_P^{(1)}| \sim r_{\text{vdW}}^{-2}$, $|r_\ell^{(0)}| \sim r_{\text{vdW}}^{-4}$. Therefore, if the energy of the particles is much smaller than the van der Waals energy $|E| \ll \dfrac{\hbar^2}{2\mu_{12} r_{\text{vdW}}^2}$, the s-wave scattering channel makes a dominant contribution, and the scattering amplitude is expressed as

$$f(k) = -\frac{1}{1/a + ik - \frac{r_{\text{eff}}}{2} k^2}. \tag{2.8}$$

In ultracold atoms, this conditions can be realized; for example, the van der Waals energy is 83 μK for ^{87}Rb atoms, while experiments are typically performed at temperature $T \lesssim 1\ \mu$K.

At this point, we can see the universality. All bound states and scattering states of the two particles are determined by the scattering amplitude, and the scattering amplitude is written as Eq. (2.8)

[§]Note that in some literature [119, 120, 121, 122], the van der Waals length is defined with coefficients different from $\dfrac{1}{2}$.

for any two-body potential at low energy. This suggests that systems with two different potentials must show the same behavior at low energy if the s-wave scattering length and the effective range are the same. Therefore, low-energy two-body physics is universally described by these two parameters. The word "universal" is used here in a sense that physically different systems behave in the same manner.

One can further proceed with the discussion of the universality by assuming the following two conditions:

1. The s-wave scattering length is much larger than the van der Waals length $|a| \gg r_{\mathrm{vdW}}$.

2. The effective range is at most of the order of the van der Waals length $|r_{\mathrm{eff}}| \lesssim r_{\mathrm{vdW}}$.

When these conditions are satisfied, the effective-range term becomes irrelevant, and we obtain

$$f(k) = -\frac{1}{1/a + ik}. \tag{2.9}$$

Thus, two-body physics at low energy is simply described by a single parameter. A bound state, corresponding to a pole on the positive imaginary axis, exists for $a > 0$ with its binding energy

$$E = -\frac{\hbar^2}{2\mu_{12}a^2}, \tag{2.10}$$

and the wave function

$$\psi(r) = \frac{1}{\sqrt{2\pi a}}\frac{e^{-r/a}}{r}. \tag{2.11}$$

It turns out that the above two conditions are satisfied in the vicinity of shape resonances for typical two-body potentials. As a specific example, in Figs. 2.1 (a) and (b), the s-wave scattering length and the effective range are shown for a soft-core van der Waals potential

$$V_{\mathrm{SCvdW}}(r) = -\frac{C_6}{r^6 + \sigma_{\mathrm{SC}}^6} \tag{2.12}$$

as a function of $r_{\mathrm{vdW}}/\sigma_{\mathrm{SC}}$. For a small $r_{\mathrm{vdW}}/\sigma_{\mathrm{SC}}$, the potential is weakly attractive, and there is no bound state. As $r_{\mathrm{vdW}}/\sigma_{\mathrm{SC}}$ is increased, the first, second, and third two-body bound states appear at $r_{\mathrm{vdW}}/\sigma_{\mathrm{SC}} = 0.607, 1.007, 1.2602$, respectively. At the point where a two-body bound state appears, the s-wave scattering length diverges. This is a general phenomenon and is called a shape resonance. While the s-wave scattering length is much larger than the van der Waals length in the vicinity of shape resonances, the effective range remains finite and of the order of the van der Waals length. For typical two-body potentials[§], the two conditions described above are satisfied close to shape resonances.

[§]One can mathematically construct a potential, where the effective range is negative with its magnitude much larger than the range of the interaction on the shape resonance $1/a = 0$ [123]. For such a potential, the second condition is not satisfied around the shape resonant point. This is analogous to a narrow Feshbach resonance, which shows a large and negative effective range.

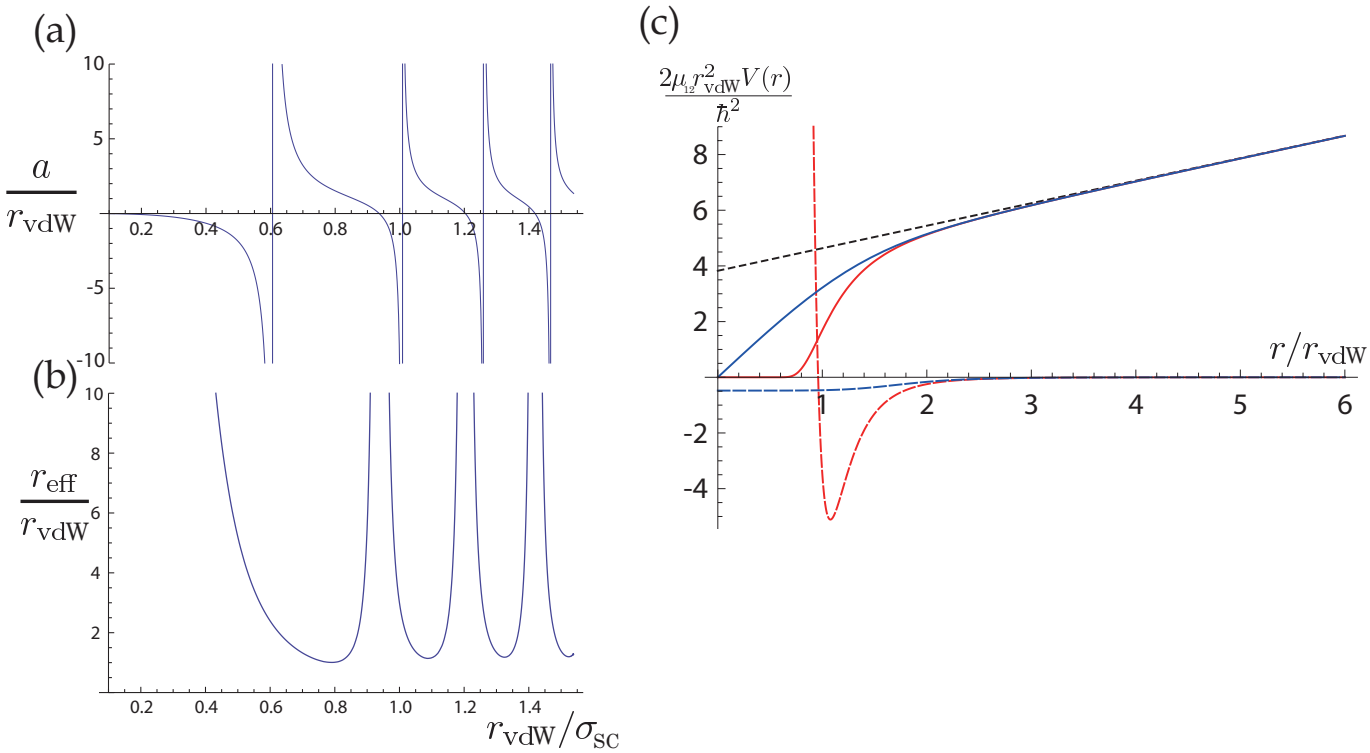

Figure 2.1: S-wave scattering length (a) and the effective range (b) for the soft-core van der Waals potential given in Eq. (2.12). A large $r_{\rm vdW}/\sigma_{\rm SC}$ corresponds to a deeper two-body potential. (c) The zero-range wave function (black dotted line) for $a/r_{\rm vdW} = -4.73$ at $E = 0$ is compared with the zero-energy solutions of the two-body Schrödinger equation for finite-range potentials. Wave functions for the Lennard-Jones potential (red solid curve) and for the soft-core van der Waals potential (blue solid curve) are shown. The Lennard-Jones potential (red dashed curve) and soft-core van der Waals potential (blue dashed curve) are tunes so that they have the same s-wave scattering length $a/r_{\rm vdW} = -4.73$ and no two-body bound state. The wave functions are unnormalized and shown in arbitrary units.

While the above argument has been made in momentum space, an alternative description is possible in real space. At low energy, a solution of the Schrödinger equation generally has the following asymptotic form

$$r\psi(r) \propto r - a \quad (r_{\rm vdW} \ll r \ll k^{-1}), \tag{2.13}$$

which can be obtained from a Fourier transformation of Eq. (2.9). In Fig. 2.1 (c), two-body wave functions at zero energy are shown for two types of potentials corresponding to the same s-wave scattering length $a/r_{\rm vdW} = -4.73$: the soft-core van der Waals potential and the Lennard-Jones potential

$$V_{\rm LJ}(r) = -\frac{C_6}{r^6}\left(1 - \frac{\sigma_{\rm LJ}^6}{r^6}\right). \tag{2.14}$$

At large inter-particle separation, the two wave functions asymptotically approach to the same limit given in Eq. (2.13) (black dashed line), while their difference becomes visible at short distance

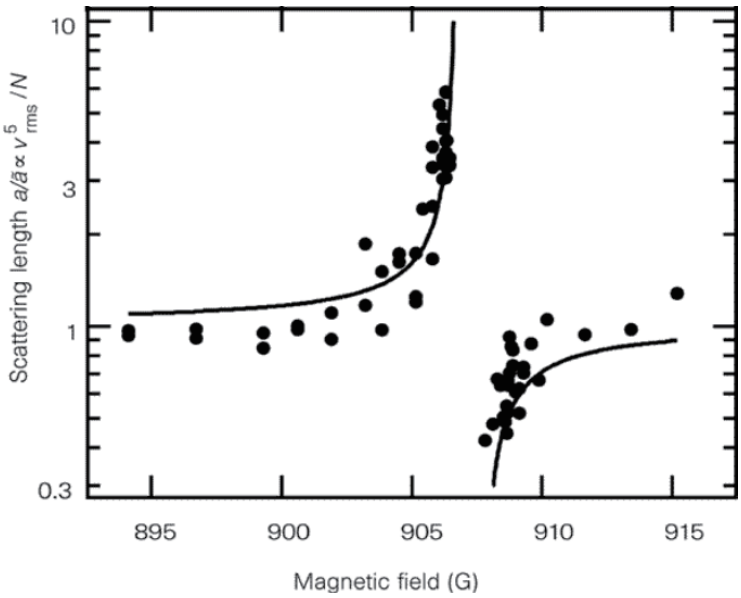

Figure 2.2: First experimental observation of a Feshbach resonance in ultracold atoms [21]. The horizontal axis is an external magnetic field, and the vertical axis shows the s-wave scattering length between ^{23}Na atoms. [Figure adapted with permission from S. Inouye *et al.*, Nature **392** 151 (1998). Copyright © (1998) Nature Publishing Group.]

$r \lesssim r_{\rm vdW}$. If we observe the wave functions with a large length scale, there is almost no difference between in the behavior of the wave function between the soft-core van der Waals potential and the Lennard-Jones potential. In other words, details of potentials are irrelevant and a two-body wave functions behave universally at long inter-particle separation. The low-energy theory in momentum space is thus equivalent to the large-distance behavior in real space.

Feshbach resonance

The Feshbach resonance is one of the most important techniques in ultracold atom experiments. It enables one to control inter-particle interactions experimentally by applying a uniform external magnetic field. In Fig. 2.2, the first experimental observation of a Feshbach resonance is shown [21]. Close to the resonant point, the s-wave scattering length gets divergently large and behaves as

$$a(B) = a_{\rm bg}\left(1 - \frac{\Delta B}{B - B_0}\right), \tag{2.15}$$

where $a_{\rm bg} \sim r_{\rm vdW}$ is the background scattering length, and ΔB characterizes the width of the Feshbach resonance.

The Feshbach resonance occurs through a coupling between different internal states of atoms. To explain the mechanism of the Feshbach resonance, let us consider two alkali atoms colliding at low energy. When the two atoms are far apart, each atom can be considered to be independent. For alkalis, internal states of atoms are characterized by the hyperfine quantum numbers. Let us denote the hyperfine states of the two atoms as α and β, respectively. As the atoms get close, they

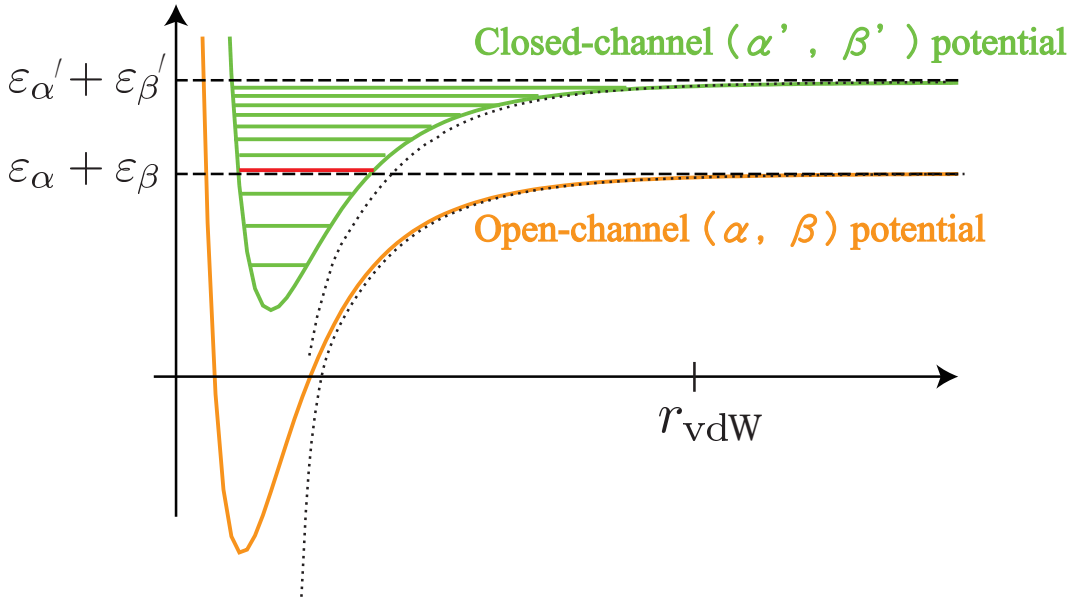

Figure 2.3: Schematic illustration of the Feshbach resonance. The diagonal potential in the two channels (α,β) and (α',β') are shown, together with bound-state levels in the (α',β') channel. The dotted curves show the asymptotic van der Waals potentials.

start to interact via the van der Waals potential[§]. Since the van der Waals part of the potential does not depend on spin states of the electrons or nuclei, the atoms experience the same van der Waals potential at large inter-atomic separation. If the two atoms get much closer, the electronic wave function of the atoms start to overlap. The electronic contribution strongly depends on spin states of the out-most electrons, and it is written as

$$\hat{V}_{\mathrm{el}}(r) = V_{\mathrm{singlet}}(r)\mathcal{P}^{\mathrm{el}}_{S=0} + V_{\mathrm{triplet}}(r)\mathcal{P}^{\mathrm{el}}_{S=1}, \tag{2.16}$$

where $V_{\mathrm{singlet}}(r)$ and $V_{\mathrm{triplet}}(r)$ are electronic contributions to the inter-atomic potential in the spin-singlet and spin-triplet channels, respectively, and $\mathcal{P}^{\mathrm{el}}_{S=0}$ and $\mathcal{P}^{\mathrm{el}}_{S=1}$ are projection operators onto the electronic spin singlet and triplet states, respectively. Since the singlet and triplet potentials behave rather differently, the inter-atomic interaction is not diagonal in the hyperfine basis any longer. This induces coupling between different hyperfine channels during the collision, and the atoms initially in the hyperfine states (α,β) can make transitions into (α',β') states. Under such circumstances, physics should be described by a multi-channel Schrödinger equation.

This channel coupling is essential for the Feshbach resonance. To see this point, let us assume that there are only two relevant channels, and label these two channels by their hyperfine quantum numbers (α,β) and (α',β'), respectively. The sums of the inter-atomic potential and the hyperfine interaction in the two channels are schematically illustrated in Fig. 2.3. At large inter-atomic separation, the inter-atomic potentials behave as $\varepsilon_\alpha + \varepsilon_\beta - C_6/r^6$ and $\varepsilon_{\alpha'} + \varepsilon_{\beta'} - C_6/r^6$ in the (α,β)

[§]Here, I neglect a dipole-dipole interaction, which is small for typical ultracold atom experiments. For some atomic species, such as Cr [124], Er [125, 126], and Dy [127, 128], the dipole-dipole interaction is unusually large and cannot be neglected.

channel and (α',β') channel, respectively. For smaller inter-atomic separation, the potentials behave differently, i.e., $V_{\alpha\beta} \neq V_{\alpha'\beta'}$. Let us consider the initial in-coming channel of the two atoms to be (α,β) channel. The in-coming (α,β) channel is often referred to as an open channel, while the (α',β') channel is referred to as a closed channel. When the two atoms come close and the channel-coupling becomes large, the transition into the (α',β') channel may occur at a length scale much smaller than $r_{\rm vdW}$. The depth of the potentials $V_{\alpha',\beta'}$ is of the order of eV, and there are many s-wave bound-state levels. If one of the bound-state levels in the (α',β') hyperfine channel (denoted as a red line in Fig. 2.3) is almost degenerate with the continuum threshold of the open channel $\varepsilon_\alpha + \varepsilon_\beta$, a resonant scattering occurs and the s-wave scattering length diverges

$$a \propto \frac{1}{\varepsilon_\alpha + \varepsilon_\beta - E_m}, \tag{2.17}$$

where E_m is the energy of the molecular level. By applying the external magnetic field, the threshold energy $\varepsilon_\alpha + \varepsilon_\beta$ can be changed by the Zeeman effect. If the change of the threshold energy as a function of the external magnetic filed is linearized around the resonant magnetic field B_0 as $\varepsilon_\alpha + \varepsilon_\beta - E_m = \delta\mu(B - B_0)$, one obtains $a \propto (B - B_0)^{-1}$. This suggests that the s-wave scattering length between the atoms can be controlled by applying an external magnetic field and fine-tuning it so that the molecular level becomes degenerate with the threshold energy of the in-coming channel.

There are two classes of Feshbach resonances: a broad Feshbach resonance, and a narrow Feshbach resonance. The width of a Feshbach resonance is characterized by the following positive, dimensionless quantity [24]

$$s_{\rm res} = \frac{4\pi}{\left(\Gamma\left(\frac{1}{4}\right)\right)^2} \frac{a_{\rm bg}}{r_{\rm vdW}} \frac{\delta\mu\Delta B}{\varepsilon_{\rm vdW}}, \tag{2.18}$$

where $\varepsilon_{\rm vdW} = \hbar^2/2\mu_{12}r_{\rm vdW}^2$ is the van der Waals energy. Crudely speaking, this quantity measures the magnetic field width in units of the van der Waals energy $s_{\rm res} \sim \delta\mu\Delta B/\varepsilon_{\rm vdW}$. When $s_{\rm res} \gg 1$, it is called a broad Feshbach resonance, which typically corresponds to a large magnetic resonance width. On the other hand, $s_{\rm res} \lesssim 1$ is called a narrow Feshbach resonance, which typically corresponds to a small resonance width. For a broad Feshbach resonance, the effective range is of the order of the van der Waals length $r_{\rm eff} \sim r_{\rm vdW}$. Therefore, the effective-range term can be safely neglected at low energy and the scattering amplitude can be described by the universal form in Eq. (2.9). On the other hand, the effective range is not necessarily small for a narrow Feshbach resonance. Indeed, in the ultra-narrow limit $s_{\rm res} \ll 1$, the effective range is negative and its magnitude gets very large $r_{\rm eff} \propto s_{\rm res}^{-1}$. In such a case, the effective-range term in Eq. (2.8) cannot be neglected. Throughout this thesis, I mainly consider the former case: few-body and many-body problems in the vicinity of a broad Feshbach resonance.

Pseudo-potential approach

In the case of a broad Feshbach resonance, the s-wave scattering length is the only relevant parameter for the interaction. Therefore, one can take any artificially constructed model potential to study low-energy two-body phenomena as long as the model potential has the same s-wave scattering length. Such a model potential is generally called a “pseudo-potential”. The most famous

pseudo-potential to model low-energy two-body systems around broad Feshbach resonances is the Huang-Yang pseudo-potential [129]:

$$V_{\mathrm{HY}}(r) = \frac{2\pi\hbar^2 a}{\mu_{12}}\delta^{(3)}(\boldsymbol{r})\frac{\partial}{\partial r}r. \tag{2.19}$$

One can easily show that the scattering amplitude calculated with this pseudo-potential reproduces Eq. (2.9), so it correctly captures the low-energy behavior close to a broad Feshbach resonance.

There is another equivalent way to reproduce the low-energy two-body physics by imposing a boundary condition when the two particles come close. The basic idea of this method can be understood easily by recalling how a two-body wave function behaves at low energy. When the two particles are placed at a distance much larger than the typical range of the interaction r_0 (in ultracold atoms, this is the van der Waals length), but much closer than the inverse of the wave number $r_0 \ll r \ll k^{-1}$, the two-body wave function behaves as

$$r\psi(r) \approx C(r-a), \tag{2.20}$$

or equivalently

$$\frac{d}{dr}\log\left[r\psi(r)\right] \approx \frac{1}{r-a}. \tag{2.21}$$

Since we are interested in low-energy behavior, the wave function at $r \lesssim r_0$ is irrelevant. By taking $r_0 \to 0$, one obtains the following zero-range boundary condition:

$$\left.\frac{d}{dr}\log\left[r\psi(r)\right]\right|_{r=0} = -\frac{1}{a}. \tag{2.22}$$

By solving the free Schrödinger equation

$$-\frac{\hbar^2}{2\mu_{12}}\nabla^2\psi(r) = E\psi(r) \tag{2.23}$$

with this boundary condition, one can easily show that the scattering amplitude becomes Eq. (2.9). Thus, the low-energy universal behavior is accurately reproduced by this pseudo-potential. This boundary condition is called the Bethe-Peierls boundary condition [130]. It is widely used to study universal physics at low energy.

The pseudo-potential method is a general and powerful tool to investigate few-body and many-body physics in the universal regime. For some light neutral atoms, realistic inter-atomic potentials are known [12], but they are rather complicated, especially at small inter-atomic separation. If one is allowed to replace such a complicated realistic potential with a simpler pseudo-potential as presented above, theoretical calculations are dramatically facilitated. For heavier atoms, it is almost impossible to obtain realistic inter-atomic potentials, since there are many electrons and one needs to take into account correlations between these electrons. Even when a realistic potential is unknown, we can still study their low-energy properties once the s-wave scattering length is known. One can construct a pseudo-potential with the corresponding s-wave scattering length and use it to investigate few-body and many-body phenomena.

In the case of a narrow Feshbach resonance, on the other hand, the above zero-range approach is no longer valid. One needs more sophisticated approaches which properly take into account

the effective range contribution, such as two-channel models. Throughout this thesis, however, we only deal with a broad Feshbach resonance, so we do not discuss them here. For more details of the Feshbach resonance, the readers are referred to Refs. [24, 131].

2.1.2 Low-energy three-body physics and the three-body parameter

Three-body boundary condition

In the Bethe-Peierls boundary condition method, effect of the original short-range potential is taken into account by the boundary condition which accurately captures the low-energy scattering phase shift. This boundary condition method can be generalized for systems with more than two particles. Let us consider three particles interacting via short-range interactions and consider its low-energy behavior. In this system, there are two types of scattering events. When two particles come close and scatter while the third particle stays far apart from them, the scattering event is essentially a two-body process. Such a scattering event can be properly taken into account by the Bethe-Peierls boundary condition. Another type of scattering is a genuine three-body one: three particles come close simultaneously and scatter with each other. The three-body scattering cannot be taken into account by the Bethe-Peierls boundary condition, because by construction it does not include any information of a three-body system. Therefore, an additional boundary condition is necessary to incorporate the phase shift induced by such a three-body scattering. The three-body boundary condition is imposed in a manner similar to the Bethe-Peierls method:

$$\frac{d}{dR}\log\left[Rf(R)\right]\bigg|_{R=R_0} = \Lambda, \tag{2.24}$$

where

$$R = \sqrt{\frac{2}{3}[r_{12}^2 + r_{13}^2 + r_{23}^2]} \tag{2.25}$$

is the hyper-radius. The hyper-radius characterizes the overall size of the three-body system, and it can be small if and only if three particles come close. In Eq. (2.24), $f(R)$ is the hyper-radial wave function, whose definition can be found in Sec. 2.2. Crudely speaking, $f(R)$ is the three-body wave function describing the overall motion of the three-body system. In Eq. (2.24), R_0 is taken in the asymptotic region $R_0 \gg r_{\mathrm{vdW}}$. The genuine three-body scattering occurs when and only when $R \lesssim r_{\mathrm{vdW}}$, and Λ characterizes the phase shift acquired by such a three-body scattering.

Note that the three-body boundary condition is, in general, independent of the two-body boundary condition even when the interaction is a sum of pair-wise interactions $V(\boldsymbol{r_1}, \boldsymbol{r_2}, \boldsymbol{r_3}) = v(\boldsymbol{r_{12}}) + v(\boldsymbol{r_{13}}) + v(\boldsymbol{r_{23}})$. In other words, one must not naively replace the two-body interaction in the Hamiltonian with the Bethe-Peierls boundary condition or the Huang-Yang pseudo-potential for systems with more than two particles. Such a replacement amounts to taking only two-body scattering into account while neglecting three-body scattering. The naive replacement is justified if and only if the effect of three-body scattering is negligibly small. Whether the three-body scattering is relevant or not is rather system dependent, and it can be known only after we have solved the three-body problem. For example, for a system of three identical bosons, the three particles can come close and scatter easily, so that the three-body boundary condition is relevant (see Sec. 2.2.1). In fact, if one

tries to solve the three-body problem without imposing the three-body boundary condition, one encounters a pathological result: the ground-state energy is unbounded from below and tends to $-\infty$ at the unitarity limit $1/a = 0$. This pathology is known as the Thomas collapse [117]. As will be discussed in Sec. 2.2.1, the Thomas collapse is closely related to the Efimov effect. The Thomas collapse clearly shows that the naive replacement of the two-body potential with the pseudo-potential is inadequate for this system. On the other hand, for systems with identical fermions, the Pauli exclusion principle can suppress the three particles from getting close. In fact, for a three-body system of two identical fermions interacting with one distinguishable particle, which corresponds to a two-component Fermi system of $\uparrow\uparrow\downarrow$ ($\uparrow$ and $\downarrow$ denote internal states of the fermions), the three particles cannot come close for an equal mass system $m_\uparrow = m_\downarrow$. Therefore, the genuine three-body scattering is negligible and the naive replacement is valid. However, when the mass imbalance is large $m_\uparrow \gg m_\downarrow$, the three particles can easily come close. Indeed, if the mass ratio exceeds a critical value $m_\uparrow/m_\downarrow > 13.6$, the three-body boundary condition becomes relevant (see Sec. 2.3.1), and the Thomas collapse occurs when one naively neglects the three-body boundary condition.

Is an N-body parameter necessary?

There is a similar issue for N-particle systems. For an N-body system, where particles interact via the sum of pair-wise interactions $\hat{V} = \sum_{i<j} v(\boldsymbol{r}_{ij})$, one needs to take great care before naively replacing the two-body interactions with the Bethe-Peierls boundary condition or the Huang-Yang pseudo-potential. The necessity of the three-body, four-body,..., and N-body boundary conditions is a highly non-trivial many-body problem. For a two-component Fermi system without mass imbalance, three-body and four-body problems have been solved, and it has been found that three-body and four-body boundary conditions are irrelevant thanks to the Pauli exclusion principle [38, 132, 133]. This justifies us to use the Hamiltonian with the sum of pair-wise pseudo-potentials in the many-body studies of the two-component Fermi system, such as the BEC-BCS crossover [134, 135, 136, 137] and its universal thermodynamics [138, 139, 140, 141, 142, 143, 144] (see Refs. [145, 146] for reviews of the BEC-BCS crossover). Since we only impose the two-body (Bethe-Peierls) boundary condition, a single parameter, the s-wave scattering length, characterizes the interaction between particles. For a two-component Fermi system with mass imbalance, three-body [38, 132] and four-body [90, 91] Efimov states have been found in a highly mass-imbalanced regime $m_\uparrow/m_\downarrow \gtrsim 13$. This suggests that the three-body and four-body boundary conditions are relevant in this system. Thus, in contrast to the BEC-BCS crossover, a highly mass-imbalanced Fermi system cannot be described by a single interaction parameter, but one needs at least several parameters: the s-wave scattering length, the three-body parameter, and the four-body parameter. For a system of more than four particles, little has been known, and further studies will be needed to make a definite statement.

The N-body parameter for $N \geq 4$ is a controversial issue in the bosonic case. In some literature [77, 78, 79], properties of four-body bound states have been claimed to be universally determined by the s-wave scattering length and the three-body parameter, so that the four-body parameter is irrelevant. Some other researchers claim the opposite [79]: the four-body parameter is indeed relevant. This issue is one of the most important issue in the field of Efimov physics. The

same issue may also exist for a system with more than four particles. Does the five-body parameter, six-body parameter,..., and N-body parameter necessary? Much work needs to be done to answer these questions.

2.2 Efimov physics for three identical bosons

In this section, low-energy universal properties of a system of three identical bosons are discussed. Since we are interested here in the universal behavior at low energy, we consider a three-body Schrödinger equaiton

$$\left[-\sum_{i=1}^{3}\frac{\hbar^2\nabla^2_{\boldsymbol{r}_i}}{2m}+U(\boldsymbol{r}_1,\boldsymbol{r}_2,\boldsymbol{r}_3)\right]\Psi(\boldsymbol{r}_1,\boldsymbol{r}_2,\boldsymbol{r}_3)=E\Psi(\boldsymbol{r}_1,\boldsymbol{r}_2,\boldsymbol{r}_3), \tag{2.26}$$

where the two-body interaction is replaced with the Huang-Yang pseudo-potential

$$U(\boldsymbol{r}_1,\boldsymbol{r}_2,\boldsymbol{r}_3)=V_{\rm HY}(\boldsymbol{r}_{12})+V_{\rm HY}(\boldsymbol{r}_{13})+V_{\rm HY}(\boldsymbol{r}_{23}), \tag{2.27}$$

and the three-body boundary condition in Eq. (2.24) is imposed at a small but nonzero hyper-radius $R=R_0$. As discussed in the previous section, this three-body problem with the pseudo-potential and the boundary condition can predict low-energy properties of various systems, including the Efimov states in ultracold atoms. Since finite-range realistic potentials are replaced by the zero-range pseudo-potential and the boundary condition, it is often referred to as the zero-range Efimov theory, or the zero-range theory.

Even in the zero-range Efimov theory, it is a genuine three-body problem. But still, we can deal with it analytically, especially at the unitarity limit. In solving the three-body problem in real space, it is convenient to introduce the Jacobi coordinates, hyper-radius, and hyper-angle:

$$\boldsymbol{R}_{\rm tot} = \frac{1}{3}(\boldsymbol{r}_1+\boldsymbol{r}_2+\boldsymbol{r}_3), \tag{2.28}$$

$$\boldsymbol{r}_{12} = \boldsymbol{r}_1-\boldsymbol{r}_2, \tag{2.29}$$

$$\boldsymbol{\rho}_3 = \boldsymbol{r}_3-\frac{1}{2}(\boldsymbol{r}_1+\boldsymbol{r}_2). \tag{2.30}$$

Using the Jacobi coordinates, the kinetic term can be rewritten as

$$-\sum_{i=1}^{3}\frac{\hbar^2\nabla_i^2}{2m}=-\frac{\hbar^2\nabla^2_{\boldsymbol{R}_{\rm tot}}}{6m}-\frac{\hbar^2\nabla^2_{\boldsymbol{r}_{12}}}{m}-\frac{3\hbar^2\nabla^2_{\boldsymbol{\rho}_3}}{4m}. \tag{2.31}$$

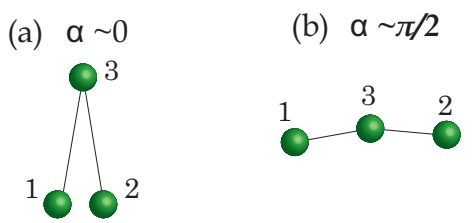

Figure 2.4: Schematic illustration of three-body configurations corresponding to (a) small and (b) large hyper-angles.

With the Jacobi coordinates, we can introduce the hyper-radius and hyper-angle[§]:

$$R^2 \equiv \frac{2}{3}\left[r_{12}^2 + r_{23}^3 + r_{31}^2\right] = r_{12}^2 + \frac{4}{3}\rho_3^2, \tag{2.32}$$

$$\alpha_3 = \arctan\left(\frac{\sqrt{3}r_{12}}{2\rho_3}\right). \tag{2.33}$$

Alternatively, the Jacobi coordinates can be written in terms of the hyper-radius and hyper-angle as

$$r_{12} = R\sin\alpha_3, \tag{2.34}$$

$$\rho_3 = \frac{\sqrt{3}}{2}R\cos\alpha_3. \tag{2.35}$$

The hyper-radius R characterizes the overall size of the three-body system, and it can be small if and only if three particles come close. The hyper-angle α_3 characterizes the relative configuration of the three particles and varies from 0 to $\pi/2$. As shown in Fig. 2.4, $\alpha_3 \to +0$ corresponds to a configuration of a sharp triangle, while $\alpha_3 \to \pi/2$ corresponds to a linearly aligned configuration. By using the hyper-radius and hyper-angle, the Schrödinger equation is written as

$$\begin{aligned} -\frac{\hbar^2}{m}\left[\frac{1}{R^{\frac{5}{2}}}\frac{\partial^2}{\partial R^2}R^{\frac{5}{2}} + \frac{1}{R^2}\frac{\partial^2}{\partial\alpha_3^2} + \frac{4}{R^2}\cot 2\alpha_3\frac{\partial}{\partial\alpha_3} - \frac{1}{R^2}\left(\frac{\hat{L}_{\boldsymbol{\rho_3}}^2}{\cos^2\alpha_3} + \frac{\hat{L}_{\boldsymbol{r_{12}}}^2}{\sin^2\alpha_3}\right)\right]\Psi(\boldsymbol{r_{12}},\boldsymbol{\rho_3}) \\ + U(\boldsymbol{r_1},\boldsymbol{r_2},\boldsymbol{r_3})\Psi(\boldsymbol{r_{12}},\boldsymbol{\rho_3}) = E\Psi(\boldsymbol{r_{12}},\boldsymbol{\rho_3}), \end{aligned} \tag{2.36}$$

where $\hat{L}_{\boldsymbol{r_{12}}}$ and $\hat{L}_{\boldsymbol{\rho_3}}$ are the angular momentum operators of the Jacobi coordinates $\boldsymbol{r_{12}}$ and $\boldsymbol{\rho_3}$, respectively.

In solving the three-body problem, it is convenient to separate the hyper-radial and the other motions in a manner similar to a separation of radial and rotational motions for a two-body problem interacting via a central potential. One essential difference between the three-body problem and the two-body problem is that the hyper-radial motion cannot be separated in general from the other part. Even when one tries to separate the hyper-radial and the other motions by an expansion

$$\Psi(\boldsymbol{r_{12}},\boldsymbol{\rho_3}) = \frac{1}{R^{5/2}}\sum_n f_n(R)\Phi_n(R,\alpha_3,\hat{\boldsymbol{r}}_{\boldsymbol{12}},\hat{\boldsymbol{\rho}}_{\boldsymbol{3}}), \tag{2.37}$$

where the basis function Φ_n is the solution to the hyper-angular Schrödinger equation

$$\begin{aligned} \left[-\frac{\partial^2}{\partial\alpha_3^2} - 4\cot 2\alpha_3\frac{\partial}{\partial\alpha_3} + \left(\frac{\hat{L}_{\boldsymbol{\rho_3}}^2}{\cos^2\alpha_3} + \frac{\hat{L}_{\boldsymbol{r_{12}}}^2}{\sin^2\alpha_3}\right) + U(\boldsymbol{r_1},\boldsymbol{r_2},\boldsymbol{r_3})\right]\Phi_n(R,\alpha_3,\hat{\boldsymbol{r}}_{\boldsymbol{12}},\hat{\boldsymbol{\rho}}_{\boldsymbol{3}}) \\ = \lambda_n(R)\Phi_n(R,\alpha_3,\hat{\boldsymbol{r}}_{\boldsymbol{12}},\hat{\boldsymbol{\rho}}_{\boldsymbol{3}}), \end{aligned} \tag{2.38}$$

[§]There are several conventions for the definition of the hyper-radius. We here chose the definition of Refs. [2, 147, 148]. In Refs. [71, 73, 149], the hyper-radius is defined as $R \equiv \sqrt{\frac{r_{12}^2 + r_{23}^3 + r_{31}^2}{\sqrt{3}}}$, which is a factor of $\frac{3^{1/4}}{\sqrt{2}} = 0.931...$ different from ours. In Refs. [32, 72, 74, 150], the hyper-radius is defined as $R \equiv \sqrt{\frac{r_{12}^2 + r_{23}^3 + r_{31}^2}{3}}$, which is a factor of $\frac{1}{\sqrt{2}} = 0.707...$ different from ours. In Refs. [115, 151], the hyper-radius is defined as $R \equiv \sqrt{\frac{r_{12}^2 + r_{23}^3 + r_{31}^2}{3\tilde{m}}}$, where $\tilde{m}$ is a normalization mass which can be chosen to be any value.

non-adiabatic couplings between different basis functions necessarily appear. Indeed, the hyper-radial Schrödinger equation can be obtained as

$$\frac{\hbar^2}{m}\left[-\frac{\partial^2}{\partial R^2}+\frac{\lambda_n(R)+\frac{15}{4}}{R^2}\right]f_n(R)+\sum_m\left[Q_{nm}(R)+2P_{nm}(R)\right]f_m(R)=E\,f_n(R). \tag{2.39}$$

This equation involves the following non-adiabatic coupling terms:

$$Q_{nm}(R)=-\frac{\hbar^2}{m}\left\langle\Phi_n\left|\frac{\partial^2}{\partial R^2}\right|\Phi_m\right\rangle, \tag{2.40}$$

$$P_{nm}(R)=-\frac{\hbar^2}{m}\left\langle\Phi_n\left|\frac{\partial}{\partial R}\right|\Phi_m\right\rangle. \tag{2.41}$$

Here, the brackets denote the hyper-angular average:

$$\langle\Phi_n\left|\hat{A}\right|\Phi_m\rangle=\int\sin^2\alpha_3\cos^2\alpha_3 d\alpha_3 d\Omega_{\hat{\boldsymbol{r}}_{12}}d\Omega_{\hat{\boldsymbol{\rho}}_3}\Phi_n^*(R,\alpha_3,\hat{\boldsymbol{r}}_{12},\hat{\boldsymbol{\rho}}_3)\hat{A}\Phi_m(R,\alpha_3,\hat{\boldsymbol{r}}_{12},\hat{\boldsymbol{\rho}}_3). \tag{2.42}$$

The hype-radial and hyper-angular wave functions are normalized as

$$\int_0^\infty dR\,|f_n(R)|^2=1, \tag{2.43}$$

$$\langle\Phi_n|\Phi_n\rangle=\int\sin^2\alpha_3\cos^2\alpha_3 d\alpha_3 d\Omega_{\hat{\boldsymbol{r}}_{12}}d\Omega_{\hat{\boldsymbol{\rho}}_3}\,|\Phi_n(R,\alpha_3,\hat{\boldsymbol{r}}_{12},\hat{\boldsymbol{\rho}}_3)|^2=1. \tag{2.44}$$

By solving this three-body problem, one can show the appearance of the Efimov states. In Sec. 2.2.2, we solve the three-body problem in a quantitatively reliable manner. Since the mathematical argument presented in Sec. 2.2.2 is involved and less intuitive, basic properties of the Efimov states will be explained in Sec. 2.2.1 in a simpler and more intuitive manner.

2.2.1 Qualitative description of the Efimov effect

In Fig. 2.5, energy spectra of a system of three identical bosons close to a two-body s-wave resonance are schematically illustrated. These energy spectra correspond to the universal behavior calculated with the zero-range Efimov theory. As discussed in Sec. 2.1.1, a two-body bound state exists on the positive side of the resonance with its binding energy having a universal form in Eq. (2.10). This is shown as a red solid line in Fig. 2.5, which corresponds to a particle-dimer continuum. Around the unitarity limit $1/a=0$, there appear an infinite number of three-body bound states (green curves), and $(1/a,E)=(0,0)$ corresponds to an accumulation point for the spectrum of the three-body bound states. At the unitarity, there exist an infinite number of trimers. Away from the unitarity, the number of trimers decreases and is finite. When the scattering length is varied toward the positive side, the trimers finally dissociate into a particle and a dimer, while they dissociate into three atoms on the negative scattering length side.

The discrete scale invariance of the Efimov states can be clearly seen in these schematic energy spectra. At the unitarity, trimers can be related to each other by a discrete scale transformation: the binding energies of the n-th and $(n+1)$-th three-body bound states are related to each other

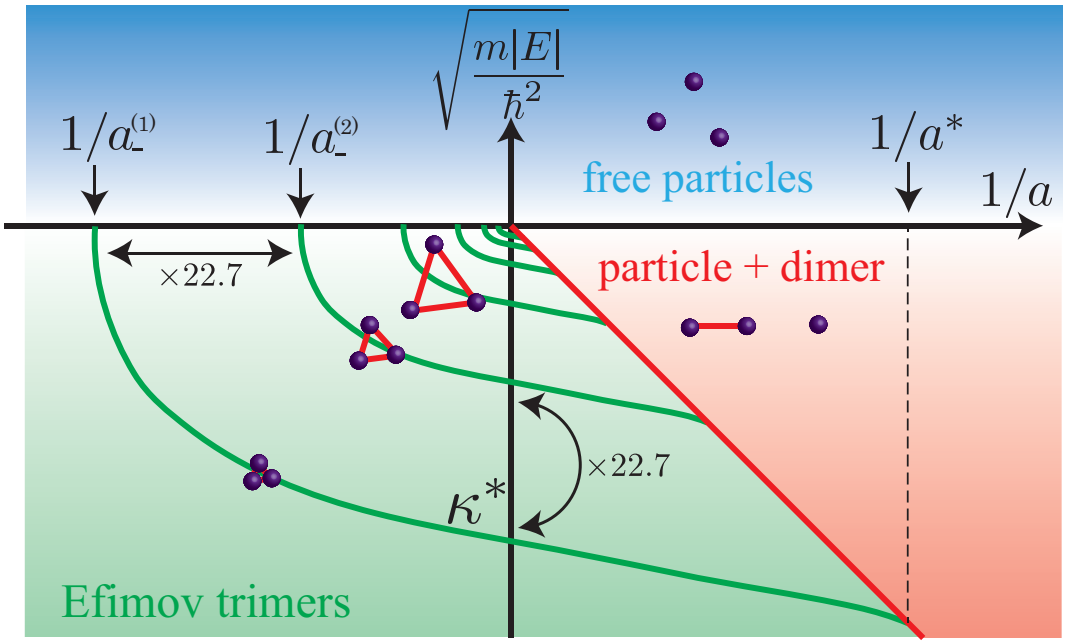

Figure 2.5: Energy spectra of a system of three identical bosons in the vicinity of a two-body resonance. Green curves show the energy spectra of Efimov trimers, and a red line is that of the universal dimer in Eq. (2.10).

as $\Psi_{n+1}(r_i) = \Psi_n(r_i e^{-\pi/s_0})$, and $E_{n+1} = e^{-2\pi/s_0} E_n$, where $e^{\pi/s_0} = 22.7\ldots$ ($s_0 = 1.0024\ldots$) is the universal scaling factor. The discrete scale invariance appears even away from the unitarity. When the radial scale transformation is performed as $1/a \to e^{n\pi/s_0}/a$, $E \to e^{2n\pi/s_0} E$ ($n = 1, 2, \ldots$), all the energy spectra of the Efimov trimers can be superimposed into a single energy spectrum. This is why the energy spectra of the Efimov trimers in Fig. 2.5 have a similar shape.

In addition to the s-wave scattering length, one additional parameter is needed to uniquely specify the energy spectra. This parameter is called the three-body parameter. There are many equivalent ways to define the three-body parameter. One way is to determine it from the binding energy of the ground-state Efimov trimer at unitarity: when the binding energy of the ground-state Efimov trimer is $E = -\frac{\hbar^2(\kappa^*)^2}{m}$, κ^* can be defined as the three-body parameter. One can alternatively define the three-body parameter as the negative scattering length at which the ground-state Efimov trimer dissociates into three particles, which is denoted as $a_-^{(1)}$ and is indicated in Fig. 2.5. The three-body parameter can also be defined as the positive scattering length at which the ground-state Efimov trimer dissociates into a particle and a dimer, which is denoted as a^* in Fig. 2.5. Since the energy spectra of the Efimov states are universal, these three quantities are related to each other in the zero-range Efimov theory as follows: $1/a^* = 14.1\kappa^*$ and $1/a_-^{(1)} = -0.64\kappa^*$ [32]. If one of these quantities is fixed, all the other can be determined. This allows us to choose any definition of the three-body parameter as long as it fixes the energy scale of the Efimov states. As will be explained in Sec. 2.2.4, $a_-^{(1)}$ can be observed experimentally by an atomic loss measurement, so this definition is often used in recent studies on the Efimov states in ultracold atoms, especially when it comes to the universality of the three-body parameter (see Sec. 2.4 and Chap. 4).

The Efimov states are often called Borromean states. A three-body bound state can exist even in the absence of a two-body bound state for $a < 0$. In this sense, it is a genuine three-body bound state in this regime. The Borromean feature can be qualitatively understood by a simple argument as follows: crudely speaking, the resonant two-body interaction means that a zero-point energy in the relative motion is exactly balanced by the attractive interaction. For three particles, on the other hand, there are two relative kinetic motions and three attractive interactions. Thus, the effect of the interactions is dominant, and three particles can be more easily bound than two particles. Such a genuine three-body binding phenomenon is similar to the "Borromean ring", and this is why the Efimov states on the negative scattering length side are often called Borromean states. With a similar argument, one can expect that $N+1$ particles are more easily bound than N particles and have a larger binding energy. This has been confirmed with recent theoretical calculations for $N \lesssim 10-40$ [77, 78, 80, 81, 82, 83, 84, 85] and in experiments for $N \leq 5$ [26, 45, 68, 88, 89].

The physical origin of the discrete scaling law is a scale-invariant behavior due to the divergence of the s-wave scattering length. Indeed, at unitarity $1/a = 0$, one can make a qualitative argument explaining the origin of the discrete scale invariance of the Efimov states as follows: at unitarity, the hyper-angular equation (2.38) does not contain any length scale. Therefore, hyper-angular eigenstates Φ_n and eigenvalues $\lambda_n(R)$ become independent of the hyper-radius: $\Phi_n(R, \alpha_3, \hat{\boldsymbol{r}}_{\mathbf{12}}, \hat{\boldsymbol{\rho}}_{\mathbf{3}}) = \Phi_0(\alpha_3, \hat{\boldsymbol{r}}_{\mathbf{12}}, \hat{\boldsymbol{\rho}}_{\mathbf{3}})$, and $\lambda(R) = \lambda_0 = \text{const.}$. The non-adiabatic couplings $Q_{nm}(R)$ and $P_{nm}(R)$ vanish, and the hyper-radial Schrödinger equation becomes

$$\frac{\hbar^2}{m}\left[-\frac{d^2}{dR^2} + \frac{\lambda_0 + \frac{15}{4}}{R^2}\right] f_0(R) = E\, f_0(R). \tag{2.45}$$

This hyper-radial Schrödinger equation can be solved analytically. Three-body bound states exist when $\lambda_0 < -4$. From the physical argument presented in the previous paragraph, one can expect that three particles can be bound more easily than the two particles and three-body bound states exist at unitarity. This suggests $\lambda_0 + 4 \equiv -s_0^2 < 0$. Thus, the hyper-radial potential in Eq. (2.45) is an inverse-square attractive potential. When such a potential appears, solutions of the Schrödinger equation show the discrete scale invariance with a scaling factor e^{π/s_0}. Indeed, a solution of the Schrondiger equation (2.45) is

$$f(R) = \sqrt{x} K_{is_0}(x), \tag{2.46}$$

where K_n is the modified Bessel function, and $x = \kappa R = \sqrt{\frac{m|E|}{\hbar^2}} R$ is the energy-scaled hyper-radius. For a small x, the modified Bessel function with an imaginary index shows the following asymptotic form:

$$K_{is_0}(x \to 0) = \sin\left[s_0 \ln\left(\frac{x}{2}\right) - \Delta\right], \qquad \Delta = \frac{1}{2}\arg\left(\frac{\Gamma(is_0+1)}{\Gamma(-is_0+1)}\right). \tag{2.47}$$

Note that this wave function is invariant under the scale transformation $x \to xe^{n\pi/s_0}$, where n is an arbitrary integer. This leads to the discrete scale invariance of the Efimov states. Indeed, by imposing the three-body boundary condition (2.24), one finds an infinite number of three-body bound states with their energy eigenvalues given as

$$|\kappa_n| = \sqrt{\frac{m|E_n|}{\hbar^2}} = \exp\left(-\frac{n\pi}{s_0}\right)\exp\left(\frac{1}{s_0}\left[\operatorname{arccot}\left(\frac{\Lambda R_0 - \frac{3}{2}}{s_0}\right) + \Delta\right]\right) \quad (n \in \mathbf{Z}). \tag{2.48}$$

These binding energies show the discrete scale invariance:

$$\frac{|E_n|}{|E_{n+1}|} = \exp\left(\frac{2\pi}{s_0}\right). \tag{2.49}$$

While the above argument is qualitative and is applicable only at unitarity, it still captures the most important features of the Efimov physics.

The log-periodic asymptotic wave function shown in Eq. (2.47) is closely related to the Thomas collapse [117]. The wave function shown in Eq. (2.47) is singular at $R = 0$. The three-body boundary condition is imposed not at $R = 0$ but at a nonzero hyper-radius $R = R_0$ to avoid this singularity. The singularity leads to a pathological result in the energy spectrum if one does not impose the three-body boundary condition at a nonzero hyper-radius. In 1935, L. H. Thomas solved the three-body problem without imposing the three-body boundary condition, and found that energies are unbound from below and the ground-state energy becomes $-\infty$ [117]. This phenomenon is known as the Thomas collapse. The Thomas collapse is closely related to the Efimov effect. Indeed, if one does not impose the three-body boundary condition, the wave function of the Efimov states (2.47) should be believed to be valid down to $R = 0$. Then, for any three-body state there always exists nodes and hence lower-lying states, since the presence of nodes suggests the existence of bound states with lower energy. Thus, the Thomas collapse is a natural consequence of the log-periodic oscillation in Eq. (2.47). Since the Efimov effect is closely related to the Thomas collapse, the Efimov effect is sometimes referred to as the Thomas-Efimov effect.

2.2.2 Quantitative description of the Efimov physics

Hyper-spherical approach

To solve Eq. (2.38), one performs the Faddeev decomposition [152]:

$$\Phi_n(R, \alpha_3, \hat{\boldsymbol{r}}_{\mathbf{12}}, \hat{\boldsymbol{\rho}}_{\mathbf{3}}) = \chi_n(R, \alpha_1, \hat{\boldsymbol{r}}_{\mathbf{23}}, \hat{\boldsymbol{\rho}}_{\mathbf{1}}) + \chi_n(R, \alpha_2, \hat{\boldsymbol{r}}_{\mathbf{31}}, \hat{\boldsymbol{\rho}}_{\mathbf{2}}) + \chi_n(R, \alpha_3, \hat{\boldsymbol{r}}_{\mathbf{12}}, \hat{\boldsymbol{\rho}}_{\mathbf{3}}). \tag{2.50}$$

Since the zero-angular-momentum channel is energetically most stable, let us restrict ourself to this channel: $\chi_n = \chi_n(R, \alpha)$. In fact, the zero-angular-momentum channel corresponds to the channel in which the Efimov effect occurs. The hyper-angular equation can then be rewritten as

$$\begin{aligned}\left[-\frac{\partial^2}{\partial\alpha_i^2} - 4\cot 2\alpha_i \frac{\partial}{\partial\alpha_i}\right]\chi_n(R, \alpha_i) \\ + \frac{mR^2}{\hbar^2} V_{\mathrm{HY}}(R\sin\alpha_i)\left[\chi_n(R, \alpha_1) + \chi_n(R, \alpha_2) + \chi_n(R, \alpha_3)\right] = \lambda_n(R)\chi_n(R, \alpha_i).\end{aligned} \tag{2.51}$$

Since the Huang-Yang pseudo-potential V_{HY} is non-zero only at $\alpha_i = 0$, this equation is equivalent to the non-interacting equation

$$\left[-\frac{\partial^2}{\partial\alpha_i^2} - 4\cot 2\alpha_i \frac{\partial}{\partial\alpha_i}\right]\chi_n(R, \alpha_i) = \lambda_n(R)\chi_n(R, \alpha_i) \tag{2.52}$$

with a boundary condition imposed at $\alpha_i = 0$. Introducing $\lambda_n(R) + 4 = -s_n^2(R)$, a solution of Eq. (2.52) is obtained as

$$\chi_n(R, \alpha) = \frac{1}{\sin 2\alpha}\left[c_1 \sinh\left(s_n(R)\alpha\right) + c_2 \cosh\left(s_n(R)\alpha\right)\right]. \tag{2.53}$$

There are two important boundary conditions. First of all, the Faddeev wave function (2.53) should not be singular at $\alpha = \frac{\pi}{2}$. This condition fixes the relative value between c_1 and c_2, giving

$$\chi_n(R,\alpha) = \frac{C}{\sin 2\alpha} \sinh\left[s_n(R)\left(\frac{\pi}{2} - \alpha\right)\right]. \tag{2.54}$$

The second boundary condition is imposed at $\alpha = 0$ such that Eq. (2.51) holds at $\alpha_i = 0$. Substituting Eq. (2.54) into Eq. (2.51) and setting $\alpha_i = 0$, the other hyper-angles become $\alpha_{j\neq i} = \dfrac{\pi}{3}$ and one obtains the following transcendental equation [2, 32]:

$$\frac{8}{\sqrt{3}} \sinh\left[s_n(R)\frac{\pi}{6}\right] - s_n(R)\cosh\left[s_n(R)\frac{\pi}{2}\right] = -\frac{R}{a}\sinh\left[s_n(R)\frac{\pi}{2}\right]. \tag{2.55}$$

When $R/a = 0$, the transcendental equation supports a single real solution $s_0 = 1.00624\ldots$ and an infinite number of pure imaginary solutions $s_1 = \pm 4.5i$, $s_2 = \pm 6.8i, \ldots$. At the unitarity, these solutions are valid for any hyper-radius. The real solution suggests an attractive inverse-square hyper-radial potential, while the pure imaginary solutions suggest repulsive inverse-square hyper-radial potentials. As argued in Sec. 2.2.1, the inverse-square attractive potential leads to the appearance of Efimov states and their discrete scale invariance. In the repulsive channel, on the other hand, no three-body bound state can exist.

Away from the unitarity, the hype-radial potential can depend non-trivially on R/a. In the Efimov channel, the inverse-square attraction appears at short distance $R/|a| \ll 1$. At larger distance $R \gtrsim |a|$, the hyper-radial potential is no longer in the inverse-square form. The breakdown of the inverse-square attraction at $R \gtrsim |a|$ suggests a decrease in the number of log-periodic oscillations in the wave function (see Eq. (2.47)). The number of three-body bound states can be estimated from the number of nodes, and one obtains an estimate of the number of three-body bound states as [1]

$$N \approx \frac{s_0}{\pi}\log\left(\kappa^*|a|\right). \tag{2.56}$$

As argued in the introduction, this estimate suggests that the scattering length must be extremely large to observe several Efimov energy levels: $\kappa^*|a| \gtrsim 500$ for two trimers, and $\kappa^*|a| \gtrsim 10^4$ for three trimers.

Some remarks on the non-adiabatic couplings are in order. At the unitarity, as argued in Sec. 2.2.1, the hyper-angular wave function is scale-invariant, and the non-adiabatic couplings vanish. On the other hand, when a is finite, the non-adiabatic couplings are non-zero, and one needs to solve the multi-channel Schrödinger equation (2.38). However, in the zero-range Efimov theory, the non-adiabatic couplings have only a minor role [32], and one can obtain the Efimov spectra shown in Fig. 2.5 even when the non-adiabatic couplings are neglected. If one wants to obtain the universal energy spectra of the Efimov states quantitatively, however, the non-adiabatic couplings should be taken into account.

The advantage of the hyper-spherical formalism is its clear physical picture. Solutions of the hyper-angular and hyper-radial equations are directly related to the three-body wave function in real space. Furthermore, the hyper-radial potential often helps us physically understand properties of a three-body system. This point will be exemplified in Chap. 4, where the physical origin of the universality of the three-body parameter is explained by using the hyper-radial potential and the

hyper-angular wave function. One disadvantage of the hyper-spherical formalism is the channel couplings. While one can manage to solve the coupled-channel Schrödinger equation numerically, it is practically easier to use an alternative approach which naturally incorporates the effect of the channel couplings. In the next few paragraphs, one of such methods is introduced.

Momentum-space approach: Skorniakov–Ter-Martirosian equation

While the hyper-spherical formalism is a real-space approach, one can alternatively solve the three-body problem in momentum space. One famous momentum-space method is use of the Skorniakov–Ter-Martirosian equation [148]. The Skorniakov–Ter-Martirosian equation is a one dimensional integral equation as follows:

$$\left[\sqrt{\frac{3}{4}p^2+\kappa^2}-\frac{1}{a}\right]a_{\mathrm{AD}}(p)=\frac{p^2}{p^2+\kappa^2}+\frac{2}{\pi}\int_0^{\Lambda}dq\frac{p}{q}\log\left(\frac{p^2+q^2+pq+\kappa^2}{p^2+q^2+pq+\kappa^2}\right)a_{\mathrm{AD}}(q), \tag{2.57}$$

where $\kappa=\sqrt{\frac{m|E|}{\hbar^2}}$ $(E<0)$ corresponds to the energy of three particles, p is the relative in-coming momentum between the particle and the dimer, and $a_{\mathrm{AD}}(q)$ is the momentum-dependent particle-dimer s-wave scattering length. The Skorniakov–Ter-Martirosian equation was originally derived to obtain the particle-dimer scattering lengths [148]. Indeed, by taking the energy at the particle-dimer threshold $E=-\frac{\hbar^2}{ma^2}$ and solving Eq. (2.57), the particle-dimer s-wave scattering length can be obtained as $a_{\mathrm{AD}}(p=0)$.

Since the three-body problem is equivalent to the particle-dimer scattering problem, one can also use Eq. (2.57) to investigate the properties of trimers. Binding energy of three-body bound states can be obtained by seeking for the value of κ at which $a_{\mathrm{AD}}(p=0)$ diverges. This can be done by finding the value of κ at which the eigenvalue of the right-hand side of Eq. (2.57) (seen as an operator acting on $a_{\mathrm{AD}}(q)$) vanishes. To avoid the Thomas collapse [117], the cut-off Λ of the momentum integration must be taken to be finite. This momentum cutoff introduces a three-body scale which fixes the energy spectra of the Efimov states. Indeed, one finds the ground-state energy of the Efimov states which is calculated with Eq. (2.57) to be $\kappa^*=0.18\Lambda$.

The Skorniakov–Ter-Martirosian equation has several advantages over the hyper-spherical equation. One advantage is its simplicity: it is a linear one-dimensional integral equation, and can be solved numerically with little difficulty. In addition, two physical quantities, the particle-dimer s-wave scattering length and the binding energy of the trimers, can be obtained from a single equation. Once a numerical code to solve the Skorniakov–Ter-Martirosian equation is prepared, these quantities can be obtained easily. Finally, the Skorniakov–Ter-Martirosian equation incorporates the channel couplings appearing in the hyper-shperical formalism.

While the above Skorniakov–Ter-Martirosian equation describes a system of three identical bosons in the $L=0$ channel, similar one-dimensional integral equations can be derived for higher angular momentum channels [148], and for three-body systems of different statistics of particles [60, 153, 154, 155, 156]. In Chap. 3, a three-body problem of two identical particles resonantly interacting in the s-wave channel with another distinguishable particle is solved numerically with the Skorniakov–Ter-Martirosian type of equation. In Sec. 3.1, I show a derivation of

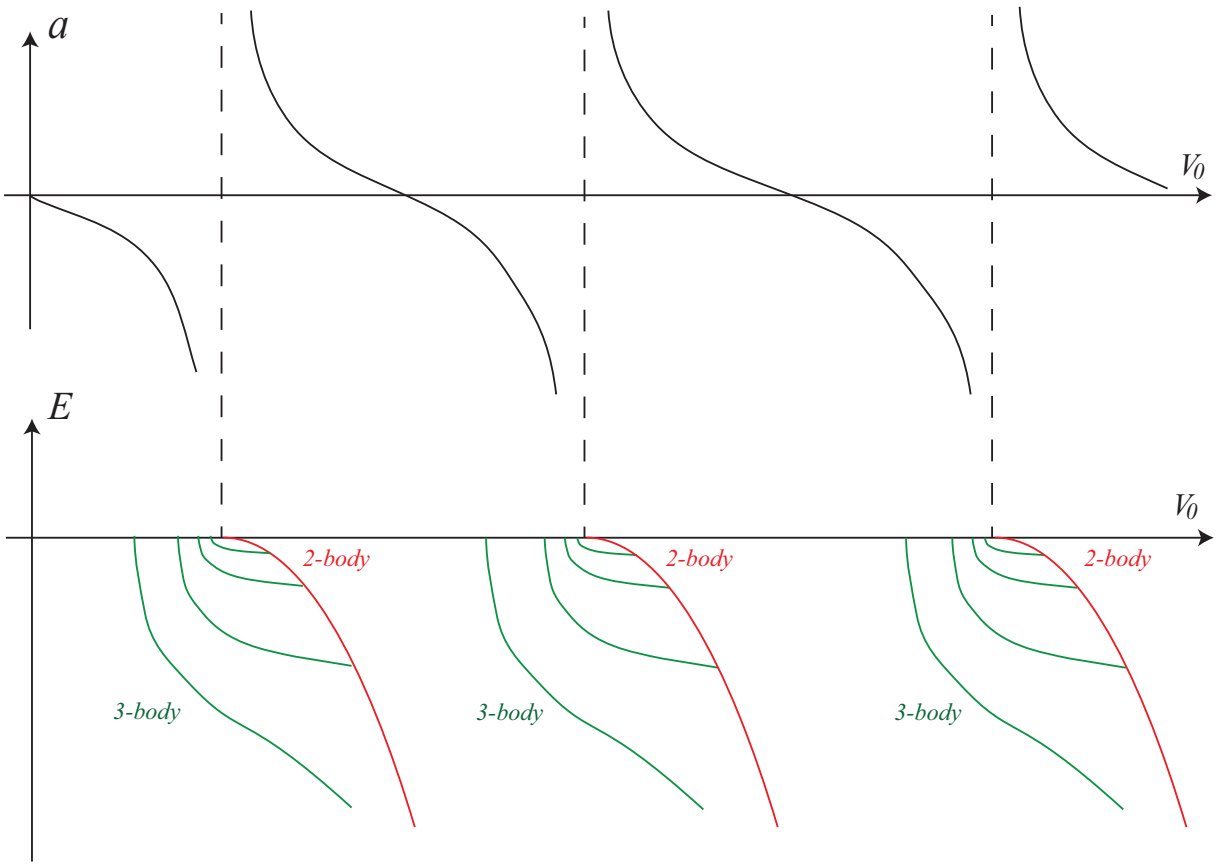

Figure 2.6: S-wave scattering length (upper panel) and energy spectra of dimers (red curves) and trimers (green ones) as a function of the strength V_0 of an attractive potential.

the Skorniakov–Ter-Martirosian type of equation for a system of two identical particles and another distinguishable particle in an arbitrary angular momentum channel and for both bosons and fermions (i.e., 2 identical bosons + 1 particle, and 2 identical fermions + 1 particle).

2.2.3 Efimov effect for finite-range potentials

In Secs. 2.2.1 and 2.2.2, the Efimov states have been introduced and discussed using the Huang-Yang pseudo-potential in (2.19) and the three-body boundary condition in (2.24). Since the pseudo-potential and the boundary condition method properly reproduce low-energy properties of any system, most properties of the Efimov states presented in Secs. 2.2.1 and 2.2.2 can also be applied to the Efimov states in a three-body system interacting via a short-range two-body potential. In Fig. 2.6, energy spectra of a three-body system interacting with an attractive two-body potential are schematically illustrated. As the two-body potential is made more attractive, successive s-wave shape resonances occur at the points where two-body bound states start to appear. In the vicinity of each of these resonances, the Efimov trimers appear, as shown by green curves. The ground-state energy of the Efimov states is of the order of the range of the interaction r_0, and the three-body parameters are $\kappa^* \approx r_0^{-1}$, $a_-^{(1)} \approx -r_0$, and $a^* \approx r_0$. For particles interacting via a potential decaying

as $-C_6/r^6$ at long distance, $\kappa^* \approx 1/r_{\rm vdW}$, $a_-^{(1)} \approx -r_{\rm vdW}$, and $a^* \approx r_{\rm vdW}$. While the three-body parameter has been known to be of the order of the range of the interaction, their precise value has been believed to be sensitive to microscopic details of two-body potentials. Recently, however, the three-body parameter has been suggested to be universally determined by the van der Waals length as $a_-^{(1)} = -8\text{-}10\ r_{\rm vdW}$. This issue will be discussed in detail in Sec. 2.4 and Chap. 4.

Some remarks on finite-range corrections are in order. The binding energy of the ground-state trimer is of the order of the range of the interaction, and thus it may not be adequate to describe it by the zero-range theory. For example, for a ^{4}He potential, the energy of the ground-state trimer disagrees significantly from what is expected from the zero-range Efimov theory [10]. Furthermore, it does not dissociate into an atom and a dimer, contrary to the behavior presented in Fig. 2.5. On the other hand, the first-excited Efimov trimer is less affected by the finite-range effect, since it is rather weakly bound thanks to a large universal scaling factor $e^{2\pi/s_0} \approx 500$. The finite-range effects of the Efimov trimers will also be studied in Chap. 3 for a three-body system of two fermions and a distinguishable particle.

While the non-adiabatic couplings have a minor role and it exactly vanishes at the unitarity limit in the zero-range theory introduced in Secs. 2.2.1 and 2.2.2, it can be relevant for finite-range potentials. In fact, even at unitarity, the non-adiabatic couplings do not vanish for finite-range potentials. As discussed in Chap. 4, the diagonal part of the non-adiabatic coupling $Q_{nn}(R)$ turns out to be crucial in explaining the physical origin of the universal three-body parameter.

2.2.4 Experiments on the Efimov physics in ultracold atoms

In ultracold atom experiments, atoms are held in a vacuum chamber by an electromagnetic potential. The number of atoms in a trap decreases gradually since atoms escape from the trap via loss processes. Among various kinds of loss processes, the Efimov states manifest themselves in a three-body recombination. The three-body recombination is a chemical reaction process in which a dimer is created via a collision of three atoms. The conservation of energy and momentum during the three-body recombination dictates that the binding energy of the dimer should be released into a kinetic energy of the atom and the dimer. The binding energy of the dimer and hence the released kinetic energy are so large that the recombination products are lost from the trap. The three-body recombination rate can be quantified by the coefficient L_3 in the rate equation

$$\frac{dn}{dt} = -L_3 n^3. \tag{2.58}$$

The recombination process is strongly affected by the Efimov states. The clearest signature of the Efimov states appear when one measures L_3 for variable s-wave scattering lengths on the negative side. In Fig. 2.7, the three-body loss rate observed by the team of the Innsbruck University is shown [27]. There is a characteristic peak in the three-body recombination coefficient. This peak corresponds to the point where the Efimov states dissociate into three atoms $a \approx a_-^{(1)}$, where the three atoms are resonantly coupled to the final state of a dimer and an atom via the Efimov states (see also Figs. 2.8 (a) and (b)). In the zero-range theory at zero temperature[§], the three-body loss

[§]Recently, the three-body loss rate has also been calculated for a finite temperature system based on the zero-range theory, and has been compared with experiments [47].

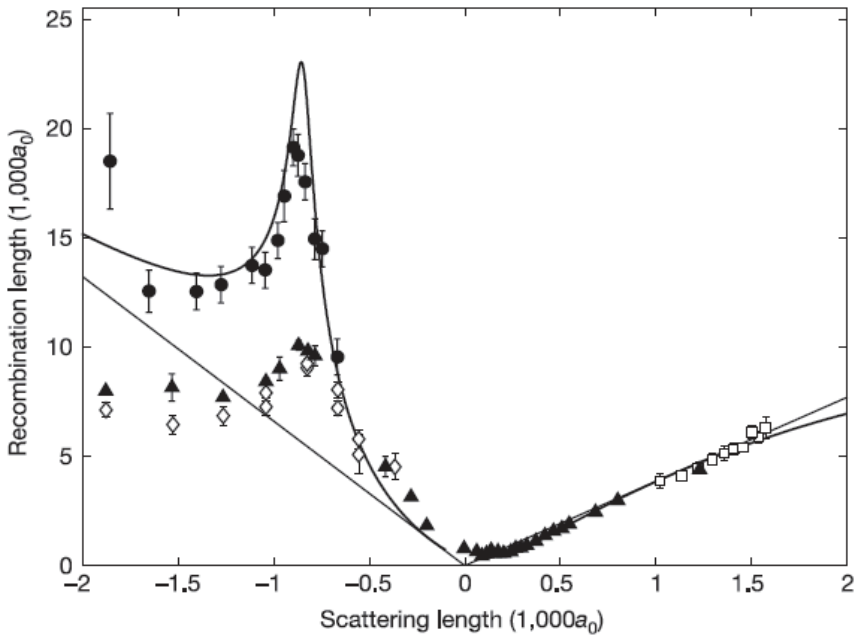

Figure 2.7: Recombination length $\rho_3 \propto L_3^{1/4}$ as a function of the s-wave scattering length [27]. The dots, filled triangles, and open diamonds correspond to data with different experimental conditions. The dots are measured at a lower temperature $T = 10$ nK, while the filled triangles and the open diamonds are measured at higher temperatures $T = 200$ nK, and 450 nK. The thick solid curve is a theoretical prediction in Eq. (2.59), and the thin lines are the $L_3 \propto a^4$ trend. [Figure adapted with permission from T. Kraemer *et al.*, Nature **440** 315 (2006). Copyright © (2006) Nature Publishing Group.]

rate coefficient is obtained as [157, 158]

$$L_3 = C\frac{\hbar a^4}{m}\frac{\sinh 2\eta_-}{s_0 \log\left(\frac{a}{a_-^{(1)}}\right) + \sinh^2\eta_-} \quad (a < 0). \tag{2.59}$$

Here, η_- is called the inelasticity parameter, which characterizes the transition probability from three atoms into a tightly bound dimer and an atom. The theoretical prediction fits fairly well with the experimental observations as shown by a solid curve in Fig. 2.7, and this is a clear signature of the appearance of the Efimov states in ultracold atoms.

The Efimov states can also be observed by the loss rate for a positive scattering length side. As shown by a black solid curve in Fig. 2.8 (b), there is no loss peak in the three-body recombination rate for a positive scattering length, but still a periodic structure characterizing the discrete scale invariance of the Efimov states appears [32]. As shown in Fig. 2.8 (c), the observed three-body recombination rate indeed shows the periodic structure. From this period, the scaling factor of the Efimov states have been estimated to be 25 ± 4, which is consistent with the universal scaling factor 22.7 of the Efimov states. While there is no clear peak in the three-body recombination rate for $a > 0$, a resonantly enhanced peak appears in the atom-dimer relaxation rate. In the atom-dimer relaxation process, a collision of weakly bound dimer and an atom ends up with a tightly bound

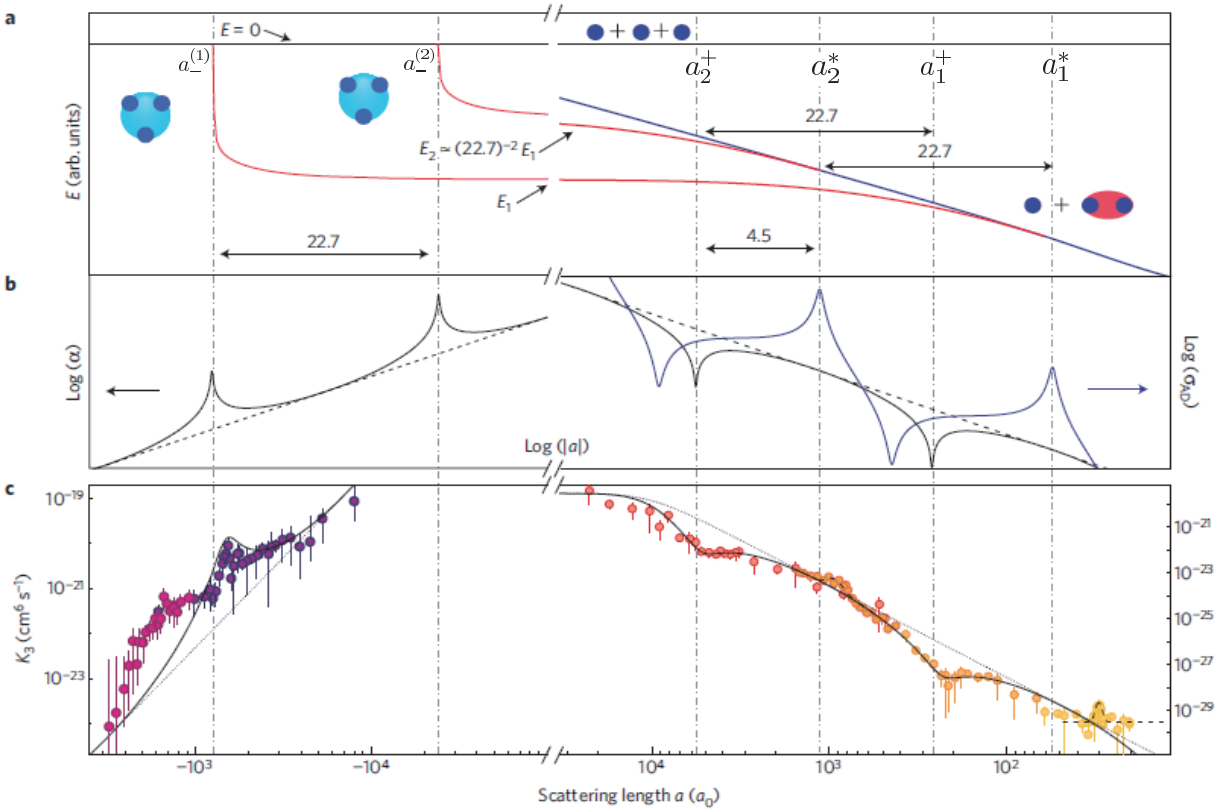

Figure 2.8: a. Schematic illustration of the energy spectrum of the Efimov states (red curve) and the dimer (blue line). b. Theoretically predicted three-body recombination rate (black curve) and the atom-dimer relaxation rate (blue curve) [32, 157]. The dotted line is the a^4 line. c. Experimentally observed three-body recombination rates. Solid curves are theoretical fits based on the zero-range Efimov theory. In a subsequent paper [66], it has been pointed out that the three-body loss peak at $a \approx -1500a_0$ is a misidentified one. The three-body loss peak corresponds to the adjacent peak located at $a \approx -600a_0$. [Figure adapted with permission from M. Zaccanti *et al.*, Nature Physics **5** 586 (2009) [28]. Copyright © (2009) Nature Publishing Group.]

dimer and an atom, which are lost from the trap. As shown by a blue solid curve in Fig. 2.8 (b), the atom-dimer relaxation rate is enhanced close to the point where the Efimov states dissociate into an atom and a dimer. This maximum in the atom-dimer relaxation rate has also been observed experimentally [159].

While the three-body recombination rate and the atom-dimer relaxation rate can lead to signatures of the Efimov states and their measurements have been quite useful for studying the Efimov states, they are not the direct evidence of the Efimov states. Recently, a direct association of the Efimov states has been realized [51, 52, 160]. In Refs. [51, 52], a gas of atoms and weakly bound dimers is initially prepared, and a microwave with variable frequency is applied. The atoms and dimers are then converted into Efimov trimers. This radio-frequency association technique has successfully been used to associate and observe the Efimov trimers in ultracold ^{6}Li atoms [51, 52]. In Refs. [160], the radio-frequency association has been applied to a gas without dimers, and Efimov

states have been created from the three-atom continuum. The radio-frequency association technique offers a direct access to the Efimov trimers, and one can measure the binding energy of the Efimov trimers.

2.3 Three-body physics for fermions

In this section, a fermionic three-body problem is reviewed. When the three particles are identical fermions with no internal degree of freedom (i.e., spinless fermions, or spin-polarized fermions), they cannot interact in the *s*-wave channel and behave as free particles at low energy. The simplest case in which non-trivial effect of the Fermi statistics on the Efimov physics can be studied is a three-body system of two identical fermions[§] and one distinguishable particle, where the fermions are resonantly interacting with the other particle in the *s*-wave channel. Such a system is often called a "2+1 system." I review this 2+1 system for a variable mass ratio. The mass ratio between the two fermions and the other particle is an important parameter which determines the presence or absence of a three-body bound state. In the previous studies [38, 59, 132], two types of three-body bound states have been demonstrated to appear in this system, the Efimov states [38, 132] and the Kartavtsev-Malykh states [59]. I describe these two trimers and discuss the role of the mass ratio in this section.

While the three-body problem can be solved exactly with the hyper-spherical method [38, 59], I present an analysis using the Born-Oppenheimer method in this section. It is far simpler and more intuitive than exactly solving the three-body problem. As we will see, three-body bound states appear when the fermions' mass is much larger than that of the other particle. Therefore, the Born-Oppenheimer method is a good approximation, and reproduces the hyper-spherical results fairly well.

2.3.1 Efimov effect and the critical mass ratio at unitarity

For resonantly interacting three identical bosons, an inverse-square attraction appears in the hyper-radial Schrödinger equation, and the Efimov states appear. For a fermionic three-body system, an essential difference from the bosonic case is that in addition to the Efimov attraction, a centrifugal repulsion appears due to the antisymmetrization between the identical fermions. To see this point, let us assume that two fermions is much heavier than the other particle, so that the Born-Oppenheimer approximation can be used [38]. In the Born-Oppenheimer approximation, we first solve the Schrödinger equation of the light particle (mass m_L) and obtain an energy eigenvalue when the positions of the heavy fermions (mass m_H) are fixed at $\boldsymbol{x_1}$ and $\boldsymbol{x_2}$. The Schrödinger equation of the light particle is ($r \equiv |\boldsymbol{x_1} - \boldsymbol{x_2}|$)

$$-\frac{\hbar^2 \nabla_{\boldsymbol{y}}^2}{2m_L}\phi(\boldsymbol{y}) = E(r)\phi(\boldsymbol{y}) \tag{2.60}$$

[§] Again, I assume throughout this thesis that fermions do not have any internal degree of freedom, i.e., spin-polarized fermions.

with the Bethe-Peierls boundary conditions at $|\boldsymbol{y}-\boldsymbol{x_1}| \to +0$ and $|\boldsymbol{y}-\boldsymbol{x_2}| \to +0$. This equation can be solved analytically, giving

$$\phi(\boldsymbol{y}) = \frac{\exp\left(-\kappa(r)\frac{|\boldsymbol{y}-\boldsymbol{x_1}|}{r}\right)}{|\boldsymbol{y}-\boldsymbol{x_1}|} + \frac{\exp\left(-\kappa(r)\frac{|\boldsymbol{y}-\boldsymbol{x_2}|}{r}\right)}{|\boldsymbol{y}-\boldsymbol{x_2}|}, \tag{2.61}$$

where $\kappa(r)$ is determined from the Bethe-Peierls boundary condition as

$$\kappa(r) - e^{-\kappa(r)} = \frac{r}{a}. \tag{2.62}$$

A solution of this transcendental equation is

$$\kappa(r) = \frac{r}{a} + W(e^{-r/a}), \tag{2.63}$$

where W is the Lambert W function. The energy eigenvalue of the light particle $E(r)$ is then obtained as

$$E(r) = -\frac{\hbar^2\kappa(r)^2}{2m_L r^2}. \tag{2.64}$$

This appears as an effective interaction in the Schrödinger equation of the relative motion between the fermions

$$\left[-\frac{\hbar^2\nabla_r^2}{m_F} + E(r)\right]\psi(r) = E\psi(r). \tag{2.65}$$

Since the wave function must be antisymmetrized, the relative angular momentum between the fermions must be an odd integer, so that a centrifugal repulsion appears. At the unitarity, the effective interaction between the heavy particles becomes

$$V(r) = \frac{\hbar^2 L(L+1)}{m_F r^2} - \frac{\hbar^2\Omega^2}{2m_L r^2}, \tag{2.66}$$

where $\Omega = W(1) = 0.5671\ldots$. The first term is the centrifugal repulsion, and the second term is the attraction induced by the light particle, i.e., the Efimov attraction. These two contributions compete, and their strength varies as the mass ratio is changed. When the mass of the fermions is much larger than that of the other particle, the Efimov attraction dominates the centrifugal repulsion, and the Efimov states appear. On the contrary, when $m_F \lesssim m_L$, the potential is repulsive and there is no three-body bound state. In the most stable $L = 1$ channel, the critical mass ratio which delimits these two behaviors is

$$\left(\frac{m_F}{m_L}\right)_E = \frac{2}{\Omega^2}\left[L(L+1) + \frac{1}{4}\right] = 13.992\ldots. \tag{2.67}$$

While the Born-Oppenheimer method has been used in the above analysis, the three-body Schrödinger equation can be solved analytically with the hyper-spherical method. One finds no qualitative difference from the Born-Oppenheimer analysis. The exact value of the Efimov's critical mass ratio is obtained as $(m_F/m_L)_E = 13.606\ldots$ [132], which is in excellent agreement with the Born-Oppenheimer result (see Table. 2.1).

Table 2.1: Critical mass ratio at which the Efimov states and the first and second Kartavtsev-Malykh states appear. The mass ratio calculated with the Born-Oppenheimer approximation and the exact hyper-spherical calculation [59, 132] are shown.

	Born-Oppenheimer	Exact
1st Kartavtsev-Malykh state	9.62	8.172
2nd Kartavtsev-Malykh state	13.74	12.917
Efimov states	13.992	13.606

2.3.2 Kartavtsev-Malykh trimer

Away from unitarity $1/a \neq 0$, the effective interaction between the heavy particles is

$$V(r) = \frac{2\hbar^2}{m_F r^2} - \frac{\hbar^2 \kappa^2(r)}{2m_L r^2} \tag{2.68}$$

In Fig. 2.9, we show $V(r)$ for various mass ratios $\alpha = m_F/m_L$. For a small mass ratio, the potential is repulsive, so that no trimer can exist. For a sufficiently large mass ratio, especially for $m_F/m_L > 13.992\ldots$, the potential is strongly attractive, so that trimers can be formed. For an intermediate mass ratio $10 \lesssim m_H/m_L < (m_F/m_L)_{\mathrm{E}}$, an attractive force appears at a distance $r \sim a$ for a positive scattering length while the short-range part is a repulsive inverse-square potential. A potential well-like structure appears, and this supports one bound state when $m_H/m_L > 9.62\ldots$, and two bound states when $m_H/m_L > 13.74\ldots$. When one uses the hyper-spherical formalism and solves the three-body problem exactly, one can show that these three-body bound states appear at mass ratios $(m_H/m_L)^{(1)}_{\mathrm{KM}} = 8.172\ldots$ and $(m_H/m_L)^{(2)}_{\mathrm{KM}} = 12.917\ldots$ [59], which agree with the Born-Oppenheimer results fairly well (see Table. 2.1).

These three-body bound states below the Efimov's critical mass ratio were found in 2007 by Kartavtsev and Malykh [59], and they are called the Kartavtsev-Malykh states. The Kartavtsev-Malykh states have distinct properties from the Efimov states. In Table. 2.2, basic properties of the Kartavtsev-Malykh states and the Efimov states are compared. First of all, the number of the bound states are different. There are an infinite number of bound states for the Efimov states, while there are only two Kartavtsev-Malykh states. Universal properties of these states also show marked contrast to those of the Efimov states. While the Efimov states depend on the two parameters, the s-wave scattering length and the three-body parameter, the there-body parameter is irrelevant for the Kartavtsev-Malykh states. This is because there exists a strong repulsive potential at short distance when $m_H/m_L < (m_F/m_L)_{\mathrm{E}}$, and it prohibits three particles from coming close. As a consequence, the Kartavtsev-Malykh states have a continuous scale invariance: if the scattering length is scaled as $a \to \beta a$, the binding energy E_n $(n = 1, 2)$ and the mean radius $\langle r \rangle$ are scaled as $E \to \beta^{-2} E$, $\langle r \rangle \to \beta \langle r \rangle$ for an arbitrary continuous value of β.

Furthermore, the stability of the Efimov trimers and that of the Kartavtsev-Malykh trimers differs significantly. The Efimov trimers are known to be unstable against a three-body loss [27]: the trimer dissociate into a tightly bound dimer and an atom, thereby releasing its binding energy into the kinetic energy and are lost from the trap. On the contrary, such a decay channel for

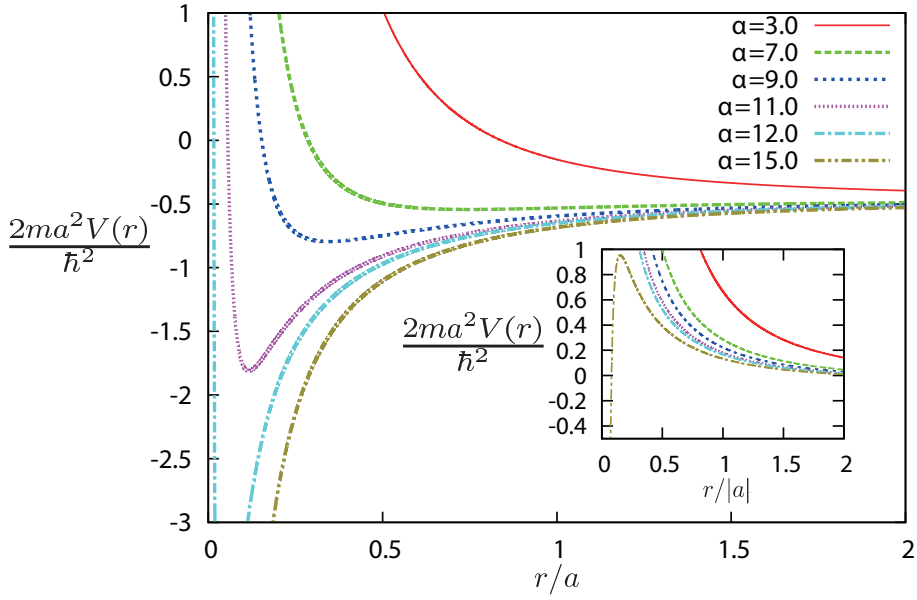

Figure 2.9: $V(r)$ in Eq. (2.68) for a positive scattering length (main figure), and a negative scattering length (inset) for several mass ratios $\alpha = m_F/m_L$.

the Kartavtsev-Malykh trimers is suppressed, since there is a large potential barrier at short distance [60]. The wave function of the Kartavtsev-Malykh states attenuates at short distance, so that there is little overlap with the wave function of the tightly bound dimer.

As a final remark, the allowed value of the scattering length is different between the Efimov states and Kartavtsev-Malykh states. The Efimov states can exist for a negative value of the scattering length. Since the two-body bound state does not exist for $a < 0$, they are sometimes termed as Borromean states: three-body bound states in the absence of a two-body bound state. This can be seen by observing the potential for $m_F/m_L > (m_F/m_L)_{\mathrm{E}}$. As shown in the inset, for a negative scattering length, the potential has an inverse-square attraction for $r/|a| \ll 1$ when the mass ratio exceeds the Efimov's critical mass ratio. Thus, the three atoms are subject to a strong enough short-range attraction when $|a|$ is large, and they can form trimers. When the mass ratio is smaller than the Efimov's critical mass ratio, on the other hand, the potential for a negative scattering length is repulsive for any r, so that no trimer can be formed. Thus, the Kartavtsev-Malykh states are not Borromean states.

In one dimension and two dimensions, three-body bound states similar to the Kartavtsev-Malykh states have been found recently [161, 162]. The three-body bound states of the Kartavtsev-Malykh character exist for $m_F/m_L > 1$ [161] and $m_F/m_L > 3.3$ [162] in one and two dimensions, respectively. These are also distinct from the Efimov states, since the Efimov states do not appear in one and two spatial dimensions [32, 115, 163]. Indeed, by generalizing the hyper-spherical formalism to a continuous number of spatial dimensions and solving the hyper-angular equation in d dimensions, one can show that the Efimov states appear for a range of dimensions $2.3 < d < 3.8$ [32, 115].

Table 2.2: Properties of the Kartavtsev-Malykh trimers and Efimov trimers are compared.

	Efimov trimers	Kartavtsev-Malykh trimers
Number of bound states	Infinite	2
Scaling property	Discrete Scaling	Continuous Scaling
Relevant parameter	S-wave scattering length Three-body parameter	S-wave scattering length
Stability	Unstable	Stable
Trimers for $a < 0$	Possible	Impossible
Other dimensions	Impossible	Possible

2.4 Universal three-body parameter

Recently, the three-body parameter of the Efimov states has attracted great theoretical and experimental interest. In Sec. 2.4.1, a short history on this issue is sketched out, followed by a review of recent developments in experimental studies of the three-body parameter. In Sec. 2.4.2, all the theoretical studies on the universal three-body parameter are listed up to the best of the author's knowledge, and they are reviewed briefly. Note that the results presented in this section is quite new, most of them reported during 2011-2013. Therefore, both experimental and theoretical results presented in this section may be subject to some revisions with updated results in the near future.

2.4.1 History and recent experiments in ultracold atoms

The three-body parameter fixes the energy scale of the Efimov states, and it is an important parameter in the Efimov physics. In the zero-range Efimov theory, the three-body parameter is introduced as a parameter characterizing a short-range three-body phase, and its value cannot be determined by itself. In fact, in ultracold atom experiments shown in Figs. 2.7 and 2.8, the three-body parameter and the inelasticity parameter are treated as fitting parameters to compare the zero-range Efimov theory with the experimental data. To determine the value of the three-body parameter for a given system, one needs to take into account a finite-range part of inter-particle interactions, and perform a three-body calculation numerically. In some literature [71], the three-body problem has been solved theoretically for some finite-range potentials, and it has been claimed that the three-body parameter is rather sensitive to details of potentials. In the language of ultracold atoms, this means that the three-body parameter is rather sensitive to atomic species, hyperfine states, and which Feshbach resonances one chooses. While the long-range part of the inter-atomic interaction share the same van der Waals form $-C_6/r^6$, the short-range part depends on electronic configurations of the atoms, and it is strongly dependent on atomic species, and hyperfine states. This non-universal short-range part of the inter-atomic interaction has been believed to alter the value of the three-body parameter significantly, rendering it non-universal. In addition to the short-range part of the two-body interaction, it has been suggested that an atomic species dependent three-body

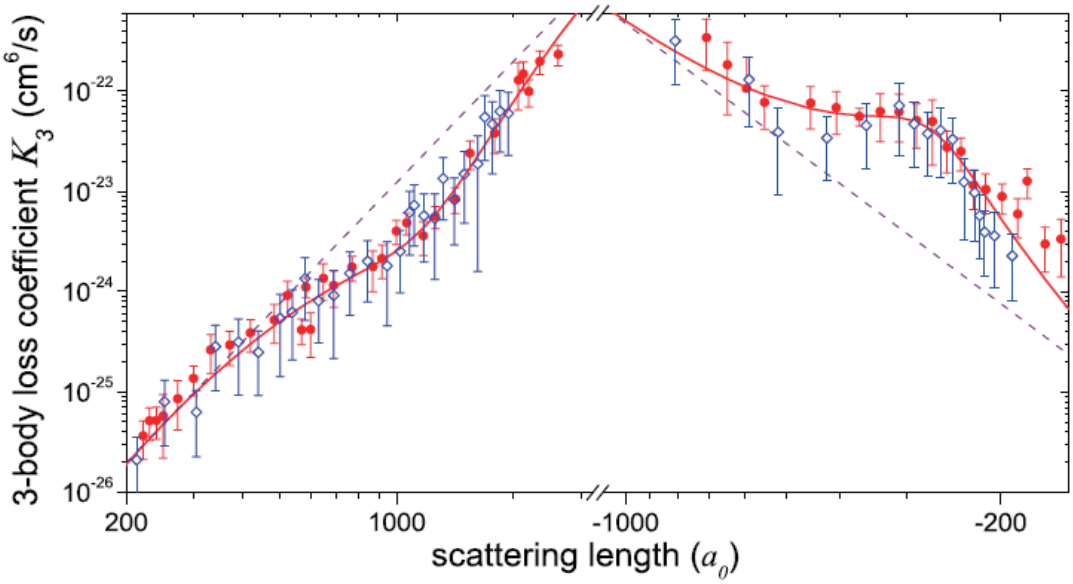

Figure 2.10: Three-body loss rate coefficient $K_3 \propto L_3$ observed experimentally for two different hyperfine states are show by red solid circles and blue open diamonds [46]. The solid curves are the zero-range Efimov theory fitted to experimental data. The dotted line shows the a^4 trend. [Figure reprinted with permission from N. Gross *et al.*, Phys. Rev. Lett. **105**, 103203 (2010). Copyright © (2010) by The American Physical Society.]

force present at short-range [164] can also significantly affect the three-body parameter, rendering the three-body parameter non-universal [71].

The first experiment suggesting the universality of the three-body parameter was performed by the team of Bar-Ilan University in 2010 [46]. In this experiment, a three-body loss was observed in the vicinity of a Feshbach resonance for two different hyperfine states. As shown in Fig. 2.10, three-body loss rates for two different hyperfine states agree excellently. This suggests that the three-body parameter and the inelasticity parameter are almost the same for the two hyperfine states. With hindsight, this experiment was the first to find the universality of the three-body parameter. However, at that time it was not clear whether the agreement is a mere coincidence or not. The universality of the three-body parameter was clearly realized in the community by a subsequent paper published in 2011 [68]. In this experiment, the team of the Innsbruck University has measured three-body loss rates for four different Feshbach resonances for ^{133}Cs atoms. Surprisingly, contrary to the conventional wisdom [71], the three-body parameters for the four different Feshbach resonances agree with each other. Furthermore, when these three-body parameters for ^{133}Cs atoms are compared with those observed for ^{7}Li atoms [44, 45, 46], they also agree when the three-body parameter is normalized by the van der Waals length $a_{-}^{(1)}/r_{\mathrm{vdW}}$ =-8-10.

These observations have surprised researchers working on the Efimov physics in ultracold atoms, and the three-body parameter for other atoms has subsequently been measured by a number of groups. Until now, the three-body parameter has been observed for four bosonic alkalis: ^{7}Li [26, 44, 45, 46, 47, 65], ^{39}K [28, 66], ^{85}Rb [67] and ^{133}Cs [68, 69]. Three-body parameters

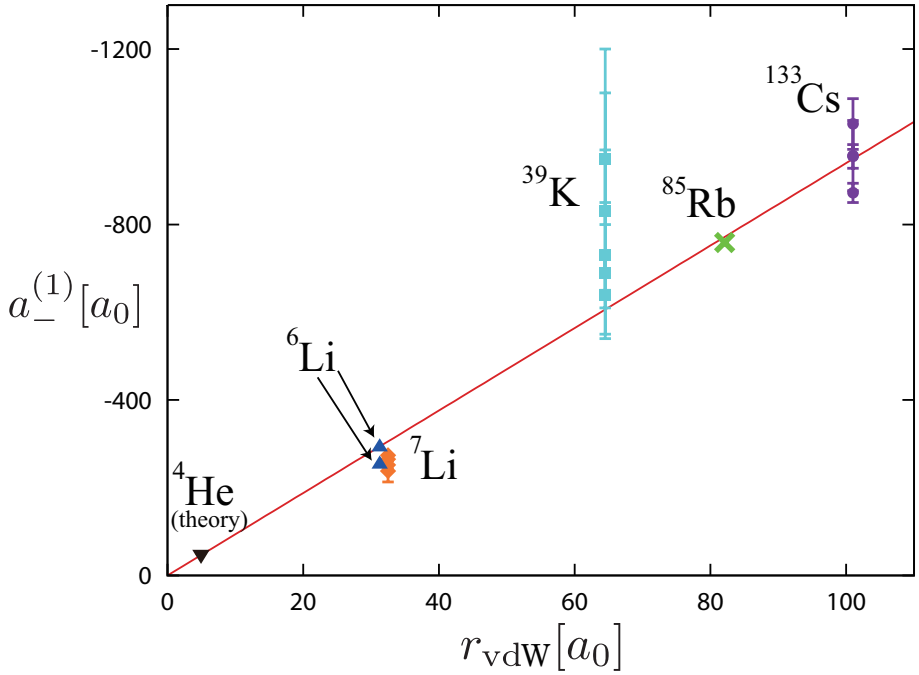

Figure 2.11: The scattering lengths at the triatomic resonance threshold, $a_-^{(1)}$, for various atomic species. The plotted data are taken from the following references (see Table. 2.4 for more detail): ^{6}Li [50, 53], ^{7}Li [26, 47, 65], ^{39}K [66], ^{85}Rb [67] and ^{133}Cs [68]. We also show the result of a theoretical calculation for a realistic ^{4}He potential [10] (see Sec. 2.4.2). The red solid line is the best fit to the data $a_-^{(1)} = -9.4 \pm 0.2 r_{\rm vdW}$.

observed so far are shown in Fig. 2.11 and Table. 2.4. Except for some data on ^{39}K atoms which will be discussed later, the three-body parameter seems to be universally determined by the van der Waals length $a_-^{(1)} = -8\text{-}10\ r_{\rm vdW}$.

The Efimov states have also been realized for a three-component Fermi system of ^{6}Li atoms [48, 49, 50, 51, 52, 53, 54]. The Efimov physics of three identical bosons and that of fermions in three different internal states are mostly the same. The only difference is that there are three inter-particle scattering lengths a_{12}, a_{23}, and a_{13}. For ^{6}Li atoms, these three scattering lengths can be simultaneously made resonant. In Ref. [50], a three-body parameter has been estimated for ^{6}Li atoms based on the assumption that the loss rate behaves in the same manner as that of identical boson in Eq. (2.59) with the mean scattering length

$$a_m^4 = \frac{1}{3}(a_{12}^2 a_{13}^2 + a_{12}^2 a_{23}^2 + a_{13}^2 a_{23}^2). \tag{2.69}$$

The three-body parameter estimated this way has been found to be $a_-^{(1)}/r_{\rm vdW} = -9.3$, which agrees excellently with the bosonic case. In Ref. [53], the three-body threshold for the first-excited Efimov trimer has been observed for ^{6}Li atoms. By using the above method and multiplying the universal scale factor, one obtains $a_-^{(1)}/r_{\rm vdW} = -8.1$. These data are also shown in Fig. 2.11.

Recently, the three-body loss rate for excited-state ^{4}He atoms has been measured [70]. While the Feshbach resonance cannot be used for the excited ^{4}He atoms, a natural scattering length be-

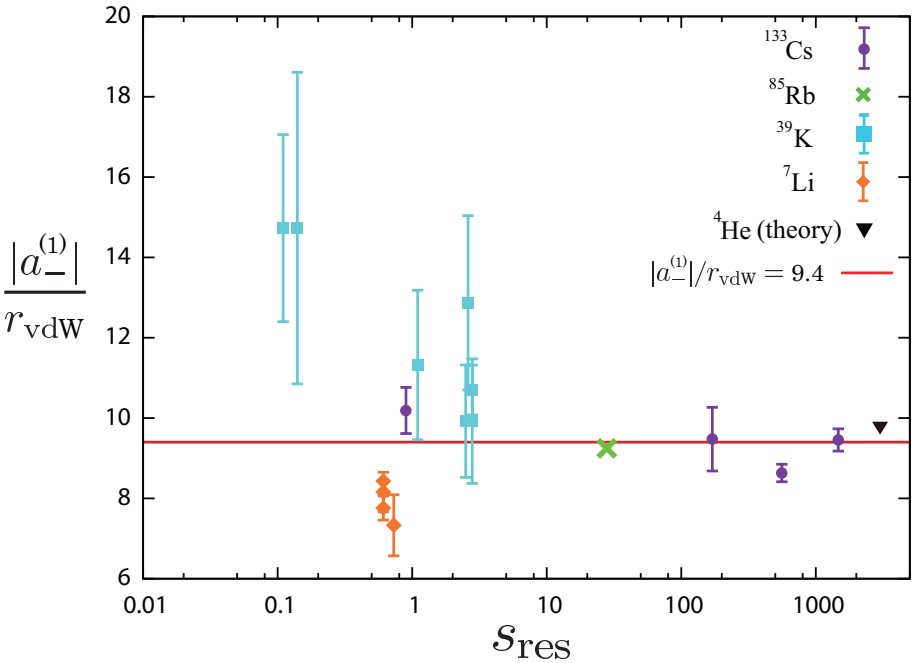

Figure 2.12: $|a_-^{(1)}|/r_{\rm vdW}$ as a function of the resonance width parameter $s_{\rm res}$ for various atomic species. The plotted data are the same as those in Fig. 2.11. The theoretical calculation for a realistic ^{4}He potential [10] corresponds to the broad Feshbach resonance limit $s_{\rm res} \to +\infty$. The red solid curve corresponds to $a_-^{(1)} = -9.4 \pm 0.2 r_{\rm vdW}$. In this figure, the data of ^{6}Li atoms is not plotted since it is not clear how one can define the mean resonance width.

tween them is resonantly large. The three-body parameter extracted from the loss rate measurement has been found to be consistent with that of alkalis, although this data is not shown in Fig. 2.11.

Two remarks are in order for experimental data not shown in Fig. 2.11. First of all, for ^{133}Cs atoms, a three-body parameter of the Feshbach resonance at $B = 818.89$ G is not shown, since it has been reported that it may suffer from a large systematic error [69]. Secondly, ^{39}K data reported in Ref. [28] is not plotted here. In Fig. 2.8, the experimental data reported in Ref. [28] is shown. For a negative scattering length, two peaks are visible. In Ref. [28], the peaks at $a = -1500a_0$ and $a = -600a_0$ are identified as three-body and four-body loss peaks, respectively. This identification results in $a_-^{(1)}/r_{\rm vdW} = -23$, in total disagreement with the universal behavior. In a subsequent paper by the same team [66], these identifications have been revised. In Ref. [66], they assigned the $a = -600a_0$ peak as the three-body loss peak, while the peak at $a = -1500a_0$ is not present in their new observation. In Fig. 2.11, the older data reported in Ref. [28] is not shown, and only the recent data reported in Ref. [66] is shown.

For a detailed list of the three-body parameters and the inelasticity parameters observed in experiments, the readers are referred to Table. 2.4 placed in the last page of this chapter.

Table 2.3: Experimental observations of the three-atom resonance $a_- < 0$ and the atom-dimer resonance $a^* > 0$ of the hetero-nuclear Efimov states of 2 identical bosons + 1 particle (A-A-B), together with values of some fundamental parameters. The van der Waals lengths for a homo-nuclear K-Rb atoms $r_{\rm vdW}^{AA}$ is taken from Ref. [165], and that for a homo-nuclear K-K atoms and Rb-Rb atoms $r_{\rm vdW}^{AB}$ are taken from Refs. [166] and [167], respectively. The background homo-nuclear s-wave scattering lengths $a_{\rm bg}^{AA}$ for ^{41}K atoms and ^{87}Rb atoms are taken from Refs. [168] and [24, 168], respectively. The dimensionless Feshbach resonance width $s_{\rm res}$ is taken from Ref. [24].

Atoms	m_A/m_B	$r_{\rm vdW}^{AA}(a_0)$	$r_{\rm vdW}^{AB}(a_0)$	$a_{\rm bg}^{AA}(a_0)$	B_0(G)	$s_{\rm res}$	$a_-^{(1)}(a_0)$	$a^*(a_0)$
^{41}K^{41}K^{87}Rb [55]	0.4713	65.30(7)	72.22(1)	62	38.4	25.8	-22(+4,-6)×10^3	-
^{87}Rb^{87}Rb^{41}K [55]	2.1217	82.59(3)	72.22(1)	100	38.4	25.8	-246(14)	-
^{87}Rb^{87}Rb^{40}K [169]	2.1747	82.59(3)	71.92(1)	100	546.62	1.96	<-3000 or >-200	230(10)

Three-body parameter for a narrow Feshbach resonance

Until 2012, all the three-body parameters for three identical bosons observed in ultracold atoms had been consistent with the universal behavior $a_-^{(1)} = -8\text{-}10\ r_{\rm vdW}$, except for those which have turned out to be unreliable (see the previous paragraph). However, in 2013, a team of LENS has observed a possible deviation from the universal behavior [66]. As one can see in Fig. 2.12, for most atoms, three-body parameters have been observed so far for broad Feshbach resonances $s_{\rm res} \gtrsim 1$. The team of LENS has observed the three-body parameters of ^{39}K atoms for various Feshbach resonances, including rather narrow Feshbach resonances of $s_{\rm res} \sim 0.1$. The results are shown as solid rectangles in Fig. 2.12. For broad Feshbach resonances, the observed three-body parameters are consistent with the universal behavior. However, for narrow Feshbach resonances, they have found that the three-body parameters get significantly larger than the universal value for ^{39}K atoms. On the other hand, the three-body parameters for ^{7}Li atoms observed at the Rice University [26, 45] and the Bar-Ilan University [44, 46, 65] show the opposite trend: it gets slightly smaller than the universal behavior. Because of such an apparent contradiction and of shortage of data, it is not yet clear whether the three-body parameter should be universal or not for narrow Feshbach resonances. As will be argued in the next section, it is also not yet understood theoretically, and requires further studies.

For a detailed list of the three-body parameters and the inelasticity parameters observed in experiments, the readers are referred to Table. 2.4 placed in the last page of this chapter.

Hetero-nuclear systems

As explained in the introduction, the Efimov states can appear for a three-body system of two identical atoms resonantly interacting with another atom whose mass is different from that of the others. Such a system is often called a hetero-nuclear system, since their atomic nuclei are different. Until now, the Efimov physics in hetero-nuclear systems have been investigated experimentally only for a mixture of Rb atoms and K atoms by two groups: LENS in 2009 [55] and JILA in 2013 [169]. In Table. 2.3, three-body parameters $a_-^{(1)}$ and atom-dimer resonant points a^* reported in these studies are summarized, together with some basic properties of these systems.

As shown in the table, the three-body parameter a_- has been reported to be observed only for two cases, ^{41}K^{41}K^{87}Rb and ^{87}Rb^{87}Rb^{41}K [55], while the atom-dimer resonance has been reported to be observed for ^{87}Rb^{87}Rb^{40}K [169]. It should be noted that the two studies report rather distinct behavior in the three-body loss rate for ^{87}Rb^{87}Rb^{41}K and ^{87}Rb^{87}Rb^{40}K: while a clear peak in the loss rate has been visible at $a = -246(14)$ in the former case [55], no peak has appeared in the region $-3000 < a < -200$ in the latter case [169]. The experimental data however is not yet sufficient, and we cannot judge yet whether the three-body parameter is universal or not for the hetero-nuclear systems.

Even if the three-body parameter is universal, it may show a different universal behavior from that of three identical bosons. In the case of three identical bosons, a long-range part of inter-atomic interactions is characterized by a single parameter r_{vdW}, so once one assumes that the three-body parameter is universally determined by this long-range part, one easily obtains the universal relation $a_-^{(1)} \approx r_{\mathrm{vdW}}$. On the other hand, there are two van der Waals lengths for the hetero-nuclear system of two A atoms and one B atom, namely a homo-nuclear van der Waals length r_{vdW}^{AA} and a hetero-nuclear van der Waals length r_{vdW}^{AB}. Even when the three-body parameter has turned out to be universal, it may non-trivially depend on these two van der Waals lengths. Furthermore, a homo-nuclear scattering length a_{bg}^{AA} remains of the order of the van der Waals length in the hetero-nuclear Efimov states, which may also affect the three-body parameter.

Note that for the atomic species and Feshbach resonances reported in Table. 2.3, the homo-nuclear scattering length a_{bg}^{AA} does not vary significantly from the background homo-nuclear scattering lengths and to a good approximation we can equate these two quantities $a^{AA} \approx a_{\mathrm{bg}}^{AA}$. This can be checked from Fig. 14.2 of Ref. [170]. For Rb atoms, this can also be checked in Table IV of Ref. [24].

2.4.2 Theoretical developments

In this section, theoretical studies on the universal three-body parameter is reviewed. To the best of the author's knowledge, all the theoretical studies on this issue until now have been listed up.

3 identical bosons for broad Feshbach resonances

Shortly after the universality of the three-body parameter has been pointed out in Ref. [68], a three-body problem of ^{4}He atoms has been numerically solved using a realistic ^{4}He potential [10]. A realistic ^{4}He potential, LM2M2 potential [12], is varied by a scaling factor as $V(r) \to \lambda V(r)$ to virtually change the s-wave scattering length of ^{4}He atoms. Then, the three-body parameter has been found to be $a_-^{(1)}/r_{\mathrm{vdW}} = -9.42$, which is in excellent agreement with the universal value observed in ultracold atom experiments. In Fig. 2.11, this theoretical value is shown as a black down-pointing triangle. Since a three-body calculation with a single-channel potential corresponds to the limit $s_{\mathrm{res}} \to +\infty$, it is shown in Fig. 2.12 in the right-most position as a black down-pointing triangle.

In Ref. [72], C. Chin attempts to explain the physical origin of the universal three-body parameter. He argues that a strongly attractive three-body potential between the atoms induces quantum

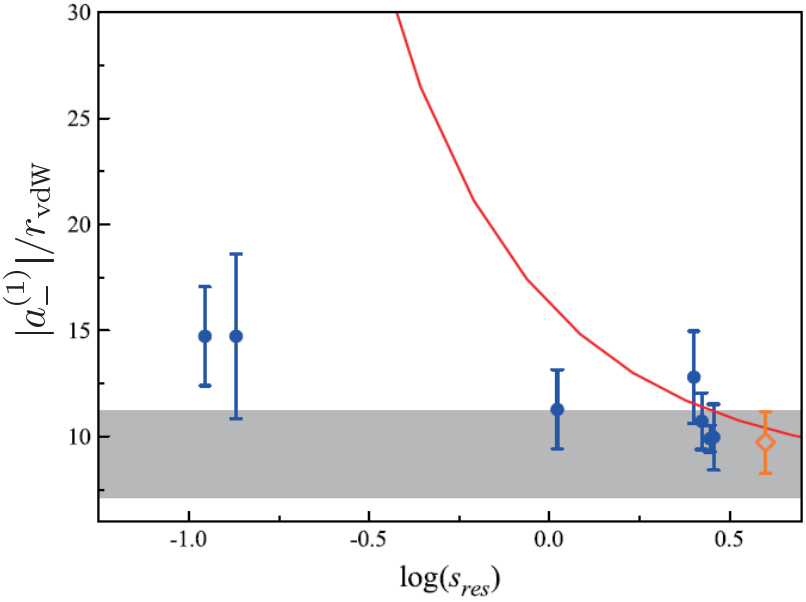

Figure 2.13: $|a_-^{(1)}|/r_{\rm vdW}$ measured for ^{39}K atoms (blue dots) [66] versus the theoretical prediction (red curve) reported in Ref. [75]. The open diamond is the mean value $|a_-^{(1)}|/r_{\rm vdW} = 9.73$ observed for broad resonances. The gray shaded region shows the variance of the experimental data. [Figure adapted with permission from S. Roy *et al.*, Phys. Rev. Lett. **111**, 053202 (2013). Copyright © (2013) by The American Physical Society.]

reflection between three atoms, so that they cannot come close and the three-body physics is determined solely by the long-range part of the inter-atomic interaction, i.e., the van der Waals interaction. He has estimated the three-body parameter with a physical model, and obtained $a_-^{(1)}/r_{\rm vdW} = -9.48$. In Ref. [73], however, J. Wang and coworkers argue that quantum reflection is insufficient to prevent three particles from coming close. By numerically solving three-body Schrödinger equation for various two-body potentials, they have shown that a strong three-body repulsion appears in the hyper-radial potential when a two-body potential either is strongly attractive or has a hard-core repulsion at short distance. They have obtained three-body parameters for various types of potentials to be $a_-^{(1)}/r_{\rm vdW} = -8 \sim 12$. In Ref. [74], P. K. Sørensen and coworkers have claimed that a repulsive barrier in the two-body potential is essential for the three-body parameter. However, in Ref. [73], J. Wang and coworkers have shown that a strong three-body repulsion can appear and the three-body parameter becomes universal even for purely attractive two-body potentials.

To summarize, for a system of three identical bosons in the vicinity of broad Feshbach resonances, the value of the three-body parameter has been found to be consistent with the experiments in most theoretical studies. However, the physical mechanisms proposed to date have been rather different from each other, and some of them are in total contradiction. In Chap. 4, the physical origin of the three-body parameter is studied, and a clear and simple physical picture will be presented.

3 identical bosons for narrow Feshbach resonances

The three-body parameter in the ultra-narrow resonance limit has been theoretically studied by D. S. Petrov in 2004 [171]. He has found that the three-body parameter is universally described by the effective range, and thus gets divergently large as $a_{-}^{(1)} \approx |r_{\mathrm{eff}}| \propto s_{\mathrm{res}}^{-1} \to +\infty$ in the ultra-narrow resonance limit. Interestingly, a slight increase of the three-body parameter for narrow resonances reported by LENS (light-blue rectangles in Fig. 2.12) [66] is consistent with this behavior, although they are yet far from the ultra-narrow resonance limit and hence the theory cannot be applied. It should be noted that there is no increase in the three-body parameter for ^{7}Li atoms (purple diamonds in Fig. 2.12) observed at the Rice University [26] and the Bar-Ilan University [44, 46].

In Ref. [75], R. Schmidt and coworkers have theoretically studied how the three-body parameter varies as the resonance width is changed. In Fig. 2.13, their theoretical prediction is shown as a red curve. It converges to $|a_{-}^{(1)}|/r_{\mathrm{vdW}} = 8.27$ in the broad resonance limit, which is consistent with the universal value. It also becomes divergently large in the ultra-narrow resonance limit, and is consistent with Ref. [171]. However, as shown in Fig. 2.13, it is inconsistent with experimental results.

Hetero-nuclear systems for broad Feshbach resonances

Until now, there is only one work on the three-body parameter for hetero-nuclear systems. In Ref. [168], Y. Wang and coworkers claim that the three-body parameter is universal even for a hetero-nuclear system of two identical bosons and one distinguishable particle. For a system of two light and one heavy particles, they have found a strong three-body repulsion similar to the case of three identical bosons. For a system of two heavy and one light particles, on the other hand, they argue that an attractive interaction between the heavy particles, rather than the three-body repulsion, makes the three-body parameter universal.

Table 2.4: Experimentally observed three-body parameters $a_-^{(1)}$ and inelasticity parameters η_- for ^{6}Li, ^{7}Li, ^{39}K, ^{85}Rb, and ^{133}Cs. For ^{4}He atoms, the three-body parameter calculated theoretically with a realistic ^{4}He potential is shown [10]. In most cases, $s_{\rm res}$ is taken from the references below or Ref. [24]. For ^{7}Li, $s_{\rm res}$ is estimated from the Feshbach resonance data in Ref. [65].

Atom	$r_{\rm vdW}[a_0]$	B_0 [G]	$a_-^{(1)}[a_0]$	$a_-^{(1)}/r_{\rm vdW}$	$s_{\rm res}$	η_-	Reference
		553.30	-1029±58	-10.188±0.574	0.9	0.12±0.01	[68]
		853.07	-955±28	-9.455±0.277	1470	0.08 ±0.01	[68]
^{133}Cs	101.0	554.71	-957±80	-9.475±0.792	170	0.19±0.02	[68]
		7.56	-872±22	-8.634±0.218	560	0.10±0.03	[68]
		818.89	-1400±150	-13.86±1.49	12	0.18±0.03	[69]
		738	-274	-8.43	0.61	0.21	[47]
^{7}Li	32.49	738	-265±16	-8.16±0.49	0.61	0.253±0.062	[46, 65]
		738	-252±10	-7.76±0.30	0.61	0.12	[26, 45]
		894	-238±25	-7.33±0.76	0.73	0.180±0.048	[44, 65]
^{6}Li	31.26	-	-292	-9.34	-	0.072	[50]
		-	-253	-8.11	-	0.016±0.010	[53]
^{4}He(Theory)	4.935	-	-48.4	-9.81	$+\infty$	-	[10]
		471.0	-640±100	-9.92±1.55	2.8	0.065±0.011	[66]
		402.6	-690±40	-10.70±0.62	2.8	0.145±0.012	[66]
		33.64	-830±140	-12.87±2.17	2.6	0.204±0.010	[66]
^{39}K	64.49	560.72	-640±90	-9.92±1.40	2.5	0.22±0.02	[66]
		162.35	-730±120	-11.32 ±1.86	1.1	0.26±0.05	[66]
		65.67	-950±250	-14.73±3.88	0.14	-	[66]
		58.92	-950±150	-14.73±2.33	0.11	-	[66]
^{85}Rb	82.10	155.04	-759±6	-9.244±0.07	28	0.057±0.002	[67]

Chapter 3

Universal three-body physics for fermions

For a three-body system of two identical fermions with no internal degree of freedom resonantly interacting in the s-wave channel with another distinguishable particle, as in introduced in Sec. 2.3, two types of trimers have been demonstrated to exist in the $L = 1$, odd parity channel: the Efimov trimers [38, 132] and the Kartavtsev-Malykh trimers [59]. When the mass ratio between the fermions and the other particle m_F/m_L is larger than the Efimov's critical mass ratio $(m_F/m_L)_{\mathrm{E}} = 13.606\ldots$ [132], the Efimov states appear. When the mass ratio is smaller than $(m_F/m_L)_{\mathrm{E}}$, the Efimov states do not appear, but still universal three-body bound states can exist. Indeed, there exist one three-body bound state when $(m_H/m_L)^{(1)}_{\mathrm{KM}} < m_F/m_L < (m_H/m_L)^{(2)}_{\mathrm{KM}}$ and two three-body bound states when $(m_H/m_L)^{(2)}_{\mathrm{KM}} < m_F/m_L < (m_F/m_L)_{\mathrm{E}}$, where $(m_H/m_L)^{(1)}_{\mathrm{KM}} = 8.172\ldots$ and $(m_H/m_L)^{(2)}_{\mathrm{KM}} = 12.917\ldots$ [59]. These three-body bound states below the Efimov's critical mass ratio are called the Kartavtsev-Malykh states after two researchers who found these three-body bound states in 2007 [59].

As compared in Table. 2.2, universal properties of the Kartavtsev-Malykh states are in marked contrast to those of the Efimov states. The Efimov states can exist for a negative value of the scattering length, and show the energy spectrum as schematically illustrated in Fig. 3.1 (b). There are an infinite number of three-body bound states featuring the discrete scale invariance. On the other hand, the Kartavtsev-Malykh states exist only for a positive scattering length. Thanks to a strong three-body repulsion originating from a centrifugal force, the three-body parameter is irrelevant for the Kartavtsev-Malykh states, and their properties are universally determined by the s-wave scattering length. For example, the binding energy of the Kartavtsev-Malykh states behaves as $E \propto a^{-2}$. When $(m_H/m_L)^{(2)}_{\mathrm{KM}} < m_F/m_L < (m_H/m_L)_{\mathrm{E}}$, two Kartavtsev-Malykh states exist, and the energy spectra behave as schematically illustrated in Fig. 3.1 (a) close to unitarity.

A natural question arises: as the mass ratio of the system is varied, how the energy spectra below the Efimov's critical mass ratio $m_F/m_L < (m_H/m_L)_{\mathrm{E}}$ shown in Fig. 3.1 (a) can change into those above the critical mass ratio $m_F/m_L > (m_H/m_L)_{\mathrm{E}}$ shown in Fig. 3.1 (b)? When the mass ratio is varied across the critical mass ratio, the number of trimers should change from two to infinite. How this can occur? The scale invariance should also change dramatically at the critical mass ratio: above the critical mass ratio, the Efimov states appear, showing the discrete scale invariance. On the other hand, the Kartavtsev-Malykh states show the continuous scale invariance: if one finds one of the Kartavtsev-Malykh states at a specific value of the s-wave scattering length, properties of

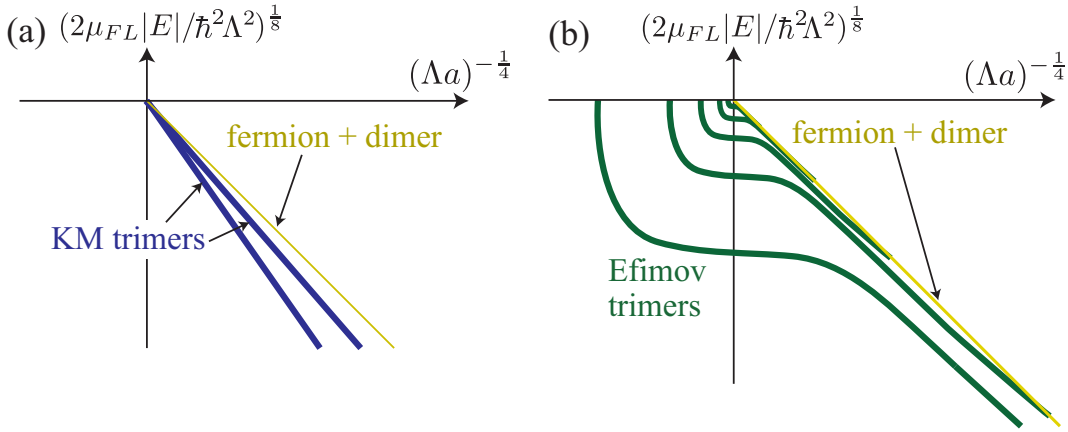

Figure 3.1: Schematic illustration of the energy spectra of (a) the Kartavtsev-Malykh (KM) trimers (thick blue lines) and (b) the Efimov trimers (thick green curves). $\mu_{FL} = \dfrac{m_F m_L}{m_L + m_F}$ is the reduced mass between the fermion and the other particle, a is the s-wave scattering length between the fermions and the other particle, and Λ is the three-body parameter, or equivalently the cutoff momentum in the Skorniakov–Ter-Martirosian equation (3.20). The rightmost thin yellow lines show the universal dimer binding energy in Eq. (2.10). [Figure adapted with permission from S. Endo *et al.*, Phys. Rev. A **86**, 062703 (2012). Copyright © (2012) by The American Physical Society.]

trimers for different values of the s-wave scattering length can be predicted by rescaling the s-wave scattering length and the energy for a continuous value of β as $a \to \beta a$, $E \to \beta^{-2}E$, and $\langle r \rangle \to \beta\langle r \rangle$. While the three-body problem of two fermions and an additional particle has been studied in some literature [59, 60, 172, 173], there has not yet been a systematic study that clarifies the relation between different types of trimers and show how the energy spectra changes as the mass ratio and s-wave scattering length are varied.

This issue is addressed in Sec. 3.2. I show in Sec. 3.2 how the Kartavtsev-Malykh states can change into the Efimov states as the mass ratio and the s-wave scattering length are varied. To this end, I first I derive in Sec. 3.1 an integral equation in the Skorniakov–Ter-Martirosian form for a system of two identical particles and one distinguishable particle for arbitrary masses, angular-momentum channels, and statistics of particles (i.e., bosons or fermions). This allows us to calculate particle-dimer ℓ-wave scattering lengths and binding energies of trimers in an arbitrary angular-momentum channel, mass ratio, and statistics from a single equation. Using this Skorniakov–Ter-Martirosian equation, I solve the three-body problem numerically by varying the mass ratio and the s-wave scattering length. I have found a new class of universal three-body bound states, "crossover trimers", which lie between the Kartavtsev-Malykh and the Efimov regimes. The crossover trimers neither show the continuous nor discrete scale invariance, but they exist between the two regimes model-independently and behave universally. As the mass ratio is increased, I have found that the trimers of the Kartavtsev-Malykh character gradually lose their continuous scale invariance and become the crossover trimers, and finally turn into the Efimov trimers.

While the Kartavtsev-Malykh states have been originally found in the fermionic 2+1 system in the $L = 1$ channel [59], in Ref. [61], it has been pointed out that they can generally exist in the

odd angular-momentum channels for the fermionic 2+1 system, and in the nonzero even angular-momentum channels for the bosonic 2+1 system. However, the Kartavtsev-Malykh states in general angular-momentum channels have been studied only in an approximate manner [61], and there has been no precise three-body calculations. In particular, precise values of the critical mass ratios at which the Kartavtsev-Malykh states appear have not been known. In Sec. 3.3, I study the three-body problem of fermionic and bosonic 2+1 systems in arbitrary angular-momentum channels with the Skorniakov–Ter-Martirosian equation derived in Sec. 3.1. I numerically obtain precise values of the critical mass ratios at which the Kartavtsev-Malykh trimers appear, their binding energies, and elastic particle-dimer scattering lengths in arbitrary angular-momentum channels for both fermionic and bosonic 2+1 systems. The result suggests that similar crossover physics studied in Sec. 3.2 may appear in the odd angular-momentum channels for the fermionic 2+1 systems and in the nonzero even angular-momentum channels for the bosonic 2+1 systems.

In Sec. 3.4, I discuss experimental implications of the results presented in Secs. 3.2 and 3.3.

3.1 Higher-partial-wave Skorniakov–Ter-Martirosian equation

The Skorniakov–Ter-Martirosian equation (2.57) is a one-dimensional integral equation, which allows us to numerically obtain the particle-dimer s-wave scattering length and binding energies of the Efimov trimers for a system of three identical bosons in the $L = 0$ channel. Similar equations have also been derived for various classes of three-body systems: three identical bosons in the higher angular momentum channels [148, 153], three identical fermions with internal degree of freedom [148], 2 bosons + 1 particle system in the $L = 0$ channel [154]. In this section, I derive a one-dimensional integral equation in the Skorniakov–Ter-Martirosian form for a three-body system of two identical particles (bosons/fermions) and one distinguishable particle in an arbitrary angular-momentum channel, for an arbitrary value of the s-wave scattering length and the mass ratio. The Skorniakov–Ter-Martirosian equation allows us to obtain precise values of particle-dimer ℓ-th wave scattering lengths and binding energies of trimers in arbitrary angular-momentum channels by varying the s-wave scattering length and the mass ratio.

The Skorniakov–Ter-Martirosian is crucial for my studies presented in Secs. 3.2 and 3.3. Compared with the other methods applied to solve the three-body problem of the 2+1 systems [59, 61, 172, 173, 174], the Skorniakov–Ter-Martirosian equation enables us to solve the three-body problem much faster and far more accurately. It facilitates the investigation of the fermionic 2+1 system for the whole parameter space of the s-wave scattering length and mass ratio and the study on the crossover physics of trimers in Sec. 3.2. It also helps us to obtain precise values of the critical mass ratios at which the Kartavtsev-Malykh trimers appear, as will be studied in Sec. 3.3.

Derivation of the Skorniakov–Ter-Martirosian equation

Let us consider a three-body problem of two identical spinless (i.e., spin-polarized) particles (mass m_F) and one distinguishable particle (mass m_L). The statistics of the identical particles can be either bosons or fermions. The interactions between the identical particles and the other particle are assumed to be nearly resonant in the s-wave channel, so that it can be modeled by the zero-range

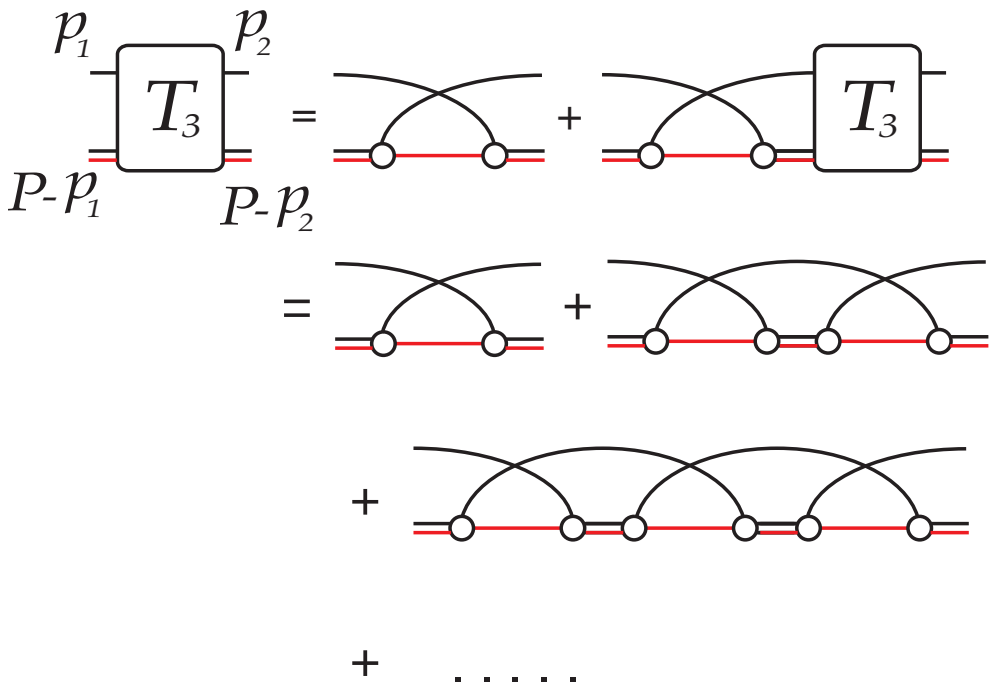

Figure 3.2: Diagrammatic representation of the Dyson equation (3.1). The single line and the double line are a single-particle Green function and a two-body T-matrix, respectively. The identical particles are shown as black lines, while the distinguishable particle is shown as a red line.

interaction (2.19) at low energy. On the other hand, the interaction between the identical particles is assumed to be non-resonant, so that it can be neglected to a good approximation. This assumption is even more justified when the identical particles are fermions, since the interaction between the fermions in the s-wave channel is prohibited.

The three-body problem is equivalent to solving the particle-dimer scattering problem, where the dimer is composed of one of the identical particles and the distinguishable particle. The particle-dimer scattering problem can be generally described by the following Dyson equation [175]

$$T_3(p_1, p_2|P) = \pm G_L(P - p_1 - p_2) \pm i \int \frac{d\omega_q d^3\boldsymbol{q}}{(2\pi)^4} G_L(P - p_1 - q) G_F(q) T_2(P - q) T_3(q, p_2|P), \quad (3.1)$$

where $T_2(q)$ is the two-body T-matrix of one of the identical particles and the other distinguishable particle, $T_3(p_1, p_2|P)$ is the particle-dimer T-matrix, and $G_F(q)$ and $G_L(q)$ are single-particle Green functions for the identical particles and the other particle, respectively; p_1 and p_2 are in-coming and out-going relative momentum and energy, respectively, and P is the total momentum and energy. All momentum indices are written in the four-momentum notation. The plus sign is when the identical particles are bosons, while the minus sign is when they are femrions. The Dyson equation is diagrammatically illustrated in Fig. 3.2. For a system interacting via the zero-range interaction (2.19), the two-body T-matrix can be analytically obtained as

$$T_2(P) = \left[\frac{\mu_{FL}}{2\pi a} - \frac{\mu_{FL}^{3/2}}{\sqrt{2}\pi} \sqrt{\frac{\boldsymbol{P}^2}{2(m_F + m_L)} - \omega_P - \imath 0^+} \right]^{-1}. \quad (3.2)$$

Let us take the on-shell processes in Eq. (3.1) for p_1 and p_2: $p_i = \overline{p_i} = \left(\frac{\boldsymbol{p_i}^2}{2m_F}, \boldsymbol{p_i}\right)$, where the overline denotes the on-shell energy and momentum. Since we are only interested in the relative motion of the atom and dimer, we take the total momentum to be zero: $P = P_0 = \left(-\frac{\hbar^2\varepsilon}{2\mu_{FL}}, 0\right)$, where $\mu_{FL} = \frac{m_F m_L}{m_F + m_L}$ is the reduced mass between one of the identical particles and the other distinguishable particle.

One can carry out the frequency integration in the second term of the right-hand side in Eq. (3.1), since $G_F(q)$ has a pole in the lower-half plane of ω_q and the other terms are analytic in the lower half-plane of ω_q. After the frequency integration, one obtains

$$T_3(\overline{p_1}, \overline{p_2}|P_0) = \pm G_L(P_0 - \overline{p_1} - \overline{p_2}) \pm i \int \frac{d^3\boldsymbol{q}}{(2\pi)^3} G_L(P_0 - \overline{p_1} - \overline{q}) G_F(\overline{q}) T_2(P_0 - \overline{q}) T_3(\overline{q}, \overline{p_2}|P_0). \quad (3.3)$$

Now, we expand the Dyson equation into independent partial waves. To this end, the Green function and the particle-dimer T-matrix are expanded as

$$-G_L(P_0 - \overline{p_1} - \overline{p_2}) = \sum_{\ell=0}^{\infty} g_\ell(p_1, p_2) P_\ell(\cos\theta_{12}), \quad (3.4)$$

$$T_3(\overline{q}, \overline{p_2}|P_0) = \sum_{\ell=0}^{\infty} t_\ell(p_1, p_2) P_\ell(\cos\theta_{12}), \quad (3.5)$$

where θ_{12} is the relative angle between $\boldsymbol{p_1}$ and $\boldsymbol{p_2}$, and $g_\ell(p_1, p_2)$ is defined as

$$g_\ell(p_1, p_2) = \frac{2\ell + 1}{2} \int_{-1}^{1} dx P_\ell(x) \frac{1}{-\frac{\varepsilon}{2\mu_{FL}} + \frac{p_1^2}{2\mu_{FL}} + \frac{p_2^2}{2\mu_{FL}} + \frac{p_1 p_2}{m_L} x}. \quad (3.6)$$

This integration can be carried out analytically by using the following mathematical formula:

$$\int_{-1}^{1} dx P_n(x) \frac{1}{1 + Ax} = 2(-1)^n \frac{1}{A} Q_n\left(\frac{1}{A}\right) \quad (0 < A < 1), \quad (3.7)$$

where $Q_n(x)$ is a Legendre function of the second kind. Then, one finds

$$g_\ell(p_1, p_2) = (2\ell + 1)(-1)^\ell \frac{m_L}{p_1 p_2} Q_\ell\left(\frac{\frac{m_L}{2\mu_{FL}}[-\varepsilon + p_1^2 + p_2^2]}{p_1 p_2}\right). \quad (3.8)$$

Substituting Eqs (3.4) and (3.5) into Eq. (3.3), one obtains

$$t_\ell(p_1, p_2) = \mp g_\ell(p_1, p_2) \mp \frac{1}{2\pi^2(2\ell + 1)} \int q^2 dq g_\ell(p_1, q) T_2(P_0 - \overline{q}) t_\ell(q, p_2), \quad (3.9)$$

where we have used the addition theorem of the spherical harmonics:

$$P_\ell(\cos\theta_{12}) = \frac{4\pi}{2\ell + 1} \sum_{m=-\ell}^{\ell} Y_{\ell m}(\theta_1, \phi_1) Y^*_{\ell m}(\theta_2, \phi_2). \quad (3.10)$$

We define the momentum-dependent scattering length as

$$a_\ell(p_1) = \frac{1}{2\ell+1}\frac{\mu_{DF}}{\mu_{FL}^2}\lim_{p_2\to 0}\frac{t_\ell(p_1,p_2)}{p_1^\ell p_2^\ell}, \tag{3.11}$$

where $\mu_{DF} = \dfrac{m_F(m_F+m_L)}{2m_F+m_L}$ is the reduced mass between one of the identical particles and the dimer. Note that the low momentum limit of $a_\ell(p)$ gives the ℓ-th wave particle-dimer scattering length when the total energy is set to the particle-dimer threshold energy $\varepsilon = a^{-2}$. To see this, recall that the particle-dimer T-matrix can be related to the particle-dimer scattering amplitude f_{AD} if we set $|\boldsymbol{p_1}| = |\boldsymbol{p_2}|$ as

$$T_3(\overline{p_1},\overline{p_2}|P_0) = -\frac{\mu_{FL}^2}{\mu_{DF}} f_{AD}(\boldsymbol{p_1},\boldsymbol{p_2})\Big|_{|\boldsymbol{p_1}|=|\boldsymbol{p_2}|}. \tag{3.12}$$

By expanding the particle-dimer scattering amplitude into partial waves as

$$f_{AD}(\boldsymbol{p_1},\boldsymbol{p_2}) = \sum_\ell (2\ell+1) f_\ell(p_1) P_\ell(\cos\theta_{12}), \tag{3.13}$$

$$f_\ell(k) = \frac{k^{2\ell}}{-\frac{1}{a_\ell}+r_\ell k^2+\cdots}, \tag{3.14}$$

one can relate the ℓ-th-wave particle-dimer scattering length a_ℓ and T_3 as follows:

$$a_\ell = -\lim_{p_1\to 0}\frac{f_\ell(p_1)}{p_1^{2\ell}} = \frac{1}{2\ell+1}\frac{\mu_{DF}}{\mu_{FL}^2}\lim_{p_1,p_2\to 0}\frac{t_\ell(p_1,p_2)}{p_1^\ell p_2^\ell}. \tag{3.15}$$

From Eqs. (3.11) and (3.15), one can clearly see that $a_\ell(p=0)$ gives the particle-dimer ℓ-th scattering length.

Substituting Eq. (3.11) into Eq. (3.9), one obtains

$$a_\ell(p_1) = \mp\frac{1}{2\ell+1}\frac{\mu_{DF}}{\mu_{FL}^2}\frac{g_\ell(p_1)}{p_1^\ell} \mp \frac{1}{2\pi^2(2\ell+1)p_1^\ell}\int dq q^{\ell+2} g_\ell(p_1,q) T_2(P_0-\overline{q}) a_\ell(q), \tag{3.16}$$

where we have defined $g_\ell(p_1)$ as

$$g_\ell(p_1) \equiv \lim_{p_2\to 0}\frac{g_\ell(p_1,p_2)}{p_2^\ell}. \tag{3.17}$$

By using the asymptotic expression for the Legendre function of the second kind

$$Q_n(z) \to \frac{2^n (n!)^2}{z^{n+1}(2n+1)!} \quad (z\to\infty), \tag{3.18}$$

g_ℓ can be obtained analytically as

$$g_n(p_1) = \frac{(-2)^n (n!)^2 m_t p_1^n}{(2n)!}\left(\frac{1}{\frac{m_L}{2\mu_{FL}}[-\varepsilon+p_1^2]}\right)^{n+1}. \tag{3.19}$$

Substituting Eq. (3.19) into Eq. (3.16), we obtain an integral equation in the Skorniakov–Ter-Martirosian form [155]:

$$\frac{a_\ell(p)}{a^{2\ell+1}} + \frac{(-1)^\ell m_L}{\mu_{FL}\pi}\int dq\left(\frac{q}{p}\right)^{\ell+1} Q_\ell\left(\frac{\frac{m_L}{2\mu_{FL}}[-\varepsilon+p^2+q^2]}{pq}\right)\frac{1}{\sqrt{-\varepsilon+\frac{\mu_{FL}}{\mu_{DF}}q^2}-\frac{1}{a}}\frac{a_\ell(q)}{a^{2\ell+1}} = \frac{(-2)^\ell(\ell!)^2}{(2\ell+1)!}\frac{\mu_{DF}m_L}{\mu_{FL}^2}\left[\frac{2\mu_{FL}}{m_L}\frac{1}{(-\varepsilon+p^2)a^2}\right]^{\ell+1}. \tag{3.20}$$

The same equation has also been derived recently in Ref. [156].

For a small ℓ, the Legendre polynominal of the second kind are given as

$$Q_{\ell=0} = \frac{1}{2}\log\left(\frac{x+1}{x-1}\right), \tag{3.21}$$

$$Q_{\ell=1} = \frac{x}{2}\log\left(\frac{x+1}{x-1}\right)-1, \tag{3.22}$$

$$Q_{\ell=2} = \frac{3x^2-1}{4}\log\left(\frac{x+1}{x-1}\right)-\frac{3}{2}x. \tag{3.23}$$

In particular, for a mass-balanced system in the $\ell = 0$ channel, Eq. (3.20) becomes

$$\left[\sqrt{-\varepsilon+\frac{3}{4}q^2}-\frac{1}{a}\right]a_{AD}(p)+\frac{1}{\pi}\int dq\left(\frac{p}{q}\right)\log\left(\frac{-\varepsilon+p^2+q^2+pq}{-\varepsilon+p^2+q^2+pq}\right)a_{AD}(q) = \frac{p^2}{(-\varepsilon+p^2)a}, \tag{3.24}$$

where

$$a_{AD}(q) = \frac{3}{8}\frac{q^2}{\sqrt{-\varepsilon+\frac{3}{4}q^2}-\frac{1}{a}}a_{\ell=0}(q). \tag{3.25}$$

Equation (3.24) is almost equivalent to Eq. (2.57). The difference in the factor in front of the integration originates from the absence of an interaction between identical particles.

By taking the energy at the dimer threshold $E = -\dfrac{\hbar^2}{2\mu_{FL}a^2}$ and solving Eq. (3.20), one can obtain the particle-dimer ℓ-th wave scattering length as $a_\ell(q = 0)$. Binding energies of trimers can also be obtained from Eq. (3.20) by seeking for the values of ε at which $a_\ell(q = 0)$ diverges. When one regards the left-hand side of Eq. (3.20) as an operator acting on $a_\ell(q)$, the divergence of $a_\ell(q = 0)$ is equivalent to one of the eigenvalues of the left-hand side being zero. Therefore, binding energies of trimers can be obtained by seeking for the values of ε at which one of the eigenvalues of the left-hand side becomes zero. In Secs. 3.2 and 3.3, particle-dimer scattering lengths and binding energy of trimers calculated with Eq. (3.20) will be presented.

When the Efimov effect does not occur, the integration in Eq. (3.20) can be taken to be infinite. Binding energies of trimers and particle-dimer scattering lengths can then be universally described by the s-wave scattering length as $E \propto -\dfrac{\hbar^2}{2\mu_{FL}a^2}$, $a_\ell \propto a^{2\ell+1}$. For a system where the Efimov effect occurs, on the other hand, an upper cutoff in the integration must be introduced in Eq. (3.20). Otherwise, the Thomas collapse occurs, and Eq. (3.20) does not have any finite solution. As long

as the energy of the system is small and it behaves universally, the cutoff can be introduced in an arbitrary manner. The most typical choice is a sharp momentum cutoff

$$\int dq \to \int_0^{\Lambda} dq. \tag{3.26}$$

The momentum cutoff can also be introduced in other ways. For example, a Gaussian type of cutoff is also possible:

$$\int dq \to \int_0^{\infty} \exp\left(-\frac{q^2}{2\Lambda^2}\right) dq. \tag{3.27}$$

Since a three-body system should behave universally at low energy, the particle-dimer scattering lengths and binding energies of trimers calculated with these two ways of the momentum cutoffs should give the same result at low energy. This can in turn be used to investigate whether the three-body system is in the universal regime or not. In Sec. 3.2.5, I study whether the 2+1 system is universal by changing the ways of the momentum cutoff and comparing them.

Discussions

The Skorniakov–Ter-Martirosian equation (3.20) can be used to obtain particle-dimer scattering lengths and binding energies of trimers for various system with a rather straightforward numerical calculation. For example, by taking $m_F/m_L = 1.0$ and $\ell = 0$ and assuming the identical particles to be fermions, the well-known value of the fermion-dimer s-wave scattering length $1.18a$ is obtained [132, 148]. Furthermore, by taking $\ell = 1$ and assuming the identical particles to be fermions, one can show that the trimers appear at mass ratios 8.172 and 12.917, as predicted in Ref. [59]. This clearly shows great advantage of the Skorniakov–Ter-Martirosian equation over other methods. In some literature [59, 61, 172], the hyper-spherical formalism has been used to study the Kartavtsev-Malykh trimers and the Efimov trimers. It has been pointed out that channel couplings should be taken into account to obtain the mass ratios $(m_H/m_L)^{(1)}_{\rm KM}$ and $(m_H/m_L)^{(2)}_{\rm KM}$ accurately. Indeed, if one neglects all the channel couplings P_{nm} and Q_{nm}, the critical mass ratios become 7.930 and 12.789 [61]. Even when the diagonal non-adiabatic term Q_{nn} is taken into account, the critical mass ratios are 8.183 and 12.929 [59]. Therefore, one needs to solve the full coupled-channel Schrödinger equation to obtain the correct critical mass ratios. Compared with the coupled-channel Schrödinger equation, the Skorniakov–Ter-Martirosian equation can be numerically solved much faster and far more accurately. This will be exemplified in Sec. 3.3, where the critical mass ratios for the appearance of the Kartavtsev-Malykh trimers and the Efimov trimers are obtained with the Skorniakov–Ter-Martirosian equation for both fermions and bosons in various angular-momentum channels and compared with the previous studies [38, 59, 61, 115, 132].

To solve Eq. (3.20) numerically, one discretizes the momentum and transforms the integral equation into a linear equation in a matrix form. The numerical calculation can be performed efficiently if the momentum is discretized with unequal spacings. In the studies presented in Secs. 3.2 and 3.3, the following exponential form of the momentum mesh has been used:

$$p_j = \exp\left(\frac{j}{N_{\rm max}} \log(\Lambda + 1)\right) - 1 \quad (j = 0, 1, ..., N_{\rm max}) \tag{3.28}$$

where $N_{\max}$ is the number of the mesh. This exponential momentum mesh suits well with the log-periodic behavior of the Efimov states at large momentum, while it gives an equally spaced mesh at small momentum. The exponentially spaced mesh allows one to obtain accurate binding energies of highly-excited Efimov states. Indeed, in Sec. 3.2.3, energy spectra of the Efimov states are obtained from up to the 4th to 8th excited trimers with a high precision.

3.2 Properties and identification of the trimers

In this section, I investigate the three-body system of two identical spinless (i.e., spin-polarized) fermions resonantly interacting in the s-wave channel with one distinguishable particle. The $L = 1^-$ channel is studied in this section, while the other channels are studied in Sec. 3.3. This channel corresponds to taking the relative angular momentum between the atom and the dimer to be $\ell = 1$ in Eq. (3.20). In this channel, two types of universal three-body bound states have been demonstrated to exist in different regimes of the mass ratio: the Kartavtsev-Malykh trimers and the Efimov trimers. While the Efimov trimers show the discrete scale invariance, the Kartavtsev-Malykh trimers feature a continuous scale invariance. In addition to the scale invariance, their energy spectra also differ significantly, as compared in Fig. 3.1.

In this section, I study how properties of the trimers change as the mass raio and the s-wave scattering length are varied. In Sec. 3.2.1, the main results of this section are summarized. In Secs. 3.2.2 to 3.2.5, the three-body problem is solved with the Skorniakov–Ter-Martirosian equation numerically and the energy spectra are obtained. In Sec. 3.2.2, properties of the trimers below the Efimov's critical mass ratio are studied. Those above the Efimov's critical mass ratio are discussed in Sec. 3.2.3. In Sec. 3.2.4, I show that there exists the third class of universal trimers, the crossover trimers, which continuously connect the Kartavtsev-Malykh trimers and the Efimov trimers. In Sec. 3.2.5, I show that the crossover trimers are indeed universal: they exist irrespective of details of the system and behave model-independently.

3.2.1 Summary of the main results

Let me summarize the main results of this section, which are enumerated from 1. to 7. First of all, I have found a new class of universal three-body bound states, which I call the "crossover trimers":

1. There exist trimers between the Efimov and the Kartavtsev-Malykh regimes, which show neither discrete nor continuous scale invariance.

2. These "crossover trimer" states are universal. They appear irrespective of short-range details of the potential, and can be universally characterized by two parameters: the s-wave scattering length and the three-body parameter.

In other words, there are three classes of universal three-body bound states in this system: the Kartavtsev-Malykh trimers, the Efimov trimers, and the crossover trimers.

As one varies the mass ratio m_F/m_L, the energy spectra of the trimers change as schematically illustrated in Fig. 3.3. Namely, I have found the following features:

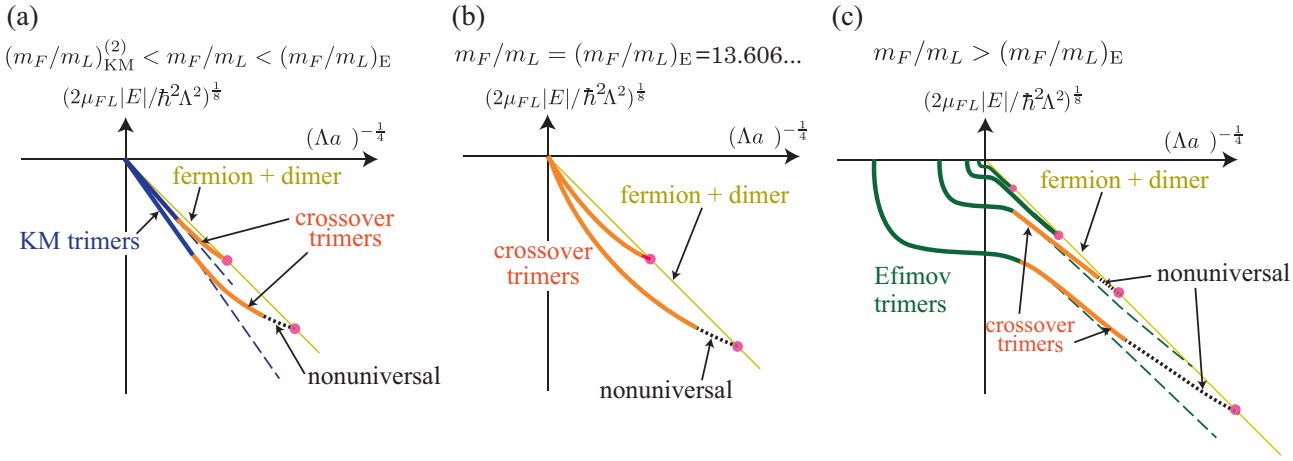

Figure 3.3: (a)-(c) Schematic illustration of energy spectra for different regimes of the mass ratio. Based on the scaling properties (see Sec. 3.2 for detail), the Kartavtsev-Malykh (KM) trimer region (thick blue curves), the Efimov trimer region (thick green curves), the crossover trimer region (thick orange curves), and the non-universal region (black dotted curves) are identified. The dashed curves in (a) and (c) are the universal prediction of the continuous scaling law of the Kartavtsev-Malykh trimers and the discrete scaling law of the Efimov trimers, respectively. The pink dots shown for $a > 0$ represent the points at which the trimer dissociates into a fermion and a dimer and the fermion-dimer p-wave scattering volume diverges. In Fig. (c), only four levels of the Efimov series are shown. [Figure adapted with permission from S. Endo *et al.*, Phys. Rev. A **86**, 062703 (2012) [176]. Copyright © (2012) by The American Physical Society.]

3. Below the Efimov's critical mass ratio $m_F/m_L < (m_F/m_L)_{\rm E}$, the trimers show the continuous scale invariance if and only if the s-wave scattering length is large and positive, $\Lambda a \gg 1$. As the s-wave scattering length gets small and one moves away from unitarity, the trimers start to depend on the three-body parameter but still they behave universally. In other words, they become the crossover trimers away from unitarity.

4. At the Efimov's critical mass ratio $m_F/m_L = (m_F/m_L)_{\rm E}$, there exist two trimers for a positive scattering length. These trimers show neither discrete nor continuous scale invariance around unitarity. In other words, the trimers are the crossover trimers close to unitarity.

5. Above the Efimov's critical mass ratio $m_F/m_L > (m_F/m_L)_{\rm E}$, the trimers satisfy the discrete scale invariance characteristic of the Efimov states close to unitarity point. Away from unitarity, on the other hand, the ground and first-excited trimers deviate significantly from the behavior predicted by the discrete scale invariance and thus become crossover trimers, while the higher-excited trimers satisfy well the discrete scale invariance for the entire region of the scattering length.

6. Both for $m_F/m_L < (m_F/m_L)_{\rm E}$ and for $m_F/m_L \geq (m_F/m_L)_{\rm E}$, the trimers dissociate into a fermion and a dimer on the positive scattering length side. At the dissociation point, a p-wave resonance occurs in the fermion-dimer scattering. However, note that the ground-state

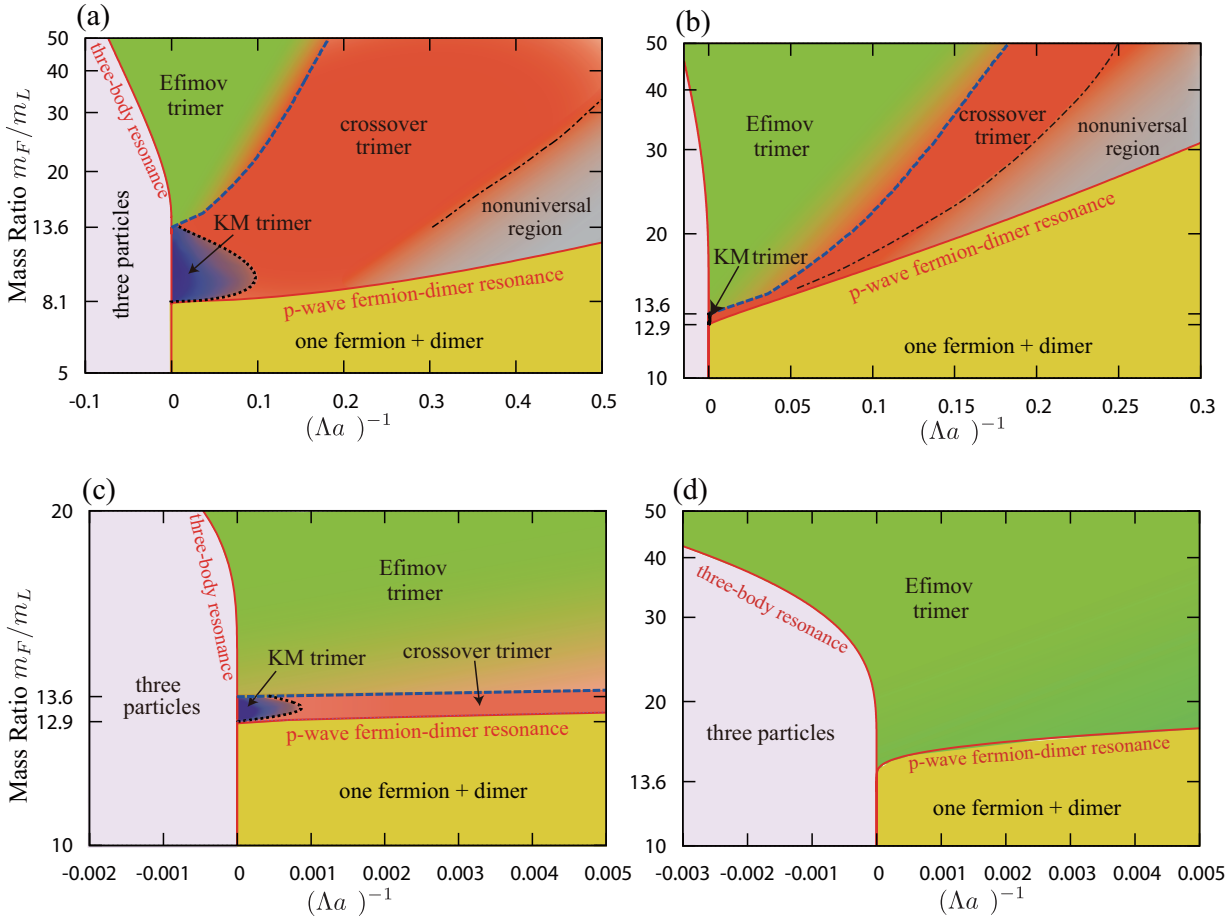

Figure 3.4: Regions of (a) the ground-state, (b)(c) first-excited, and (d) second-excited trimers as a function of the mass ratio and $(\Lambda a)^{-1}$, where a is the s-wave scattering length and Λ is the cutoff momentum, which corresponds to the three-body parameter. For the ground-state and first-excited trimers, four regimes exist: the Efimov, Kartavtsev-Malykh (KM), crossover, and non-universal regimes. For the second-excited trimer, only the Efimov region appears. A trimer dissociates into a fermion and a dimer at the fermion-dimer p-wave resonance shown as a red curve on the positive a side, while it dissociates into three particles at the three-body resonance shown as a red curve on the negative a side. The black dotted curves and the blue dashed curves correspond to $r_n = 0.40$ (see Eq. (3.29)) and $q_n = 0.40$ (see Eq. (3.32)), which delimit the Kartavtsev-Malykh trimer region and the Efimov trimer region, respectively. The black dashed-dotted curves correspond to $s_n = 0.90$ (see Eq. (3.35)), which separates the crossover and non-universal (i.e., model-dependent) trimer regions. The color contour is used for the sake of clarity. The non-universal region gets large with increasing the mass ratio, and the Efimov region disappears for the mass ratio well above 50 due to non-universal corrections (see discussions in Sec. 3.2.5). [Figure adapted with permission from S. Endo *et al.*, Phys. Rev. A **86**, 062703 (2012) [176]. Copyright © (2012) by The American Physical Society.]

trimer may not do so, since non-universal finite-range effects are significant for them in this region.

7. Close to the fermion-dimer dissociation point, non-universal finite-range effects are significant for the ground-state trimer. For the first-excited trimer, except for a very small region close to the fermion-dimer dissociation boundary, it behaves rather universally. The higher excited trimers are universal over the entire region.

These results are summarized in Fig. 3.4, where properties of the ground, first-excited, and second-excited trimers are shown as a function of the mass ratio and the s-wave scattering length. The trimers are classified into the Kartavtsev-Malykh region (blue region), the Efimov region (green region), and the crossover trimer region (orange region) according to their scaling features:

- Kartavtsev-Malykh trimer [59]: universal trimer with a continuous scale invariance.
- Efimov trimer [38, 132]: universal trimer with a discrete scale invariance.
- Crossover trimer: universal trimer with no scale invariance.

The gray region show the non-universal region, where finite-range effects are significant. This has been judged by seeing whether the results are independent of the way one introduces the cutoff in the momentum integration (see Sec. 3.2.5 for more details).

3.2.2 Energy spectra for $m_F/m_L < (m_F/m_L)_{\rm E}$

In this section, binding energies of trimers calculated with the Skorniakov–Ter-Martirosian equation (3.20) are discussed. Here, I have chosen the sharp momentum cutoff in Eq. (3.26). In the inset of Figs. 3.5 (a) and (b), binding energies of trimers are shown as a function of $1/\Lambda a$ for several mass ratios. As predicted in Ref. [59], the ground trimer and the first-excited trimer appear for $m_F/m_L > (m_H/m_L)^{(1)}_{\rm KM} = 8.172...$ and $m_F/m_L > (m_H/m_L)^{(2)}_{\rm KM} = 12.917....$ These three-body bound states exist only on the positive scattering length side and lie slightly below the dimer energy, which suggests that the three-body bound states are only loosely bound. This is consistent with what has been found in Ref. [59]: binding energies of the Kartavtsev-Malykh trimers are small except for $m_F/m_L \approx (m_F/m_L)_{\rm E}$.

To see the energy spectra of these trimers in more details, in the main panel of Figs. 3.5 (a) and (b), binding energies of trimers measured from the particle-dimer threshold are shown. As one can see in Fig. 3.5 (a), the ground trimer exists for $m_F/m_L > (m_H/m_L)^{(1)}_{\rm KM} = 8.172....$ The binding energy gets large as the mass ratio is increased. One finds that the energy spectra are almost linear close to unitarity. The linear behavior suggests that the three-body parameter is irrelevant and the trimers are universally described by the s-wave scattering length as $E \propto a^{-2}$. Thus, the linear behavior in Fig. 3.5 suggests the continuous scale invariance. These trimers with the continuous scale invariance close to the unitarity have been studied in Ref. [59]. Indeed, the scattering length is assumed to be much larger than any other quantities in Ref. [59], so it corresponds to taking $1/\Lambda a \to +0$ in our system.

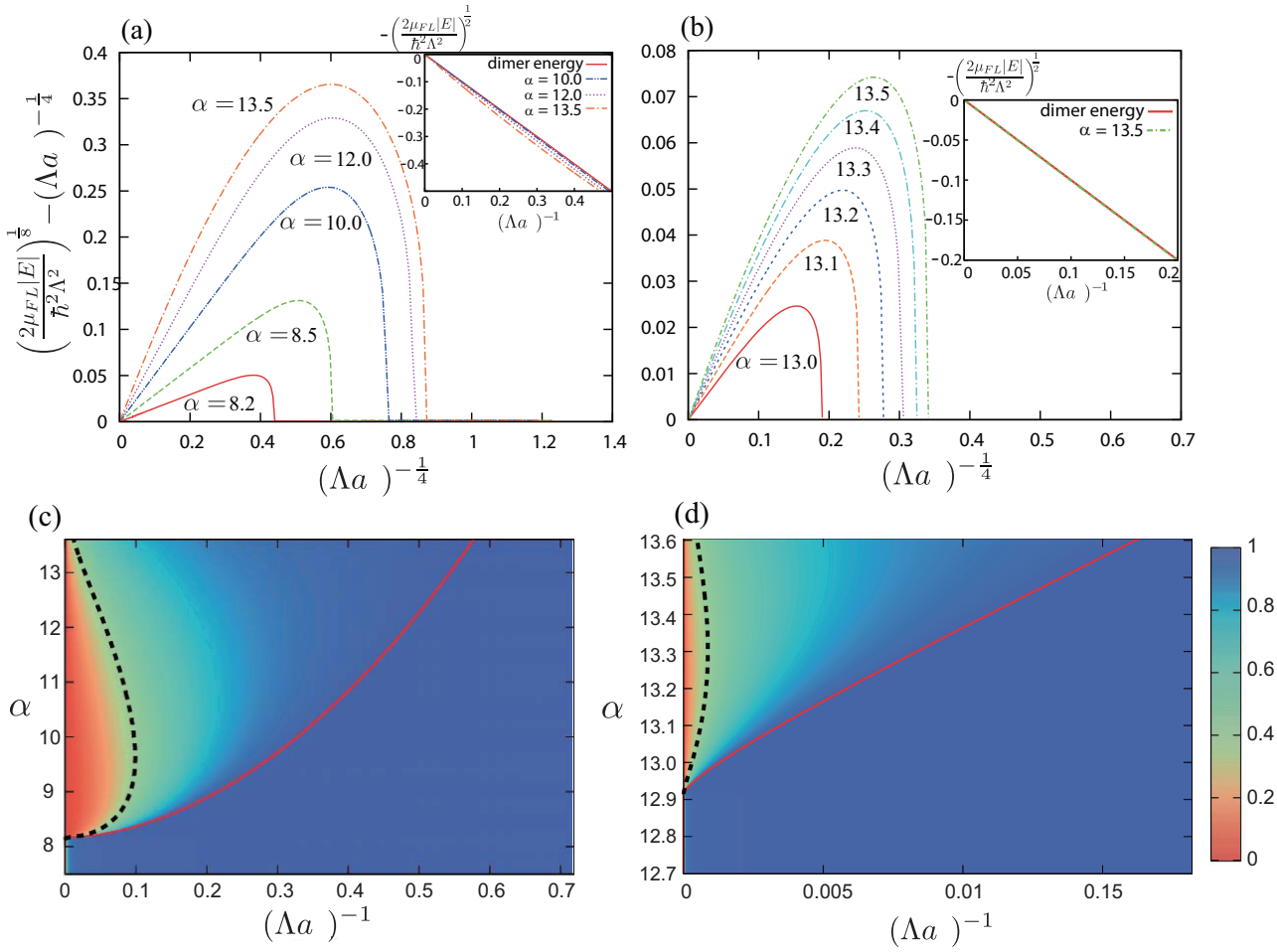

Figure 3.5: (a)(b) Energy spectra of the trimers with several different mass ratios $\alpha = m_F/m_L$ as measured from the dimer binding energy for (a) the ground-state trimer and (b) the first-excited trimer. The insets show the binding energies of the trimers as measured from the vacuum, together with the dimer binding energy shown as the red solid curve. (c)(d) Contour plots of r_n defined in Eq. (3.29) for (c) the ground-state trimer and (d) the first-excited trimer. The red solid curves are the fermion-dimer dissociation threshold. The black-dotted curves represent the $r_n = 0.40$ curves, which delimit the region in which the continuous scale invariance is well satisfied (i.e., the Kartavtsev-Malykh trimer regime). [Figure adapted with permission from S. Endo *et al.*, Phys. Rev. A **86**, 062703 (2012) [176]. Copyright © (2012) by The American Physical Society.]

As one moves away from unitarity, the linear behavior deteriorates and finally energy spectra of the trimers merge into that of the dimer. Therefore, the trimers dissociate into a fermion and a dimer when $1/\Lambda a$ is varied toward the positive side. This means that there occurs a scattering resonance in the fermion-dimer scattering. Since we are dealing with trimers in the $L = 1^-$ channel, the fermion-dimer scattering resonance occurs in the p-wave channel. This p-wave resonance will be studied in details in Secs. 3.3 and 3.4 (see Figs. 3.12 and 3.16). Thus, we have arrived at the following conclusions (c.f. see statements 3. and 6. in Sec. 3.2.1):

- Close to unitarity $\Lambda a \gg 1$, the trimers show the continuous scale invariance.
- Away from unitarity, the continuous scale invariance deteriorates, and the trimers finally dissociate into a fermion and a dimer.

As discussed in Sec. 3.2.5, the first feature is universal. On the other hand, trimers are rather sensitive to non-universal finite-range effects close to the particle-dimer dissociation point. Therefore, when one considers a system with different short-range details, or different ways of the momentum cutoff, the trimers may not dissociate into an atom and a dimer.

The continuous scale invariance of the trimers can be quantified by introducing the following quantity ($x \equiv (\Lambda a)^{-1}$):

$$r_n(x) = \frac{K_n(x) - K_{\rm dimer}(x)}{K_n^{\rm (KM)}(x) - K_{\rm dimer}(x)}, \tag{3.29}$$

where $K_{\rm dimer}(x) = x$ is the binding energy of the dimer, and $K_n^{\rm (KM)}(x) = \sqrt{\frac{2\mu_{FL}|E_n|(x)}{\hbar^2\Lambda^2}} = C_n x$ is the trimer binding energy in the limit $1/\Lambda a \to +0$ for the ground-state trimer ($n = 1$), and the first-excited trimer ($n = 2$). Here, $C_n \geq 1$ characterizes the binding energies of the trimers in the universal limit $\Lambda a \gg 1$ studied in Ref. [59]; $r_n(x)$ is 1 when the continuous scaling law holds exactly, while it vanishes when the trimers dissociate into an atom and a dimer. In Figs. 3.5 (c) and (d), r_n as a fucntion of $1/\Lambda a$ and the mass ratio are shown for the ground-state and first-excited trimers, respectively. Close to the unitarity limit, $r_n \approx 1$, suggesting that the trimers show the continuous scale invariance. We can regard this region as the Kartavtsev-Malykh trimer region. Away from unitarity, the continuous scaling deteriorates and r_n gets small, and they finally become $r_n = 0$ at the particle-dimer dissociation point. In Figs. 3.4 (a)-(c) and Figs. 3.5 (c)(d), the black dotted curves corresponding to $r_n = 0.40$ are shown. These can be regarded as curves delimiting a regime with the continuous scaling and that with no scaling.

As the mass ratio is increased from $(m_H/m_L)^{(1)}_{\rm KM}$ for the ground trimer and from $(m_H/m_L)^{(2)}_{\rm KM}$ for the first-excited trimer, the Kartavtsev-Malykh trimer region initially gets large. This is because the trimers get more bound as the mass ratio is increased, leading to a larger universal region. As the mass ratio is increased further, the Kartavtsev-Malykh trimer region gets smaller. This is physically natural because the short-range repulsive barrier in the hyper-radial potential gets small toward $(m_H/m_L)_{\rm E}$ (see Fig. 2.9). It then becomes easier for the three particles to come close and the system becomes more sensitive to the three-body parameter.

3.2.3 Energy spectra for $m_F/m_L > (m_F/m_L)_{\rm E}$

In this section, the energy spectra of trimers for $m_F/m_L > (m_F/m_L)_{\rm E}$ are calculated with the Skorniakov–Ter-Martirosian equation for a sharp momentum cutoff. Above the critical mass ratio $(m_F/m_L)_{\rm E}$, the Efimov states appear [38, 115, 132]. With the zero-range theory applied at unitarity, the discrete scale factor of the Efimov states above the critical mass ratio has been demonstrated to be $e^{\pi/\gamma}$, where γ is determined from the transcendental equation [59, 115]

$$0 = \frac{1+\gamma^2}{\gamma}\tanh\gamma\frac{\pi}{2} - \frac{2}{\sin 2\omega}\frac{\cosh\gamma\omega}{\cosh\gamma\frac{\pi}{2}} + \frac{\sinh\gamma\omega}{\gamma\sin^2\omega\cosh\gamma\frac{\pi}{2}}, \tag{3.30}$$

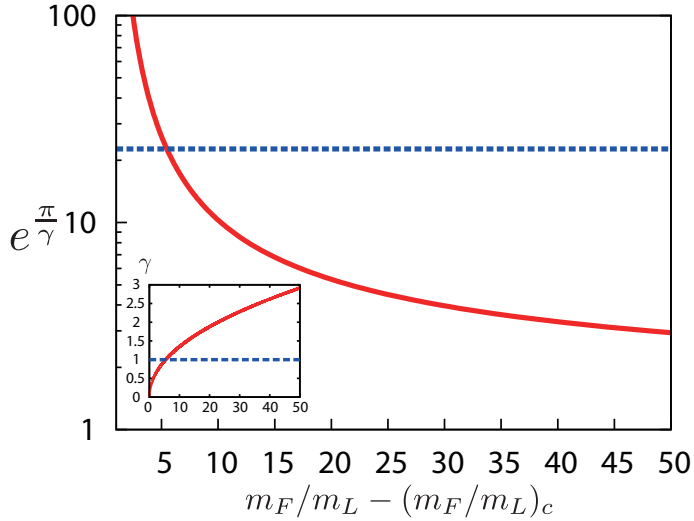

Figure 3.6: The scaling factor $e^{\frac{\pi}{\gamma}}$ as a function of the mass ratio (red solid curve). The blue dotted curve is the scaling factor for three identical bosons $e^{\frac{\pi}{s_0}} = 22.7\ldots$. The inset shows the strength of the effective attraction γ as a function of the mass ratio, together with $s_0 = 1.00624$ for three identical bosons.

where

$$\cot\omega = \frac{\sqrt{1+2\alpha}}{\alpha}. \tag{3.31}$$

The mass ratio dependence of γ and the scaling factor $e^{\frac{\pi}{\gamma}}$ is shown in Fig. 3.6. Right above the critical mass ratio $m_F/m_L \gtrsim 13.606$, the strength of the hyper-radial attraction is small, so that the scaling factor is large. As the mass ratio increases, the scaling factor gets small. For the mass ratio $m_F/m_L \gtrsim 20.0$, the scaling factor becomes smaller than that of three identical bosons or three distinguishable fermions $e^{\frac{\pi}{s_0}}$, $s_0 = 1.00624$ [27, 51]. In ultracold atom experiments, the scaling symmetry of Efimov states has been observed for at most a few sequences. The small scaling factor in the large mass ratio helps observe a longer series of Efimov states [69, 116].

In Fig. 3.5 (a), the energy spectra of the trimers are shown. Note that the following radial scale transformation has been performed for the first-excited and second-excited trimers

$$\begin{aligned} \text{first} - \text{excited} : & K_2 \to K_2 e^{\frac{\pi}{\gamma}}, \qquad (\Lambda a)^{-1} \to (\Lambda a)^{-1} e^{\frac{\pi}{\gamma}}, \\ \text{second} - \text{excited} : & K_3 \to K_3 e^{\frac{2\pi}{\gamma}}, \qquad (\Lambda a)^{-1} \to (\Lambda a)^{-1} e^{\frac{2\pi}{\gamma}}. \end{aligned}$$

The energy spectra almost superimpose into a single universal curve, suggesting that the discrete scale invariance of the Efimov states is satisfied well for most of the region of $1/\Lambda a$. In particular, the discrete scaling holds excellently at unitarity. In Fig. 3.8 (a), binding energies of the ground up to the fourth-excited trimers at unitarity are shown after multiplied by the scale factor $e^{\frac{n\pi}{\gamma}}$. The binding energies of the trimers evolve smoothly from the critical mass ratio. The same behavior is also reported in Ref. [177] for a system interacting with a narrow resonance. The energy spectra superimpose into a single universal curve close to the critical mass $(m_F/m_L)_{\mathrm{E}}$, while the ground-state trimer deviates from the other when the mass ratio gets as large as $m_F/m_L \gtrsim 50$. This means

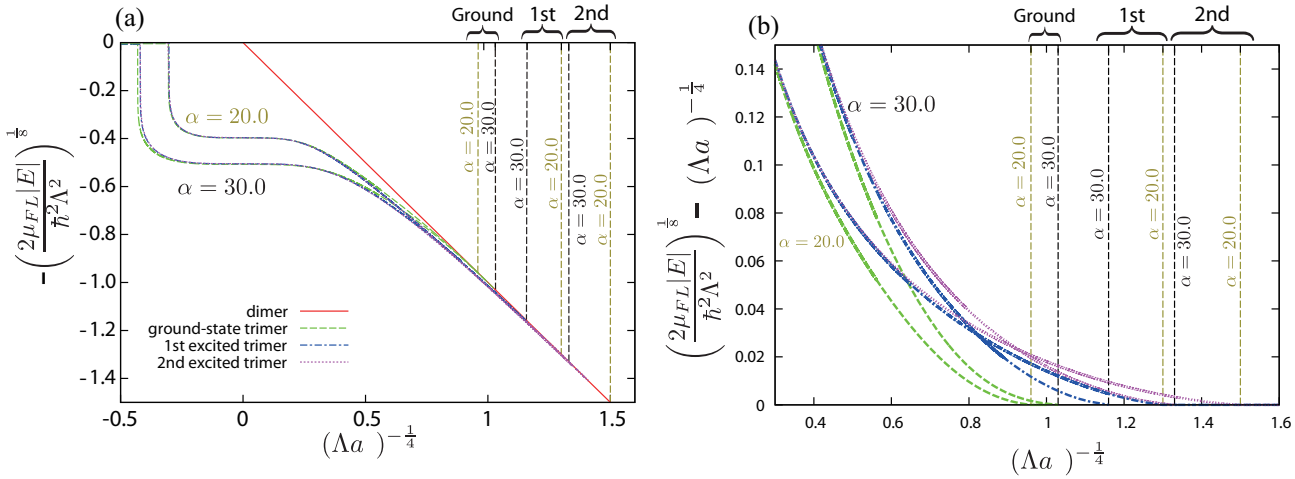

Figure 3.7: (a) Energy spectra of the ground-state, first-excited, and second-excited trimers for $m_F/m_L = 20.0$ and $m_F/m_L = 30.0$. The binding energy is measured from the vacuum. For the first and second-excited trimers, the radial scaling transformation has been performed. On the positive a side, the fermion-dimer dissociation points are shown for each trimer state. (b) Energy spectra close to the atom-dimer dissociation point as measured from the dimer binding energy for $m_F/m_L = 20.0$ and $m_F/m_L = 30.0$. The same radial scaling transformation is performed as in (a). [Figure adapted with permission from S. Endo *et al.*, Phys. Rev. A **86**, 062703 (2012) [176]. Copyright © (2012) by The American Physical Society.]

that all the trimers show the discrete scale invariance with the scale factor predicted in Eq. (3.30) at unitarity when $m_F/m_L \lesssim 50$, while the ground-state trimer deviates from the universal scale factor when $m_F/m_L \gtrsim 50$. This can be quantified further by taking the ratio of the binding energies of the adjacent trimers $\sqrt{\frac{E_n}{E_{n+1}}}$. The results are shown in Fig. 3.8 (b), together with the universal prediction $e^{\frac{n\pi}{\gamma}}$ shown as a black solid curve. For mass ratios $m_F/m_L \lesssim 50$, the discrete scaling law holds for all the trimers including the ground-state and first-excited trimers. This suggests that the Kartavtsev-Malykh trimers for $m_F/m_L < (m_F/m_L)_{\mathrm{E}}$ and $a > 0$ change continuously into the Efimov trimers for $m_F/m_L > (m_F/m_L)_{\mathrm{E}}$ and $1/a = 0$ as the scattering length and the mass ratio are varied. As the mass ratio increases further and so does the binding energy of trimers, the Efimov states gradually become dependent on non-universal short-range details. This is why there appear slight deviations from the universal scaling law in Figs. 3.8 (a) and (b).

As one moves away from the unitarity toward the positive scattering length side, the discrete scale invariance deteriorates. In Fig. 3.7 (b), binding energies of trimers as measured from the fermion-dimer threshold are shown. Again, the radial scale transformation with the scale factor $e^{\pi/\gamma}$ has been performed, so that trimers superimpose into a single curve when the discrete scale invariance is precisely satisfied. One can see that the trimers become less scale invariant as one moves toward the fermion-dimer dissociation point. This can be quantified by observing the position of the fermion-dimer dissociation point $a_n^{(\mathrm{FD})}$. In Fig. 3.8 (d), the ratios of $a_n^{(\mathrm{FD})}$ between the adjacent levels are shown. There are two important features:

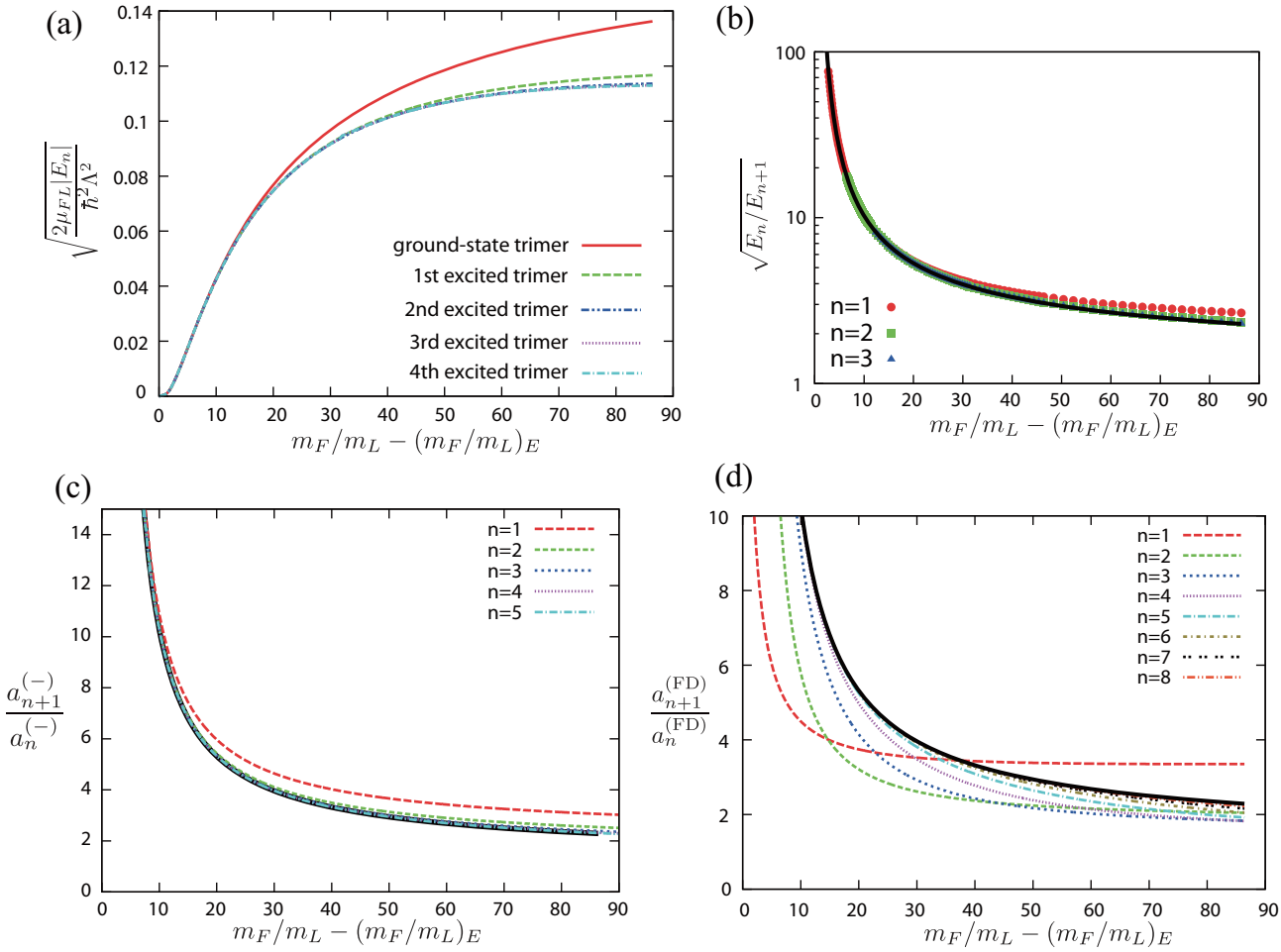

Figure 3.8: (a) Binding energy of the ground to fourth excited trimers at the unitarity limit. The radial scaling transformation has been performed. (b) Ratio of the binding energy between the adjacent trimers at the unitarity limit. (c) Ratio of the *s*-wave scattering length at which the trimer dissociates into three particles. (d) Ratio of the *s*-wave scattering length at which a trimer dissociates into a fermion and a dimer. In (b)-(d), the universal scaling ratio obtained from Eq. (3.30) is also shown as black solid curves. [Figure adapted with permission from S. Endo *et al.*, Phys. Rev. A **86**, 062703 (2012) [176]. Copyright © (2012) by The American Physical Society.]

- For $n = 1$ (ground – first-excited trimers) and $n = 2$ (first-excited – second-excited trimers), the ratio $a_{n+1}^{(\mathrm{FD})}/a_n^{(\mathrm{FD})}$ deviates significantly from the universal value $e^{\pi/\gamma}$.
- For $n \geq 3$, the ratio agrees with the universal value if the mass ratio is not too large $m_F/m_L - (m_F/m_L)_{\mathrm{E}} \lesssim 20$.

The clear difference between the highly excited trimers (≥ 3) and the ground and first-excited trimers is the consequence of the presence of two Kartavtsev-Malykh trimers below the Efimov's critical mass ratio. Indeed, as shown in Fig. 3.5, the ground-state and first-excited trimers exist on the positive a side below the critical mass ratio, and the fermion-dimer dissociation points are well separated from the unitarity (see red solid curves for $a > 0$ in Figs. 3.4 (a)-(c)). This is in marked

contrast with the highly excited trimers. The highly excited trimers appear at the critical mass ratio, so that their fermion-dimer dissociation points are located close to the unitarity point when $m_F/m_L \gtrsim (m_F/m_L)_{\mathrm{E}}$ (see a red solid curve for $a > 0$ in Fig. 3.4 (d)). This is why the ground-state and first-excited trimers are no longer scale invariant close to the fermion-dimer dissociation point, whereas they show a good scaling invariance for $n \geq 3$.

While the ground and first-excited trimers become less scale invariant on the positive scattering length side, they remain scale invariant on the negative scattering length side. One can see this point by observing the position of the three-body threshold $a_n^{(-)}$. In Fig. 3.8 (c), the ratios of the three-body threshold $a_n^{(-)}$ between adjacent levels are shown. One finds that the discrete scaling law holds rather well for most of the region. In contrast to the fermion-dimer dissociation point, the three-body thresholds for all the trimers (red solid curve for $a < 0$ in Figs. 3.4 (a) to (d)) appear from the unitarity point at the critical mass ratio, and the Kartavtsev-Malykh trimers do not affect the behavior of the three-body threshold significantly. For a large mass ratio $m_F/m_L \gtrsim 50$, a slight deviation from the universal discrete scaling law is visible in Fig. 3.8 (c), especially for small n. In this region, the binding energy of the trimers is large, so that the non-universal finite-range effects cannot be neglected.

We note that it is possible in general that the three-body thresholds may appear in the region $8.62 < m_F/m_L < (m_F/m_L)_{\mathrm{E}}$ if the interaction between the fermions is present and its strength is fine-tuned [172]. In this work, the interaction between the fermions is not included, so we do not find such three-body resonance below the Efimov's critical mass ratio.

To summarize, we have arrived at the following conclusions in this section (c.f. statements 5 and 6 in Introduction):

- Close to the unitarity point, the trimers satisfy the discrete scaling law of the Efimov states. Away from the unitarity, the two lowest trimers deviate from the discrete scaling law, while the shallower trimers satisfy the discrete scaling law well for most of the region.

- The trimers dissociate into a fermion and a dimer on the positive a side.

These statements are valid as long as the mass ratio is not too large, so that non-universal short-range effects are negligible. The finite-range effects are discussed in more detail in Sec. 3.2.5.

3.2.4 Crossover trimers

From the discussions so far, the following properties for the ground-state and first-excited trimers have been obtained:

- For $m_F/m_L < (m_F/m_L)_{\mathrm{E}}$, the two trimers satisfy the continuous scale invariance fairly well if and only if the s-wave scattering length is large, $\Lambda a \gg 1$. This Kartavtsev-Malykh region gets small as the mass ratio is increased toward the Efimov's critical mass ratio (see Figs. 3.5 (c) and (d)).

- For $m_F/m_L > (m_F/m_L)_{\mathrm{E}}$, the two trimers show the discrete scale invariance fairly well and thus are the Efimov trimers close to the unitarity limit (see Fig. 3.8 (b)). However, the discrete scale invariance deteriorates close to the fermion-dimer dissociation point (see Fig. 3.8 (d)).

For $m_F/m_L < (m_F/m_L)_{\rm E}$, the Kartavtsev-Malykh trimer regime is identified by r_n, as shown in Figs. 3.4 (a)-(c) and Figs. 3.5(c)(d). In a similar manner, we introduce the following quantity to identify the Efimov trimer region:

$$q_n\left(e^{\frac{\pi}{\gamma}}x\right) \equiv \frac{\left|e^{-\frac{\pi}{\gamma}}K_n\left(e^{\frac{\pi}{\gamma}}x\right) - K_{n+1}(x)\right|}{|K_{n+1}(x) - x|} \quad x \equiv (\Lambda a)^{-1}. \tag{3.32}$$

Here, q_n is zero when the discrete scale invariance holds precisely, and it quantifies how well the trimers show the discrete scaling. In Fig. 3.4, the contours of $q_n = 0.40$ are shown as blue dashed curves. Close to the unitarity point, the discrete scaling law holds well, so that q_n is small. As we move away from the unitarity, the deviation from Efimov's discrete scaling law becomes significant, and q_n increases. We can identify the Efimov trimer as a region with small q_n. As discussed in Fig. 3.8 (d), the breakdown of the scale invariance is significant for the ground-state and the first-excited trimers, while the higher excited trimers are rather scale invariant. If we delimit the Efimov region according to the value of q_n, the Efimov region shrinks as the mass ratio is decreased toward the critical mass ratio, as shown in Fig. 3.4. Close to the critical mass ratio, both the Kartavtsev-Malykh trimer region and the Efimov trimer region shrink, suggesting that the trimers have neither discrete nor continuous scaling invariance. Thus, we arrive at the following conclusions:

- The Kartavtsev-Malykh trimers for $m_F/m_L < (m_F/m_L)_{\rm E}$ change continuously into Efimov trimers for $m_F/m_L > (m_F/m_L)_{\rm E}$ as the mass ratio and the s-wave scattering length are varied.
- In between the Kartavtsev-Malykh and Efimov trimer regions, there exist "crossover trimers," which have neither discrete nor continuous scale invariance.

A change in the scale invariance occurs as a crossover, rather than as an abrupt change. In Fig. 3.4, the crossover trimer regions are shown as red regions. At the critical mass ratio, the trimers exist but they show neither the discrete nor continuous scaling invariance. Thus, we arrive at the first and fourth conclusions listed in Sec. 3.2.1.

The absence of both of the scale invariance can be understood when one sees the hyper-radial potential. At the critical mass ratio, the hyper-radial potential becomes a Coulomb-type attraction $-1/R$ at short distance. This attraction is strong enough to support two bound states when $a > 0$. However, since it is no longer an inverse square attraction, the trimers do not show the discrete scale invariance. Furthermore, the three particles can get close easily since there is no repulsive hyper-radial potential, suggesting that the three-body parameter is relevant for these trimers.

3.2.5 Universal and non-universal trimers

From Sec. 3.2.2 to Sec. 3.2.4, properties of the trimers have been studied by the Skorniakov–Ter-Martirosian equation with a sharp momentum cutoff. The introduction of the momentum cutoff amounts to assuming a certain form of a finite-range boundary condition when the atom and the dimer come close, thereby imposing a specific value of the three-body parameter. However, one can take other forms of short-range models, in general. Thus, one may ask the following question: do the results obtained from Sec. 3.2.2 to Sec. 3.2.4 represent universal features of the trimers for the

two fermions plus one particle system, or do they represent special features of the sharp momentum cutoff? The word "universal" is used here in the sense that the trimers can be characterized only by the three-body parameter and the s-wave scattering length. One way to answer this question is to perform the three-body calculation with different short-range models and compare the results. In this section, the results of the Skorniakov–Ter-Martirosian equation calculated with the two different ways of the momentum cutoffs are compared: the sharp cutoff

$$\int_0^\infty dq \to \int_0^{\Lambda_{\rm S}} dq, \tag{3.33}$$

and the Gaussian cutoff

$$\int_0^\infty dq \to \int_0^\infty dq \exp\left(-\frac{q^2}{2\Lambda_{\rm G}^2}\right). \tag{3.34}$$

If the trimers are universal, the change in the choice of the momentum cutoff is equivalent to changing the value of the three-body parameter. The energy spectra for the two models then differ only by their energy scales specified by their three-body parameters. Thus, by rescaling the energy spectra and thereby taking a common three-body parameter, one should obtain a common universal energy spectrum for the two models. If the energy spectrum $K_{\rm G,S} = \sqrt{\frac{2\mu_{FL}|E_{\rm G,S}|}{\Lambda_{\rm G,S}^2}}$ is plotted as a function of $(\Lambda_{\rm G,S}a)^{-1}$, or $K_{\rm G,S}^{\frac{1}{4}}$ as a function of $(\Lambda_{\rm G,S}a)^{-\frac{1}{4}}$, then the rescaling of the three-body parameter corresponds to a radial scale transformation. Thus, one can study the universality of the trimers by performing a radial scale transformation of the energy spectra and seeing whether they superimpose upon each other.

Note that the universal and non-universal regions determined this way are closely related to the level of approximation of the Skorniakov–Ter-Martirosian approach. In the Skorniakov–Ter-Martirosian equation, inter-particle interactions are replaced by two-body and three-body boundary conditions, representing the s-wave scattering length and three-body parameter, respectively. This approximation is justified by the universality: as long as the scattering length and the three-body parameter are taken to be the same value, energy spectra calculated with the Skorniakov–Ter-Martirosian equation should quantitatively agree with those calculated with other models. If the system is non-universal, short-range details which are not incorporated in the Skorniakov–Ter-Martirosian equation cannot be ignored, so that the results obtained with the Skorniakov–Ter-Martirosian equation will in general deviate from the full quantum calculation with a realistic potential.

The main conclusions in this section are statements 2 and 7 described in Sec. 3.2.1. More specifically, we have found the following:

- For $m_F/m_L < (m_F/m_L)_{\rm E}$, the ground-state trimer is non-universal close to the fermion-dimer dissociation point, while they are universal for the other region. The first-excited and higher-excited trimers are universal for the most region.

- For $m_F/m_L > (m_F/m_L)_{\rm E}$, the ground-state and first-excited trimers are non-universal close to the fermion-dimer dissociation point, while they are universal for the other region.

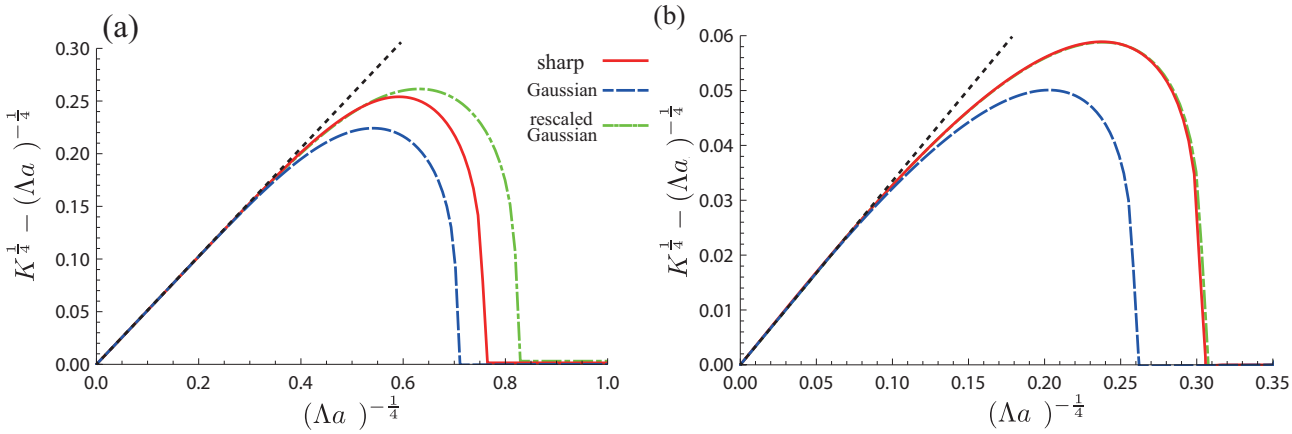

Figure 3.9: Binding energy of the trimers as measured from the dimer binding energy for (a) the ground-state trimer at $m_F/m_L = 10.0$ and (b) the first-excited trimer at $m_F/m_L = 13.3$. The binding energy for the sharp momentum cutoff (red solid curve) and Gaussian momentum cutoff (blue dashed curve) are compared. The binding energy of the Gaussian cutoff after a rescaling of the three-body parameter is also shown as green dashed-dotted curves. The scaling factors are taken to be 1.85 for (a) and 1.90 for (b). The black dotted lines are the linear fits in the large a region. [Figure adapted with permission from S. Endo *et al.*, Phys. Rev. A **86**, 062703 (2012) [176]. Copyright © (2012) by The American Physical Society.]

- For $m_F/m_L > (m_F/m_L)_{\mathrm{E}}$, the higher excited trimers are universal for the entire region, even close to the fermion-dimer dissociation point.
- For a mass ratio well above 50, the binding energy of the trimers becomes so large that the non-universal short-range effects can no longer be neglected.

These results are summarized in Figs. 3.4 and 3.3, in which the universal and non-universal regions are identified.

A. $m_F/m_L < (m_F/m_L)_{\mathrm{E}}$

In Fig. 3.9, the energy spectra of the trimers as measured from the dimer binding energy are shown for $m_F/m_L < (m_F/m_L)_{\mathrm{E}}$. The energy spectra for the sharp and Gaussian momentum cutoffs agree close to the unitarity. This is a direct consequence of the continuous scale invariance of the Kartavtsev-Malykh trimers: they only depend on the s-wave scattering length, so that a change in the momentum cutoff does not affect the energy spectrum.

Away from unitarity, the energy spectra for the sharp and Gaussian cutoffs deviate from the linear behavior of the Kartavtsev-Malykh trimers, and they show different binding energy curves. The two spectra, however, can be superimposed into a single universal curve after performing the rescaling and setting a common value of the three-body parameter if the result is model-independent. The energy spectra after the rescaling are shown in Fig. 3.9. The energy spectra overlap for $(\Lambda a)^{-1/4} \lesssim 0.6$ for the ground-state trimer. This suggests that the trimers are model-independent

in this region. Close to the fermion-dimer dissociation point the two curves do not overlap, which suggests that the ground-state trimer depends on non-universal short-range effects in this region. On the other hand, the first-excited trimer is universal for almost the entire region, as we can see in Fig. 3.9 (b). This difference originates from a smaller binding energy of the first-excited trimer. Since they have smaller binding energy, the non-universal short-range effects are less significant for the first-excited trimer. In particular, the position of the fermion-dimer p-wave resonance is rather universal for the first-excited trimer, while it is non-universal for the ground-state trimer.

Note that the universal region is larger than the Kartavtsev-Malykh region both in Fig. 3.9 (a) and (b). This fact supports our main conclusion schematically illustrated in Fig. 3.3 (a): below the Efimov's critical mass ratio, two trimers exist, which show the continuous scale invariance for a large s-wave scattering length region. These trimers are the Kartavtsev-Malykh trimers. As we vary the s-wave scattering length toward the positive scattering length side, the trimers lose their continuous scale invariance in a model-independent manner. Thus, the Kartavtsev-Malykh trimers changes into the crossover timers. As the s-wave scattering length is varied further, the non-universal short-range effects become significant for the ground-state trimer, while the first-excited trimer is universal for most of the region. As the mass ratio is increased toward the critical value, the Kartavtsev-Malykh region shrinks. The ground-state and first-excited trimers then turn into the crossover trimers for most of the region.

Since the non-universal effects are significant for the ground-state trimer close to the fermion-dimer dissociation point, the fermion-dimer dissociation point may not appear when one considers a system with different short-range details, or different ways of momentum cutoff. In the case of three identical bosons, it has been shown that non-universal finite-range effects can prevent the ground-state Efimov trimer from dissociating into a fermion and a dimer. This is the case for instance for ^{4}He atoms with a scaled realistic potential [10]. For the two fermions and one particle system we study here, a similar situation may occur for the ground-state trimer. In contrast, the finite-range effects are less significant for the first-excited and higher-excited trimers, so they are very likely to dissociate into a fermion and a dimer.

B. $m_F/m_L > (m_F/m_L)_{\mathrm{E}}$

In the inset of Fig. 3.10 (a), the energy spectra at the unitarity limit for the sharp and Gaussian cutoffs are shown. As one can see, the energy spectra seem to be different for the two models. But if the trimers are universal, the two spectra can be superimposed into a single universal curve by rescaling the momentum cutoff and thereby taking a common three-body parameter as we did for the lower mass-ratio region. In the main panel of Fig. 3.10 (a), the ratio of the binding energies at unitarity for the two models are shown. The ratios are almost the same for all the trimer levels at unitarity. This suggests that a common universal scaling factor can be used to perform the radial scale transformation so that the energy spectra calculated with the sharp and Gaussian cutoffs give the common curves. Therefore, the trimers are model-independent and hence universal at unitarity. Note that the universality deteriorates slightly for a large mass ratio $m_F/m_L \gtrsim 50$, since the binding energy of the trimers is too large in this region.

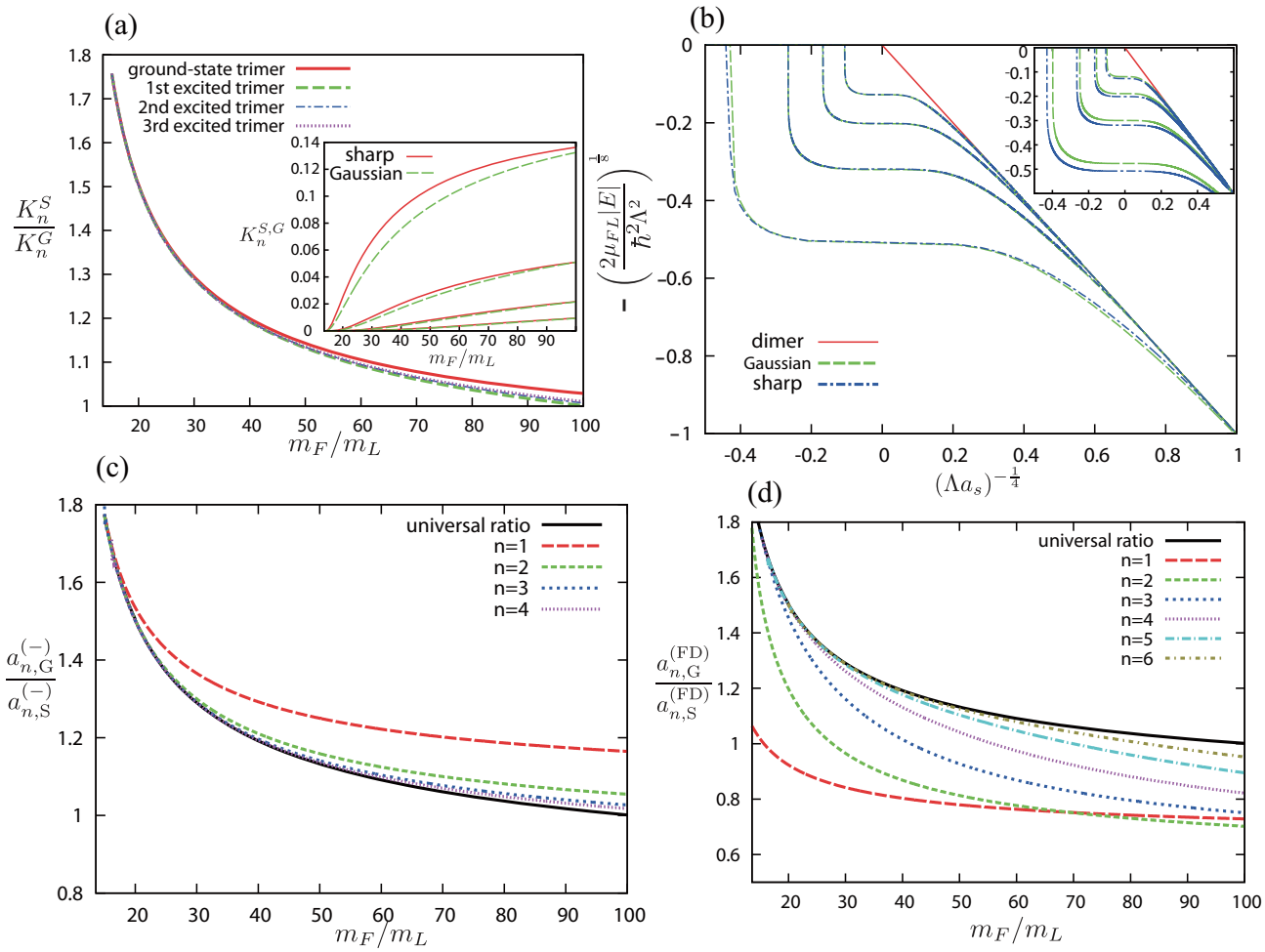

Figure 3.10: (a) Ratio of the binding energy between adjacent trimers at unitarity. Two models are compared: the Skorniakov–Ter-Martirosian equation with a sharp momentum cutoff and the Gaussian cutoff. (b) Energy spectra of the ground-state trimer up to the fourth-excited trimer at $m_F/m_L = 30.0$ for the sharp momentum cutoff (blue dashed-dotted curves) and the Gaussian momentum cutoff (green dashed curves). The radial scaling transformation has been performed, so that the energy spectra with the different cutoffs are superimposed onto universal curves. In the inset, the energy spectra before the radial scaling transformation are shown. (c) Ratio of the *s*-wave scattering length at which the trimer dissociates into three particles. (d) Ratio of the *s*-wave scattering length at which the trimer dissociates into a fermion and a dimer. In (c) and (d), the universal scaling curves between the two models obtained from Fig. 3.10 (a) are shown as the black solid curves. [Figure adapted with permission from S. Endo *et al.*, Phys. Rev. A **86**, 062703 (2012) [176]. Copyright © (2012) by The American Physical Society.]

The rescaling factor between the two models obtained at the unitarity limit can be used to perform the radial scaling transformation, which amounts to setting the same three-body parameter. The energy spectra after this rescaling are shown in Fig. 3.10 (b). One can see that they give the same universal binding energy curves for most of the region, which suggests that most of the

features of the trimers are model-independent. A small disagreement is visible in regions well separated from the unitarity point.

To investigate the universality of the trimers away from the unitarity in more detail, the fermion-dimer dissociation point for $a > 0$ and the three-particle dissociation point for $a < 0$ are studied. In Figs. 3.10 (c) and (d), the ratios between the a's at which the three-body resonance and the fermion-dimer resonance occur are shown. As shown in Fig. 3.10 (c), the ratio of the three-body thresholds agree excellently with each other. They are consistent with the universal scale factor between the sharp and Gaussian cutoffs obtained at unitarity from Fig. 3.10 (a). This suggests that the trimers are model-independent in the negative side of $1/\Lambda a$. Small deviations are visible only when the mass ratio becomes too large and the binding energy of the trimers becomes large. In Fig. 3.10 (d), the ratios of a at which the trimer dissociates into a fermion and a dimer are shown. The ratio between the ground and first-excited trimer ($n = 1$) shows a significant deviation from the universal rescaling factor between the sharp and Gaussian cutoff. This suggests that the non-universal corrections are significant for the ground-state trimer close to the fermion-dimer dissociation point. For the first-excited and higher-excited trimers, on the other hand, the deviation is less significant. This is because the binding energy is small for these trimers, so that they are less affected by the non-universal effects.

These results support our conclusions illustrated in Fig. 3.3 (c). For the second and higher excited trimers, the spectra satisfy Efimov's discrete scaling law, as discussed in Fig. 3.8, and they are universal for the entire region. For the ground-state and first-excited trimers, the spectra satisfy Efimov's discrete scaling law for $1/a < 0$ or close to the unitarity limit. As we change Λa toward the fermion-dimer dissociation point, there is a deviation from the discrete scaling law as presented in Fig. 3.8 (d). This deviation is a universal feature due to the presence of the Kartavtsev-Malykh states below the critical mass ratio, and it is distinct from that induced by non-universal short-range effects. Indeed, one can define the following quantity to characterize the model-independence:

$$s_n(x) \equiv \frac{\left|K_n^{\mathrm{S}}(x) - \beta_{\mathrm{SG}} K_n^{\mathrm{G}}(\beta_{\mathrm{SG}}^{-1} x)\right|}{\left|K_n^{\mathrm{S}}(x) - x\right|} \qquad x \equiv (\Lambda a)^{-1}, \tag{3.35}$$

where $\beta_{\mathrm{SG}} \equiv K_n^{\mathrm{S}}/K_n^{\mathrm{G}}$ is a scaling factor between the two models obtained by taking the ratio of the binding energies at unitarity (c.f. see Fig. 3.10 (a)). Note that this quantity can be defined only above the critical mass ratio $m_F/m_L > (m_F/m_L)_{\mathrm{E}}$. Close to the unitarity limit, s_n is small, indicating that the trimers are model-independent. As we move away from unitarity toward the positive scattering length side, s_n increases, suggesting that the non-universal effects become significant for the ground-state and first-excited trimers. In Figs. 3.4 (a) and (b), the contours of $s_n = 0.90$ are shown as black dashed-dotted curves. These curves can be regarded as boundaries between the universal (model-independent) regions and non-universal (model-dependent) regions. While the boundaries between the Kartavtsev-Malykh trimer region and the Efimov trimer region shrink toward the critical mass ratio, the curves delimiting the universal and non-universal regions are well separated from the unitarity limit. Therefore, the trimers at the critical mass ratio are universal states which are distinct from the Kartavtsev-Malykh trimers or Efimov trimers, as schematically shown in Fig. 3.3 (b). These are universal three-body bound states which show neither continuous nor discrete scale invariance, which we identify as the crossover trimers.

3.3 Kartavtsev-Malykh states and Efimov states in the other systems

In the previous section, the three-body problem of two identical fermions and one distinguishable particle is studied in the $L = 1$, odd parity channel. In this channel, there exist Kartavtsev-Malykh states, Efimov states, and crossover states. In some previous studies, the Kartavtsev-Malykh states and Efimov states have also been demonstrated to exist in other angular-momentum channels [61, 115]: it has been demonstrated that they exist in the odd angular-momentum channels for a system of two identical fermions and one distinguishable particle. They can also exist for a system of two identical bosons and one distinguishable particle in the non-zero even angular-momentum channels. While precise values of the Efimov's critical mass ratios have been obtained in Ref. [115], the Kartavtsev-Malykh states in these higher angular-momentum channels have been studied only in an approximate manner [61], and there has been no precise three-body calculations. In particular, precise values of the critical mass ratios at which the Kartavtsev-Malykh states appear have not been known. In this section, I study the three-body problem of both fermionic and bosonic 2+1 systems in arbitrary angular-momentum channels with the Skorniakov–Ter-Martirosian equation derived in Sec. 3.1. I numerically obtain precise values of the critical mass ratios at which the Kartavtsev-Malykh trimers appear and their binding energies in arbitrary angular-momentum channels for both fermionic and bosonic 2+1 systems. The elastic particle-dimer scattering lengths are also calculated precisely with the Skorniakov–Ter-Martirosian equation. As we will see, the particle-dimer resonances occur at the point where the trimer dissociates into an atom and a dimer. The resonances originating from the Kartavtsev-Malykh states occurs in higher partial-wave channels. As the mass ratio is varied, we find that the Kartavtsev-Malykh states change into the Efimov states. This suggests that similar crossover physics found in Sec. 3.2 may generally appear in the odd angular-momentum channels for the fermionic 2+1 systems and in the nonzero even angular-momentum channels for the bosonic 2+1 systems.

The binding energies of the elastic particle-dimer scattering lengths are obtained by solving Eq. (3.20) numerically. The momentum cutoff is introduced to avoid the Thomas collapse. We use the sharp momentum cutoff in this section. We have taken large cutoff momenta $\Lambda a \gtrsim 1000$ to obtain the universal behavior of the Kartavtsev-Malykh trimers, since as we have shown in Sec. 3.2, the trimers become crossover ones and thus depend on Λ when Λa is not large. By comparing the results calculated for different values of cutoff momenta, one can see whether the results are universally determined by the s-wave scattering length or it explicitly depends on the three-body parameter.

In Fig. 3.11, the particle-dimer elastic scattering lengths and binding energies of the trimers in the $\ell = 0$ channel are shown for both bosonic and fermionic 2+1 systems. Here, I only investigate the positive scattering length side $a > 0$. One can clearly see that the trimers and their associated particle-dimer s-wave resonances exist for the bosonic 2+1 systems while there is no trimer for the fermionic 2+1 system. For the bosonic 2+1 system in this channel shown in the left panel of Fig. 3.11, the Efimov states appear for any mass ratio [115]. The cutoff momentum corresponding to the three-body parameter is relevant for the Efimov states, so that the binding energies and particle-dimer scattering lengths depend explicitly on Λ. On the other hand, as shown in the right

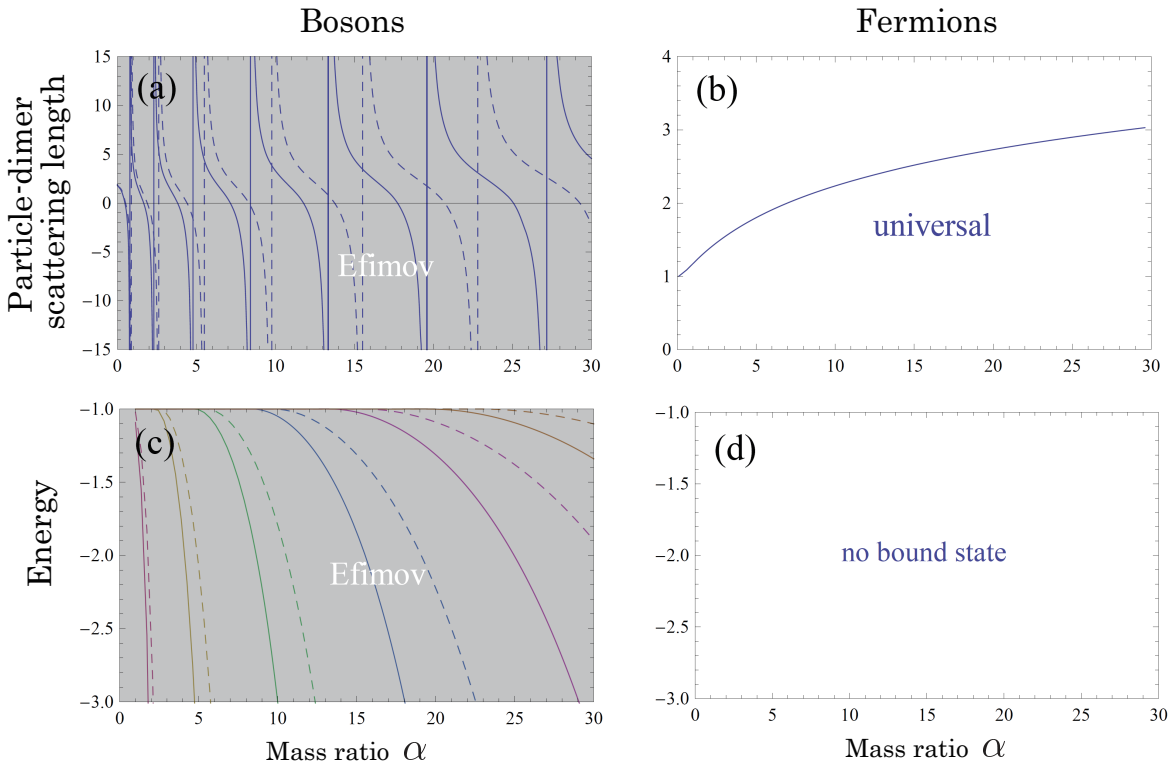

Figure 3.11: S-wave scattering length and binding energy for the bosonic and fermionic cases [155]. (a),(b) S-wave scattering length in units of a, and (c), (d) binding energy of trimers in units of $\frac{\hbar^2}{2ma^2}$ are shown. The gray and white regions are the universal and non-universal regions, respectively. The dashed curves correspond to a momentum cutoff of $\Lambda a = 2000$ and the solid curve to $\Lambda a = 4000$. [Figure reprinted with kind permission from Springer Science+Business Media: S. Endo *et al.*, Few-Body Systems **51**, 207 (2011). Copyright © Springer-Verlag 2011.]

pannel of Fig. 3.11, no trimer appears in this channel. Since there is no trimer and hence no Efimov effect, the three-body system can be universally characterized by the s-wave scattering length. The elastic particle-dimer scattering lengths for $\Lambda a = 2000$ and $\Lambda a = 4000$ agree excellently, suggesting that the elastic particle-dimer scattering length is indeed universal. At equal mass we obtain $a_{AD} = 1.18a$, which is consistent with the well-known value of the fermion-dimer scattering length [132, 148]. The result presented in the top right panel is the same as what was previously reported in Refs. [132, 178].

In the higher angular-momentum channel, the mass ratio plays a crucial role. In Fig. 3.12, the particle-dimer elastic scattering lengths and binding energies of the trimers in the $\ell = 1$ channel are shown. There is no trimer and hence no scattering resonance for the bosonic 2+1 system. Since the Efimov effect does not occur, the particle-dimer p-wave scattering volume is universal and hence it does not depend on the cutoff momentum if $\Lambda a \gg 1$. On the other hand, as shown in the right panel of Fig. 3.12, the fermionic system in the $\ell = 1$ channel supports three-body bound states. This channel is what has been studied in Sec. 3.2. Two Kartavtsev-Malykh states appear at mass ratios 8.172.. and 12.917... [59], and the Efimov effect occurs for $m_F/m_L > 13.606$ [38, 132]. The region above the Efimov's critical mass ratio is shown in gray. Below the Efimov's critical mass ratio, the

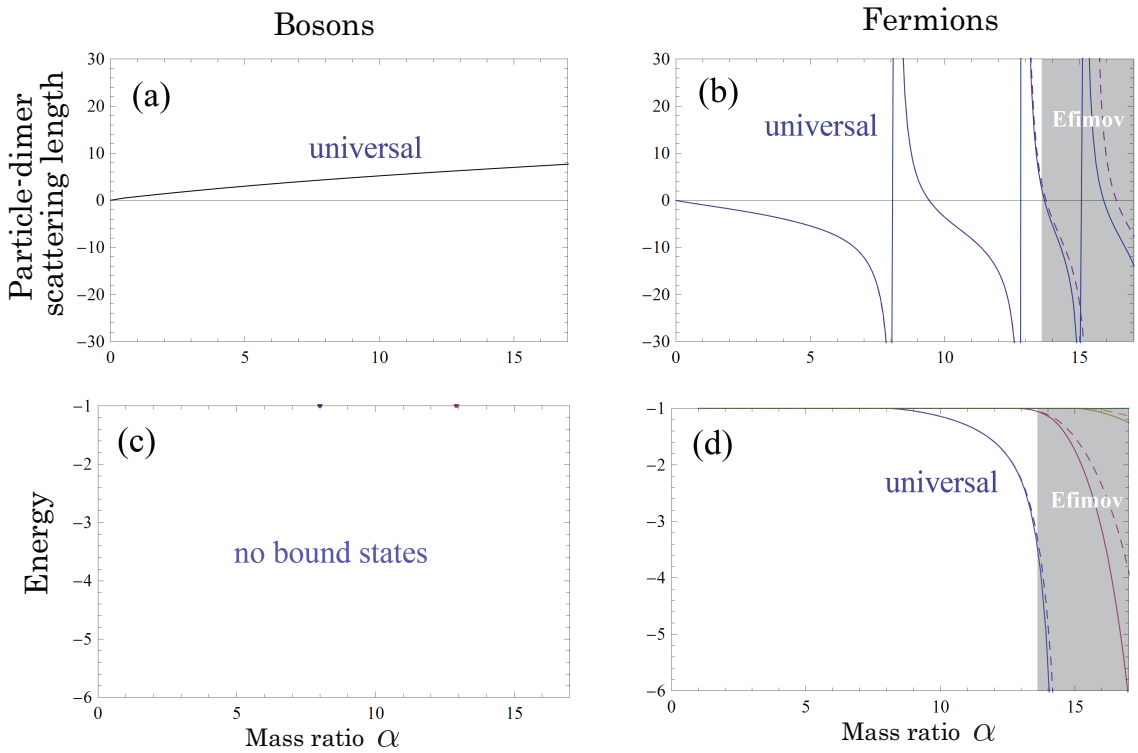

Figure 3.12: P-wave scattering volume, which is denoted here as the "particle-dimer scattering length," and binding energy in units of a^3 and $\frac{\hbar^2}{2ma^2}$, respectively [155]. Notations are the same as those in Fig. 3.11. [Figure reprinted with kind permission from Springer Science+Business Media: S. Endo *et al.*, Few-Body Systems **51**, 207 (2011). Copyright © Springer-Verlag 2011.]

binding energies and the elastic particle-dimer scattering lengths for $\Lambda a = 2000$ and $\Lambda a = 4000$ agree excellently, suggesting that they are universal. For a larger mass ratio $m_F/m_L \gtrsim 13.606$, the binding energies and the elastic particle-dimer scattering lengths for $\Lambda a = 2000$ and $\Lambda a = 4000$ disagree, suggesting that the Efimov effect occurs and the cutoff momenta corresponding to the three-body parameter becomes relevant.

In Fig. 3.13 to Fig. 3.15, the particle-dimer elastic scattering lengths and binding energies of the trimers in the $\ell \geq 2$ channels are shown. Generally, trimers appear in the odd angular-momentum channels for the fermionic 2+1 systems and in the even angular-momentum channels for the bosonic 2+1 systems. This reconfirms the conclusion of the previous pieces of work [61, 179]. Here, we note that the fermionic 2+1 systems in the odd angular-momentum channels and for the bosonic 2+1 systems in the nonzero even angular-momentum channels, the energy spectra and particle-dimer scattering lengths behave in a manner similar to Fig. 3.12. At lower mass ratio, the binding energies of the trimers and the particle-dimer scattering lengths are universal. There are three, four, and five Kartavtsev-Malykh states in the $\ell = 2$, $\ell = 3$, and $\ell = 4$ channels, respectively. The critical mass ratios at which the Kartavtsev-Malykh states appear are shown in Table. 3.1. In Ref. [61], these Kartavtsev-Malykh states have been predicted to exist in these channels, and approximate values of the critical mass ratios have been obtained by solving the hyper-radial Schrödinger equation in the single-channel approximation. Since the Skorniakov–Ter-Martirosian

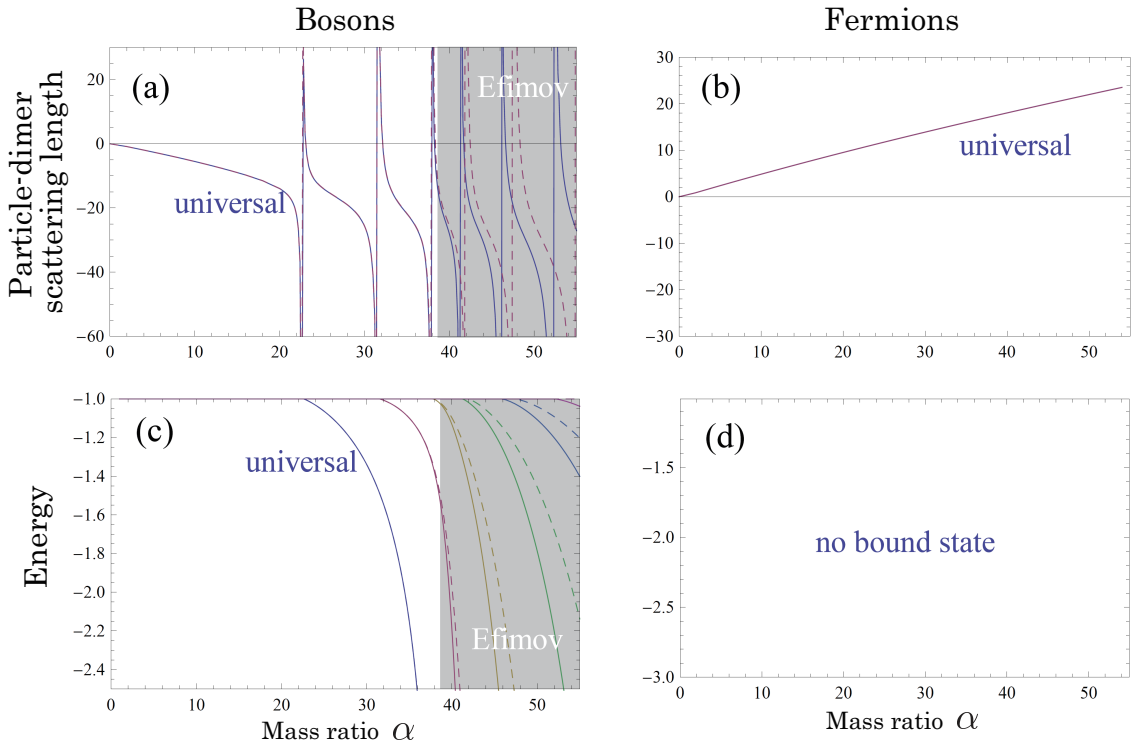

Figure 3.13: D-wave scattering length and binding energy in units of a^5 and $\frac{\hbar^2}{2ma^2}$, respectively [155]. Notations are the same as those in Fig. 3.11. [Figure reprinted with kind permission from Springer Science+Business Media: S. Endo *et al.*, Few-Body Systems **51**, 207 (2011). Copyright © Springer-Verlag 2011.]

equation naturally incorporates all the channel couplings, the mass ratios we find in Table. 3.1 are precise values, refining the approximate mass ratios reported in Ref. [61].

In Table. 3.1, we also show the widths of the particle-dimer resonances in terms of the mass ratio Δ_α for the resonances corresponding to the Kartavtsev-Malykh states. They are obtained by fitting

$$\frac{a_{AD}}{a^{2\ell+1}} \approx \frac{\Delta_\alpha}{\alpha - \alpha_0}, \tag{3.36}$$

where α_0 is the mass ratio at which the Kartavtsev-Malykh states appear. Note that the width of the resonances at $m_F/m_L = 8.172...$ for the fermionic 2+1 system corresponding to the first Kartavtsev-Malykh states is rather broad. Therefore, even when the mass ratio of the system is not close to $m_F/m_L = 8.172...$, a signature of the first Kartavtsev-Malykh states can be observed from an enhanced particle-dimer p-wave cross section. Note that an enhancement of the p-wave particle-dimer scattering well below the mass ratio 8.172 was previously reported in Refs. [59, 60]. The broad width of the resonance is closely related to the small binding energy of the Kartavtsev-Malykh states, as one can see the insets of Figs. 3.5 (a) and (b). This enhancement of the particle-dimer p-wave cross section has been observed in 2013 by the Innsbruck University in a mass-imbalanced fermionic mixture of ^{6}Li-^{40}K (mass ratio 6.64) [62]. We also note that the width of the resonances for some of the Kartavtsev-Malykh states in the other channels are also broad. In

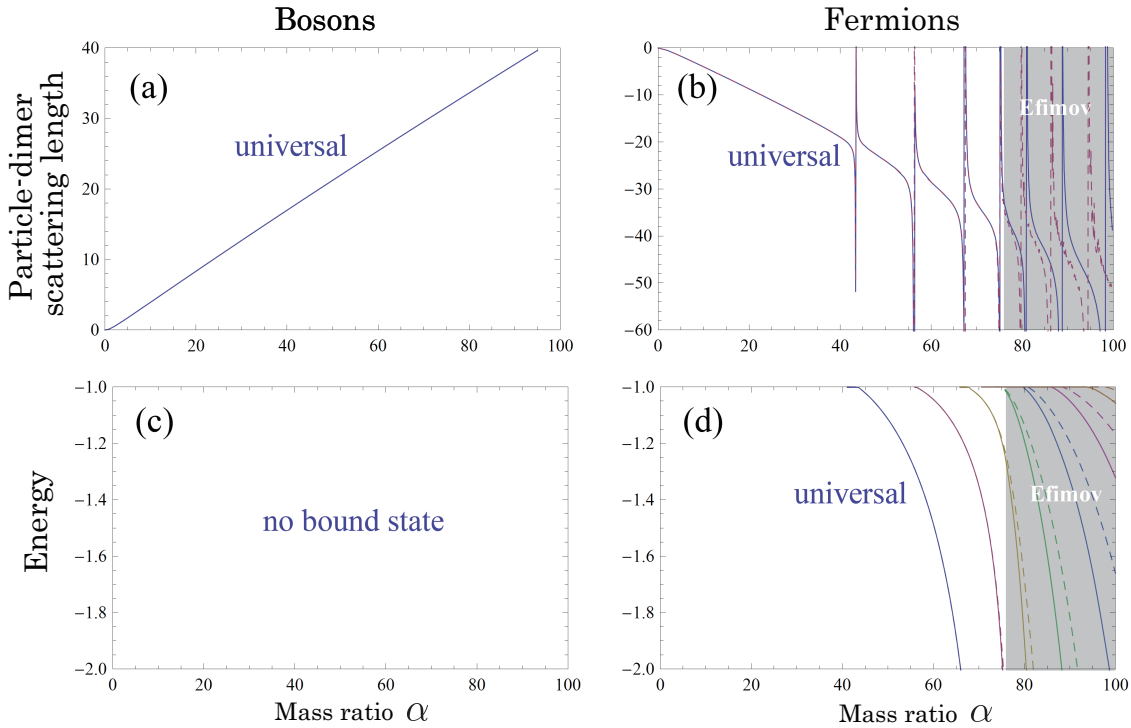

Figure 3.14: F-wave scattering length and binding energy in units of a^7 and $\frac{\hbar^2}{2ma^2}$, respectively [155]. Notations are the same as those in Fig. 3.11. [Figure reprinted with kind permission from Springer Science+Business Media: S. Endo *et al.*, Few-Body Systems **51**, 207 (2011). Copyright © Springer-Verlag 2011.]

particular, the bosonic 2+1 system shows a broad d-wave atom-dimer resonance around $m_F/m_L = 22.637$ and $m_F/m_L = 31.523$. These mass ratios are surprisingly close to that of ^{6}Li-^{133}Cs (mass ratio 22.095) [180, 181] and that of ^{6}Li-^{174}Yb-^{174}Yb (mass ratio 28.917) [57, 58]. These highly mass-imbalanced atomic mixtures have recently been realized in ultracold atoms, and one may observe a signature of the Kartavtsev-Malykh states in the $\ell = 2$ channel from the enhanced atom-dimer d-wave cross section, in a manner similar to what has been done in Ref. [62]. As the angular momentum gets larger, the widths of the resonances tend to get smaller, suggesting that observing the Kartavtsev-Malykh states from the resonant atom-dimer scattering would be more challenging, especially for $\ell \geq 4$.

The behavior of the binding energies and the particle-dimer scattering length presented in Fig. 3.12 are similar to those in Figs. 3.13 to 3.15. This implies that the crossover physics studied in Sec. 3.2 may also apper in the higher angular-momentum channels $\ell \geq 2$. Indeed, when one closely looks at Fig. 3.12 to 3.15, one finds that the binding energies and particle-dimer scattering lengths for $\Lambda a = 2000$ and $\Lambda a = 4000$ deviate from each other not abruptly but gradually. This suggests that the universality gradually deteriorates and turn into the Efimov trimers, as what have been found in Sec. 3.2. Therefore, it is likely that the crossover trimers also appear in the higher angular-momentum channel $\ell \geq 2$, although this point should be studied in more detail in future studies.

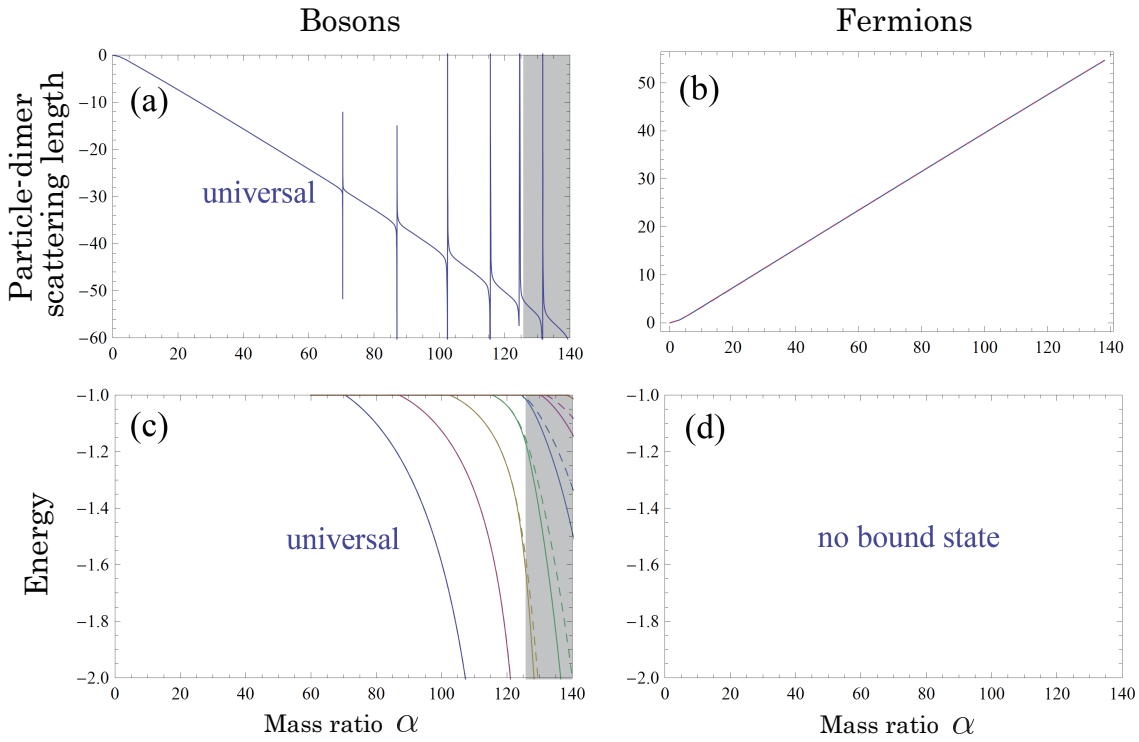

Figure 3.15: G-wave scattering length and binding energy in units of a^9 and $\frac{\hbar^2}{2ma^2}$, respectively [155]. Notations are the same as those in Fig. 3.11. [Figure reprinted with kind permission from Springer Science+Business Media: S. Endo *et al.*, Few-Body Systems **51**, 207 (2011). Copyright © Springer-Verlag 2011.]

3.4 Experimental implications

In this section, I discuss experimental implications of the results presented in Sec. 3.2 and Sec. 3.3. To experimentally observe the properties of the three-body system of two identical fermions and another particle discussed in Sec. 3.2, the following conditions are necessary:

- We need a mixture of fermions without internal degree of freedom (i.e. spin-polarized fermions) and another particle. The statistics of the other particle is arbitrary.
- The interaction between the fermions and the other particle is resonant: $a \gg \Lambda^{-1} \sim r_0$, where r_0 is the range of the interaction.
- The fermions should be much heavier than the other one, i.e., $m_F/m_L \gtrsim 5$.

In ultracold atoms, one can prepare a mixture of two different atomic species. The s-wave scattering length between atoms can be fine-tuned by using a Feshbach resonance [27]. So the first and second conditions seem plausible. It is not easy to realize an atomic mixture with a large mass imbalance, but still it is still feasible. For example, a mixture of ^{6}Li and ^{40}K has been realized, and the Feshbach resonances between ^{6}Li atoms and ^{40}K atoms have been performed [56, 62]. A fermionic mixture with a large mass imbalance is also available, such as a mixture of ^{6}Li and

Table 3.1: Mass ratios at which the Kartavtsev-Malykh states appear, the width of the particle-dimer resonance, and the Efimov threshold for various angular-momentum channels and statistics. For the case of $\ell = 1$, the results are the same as those obtained in Ref. [59]. For higher-angular momenta, we refine the values obtained in Ref. [61]. The Efimov's critical mass ratios shown in the rightmost column are taken form Ref. [115]. Note that the fourth Kartavtsev-Malykh states for $\ell = 3$ has been overlooked in Ref. [155].

ℓ	statistics	Kartavtsev-Malykh state	width of the resonance	Efimov threshold
1	fermions	8.172	9.2	13.607
		12.917	8.1	
2	bosons	22.637	5.9	38.630
		31.523	11.9	
		37.766	8.1	
3	fermions	43.395	1.3	75.994
		56.166	3.7	
		67.336	5.4	
		74.822	9.9	
4	bosons	70.457	0.14	125.765
		87.027	0.50	
		115.534	0.99	
		102.486	1.27	
		124.167	0.81	

^{173}Yb atoms [57, 58]. Although the Feshbach resonance between ^{6}Li and ^{173}Yb atoms has not been realized yet since its width is rather narrow [182], in 2012, the magnetically controlled Feshbach resonance has been observed between Yb atoms by transferring atoms into a metastable excited state [63]. It is expected that with the same technique one may overcome the difficulty and perform the magnetically controlled Feshbach resonant between Yb and Li atoms [64]. We also note that other atoms with a very large mass are currently being cooled down, such as Dy [127, 128], and Er [125, 126]. Atomic mixtures with a large mass imbalance can be realized in ultracold atom experiments.

In Table. 3.2, the mass ratios for some atomic combinations are presented. To observe three-body bound states, one needs a mass ratio larger than $(m_F/m_L)^{(1)}_{\rm KM} = 8.172....$ To realize such a highly mass-imbalanced atomic mixture, one must prepare light atoms, such as Li, and heavy atoms, such as Sr, Yb, Er, and Dy. One can see from Table. 3.2 that among those satisfying $m_F/m_L > (m_F/m_L)^{(1)}_{\rm KM}$, most of them are in the region $m_F/m_L > (m_F/m_L)_{\rm E} = 13.606....$ The Efimov trimers and the crossover trimers can be observed with those atomic combinations. To observe the Kartavtsev-Malykh trimers and associated crossover trimers, on the other hand, there are only a few candidates. With current technique, it seems rather challenging to prepare these atomic mixtures and utilize a Feshbach resonance. We note that in ultracold atoms, the effective masses of the atoms can be varied by an optical lattice [183]. If the s-wave scattering length is fine-tuned to be much larger than the lattice spacing of the optical lattice, the effect of the lattice is only to alter the

Table 3.2: Mass ratios for some atomic species. The horizontal lines corresponds to the critical mass ratios for the appearance of the Kartavtsev-Malykh states $(m_F/m_L)^{(1)}_{\rm KM} = 8.172...$ and the Efimov states $(m_F/m_L)_E = 13.606...$, respectively.

Species	Mass ratio
^{7}Li–^{40}K	5.70
^{7}Li–^{43}Ca	6.12
^{6}Li–^{40}K	6.64
^{23}Na–^{161}Dy	7.00
^{23}Na–^{167}Er	7.26
^{23}Na–^{173}Yb	7.52
^{7}Li–^{53}Cr	7.55
^{6}Li–^{53}Cr	8.80
^{9}Be–^{87}Sr	9.64
^{7}Li–^{87}Sr	12.39
^{6}Li–^{87}Sr	14.45
^{7}Li–^{161}Dy	22.94
^{7}Li–^{167}Er	23.79
^{7}Li–^{173}Yb	24.65

effective mass of the atoms. By tailoring the shape and depth of the optical lattice, one may alter the masses of the particles and study the three-body system by varying both the mass ratio and the s-wave scattering length. We also note that the Kartavtsev-Malykh trimers appear for smaller mass ratios in one and two spatial dimensions [161, 162], although the crossover physics may not appear in these systems due to the absence of the Efimov effect in one and two dimensions [32, 115].

In ultracold atoms, Efimov states has often been observed indirectly by measuring the atomic losses [27, 69], but recently a photoassociation technique has been used to observe the Efimov trimers directly [51, 52, 160]. With this technique, one can directly associate the trimers and measure their binding energy. By precisely measuring the binding energies of the trimers by varying the s-wave scattering length, one can check how well the continuous or discrete scaling law holds. The deviation from the scale invariance as described in Fig. 3.3 (a) and (c) can be a clear signature of the crossover trimers. Note that the breakdown of the continuous and discrete scaling is essentially different from that induced by non-universal corrections discussed for the ground-state Efimov trimer in Refs. [54, 69]. While the latter depends significantly on short-range details of each atoms, the continuous and discrete scaling is lost in a universal manner, which can be quantitatively predicted theoretically with the universal theories, such as the Skorniakov–Ter-Martirosian equation, or the effective field theory [32].

The three-body bound states can be also studied by observing the p-wave atom-dimer resonance. The atom-dimer cross section is easier to observe than directly measuring binding energies of the trimers. In Fig. 3.16 the atom-dimer s-wave scattering length (inset) and p-wave scattering volume (main panel) are shown as a function of $1/\Lambda a$ for several mass ratios $m_F/m_L > 8.172$. The

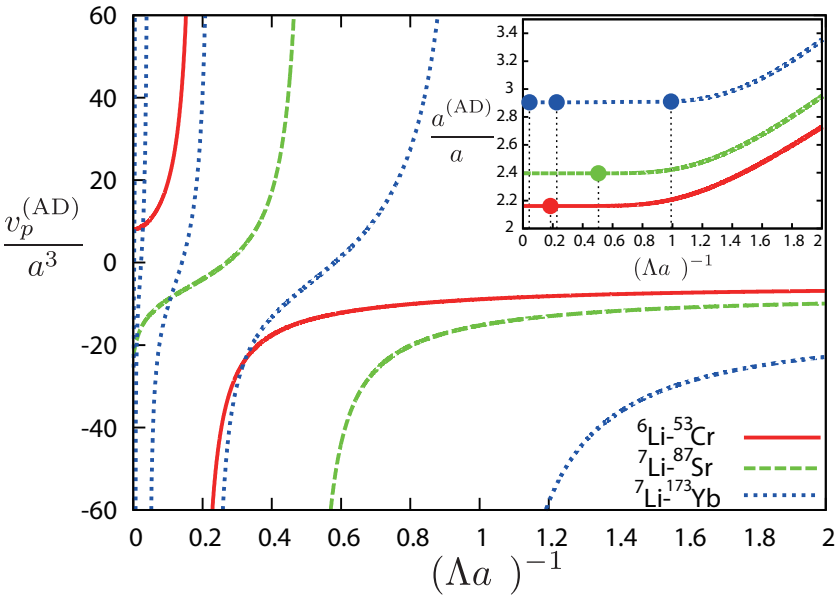

Figure 3.16: Atom-dimer P-wave scattering volume $v_p^{(\mathrm{AD})}$ for ^{6}Li–^{53}Cr (red solid curve, m_F/m_L = 8.80), ^{7}Li–^{87}Sr (green dashed curve, m_F/m_L = 12.39), and ^{7}Li–^{173}Yb (blue dotted curve, m_F/m_L = 24.65), calculated with the Skorniakov–Ter-Martirosian equation with the sharp momentum cutoff. In the inset, the s-wave atom-dimer scattering length for each atomic combination is shown. The points show the p-wave atom-dimer resonance positions for each atomic combination. [Figure adapted with permission from S. Endo *et al.*, Phys. Rev. A **86**, 062703 (2012) [176]. Copyright © (2012) by The American Physical Society.]

three-body bound states induce atom-dimer scattering resonances, as discussed in Sec. 3.3. Close to the atom-dimer dissociation point, the atom-dimer p-wave scattering volume becomes resonantly large, while the atom-dimer s-wave scattering length remains of the order of the atom-atom s-wave scattering length. For $8.172 < m_F/m_L < 13.606$, the atom-dimer p-wave resonance is a smoking gun for the existence of the crossover trimer: the trimers can dissociate into an atom and a dimer due to the breakdown of the continuous scaling of the Kartavtsev-Malykh states as illustrated in Fig. 3.3 (a). In particular, the position of the p-wave atom-dimer resonance for the first-excited trimer is determined universally.

Even when $m_F/m_L < 8.172$ and no trimer exists, one can observe a signature of the trimers by measuring the p-wave atom-dimer cross section. As studied in Ref. [60] and Sec. 3.3, the width of the atom-dimer p-wave resonance in terms of the mass ratio is rather broad and one can still observe a signature of the Kartavtsev-Malykh trimer even for a fermionic mixture with a smaller mass imbalance. In 2013, the enhancement of the atom-dimer p-wave cross section has been observed spectroscopically for a mass-imbalanced fermionic mixture of ^{6}Li-^{40}K (mass ratio 6.64) [62]. While the Kartavtsev-Malykh trimer has not been observed yet, this experiment is a good evidence for the Kartavtsev-Malykh trimer in the fermionic 2+1 system. From the results presented in Sec. 3.3, I predict that a similar enhancement of the atom-dimer scattering can be observed in a Bose-Fermi mixture of ^{6}Li-^{133}Cs atoms (mass ratio 22.095) [180, 181] and ^{6}Li-^{174}Yb

atoms (mass ratio 28.917) [57, 58]. The mass ratios for these atomic mixtures are surprisingly close to the mass ratios at which the Kartavtsev-Malykh trimers appear in the $\ell = 2$ channel, 22.637 and 31.523. This suggests that the d-wave atom-dimer scattering length is enormously large for these atomic mixtures. In fact, the d-wave atom-dimer scattering lengths are $a_{AD}/a^5 = -24.18$ and $a_{AD}/a^5 = -21.14$ for mass ratios corresponding to ^{6}Li-^{133}Cs and ^{6}Li-^{174}Yb, respectively. A mixture of ^{6}Li and ^{133}Cs atoms have been realized and the inter-species Feshbach resonance has been performed recently [180, 181]. Although the Efimov states in the $\ell = 0$ induces an atomic loss in this system, the enhanced d-wave atom-dimer cross section may be observed in this system. For ^{6}Li and ^{174}Yb atoms, the Feshbach resonance has not been realized yet, but may be realized in near future by transferring atoms into long-lived excited states [63, 64].

Chapter 4

Universal three-body parameter of the Efimov states

As explained in detail in the introduction and in Sec. 2.4, the Efimov states have recently been observed in ultracold atom experiments for various atomic species, and their three-body parameters have been found to be universally determined by the van der Waals length for a system of three identical bosons in the vicinity of a broad Feshbach resonance. These observations have surprised researchers working on the Efimov physics in ultracold atoms. While the long-range part of the inter-atomic interaction share the same van der Waals form $-C_6/r^6$, the short-range part depends on details of electronic configurations of the atoms, and it can thus vary significantly for different atoms and hyperfine states. Until quite recently, it had been widely held that this non-universal short-range part can significantly affect the short-range three-body phase, rendering the three-body parameter non-universal.

In this chapter, I elucidate the physical origin of the universal three-body parameter, explaining under what conditions and why the three-body parameter can be universal. But before proceeding to the main part of this chapter, let me first rephrase the issue in more theoretical terms and try to define when the three-body parameter is called "universal" or "non-universal". In this chapter, we consider a system of three identical bosons in the vicinity of a broad Feshbach resonance. For two particles interacting via a broad Feshbach resonance, the particles mostly reside in an open channel, so that one can model their low-energy behavior accurately by a single-channel potential in the vicinity of a shape resonance (see Sec. 2.1.1 and Ref. [24]). Let us therefore consider a three-body Schrödinger equation

$$\left[-\sum_{i=1}^{3}\frac{\hbar^2\nabla_{\boldsymbol{r}_i}^2}{2m}+V(r_{12})+V(r_{23})+V(r_{13})+V_{3B}(\boldsymbol{r_1},\boldsymbol{r_2},\boldsymbol{r_3})\right]\Psi(\boldsymbol{r_1},\boldsymbol{r_2},\boldsymbol{r_3})=E\Psi(\boldsymbol{r_1},\boldsymbol{r_2},\boldsymbol{r_3}), \tag{4.1}$$

where $V(r)$ is a two-body potential which is fine-tuned to be in the vicinity of a shape resonance, and V_{3B} is a three-body potential. For neutral atoms, the inter-atomic potential has the van der Waals tail, so let us assume here that $V(r)\to-\dfrac{C_6}{r^6}$ at long distance. The three-body potential V_{3B} is effective only when three particles get close simultaneously. For neutral atoms, its range is known to be rather small $r_0 \ll r_{\mathrm{vdW}}$ [164], so we assume that the range of V_{3B} is much smaller than the van der Waals length. By solving the three-body Schrödinger equation for a specific choice of V

and V_{3B}, one obtains the three-body parameter numerically. Now, let us prepare another pair of V and V_{3B} by changing the short-range part of the two-body or three-body potentials while keeping the s-wave scattering length:

$$V' = V(r) + \Delta V(r), \tag{4.2}$$

$$V'_{3B} = V_{3B}(r) + \Delta V_{3B}(r). \tag{4.3}$$

Here, $\Delta V(r)$ and $\Delta V_{3B}(r)$ are introduced to model changes in the short-range part of the inter-atomic potentials when an atomic species or a hyperfine state is varied. The ranges of $\Delta V(r)$ and $\Delta V_{3B}(r)$ are assumed to be much smaller than $r_{\rm vdW}$. Now, let us solve the three-body Schrödinger equation for V' and V'_{3B} and compare its three-body parameter with that of V and V_{3B}. If the three-body parameters for V and V_{3B} and for V' and V'_{3B} agrees with high precision for a wide variety of choice of $\Delta V(r)$ and $\Delta V_{3B}(r)$, the three-body parameter is regarded as universal.

To the best of the author's knowledge, it has not yet been defined clearly in any literature what is the theoretical definition of the universality in the three-body parameter, but it seems that the above definition has been used implicitly in most theoretical studies on this issue [72, 73, 147, 168, 184]. Therefore, I adopt this definition in this chapter too. Note however that the definition is rather subjective and mathematically not well-defined: it depends on what one regards as "high precision" or " a wide variety of potentials". For the criterion of the "high precision", the universal scale factor is one possible reference value to compare with. If one assumes that $\Delta V(r)$ and $\Delta V_{3B}(r)$ can alter the short-range three-body phase significantly, the three-body parameter should vary randomly within a factor of the fundamental period $e^{\pi/s_0} = 22.7....$ If the ratio between the three-body parameters for different pairs of V and V_{3B} is much smaller than 22.7, one may regard it as universal. Another experiments-based criterion is to compare with the experimental results $a_-^{(1)}/r_{\rm vdW}$ =-8-10 and see whether the theoretically found three-body parameter is consistent or not.

Now that the universality has been defined from a theoretical point of view, let us introduce some relevant previous studies. In Ref. [72], C. Chin points out that a strongly attractive van der Waals interaction is essential. For typical neutral atoms, an inter-atomic potential supports many two-body bound states, which implies that the strength of the van der Waals interaction C_6 is rather strong. He assumes that the strong two-body van der Waals attraction leads to a strong hyper-radial potential $-3 \times C_6/R^6$. Since C_6 is large and the hyper-radial potential is strongly attractive, he then argues that it can induce quantum reflection between three atoms. Since three particles are reflected in the van der Waals region $R \gtrsim r_{\rm vdw}$, they are insensitive to a change in the short-range part of an inter-atomic potential, so that three-body physics is determined solely by the long-range part of the inter-atomic interaction, i.e., the van der Waals interaction. At first sight this argument seems plausible, but there are several problems. First of all, in Ref. [10], the three-body parameter for ^{4}He atoms has been calculated theoretically by using a realistic ^{4}He potential (LM2M2), and found to be $a_-^{(1)}/r_{\rm vdW} = -9.42$, which is in excellent agreement with the universal value observed in ultracold atom experiments. Since the van der Waals interaction between ^{4}He atoms is rather weak and supports only one two-body bound state, the argument presented in Ref. [72] cannot explain why the three-body parameter for ^{4}He atoms agrees with the universal value reported in ultracold atom experiments. Furthermore, the quantum reflection scenario can be similarly applied to two particles, and it suggests that that the s-wave scattering length should also be universally

determined by van der Waals length. However, this is not the case: the s-wave scattering length is known to vary almost randomly between different atomic species and hyperfine states.

This second point is worthwhile to note. For ultracold atoms, the s-wave scattering length, which characterizes a two-body short-range phase, is known to be strongly dependent on atomic species and hyperfine states. On the other hand, the three-body parameter, which characterizes a three-body short-range phase, has been found to be independent of atomic species and hyperfine states. Why is two-body physics non-universal, while three-body physics is universal? If one tries to explain the physical origin of the universal three-body parameter, one must at the same time explain consistently why the s-wave scattering length is non-universal.

In Ref. [73], J. Wang and coworkers have numerically solved the three-body problem for various types of two-body potentials, and they have shown that a strong three-body repulsion appears in the hyper-radial potential when a two-body potential is strongly attractive or has a hard-core repulsion at short distance. Typical neutral atoms correspond to the former, while the ^{4}He potential corresponds to the latter. The shape of the three-body repulsion has been found to be rather universal, in the sense that it is independent of details of a two-body potential. The repulsion appears at a rather large distance $R \approx 2r_{\rm vdw}$, rendering changes in the short-range part $\Delta V(r)$ and $\Delta V_{3B}(r)$ irrelevant. By solving the three-body Schrödinger equation numerically, they have obtained the three-body parameter $a_-^{(1)} = -(8\text{-}12)r_{\rm vdW}$ for various types of strongly attractive two-body potentials and for potentials with a hard-core repulsion. While it has become clear with this work that the three-body parameter should be universal for a strongly attractive two-body potential or a two-body potential with a hard-core repulsion, the physical mechanism still remains unclear. Namely, the following questions remain unresolved:

Q1. What is the physical origin of the three-body repulsion?

Q2. Why is the three-body repulsion universal?

Q3. Why are a strongly attractive two-body potential and a two-body potential with a hard-core repulsion relevant?

Q4. Why is the s-wave scattering length non-universal, while the three-body parameter is universal?

I address the physical origin of the universal three-body parameter and give clear answers to all these questions[§]. In Sec. 4.1, I present answers to the above questions as follows:

A1. When three particles get close, a non-adiabatic deformation of the three-body wave function occurs due to a suppression of probability which occurs when two particles get close. This deformation of the three-body wave function results in a strong three-body repulsion.

A2. Because the suppression of the two-body probability occurs in a universal manner.

[§]*A remark on the contribution:* The work presented in this chapter has been done in close collaboration with P. Naidon at RIKEN. The author's contribution and the coworker's contribution are rather complimentary, so I include in this thesis some of the results obtained by the coworker in addition to my contribution.

A3. Because the suppression of the two-body probability occurs for a strongly attractive two-body potential and for a two-body potential with a hard-core repulsion.

A4. Because the deformation can occur only for a system with more than two particles: a three-body system has the hyper-angular degree of freedom which characterizes the deformation of the three-body configuration, while a two-body system has no such degree of freedom.

In Sec. 4.2, the three-body parameter for non-van der Waals types of potentials is discussed based on the physical mechanism elucidated in Sec. 4.1. It is argued in Sec. 4.2.1 that the three-body parameters for a wide class of potentials should be characterized by the effective range. This conjecture is confirmed numerically in Sec. 4.2.2, and two classes of two-body potentials are identified, for which the three-body parameter has a universal value in units of their effective range. One class corresponds to short-range two-body potentials decaying as a power law, relevant to atomic interactions, for which the two-body correlation behaves smoothly. The other corresponds to deep two-body potentials decaying exponentially, relevant to nuclear systems, for which the two-body correlation shows a discontinuity.

4.1 Physical origin of the universal three-body parameter for atomic Efimov states

In this section, we elucidate the physical origin of the universal three-body parameter for particles interacting via a van der Waals type of potential. Throughout this section, we use the low-energy Faddeev equation to deal with the three-body problem [150]. There are several different ways of formulating the low-energy Faddeev equation [32, 115, 150], which can often confuse the readers. Therefore, in Sec. 4.1.1, I briefly summarize the low-energy Faddeev equation we use in this chapter. The advantage of the low-energy Faddeev equation is its simplicity: it is a one-dimensional linear integro-differential equation, which is much simpler than solving the original three-body Schrödinger equation. One drawback of the low-energy Faddeev equation is that it neglects higher-partial-wave channels. In Sec. 4.1.1 solutions of the low-energy Faddeev equation are compared with those obtained in Ref. [73], which includes most of the higher-partial-wave channels. It is then shown that the low-energy Faddeev equation qualitatively reproduce all the features reported in Ref. [73], justifying the use of the low-energy Faddeev equation to study the universality of the three-body parameter. Thus, Sec. 4.1.1 is devoted mostly to review and confirm the previous results.

One of the main parts of our work[§] is presented in Sec. 4.1.2. I explain in Sec. 4.1.2 the physical mechanism why the three-body parameter becomes universal, giving answers to all the questions listed above.

[§] *A remark on the contribution:* Contributions of the author and the coworker P. Naidon in this section are as follows:
- Numerical calculations of the low-energy Faddeev equation: P. Naidon
- Proposal of the non-adiabatic deformation scenario described in Sec. 4.1.2: S. Endo
- Proposal of the model wave function in Eq. (4.19) and calculations with it: S. Endo

4.1.1 Hyper-radial potential in the low-energy Faddeev formalism

Low-energy Faddeev equation

While the low-energy Faddeev equation was first derived in Ref. [150], we use a slightly different formalism from the original one. Throughout this chapter, we use the low-energy Faddeev equation formulated in Ref. [115]. It turns out that the theoretical description becomes much simpler in this formalism compared with that in Refs. [32, 150].

In the formalism introduced in Ref. [115], one first expands the three-body wave function by adiabatic hyper-angular bases as in Eq. (2.37). One then decomposes the hyper-angular wave function $\Phi_n(R, \alpha_3, \hat{\boldsymbol{r}}_{\mathbf{12}}, \hat{\boldsymbol{\rho}}_{\mathbf{3}})$ into Faddeev components (see Eq. (2.50)):

$$\Phi_n(R, \alpha_3, \hat{\boldsymbol{r}}_{\mathbf{12}}, \hat{\boldsymbol{\rho}}_{\mathbf{3}}) = \frac{\psi_n(R, \alpha_1)}{\sin 2\alpha_1} + \frac{\psi_n(R, \alpha_2)}{\sin 2\alpha_2} + \frac{\psi_n(R, \alpha_3)}{\sin 2\alpha_3}. \tag{4.4}$$

Here, we have neglected the angular dependence of the Faddeev component $\psi_n(R, \alpha_i, \hat{\boldsymbol{r}}_{\boldsymbol{jk}}, \hat{\boldsymbol{\rho}}_{\boldsymbol{i}}) \approx \psi_n(R, \alpha_i)$, since the zero-angular-momentum channel is energetically most favored and gives the most dominant contribution. The Faddeev components then obey the following equation (see Eq. (2.52)):

$$\begin{aligned} 0 = &\left[-\frac{\partial^2}{\partial\alpha_3^2} - 4 + R^2 u(R\sin\alpha_3) - \lambda_n(R)\right]\psi_n(R, \alpha_3) \\ &+ R^2 u(R\sin\alpha_3)\left[\frac{\sin 2\alpha_3}{\sin 2\alpha_1}\psi_n(R, \alpha_1) + \frac{\sin 2\alpha_3}{\sin 2\alpha_2}\psi_n(R, \alpha_2)\right], \end{aligned} \tag{4.5}$$

where

$$u(x) = \frac{m}{\hbar^2}V(x). \tag{4.6}$$

By taking the angular average of Eq. (4.5) with respect to $\hat{\boldsymbol{r}}_{\mathbf{12}}$ and $\hat{\boldsymbol{\rho}}_{\mathbf{3}}$, the last term written in terms of α_1 and α_2 can be rewritten by the coordinate α_3:

$$\left\langle \frac{\sin 2\alpha_3}{\sin 2\alpha_1}\psi_n(R, \alpha_1)\right\rangle_{\hat{\boldsymbol{r}}_{\mathbf{12}}, \hat{\boldsymbol{\rho}}_{\mathbf{3}}} = \left\langle \frac{\sin 2\alpha_3}{\sin 2\alpha_2}\psi_n(R, \alpha_2)\right\rangle_{\hat{\boldsymbol{r}}_{\mathbf{12}}, \hat{\boldsymbol{\rho}}_{\mathbf{3}}} = \frac{2}{\sqrt{3}}\int_{\left|\alpha_3 - \frac{\pi}{3}\right|}^{\frac{\pi}{2} - \left|\frac{\pi}{6} - \alpha_3\right|} d\beta\psi_n(R, \beta). \tag{4.7}$$

This procedure is called the kinematic rotation [32, 115, 150]. One then obtains the low-energy Faddeev equation:

$$0 = \left[-\frac{\partial^2}{\partial\alpha_3^2} - 4 + R^2 u\left(R\sin\alpha_3\right) - \lambda_n(R)\right]\psi_n(R, \alpha_3) + \frac{4}{\sqrt{3}}R^2 u\left(R\sin\alpha_3\right)\int_{\left|\alpha_3 - \frac{\pi}{3}\right|}^{\frac{\pi}{2} - \left|\frac{\pi}{6} - \alpha_3\right|} d\beta\psi_n(R, \beta). \tag{4.8}$$

Solving this one-dimensional integro-differential equation numerically, one obtains $\lambda_n(R)$ and $\psi_n(R, \alpha)$. The hyper-radial part obeys the hyper-radial Schrödinger equation (2.39). Once ψ_n is obtained numerically, the non-adiabatic couplings Q_{nm} and P_{nm} can be computed numerically from Eqs. (2.40), (2.41), and (4.4).

The low-energy Faddeev equation is a simple one-dimensional integro-differential equation so it can easily be solved numerically. The hyper-radial equation is a coupled one-dimensional second-order differential equation, and it is also numerically feasible. Note that these procedures are far easier than solving the full three-body Schrödinger equation. One major disadvantage is that we have assumed that the higher-partial-wave contributions to the Faddeev component is small, and we have taken it to be $\psi_n(R, \alpha_i, \hat{\boldsymbol{r}}_{\boldsymbol{jk}}, \hat{\boldsymbol{\rho}}_{\boldsymbol{i}}) \approx \psi_n(R, \alpha_i)$. Crudely speaking, this approximation amounts to assuming that the i-th particle affects the relative motion between the j-th and k-th particles in a manner similar to the "mean field", which is averaged out for all possible angular configurations. As we will discuss later, this approximation does not affect our qualitative argument on the physical origin of the three-body parameter, but it does affect some quantitative details.

From the normalization of the hyper-angular wave function in Eq. (2.44), the diagonal part of the non-adiabatic couplings can be shown to be

$$P_{nn}(R) = 0, \tag{4.9}$$

$$Q_{nn}(R) = -\frac{\hbar^2}{m}\left\langle \Phi_n \left| \frac{\partial^2}{\partial R^2} \right| \Phi_n \right\rangle = \frac{\hbar^2}{m}\left\langle \frac{\partial \Phi_n}{\partial R} \middle| \frac{\partial \Phi_n}{\partial R} \right\rangle \geq 0. \tag{4.10}$$

Thus, if one neglects the couplings to different channels, one obtains a single-channel hyper-radial equation:

$$\left[-\frac{\hbar^2}{m}\frac{\partial^2}{\partial R^2} + U_n(R) - \frac{\hbar^2}{4mR^2} \right] f_n(R) = E\, f_n(R), \tag{4.11}$$

$$U_n(R) = \frac{\hbar^2\left[\lambda_n(R) + 4\right]}{mR^2} + Q_{nn}(R). \tag{4.12}$$

One can see that the effect of the non-adiabatic part is to add a repulsive hyper-radial potential $Q_{nn}(R) \geq 0$. As we will find in Sec. 4.1.2, this repulsive non-adiabatic term plays a crucial role in explaining the physical origin of the universal three-body parameter.

In Refs. [32, 150], the low-energy Faddeev equation has been introduced in a manner slightly different from above. In the above formalism, the Faddeev decomposition is performed after the three-body wave function is expanded by the hyper-angular bases. On the other hand, in Refs. [32, 150], the three-body wave function is first decomposed into Faddeev components, and then the Faddeev component is expanded by the hyper-angular bases. This difference in the order of the Faddeev decomposition and the expansion by the hyper-angular bases leads to a rather different behavior in P_{nm} and Q_{nm}. In the latter formalism, the diagonal part P_{nn} does not vanish in general [32, 150]. Similarly, one cannot perform the integration by parts for Q_{nm}, as has been performed in Eq. (4.10). The difference originates from the normalization of the hyper-angular wave function and the Faddeev component. In the above formalism, the non-adiabatic couplings are defined in terms of the hyper-angular wave function (see Eqs. (2.40) and (2.41)), which is normalized indeed. On the other hand, the Faddeev component itself is not normalized, but only their sum (i.e., the hyper-angular wave function in Eq. (4.4)) is normalized.

Numerical Solutions of the low-energy Faddeev equation

Let us solve Eq. (4.8) numerically for various van der Waals type of potentials, and show the diagonal hyper-radial potential $U_n(R)$. Here, we consider three classes of potentials: the soft-

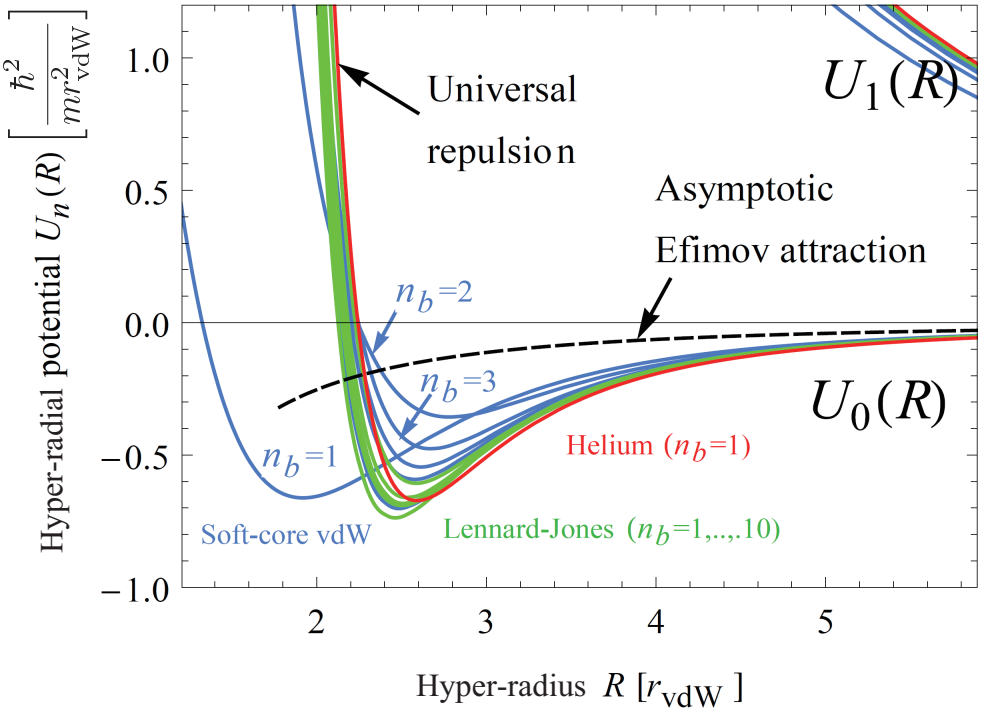

Figure 4.1: Hyper-radial potentials $U_n(R)$ for different two-body potentials at unitarity [147]: the soft-core van der Waals potential in Eq. (2.12) (blue curves) with $n_b = 1$ up to 10 s-wave two-body bound states, the Lennard-Jones potential in Eq. (2.14) (green curves) with $n_b = 1$ up to 10 s-wave two-body bound states, the ^{4}He potential [12] (red curve) rescaled to reach unitarity with $n_b = 1$ s-wave two-body bound state. $U_0(R)$ and $U_1(R)$ are the hyper-radial potentials for the Efimov channel and non-Efimov channel, respectively. There are many non-Efimov channels, but only the one adjacent to the Efimov channel is drawn. The black dashed curve shows the asymptotic Efimov attraction $-\frac{\hbar^2 s_0^2}{mR^2}$. [Figure adapted from Ref. [147] with permission. Copyright © (2014) by The American Physical Society.]

core van der Waals potential in Eq. (2.12), the Lennard-Jones potential in Eq. (2.14), and the ^{4}He potential (LM2M2 potential) [12]. For the soft-core van der Waals potential and the Lennard-Jones potential, the parameters $\sigma_{\rm SC}$ and $\sigma_{\rm LJ}$ are chosen so that the system is at the shape resonance point $1/a = 0$. As can be seen in Fig. 2.1, there are many possible choices of $\sigma_{\rm SC}$ and $\sigma_{\rm LJ}$, corresponding to different potential well depths, or equivalently different numbers of s-wave two-body bound states. We therefore consider various shape resonances corresponding to the appearance of the first two-body bound state ($n_b = 1$) up to the tenth two-body bound state ($n_b = 10$). The ^{4}He potential is known to be close to a shape resonance, and support one weakly bound two-body bound state [12]. To compare it with the results calculated for the soft-core van der Waals potential and the Lennard-Jones potential at unitarity, we multiply the ^{4}He potential by a scale factor $V(r) \to \lambda V(r)$ so that the ^{4}He potential is artificially fine-tuned to be at unitarity: $\lambda = 0.97412$ [10].

Note that there are an infinite number of solutions for Eq. (4.8), but here we mainly focus on

the solution which shows the Efimov effect. Namely, there exists a channel n where the solution asymptotes to $U_n(R) \to -\frac{\hbar^2 s_0^2}{mR^2}$ when $r_{\rm vdW} \ll R \ll |a|$. We call this channel as the Efimov channel, and denote it as $n = 0$.

In Fig. 4.1, $U_0(R)$ for the three classes of potentials is shown. One can see that all the curves corresponding to the Efimov channel $n = 0$ asymptotically approaches to the universal Efimov attraction curve (black dashed curve) when $r_{\rm vdW} \ll R$, while they deviate significantly from it when $R \lesssim r_{\rm vdW}$. One of the non-Efimov channels $U_1(R)$ is also shown in Fig. 4.1 .

One important feature in Fig. 4.1 is that most of the $U_0(R)$ curves almost superimpose onto each other. Indeed, the ^{4}He potential, the Lennard-Jones potential for all n_b, and the soft-core van der Waals potential for $n_b \gtrsim 5$ almost superimpose into a single universal curve. This behavior is rather non-trivial if one recall a huge difference in the two-body potentials. While the potentials behave as $-C_6/r^6$ at long distance, they differ significantly at short distance: the soft-core van der Waals potential behaves smoothly at short distance, while the Lennard-Jones potential and the ^{4}He potential has a steep repulsive core. Furthermore, the depth of the potential differs significantly when n_b is changed. For example, the ratios of the depth of the soft-core van der Waals potential are

$$\frac{V_{\rm SCvdW}(r=0)|_{n_b=2}}{V_{\rm SCvdW}(r=0)|_{n_b=1}} = 21, \quad \frac{V_{\rm SCvdW}(r=0)|_{n_b=5}}{V_{\rm SCvdW}(r=0)|_{n_b=1}} = 401, \quad \frac{V_{\rm SCvdW}(r=0)|_{n_b=10}}{V_{\rm SCvdW}(r=0)|_{n_b=1}} = 3366 \tag{4.13}$$

The difference in $U_0(R)$ shown in Fig. 4.1 is much smaller than this huge difference in the depth of the two-body potential.

Another important feature is that $U_0(R)$ agrees with each other excellently for the ^{4}He potential and the Lennard-Jones potential for all n_b, while $U_0(R)$ for the soft-core van der Waals potential gradually converges to those for the ^{4}He potential and the Lennard-Jones potential as n_b is increased. Thus, for two-body potentials with a hard core, the hyper-radial potential is universal for any depth. On the other hand, for the soft-core van der Waals potential which does not have a hard core, the hyper-radial potential becomes universal when the two-body potential is deep enough $n_b \gg 1$. The universal hyper-radial potential shows a strong universal repulsion at $R \approx 2r_{\rm vdW}$[§]. This universal repulsion prevents three particles from coming close, so that the system becomes insensitive to short-range details.

All these features shown above are the same as what have been previously reported in Ref. [73], in which the three-body problem has been solved with all the higher-partial-wave channels and the channel couplings included. This suggests that it is adequate to use the low-energy Faddeev equation to address the issue of the universal three-body parameter at least qualitatively. We therefore mainly use the low-energy Faddeev equation in this section.

We finally note that the repulsive barrier at $R \approx 2r_{\rm vdW}$ appears even for a purely attractive potential: the soft-core van der Waals potential is monotonical and thus purely attractive, but still it shows a strong three-body repulsion. In Ref. [73], the hyper-radial repulsion has also been found to appear for other types of purely attractive potentials. These results suggest that the repulsive barrier

[§]Note that the hyper-radius used here is different by a factor of $\frac{3^{1/4}}{\sqrt{2}} = 0.931...$ from the hyper-radius used in Ref. [73]. See a footnote in P. 27.

at $R \approx 2r_{\rm vdW}$ does not originate from a repulsion in the two-body potential. In Ref. [74], P. K. Sørensen and coworkers have claimed that a repulsive barrier in the two-body potential is essential for determining the three-body parameter, but this is inconsistent with our result and Ref. [73].

4.1.2 Non-adiabatic deformation as the physical origin of the universal three-body parameter

As shown in Ref. [73] and in the previous section, the hyper-radial potential behaves universally and shows strong universal repulsion at $R \approx 2r_{\rm vdW}$ for a two-body potential with a hard core at short distance and for a deep two-body potential. The following questions, however, have yet to be answered:

- What is the origin of the strong universal repulsion at $R \approx 2r_{\rm vdW}$?
- Why does the three-body potential behave universally?
- Why does it appear for a two-body potential with a hard-core or a deep two-body potential? What is special about these potentials?

In this section, we answer these questions. We first point out that a significant suppression of probability occurs for two particles interacting via a two-body potential with a hard-core or a deep two-body potential. This suppression of probability occurs in a rather universal manner. Using this universal two-body suppression of probability, we answer why there appears a strong three-body repulsion. Namely, we show that the universal two-body suppression of probability induces an abrupt change in the shape of the three-body wave function when three particles get close. This deformation results in a large non-adiabatic force $Q_{00}(R)$ and leads to a strong universal repulsion at $R \approx 2r_{\rm vdW}$. The resulting hyper-radial potential is universal because the two-body suppression of probability occurs in a universal manner. We confirm this scenario by reproducing the hyper-radial potential shown in Fig. 4.1 with a simple model wave function which incorporates the universal two-body suppression of probability into the Efimov wave function.

Universal two-body correlation

Let us consider a two-body Schrödinger equation at zero energy:

$$\left[-\frac{\hbar^2}{m}\frac{d^2}{dr^2} + V(r)\right]\varphi(r) = 0. \tag{4.14}$$

In Fig. 4.2, two-body probability density distributions $|\varphi(r)|^2$ are shown for the soft-core van der Waals potential, the Lennard-Jones potential, and the rescaled ^{4}He potential. Here, the s-wave scattering length is taken to be at unitarity $1/a = 0$. At large distance, the two-body wave function asymptotically approaches to the zero-range result $\varphi(r) = \text{Const.}$ (see Eq. (2.20)). In Fig. 4.2, the wave function is normalized so that $\varphi(r) \to 1$ at large distance. As two particles get close $r \lesssim r_{\rm vdW}$, the two-body probability becomes smaller than the zero-range prediction $\varphi(r) = 1$. One remarkable feature is that the two-body wave functions behave rather similarly for the Lennard-Jones potential

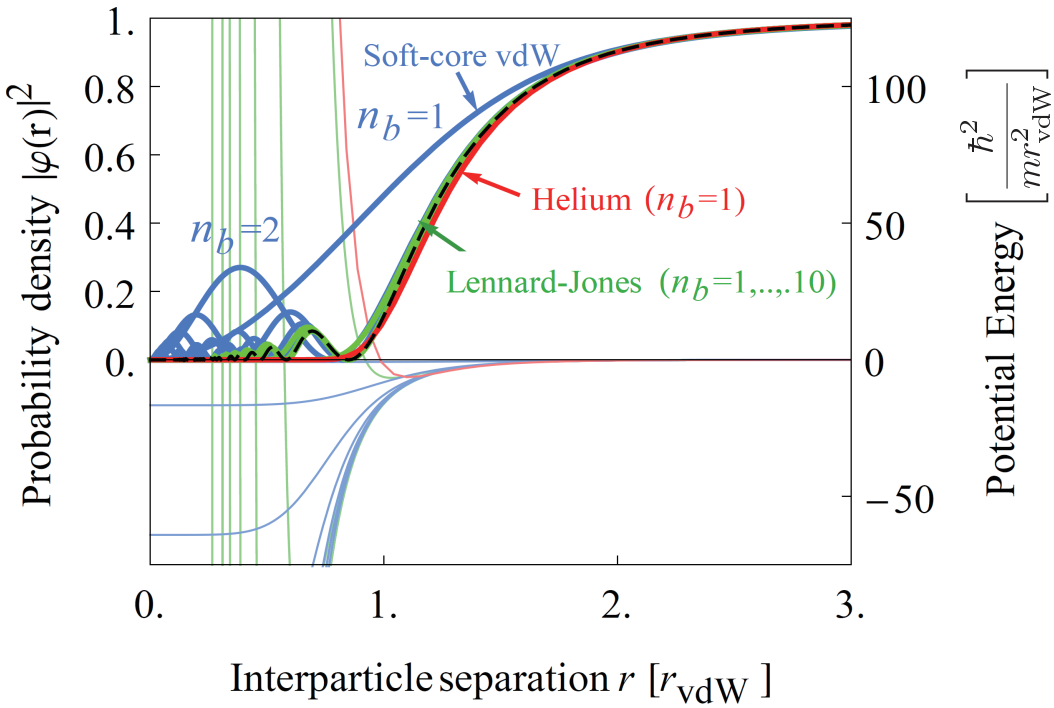

Figure 4.2: Zero-energy two-body probability density distribution $|\varphi(r)|^2$ as a function of interparticle distance for different two-body potentials [147]: the soft-core van der Waals potential (blue curves) with $n_b = 1$ up to 8 s-wave bound states, Lennard-Jones potential (green curves) with $n_b = 1$ up to 8 s-wave bound states, ^{4}He potential (red curve) rescaled to reach the unitarity with 1 s-wave bound state. The corresponding potentials are shown as thin curves. The probability density corresponding to the universal van der Waals correlation given in Eq. (4.15) is also shown by the dashed black curve. [Figure adapted from Ref. [147] with permission. Copyright © (2014) by The American Physical Society.]

for all n_b, for the ^{4}He potential, and for the deep soft-core van der Waals potential $n_b \gtrsim 4$. As discussed later, this universal suppression of the two-body probability is crucial for the origin of the universal three-body repulsion found in Ref. [73] and in Sec. 4.1.1. For the ^{4}He potential and the shallowest Lennard-Jones potential, the suppression of probability occurs at a distance where a hard-core repulsion appears. This suppression can be ascribed to the hard-core repulsion. For a deeper Lennard-Jones potential $n_b \geq 2$, however, the suppression of the two-body probability occurs at a distance much larger than the hard-core radius. In this case, the suppression of the probability is induced not by a hard-core repulsion, but rather by quantum reflection. Quantum reflection is a phenomenon where particles get reflected by a strong attractive potential due to an impedance mismatch [185]. The attractive part of the Lennard-Jones potential for $n_b \geq 2$ is so strong that quantum reflection occurs and the two-body probability is suppressed at $r \approx r_{\rm vdW}$. Quantum reflection also explains the suppression of the probability for the deep soft-core van der Waals potential. While the origin of the reflection mechanism is different for a deep potential and a potential with a hard core, their wave functions behave in the universal manner. Indeed, they can

be characterized by the analytical solution of the two-body Schrödinger equation for the van der Waals potential at zero energy [119, 121, 122]

$$\varphi(r) = \Gamma\left(\frac{5}{4}\right)\sqrt{x}J_{\frac{1}{4}}\left(\frac{2}{x^2}\right) - \frac{r_{\rm vdW}}{a}\Gamma\left(\frac{3}{4}\right)\sqrt{x}J_{-\frac{1}{4}}\left(\frac{2}{x^2}\right) \qquad x \equiv \frac{r}{r_{\rm vdW}}, \tag{4.15}$$

where Γ and J_n are the Gamma and Bessel functions, respectively. This is shown in Fig. 4.2 as a black dashed curve. The universal two-body suppression of the probability can be characterized rather accurately by this two-body wave function.

The only notable different between the two-body wave functions for the Lennard-Jones potential for all n_b, for the ^{4}He potential, and for the deep soft-core van der Waals potential $n_b \gtrsim 4$ is a small oscillations occurring at short distance. The number of oscillations characterizes the number of two-body bound states and thus changes when n_b is varied. This difference however does not affect the three-body physics so much, since the probability of finding particles in this region is already very small.

Non-adiabatic deformation of the three-body wave function

In the hyper-radial potential $U_0(R)$, there are two contributions: the adiabatic term $\hbar^2[\lambda_0(R) + 4]/mR^2$ and the non-adiabatic term $Q_{00}(R)$. In the left panel of Fig. 4.3, the adiabatic term (dotted curves), the non-adiabatic term (dashed curves), and the total hyper-radial potential (solid curves) are shown for the Lennard-Jones potential from $n_b = 1$ up to $n_b = 5$. While the adiabatic part is attractive except for a very small hyper-radius, the non-adiabatic part shows a strong repulsion. Indeed, as shown in Eq. (4.10), the non-adiabatic part $Q_{00}(R)$ is a positive definite quantity, so that it leads to a repulsive force. As can be seen from Eq. (4.10), $Q_{00}(R)$ describes a change in the hyper-angular wave function as the hyper-radius is varied. A large non-adiabatic contribution shown in the left panel of Fig. 4.3 suggests that the hyper-angular wave function changes rather abruptly as the hyper-radius is varied. To visualize this point, in Fig. 4.4, we plot the probability of finding a particle 3 when we put particles 1 and 2 at a given separation r_{12}. To be more specific, we show a contour plot of the following quantity in Fig. 4.4:

$$P_{\boldsymbol{r_1},\boldsymbol{r_2}}(\boldsymbol{r_3}) = \sin^2\alpha_3\,|\Phi_n(R,\alpha_3,\hat{\boldsymbol{r}}_{\boldsymbol{12}},\hat{\boldsymbol{\rho}}_{\boldsymbol{3}})|^2\,. \tag{4.16}$$

In the zero-range theory at unitarity, shown in the left panels, the hyper-angular wave function can be written analytically as

$$\Phi_0^{(\rm ZR)}(R,\alpha_3,\hat{\boldsymbol{r}}_{\boldsymbol{12}},\hat{\boldsymbol{\rho}}_{\boldsymbol{3}}) = \sum_{k=1,2,3}\frac{\psi_n^{(\rm ZR)}(R,\alpha_k)}{\sin 2\alpha_k}, \tag{4.17}$$

where $\psi_n^{(\rm ZR)}$ is the solution of the hyper-angular equation for the zero-range interactions at unitarity (see Eq. (2.54)):

$$\psi_0^{(\rm ZR)}(R,\alpha) = \sinh\left[s_0\left(\frac{\pi}{2}-\alpha\right)\right]. \tag{4.18}$$

This hyper-angular wave function does not involve any scale. Therefore, even when the hyper-radius is varied, the shape of the hyper-angular wave function remains unchanged. The probability

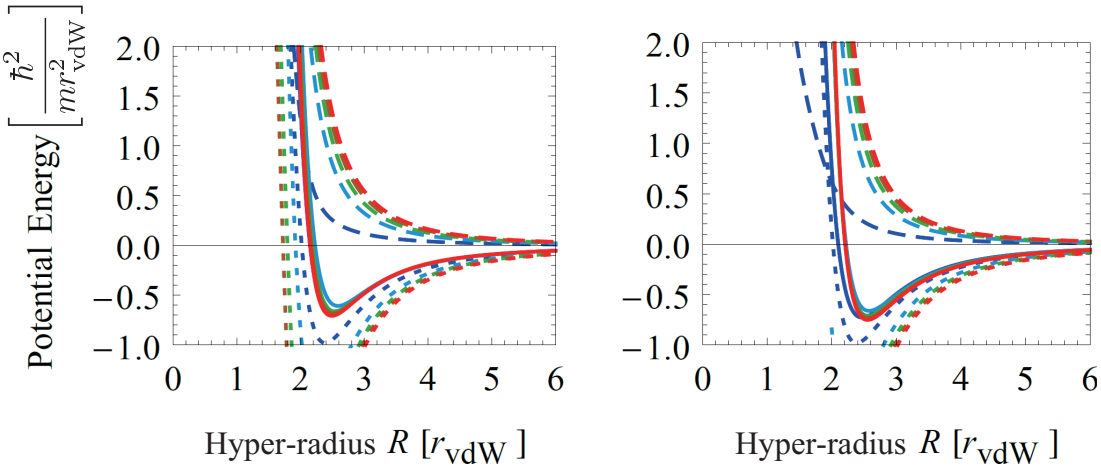

Figure 4.3: Hyper-radial potentials calculated with the Faddeev three-body calculations (left) and the simple two-body correlation model described in the main text (right) [147]. The dashed curves show the non-adiabatic kinetic energy $Q_{00}(R)$ for the Lennard-Jones potentials of different depths, corresponding to the unitarity limit with different numbers of two-body bound states ranging from $n_b = 1$ (blue) to $n_b = 5$ (red). The solid curves show the full three-body potential $U_0(R)$ obtained by adding the adiabatic contribution $\hbar^2[\lambda(R) + 4]/mR^2$ (dotted curves) obtained from Faddeev calculations, which is shown by the dotted curves. [Figure adapted from Ref [147] with permission. Copyright © (2014) by The American Physical Society.]

density therefore remains the same up to a scale transformation, as shown in the left panel of Fig. 4.4. The third particle is always located close to one of the two particles, as shown by green dots in Fig. 4.4. This invariance of the hyper-angular wave function with respect to the hyper-radius results in $Q_{00}(R) = 0$.

On the other hand, for a finite-range potential, the hyper-angular wave function can have a scale. It can therefore change its shape as the hyper-radius is varied, leading to $Q_{00}(R) > 0$. In the right panels of Fig. 4.4, the hyper-angular wave functions calculated with the low-energy Faddeev equation for the Lennard-Jones potential ($n_b = 4$) are shown. At large inter-particle separation, the hyper-angular wave functions look almost similar to the zero-range one. One clear difference is that there are two regions where the probability gets suppressed compared with the zero-range counterpart. In these two spherical regions with their radius $\sim r_{\rm vdW}$, two of the three particles come close, so that the universal two-body suppression of the probability seen in Fig. 4.2 occurs. At large inter-particle separation, these excluded regions do no affect $Q_{00}(R)$ significantly, and $Q_{00}(R)$ is small. However, as the two particles come close $r_{12} \approx r_{\rm vdW}$, this two-body suppression leads to an abrupt change in the hyper-angular wave function. Indeed, the two-body suppression pushes out the wave function to a region forming a ring in-between the two particles, corresponding to an equilateral shape. This change of shape happens very suddenly, making it difficult for the system to follow the Efimov channel adiabatically and resulting in a strong repulsion $Q_{00}(R) > 0$. As argued above, the two-body suppression occurs in a universal manner for a deep potential or a potential with a hard-core, so the abrupt change in the hyper-angular wave function also occurs universally

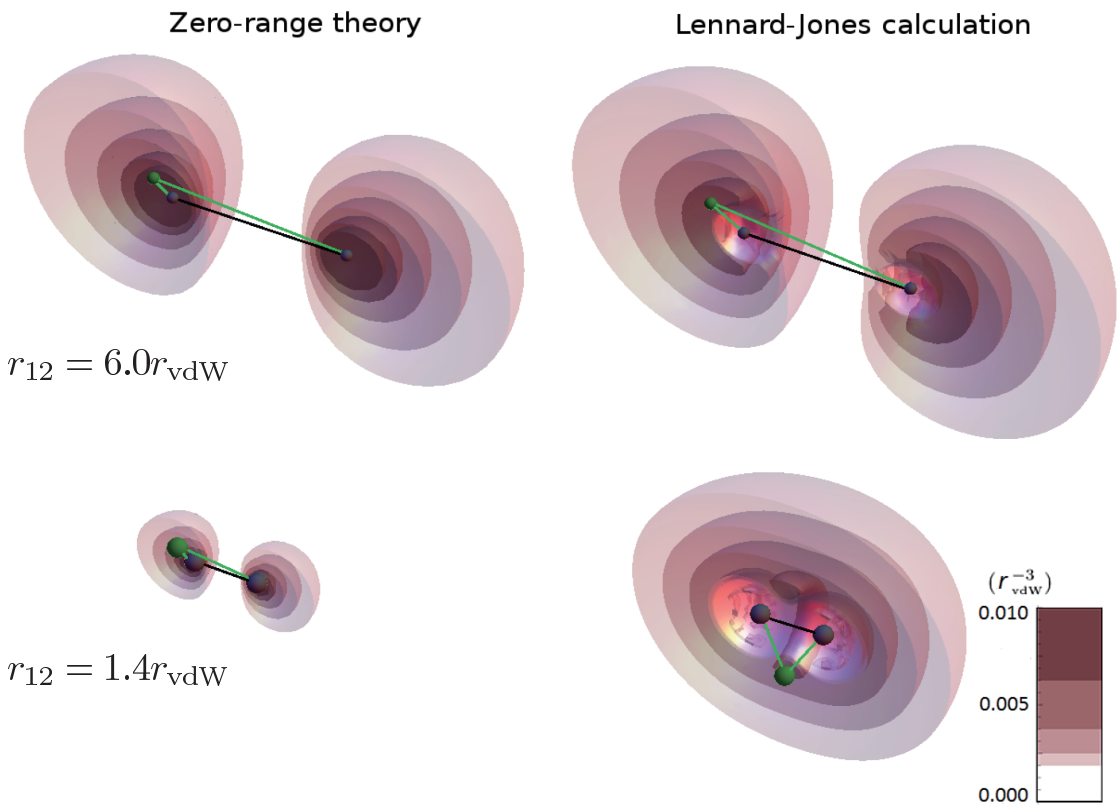

Figure 4.4: Three-dimensional contour plots of the probability distribution in Eq. (4.16) of finding a third particle for a given separation of the two other particles (indicated by a pair of small gray balls connected by a black line) [147]. For clarity, the view is cut along a plane containing the two particles. The top figures correspond to a separation of $6.0r_{\rm vdW}$, while the bottom ones to a separation of $1.4r_{\rm vdW}$. The darker, the higher the probability of finding the third particle. In order to appreciate the change in configuration between the figures, a typical location of the third particle is indicated by a small green ball connected to the other two particles by green lines. The left figures are calculated from the zero-range Efimov theory at unitarity. The right figures are calculated for the Lennard-Jones potential at unitarity supporting four two-body bound states. [Figure adapted from Ref. [147] with permission. Copyright © (2014) by The American Physical Society.]

for these classes of potentials.

Pair correlation model

To verify the above scenario, let us consider a trial hyper-angular wave function of the Bijl-Jastrow form [186, 187]:

$$\Phi_0^{(\rm model)} = \Phi_0^{(\rm ZR)} \varphi(r_{12})\varphi(r_{23})\varphi(r_{13}), \tag{4.19}$$

where φ is the solution of the zero-energy Schrödinger equation (4.14). In this model hyper-angular wave function, the zero-range Efimov configuration is taken into account by $\Phi_0^{(\rm ZR)}$, while the two-body suppression of the probability is taken into account by φ's. This model wave function may be

seen as the simplest wave function ni which both the Efimov effect and the two-body suppression of probability are properly taken into account, while all the other complicated effects are neglected. If the hyper-angular wave function in Fig. 4.4 and the hyper-radial potential in Fig. 4.3 can be reproduced with this model wave function, one can be rather sure that the non-adiabatic deformation scenario explains the physical origin of the universal three-body repulsion and the universal three-body parameter.

We have confirmed that the model wave function in Eq. (4.19) shows a probability density distribution which looks almost the same as those shown in the right panel of Fig. 4.4, with almost no notable difference. We have also calculated the non-adiabatic term Q_{00} from Eq. (4.19), which are shown as dashed curves in the right panel of Fig. 4.3. The non-adiabatic potentials Q_{00} agrees excellently with the one presented in the left panel, which shows the solution of the low-energy Faddeev equation. This confirms our claim that the non-adiabatic deformation of the three-body configuration originates from the suppression of two-body probability.

Summary

We have elucidated the physical origin of the universal three-body parameter as follows: for particles interacting via a deep two-body potential or a two-body potential with a hard core at short distance, the probability gets suppressed when two particles come close due to quantum reflection or a hard-core repulsion, respectively. The two-body suppression leads to a non-adiabatic deformation of the three-body wave function, resulting in a large non-adiabatic repulsion $Q_{00}(R)$. This non-adiabatic deformation is the origin of the hyper-radial repulsion found in Ref. [73] and Sec. 4.1.1. Since the two-body suppression occurs universally for a deep two-body potential or a two-body potential with a hard core, the non-adiabatic repulsion also appears universally for these potentials.

Our scenario can naturally explains why the three-body parameter is universal while the s-wave scattering length is non-universal: the deformation of the wave function can occur for three particles thanks to the hyper-angular degree of freedom, whereas there is no such degree of freedom for two particles.

4.1.3 Some remarks

In Secs. 4.1.1 and 4.1.2, we present our argument based on the low-energy Faddeev equation and on the single-channel approximation. These approximations have facilitated the physical argument greatly. As shown in Sec. 4.1.1, they successfully reproduce most features of the hyper-radial potential obtained with a full three-body calculation, so they give qualitatively correct results. However, the low-energy Faddeev equation and the single-channel approximation are not quantitatively reliable. Indeed, if one calculates the three-body parameter with the low-energy Faddeev equation and with the single-channel approximation, the value of the three-body parameter disagrees with experimentally observed value by a factor of about 50%. One therefore needs to take into account higher-partial-wave contributions and solve the coupled equation to obtained the precise theoretical values reported in Refs. [10, 73]. In Sec. 4.2, an alternative approach to calculate the three-body parameter is introduced, which is inspired by the physical mechanism presented in this section. It

turns out that the method is much more quantitatively accurate than the single-channel low-energy Faddeev equation, successfully reproducing the experimentally observed universal value of the three-body parameter.

4.2 Three-body parameter for general two-body potentials

4.2.1 Physical argument

In the previous section, the physical origin of the universal three-body parameter has been clarified for potentials with the van der Waals tail. It is pointed out that the universal suppression of the two-body probability is essential, because it induces a strong non-adiabatic repulsion and renders the three-body parameter universal. Here, we recall that properties of the van der Waals interaction have been used only to show that the suppression of the two-body probability occurs universally. Therefore, even for a non-van der Waals type of potential, one can naturally expect that the three-body parameter becomes universal from the same physical mechanism if the universal suppression of the two-body probability occurs.

In Fig. 4.6, I show the zero-energy two-body wave functions at unitarity for various potentials: the Lennard-Jones potential, the 8-4 potential

$$V_{84}(r) = -\frac{C_4}{r^4}\left(1 - \frac{\sigma^4}{r^4}\right), \tag{4.20}$$

the Gaussian potential

$$V_{\mathrm{Gauss}}(r) = -C_{\mathrm{G}} \exp\left(-\frac{r^2}{r_0^2}\right), \tag{4.21}$$

the Yukawa potential

$$V_{\mathrm{Y}}(r) = -C_{\mathrm{Y}} \frac{\exp\left(-\frac{r}{r_0}\right)}{r}, \tag{4.22}$$

the Pöschl-Teller potential[§] (see Fig. 4.5 (a) for its shape) [188, 189]

$$V_{\mathrm{PT}}(r) = C_{\mathrm{PT}}\left[\frac{\alpha(\alpha-1)}{\sinh^2\left(\frac{r}{r_0}\right)} - \frac{\alpha(\alpha+1)}{\cosh^2\left(\frac{r}{r_0}\right)}\right], \tag{4.23}$$

and the Morse potential (see Fig. 4.5 (b) for its shape) [189, 190]

$$V_{\mathrm{M}}(r) = C_{\mathrm{M}}\left(\exp\left[-2\frac{r-\beta r_0}{r_0}\right] - 2\exp\left[-\frac{r-\beta r_0}{r_0}\right]\right). \tag{4.24}$$

All these potentials are assumed to be at unitarity with six s-wave bound states ($n_b = 6$) by adjusting the parameters σ or C. One can see that the suppression of the two-body probability occurs for all the potentials. Another notable feature is that the suppression occurs at a length scale characterized by the effective range r_{eff} for all the potentials. Indeed, for most physical potentials, the length scale

[§]The Pöschl-Teller potential with $\alpha = 1$ is sometimes referred to as the modified Pöschl-Teller potential, and it has a hard repulsive core at short distance when $\alpha > 1$, while it is a smooth attractive potential when $\alpha = 1$

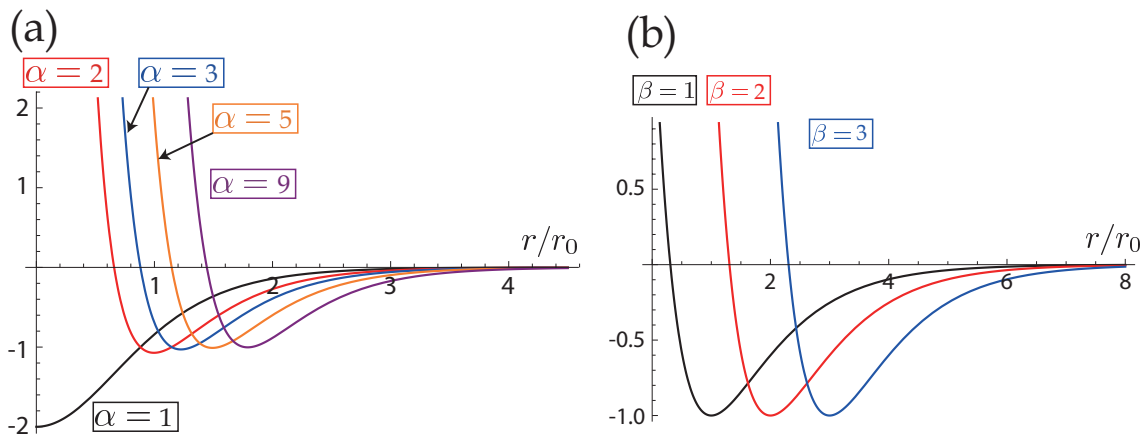

Figure 4.5: (a) Pöschl-Teller potential with $\alpha = 1$ (black), $\alpha = 2$ (red), $\alpha = 3$ (blue), $\alpha = 5$ (orange), and $\alpha = 9$ (purple). (b) Morse potential with $\beta = 1$ (black), $\beta = 2$ (red), and $\beta = 3$ (blue). An arbitrary unit is taken for the vertical axis.

for this suppression can be generally characterized by the effective range through the following formula [118]:

$$r_{\text{eff}} = 2\int_0^\infty dr\left[|\varphi_{\text{ZR}}(r)|^2 - |\varphi(r)|^2\right], \tag{4.25}$$

where $\varphi(x)$ and $\varphi_{\text{ZR}}(x) = 1 - \dfrac{r}{a}$ are the two-body wave functions at zero energy for a finite-range potential $V(x)$ and for a zero-range potential, respectively. While the effective range is conventionally defined as a low-energy expansion parameter of the phase shift (see Eq. (2.4)), this formula relates the effective range to a length scale associated with the pair correlation at zero energy.

As discussed in the previous section, this suppression of the two-body probability creates the three-body repulsion through the non-adiabatic deformation of the three-body wave function. Although the precise shape of the repulsive barrier may depend on shape of the two-body potential, the effective range sets the location of the suppression of probability, and hence the hyper-radius at which the universal hyper-radial repulsion appears. For most physical potentials, the two-body wave function gets suppressed at short distance as the depth of the two-body potential is increased. Therefore, one can expect that the three-body parameter can be characterized by the effective range for most two-body potentials when they get sufficiently deep and the suppression of the two-body probability occurs. This conjecture will be numerically confirmed in Sec. 4.2.2.

For a single-channel potential with the van der Waals tail, the effective range can be related to the van der Waals length and the s-wave scattering length as [119, 120, 122]

$$r_{\text{eff}} = \frac{2}{3\pi}\Gamma^2\left(\frac{1}{4}\right)\left[\left(1 - \frac{\bar{a}}{a}\right)^2 + \left(\frac{\bar{a}}{a}\right)^2\right] r_{\text{vdw}}, \tag{4.26}$$

where

$$\bar{a} = \frac{4\pi}{\Gamma^2\left(\frac{1}{4}\right)} r_{\text{vdw}}. \tag{4.27}$$

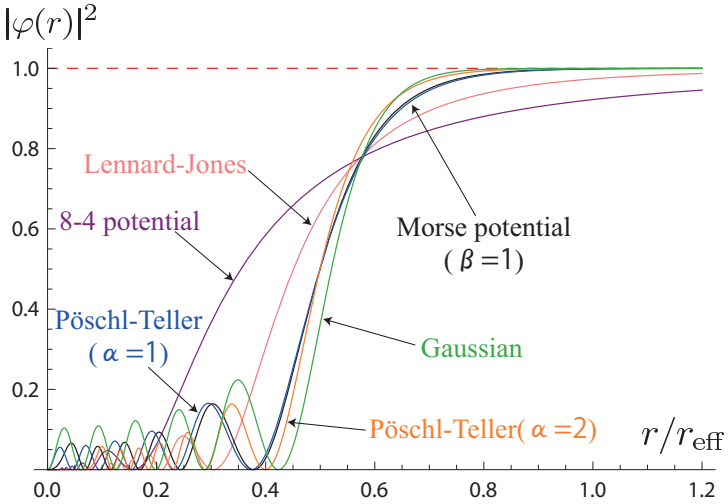

Figure 4.6: Two-body wave functions for the Lennard-Jones potential in Eq. (2.14) (pink), the 8-4 potential in Eq. (4.20) (purple), the Gaussian potential in Eq. (4.21) (green), the Pöschl-Teller potential in Eq. (4.23) with $\alpha = 1$ (blue) and $\alpha = 2$ (orange), the Morse potential with $\beta = 1$ (black). The depth of these potentials is set to be at unitarity $1/a = 0$ with 6 s-wave two-body bound states $n_b = 6$. The wave function is normalized so that $\varphi(r) \to 1$ at large distance. The red dashed line $\varphi(r) = 1$ corresponds to the zero-range two-body wave function at unitarity.

In particular, the effective range is proportional to the van der Waals length at unitarity:

$$r_{\rm eff} = \frac{2}{3\pi}\Gamma^2\left(\frac{1}{4}\right) r_{\rm vdw} = 2.79 r_{\rm vdw}. \tag{4.28}$$

Therefore, the conjectured relation between the three-body parameter and the effective range incorporates the van der Waals class of potentials studied in Sec. 4.1, and can be regarded as a natural generalization to systems interacting with a non-van der Waals type of potentials.

For most classes of potentials, the two-body wave function shows the suppression of the two-body wave function as the depth of the two-body potential is increased. However, for some pathological cases, there is no well-converged universal pair correlation. One clear example is the square-well potential. For the square-well potential $V(r) \propto -\Theta(r_0 - r)$, the zero-energy two-body probability density distribution $|\varphi(r)|^2$ at unitarity is

$$|\varphi(r)|^2 = \begin{cases} 1 & (r > r_0) \\ \sin^2\left[\frac{(2n_b-1)\pi}{2}\frac{r}{r_0}\right] & (r < r_0) \end{cases} \tag{4.29}$$

This is shown in Fig. 4.7 for various n_b. One can see that the two-body wave functions do not show any suppression of probability. This may be due to the discontinuity in the two-body potential. If a two-body potential is continuous, particles can be accelerated in a semiclassical manner when the two-body potential is attractive. This accelerated motion can lead to a mismatch in the impedance, resulting in the suppression of probability when two particles get close. On the other hand, a discontinuous jump does not allow any semiclassical acceleration of particles. This may explain

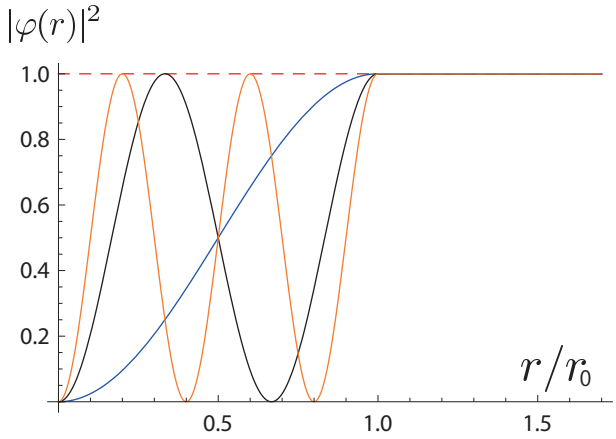

Figure 4.7: Zero-energy two-body wave functions for the square-well potential at unitarity for $n_b = 1$ (blue), $n_b = 2$ (black), and $n_b = 3$ (orange) two-body bound states. A red dashed line $\varphi(r) = 1$ which corresponds to the zero-range two-body wave function at unitarity.

why the wave function is not suppressed for the square-well potential near unitarity. Since the suppression of the probability does not occur, one can expect that the three-body parameter for the square-well potential does not converge to any universal value when the depth of the potential is increased.

To summarize, for most physical interactions (except for some pathological cases such as the square-well potential), the suppression of the two-body probability occurs at a length scale on the order of the effective range when the depth of the potential is increased. This fact and the physical mechanism shown in Sec. 4.1 suggest that for a wide class of deep two-body potentials, the three-body parameter should be universal and can be characterized by the effective range. This conjecture will be confirmed numerically in the next section.

Note that in Ref. [73], the three-body parameter of the Pöschl-Teller potential with $\alpha = 1$ has been obtained numerically by varying its depth, and it has been found to converge to a universal value characterized by the effective range in the deep potential limit. While the relation between the three-body parameter and the effective range has been shown only for the Pöschl-Teller potential with $\alpha = 1$ in Ref. [73], with hindsight it was the first example of the universal relation. Our argument presented above elucidates why the three-body parameter should be characterized by the effective range in their work. The physical argument presented in this section also suggests that this relation is not a special feature of the Pöschl-Teller potential, but rather should hold universally for a broad class of potentials.

4.2.2 Universality classes of the three-body parameter

In this section, we study the three-body parameter for various classes of two-body potentials. In general, a three-body calculation with a deep two-body potential is rather formidable and requires sophisticated numerical methods [73]. This is due to coexistence of a large length scale $\sim |a_-^{(1)}|$ associated with the Efimov physics and a short wave length appearing inside the strongly

attractive potential region for a deep two-body potential $\sim \sqrt{\frac{\hbar^2}{mV_0}}$, where V_0 is the typical depth of the two-body potential. To circumvent this difficulty, a simpler method is introduced. We use a separable potential, which is constructed to reproduce the universal pair correlation of the original two-body potential at zero energy. The separable potential constructed in this way naturally reproduces two-body properties at low energy, such as the effective range. A three-body problem with the separable potential reduces to the Skorniakov–Ter-Martirosian type of one-dimensional integral equation, which is much simpler than solving the three-body Schrödinger equation with the original two-body potential. It is first shown that the three-body parameter calculated with the separable potential agrees excellently with that obtained by solving the three-body Schrödinger equation. This justifies us to use the separable potential as a much simpler and efficient way to evaluate the three-body parameter of a system interacting with rather deep two-body potentials, facilitating our study dramatically. Using the separable potential, the three-body parameter is calculated for various classes of two-body potentials for a variable depth. It is shown that the three-body parameter becomes universal when expressed in units of the effective range when the depth of the potential gets large, confirming the conjecture presented in Sec. 4.2.1. We identify two classes of two-body potentials, for which the three-body parameter shows the universality. One class corresponds to short-range two-body potentials decaying as a power law, for which the two-body probability is suppressed at short distance in a smooth fashion. The other corresponds to potentials decaying faster than any power law, for which the two-body probability is suppressed abruptly when $r < \frac{1}{2}r_{\rm eff}$. The former one is relevant for the Efimov states in atomic physics, such as ^{4}He cluster [7, 8, 9, 10] and ultracold atoms in the vicinity of a broad Feshbach resonance, while the latter is relevant for the Efimov states in nuclear systems, such as halo states in the neutron rich nuclei [3, 4, 5].

Separable potential constructed to reproduce the pair correlation

A separable potential is a non-local potential first introduced by Y. Yamaguchi [191]:

$$\hat{V} = \frac{\hbar^2}{m}\xi\,|\chi\rangle\langle\chi|\,. \tag{4.30}$$

The advantage of the separable potential is its simplicity: the two-body Schrödinger equation with the separable potential can be solved analytically, and the scattering amplitude and the wave function are obtained as

$$f(\boldsymbol{k}) = -\frac{|\chi(\boldsymbol{k})|^2}{4\pi}\left(\frac{1}{\xi} + \int \frac{d^3\boldsymbol{q}}{(2\pi)^3}\frac{|\chi(\boldsymbol{q})|^2}{q^2 - k^2 - \imath 0^+}\right)^{-1}, \tag{4.31}$$

and

$$\psi_{\boldsymbol{k}}(r) = e^{i\boldsymbol{kr}} + 4\pi f(\boldsymbol{k})\int \frac{d^3\boldsymbol{q}}{(2\pi)^3}\frac{e^{i\boldsymbol{qr}}}{q^2 - k^2 - \imath 0^+}\frac{\chi(\boldsymbol{q})}{\chi(\boldsymbol{k})}. \tag{4.32}$$

By assuming an isotropic separable potential $\chi(\boldsymbol{k}) = \chi(k)$ and taking the low-energy limit, the scattering length is obtained as

$$\begin{aligned} a &= -f(k=0) \\ &= \left(\frac{4\pi}{\xi} + \frac{2}{\pi}\int_0^\infty dq\,|\chi(q)|^2\right)^{-1}|\chi(0)|^2\,. \end{aligned} \tag{4.33}$$

The zero-energy wave function is obtained as

$$\psi_0(r) = -\frac{a}{r}\varphi(r), \tag{4.34}$$

where

$$\varphi(r) = \frac{2}{\pi}\int_0^\infty dq \frac{\sin qr}{q}\frac{\chi(q)}{\chi(0)} - \frac{r}{a}. \tag{4.35}$$

One can easily see that this is consistent with the long-distance behavior shown in Eq. (2.13) if one uses

$$\lim_{r\to\infty}\int_0^\infty dq \frac{\sin qr}{q}\frac{\chi(q)}{\chi(0)} = \frac{\pi}{2}. \tag{4.36}$$

The separable potential is one of the most commonly used pseudo-potential. Typically, for a few-body problem in the vicinity of a broad Feshbach resonance, the separable potential is constructed to reproduce the s-wave scattering length of the original two-body potential, since the low-energy two-body problem in the vicinity of a broad Feshbach resonance can be universally characterized by the s-wave scattering length (see Sec. 2.1). In this approach, the value of ξ is determined from Eq. (4.33) by fixing a, while $\chi(q)$ can be taken at one's discretion. Therefore, simple functions such as the Gaussian or the exponential functions are often used for $\chi(q)$. With the separable potential, the three-body problem can also be solved much more easily than solving the three-body Schrödinger equation for a system interacting with a pair-wise potential. Indeed, the three-body problem with the separable potential reduces to the following Skorniakov–Ter-Martirosian type of one-dimensional integral equation:

$$D(P)F(P) + \int_0^\infty \frac{q^2 dq}{2\pi^2} H(P,q)F(q), \tag{4.37}$$

where

$$D(P) = \frac{1}{\xi} + \int_0^\infty \frac{dq}{2\pi^2}\frac{q^2\,|\chi(q)|^2}{q^2 - \frac{mE}{\hbar^2} + \frac{3}{4}P^2}, \tag{4.38}$$

and

$$H(P,q) = \int_{-1}^{1} du \frac{\chi^*\left(\sqrt{q^2 + \frac{1}{4}P^2 + qPu}\right)\chi\left(\sqrt{P^2 + \frac{1}{4}q^2 + qPu}\right)}{P^2 + q^2 + Pqu - \frac{mE}{\hbar^2}}. \tag{4.39}$$

Equation (4.37) can be easily solved numerically[§] with the same technique as was done for Eq. (3.20) in Chapter 3.

While choosing a simple functional form such as Gaussian for $\chi(q)$ simplifies the calculations, one disadvantage of this treatment is that the two-body correlation of the original two-body potential is not correctly reproduced except for the s-wave scattering length. Since the two-body correlation at low-energy is important in determining the value of the three-body parameter as has been argued in Sec. 4.1, the three-body parameter calculated with the separable potential constructed above would differ significantly from that of the original two-body potential. Therefore, it would be inadequate to use this naive pseudo-potential.

[§] *A remark on the contribution:* Most of the three-body numerical calculations in this section has been performed by P. Naidon.

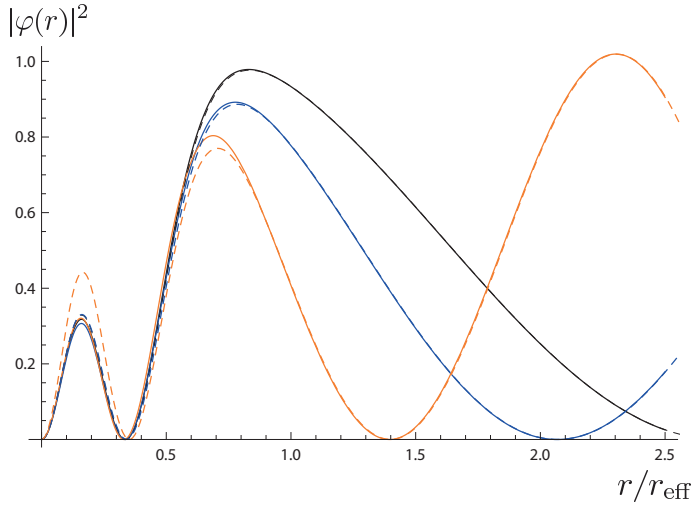

Figure 4.8: Solutions of the two-body Schrödinger equation at unitarity for the Gaussian potential in Eq. (4.21) corresponding to $n_b = 2$ (solid curves) and the separable potential calculated from Eqs (4.30), (4.33), and (4.40) (dashed curves). The energies are taken as $E = \dfrac{\hbar^2}{2mr_{\rm eff}^2}$ (black), $E = \dfrac{\hbar^2}{mr_{\rm eff}^2}$ (blue), and $E = \dfrac{3\hbar^2}{mr_{\rm eff}^2}$ (orange).

However, taking advantage of the freedom of choice for $\chi(q)$, we can choose $\chi(q)$ such that the zero-energy wave function for the separable potential exactly reproduces the pair correlation of the original two-body potential. From Eq. (4.35), one obtains the relation between $\chi(q)$ and the zero-energy pair correlation as

$$\begin{aligned}\frac{\chi(q)}{\chi(0)} &= 1 + q\int_0^\infty dr\left[\frac{r}{a}\left(1-\frac{a}{r}-\psi_0(r)\right)\right]\sin qr \\ &= 1 - q\int_0^\infty dr\left(1-\frac{r}{a}-\varphi(r)\right)\sin qr.\end{aligned} \tag{4.40}$$

One can reproduce any form of the zero-energy pair correlation exactly by constructing $\chi(q)$ from Eq. (4.40). To be more specific, we construct a separable potential and solve the three-body problem according to the following procedure:

1. Solve the two-body Schrödinger equation for the two-body potential one wants to deal with, and obtain $\psi_0(r)$ (or equivalently the pair correlation $\varphi(r)$).
2. Substitute $\psi_0(r)$ (or $\varphi(r)$) into Eq. (4.40) and obtain $\chi(q)$.
3. Substitute $\chi(q)$ into Eq. (4.33) and obtain ξ for a fixed value of a.
4. Using $\chi(q)$ and ξ obtained in 2. and 3., solve the three-body problem with Eq. (4.37).

The separable potential constructed in this way has the advantage of being easily tractable thanks to its separability while at the same time reproducing the zero-energy pair correlation accurately.

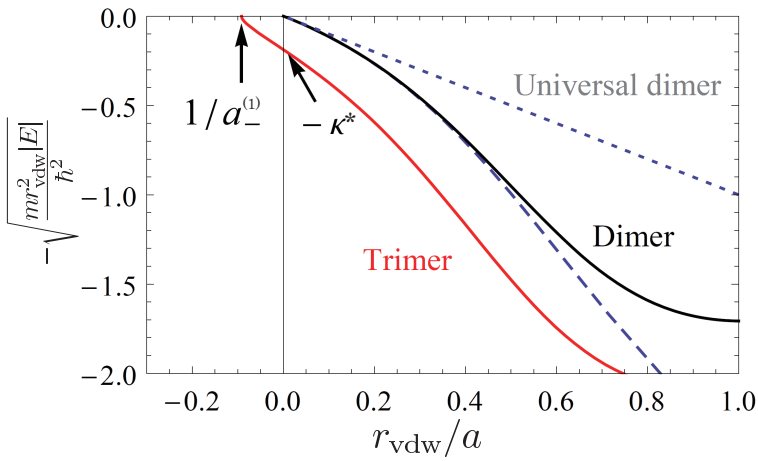

Figure 4.9: Trimer (red solid curve) and dimer (black solid curve) energies for the separable potential in Eqs (4.30), (4.33), and (4.40) as a function of the inverse scattering length [184]. The trimer curve is calculated with the pair correlation of a sufficiently deep van der Waals potential in Eq. (4.15). The dotted line represents the universal dimer energy in Eq. (2.10). The dashed curve represents the dimer energy for a sufficiently deep van der Waals potential obtained by solving the two-body Schrödinger equation numerically. [Figure adapted from Ref. [184] with permission. Copyright © (2014) by The American Physical Society.]

Furthermore, from Eq. (4.25), one can see that the separable potential also reproduces the effective range of the original two-body potential. This suggests that the separable potential reproduces not only the zero-energy two-body physics but also finite-energy properties. In Fig. 4.8, I compare two-body wave function of the Gaussian potential and the separable potential constructed as above at finite energy. One can see that the two-body wave functions agree excellently for most of the region when $E \lesssim \frac{\hbar^2}{mr_{\rm eff}^2}$. A slight discrepancy is barely visible at short distance, which gets larger at higher energy.

In addition to the low-energy continuum states, weakly bound two-body bound states can also be reproduced fairly well with the separable potential. In Fig. 4.9, binding energy of a weakly bound dimer for a deep van der Waals potential is compared with that calculated with the separable potential. They agree excellently at low energy, while they deviate from each other when $|E| \gtrsim \frac{\hbar^2}{mr_{\rm vdw}^2}$. Note that the agreement is much better than the universal dimer energy $\frac{\hbar^2}{ma^2}$. This can be naturally understood by noting that the effective range is accurately reproduced with the separable potential, while the universal dimer formula amounts to taking $r_{\rm eff} = 0$.

In Fig. 4.9, we also show the binding energy of the ground-state Efimov trimer calculated with the separable potential for the van der Waals correlation in Eq. (4.15), corresponding to an infinitely deep van der Waals potential. We found the universal values of the binding energy at unitarity and the three-body threshold to be $\kappa^* = 0.187(1)r_{\rm vdW}^{-1}$ and $a_-^{(1)}/r_{\rm vdW} = -10.86(1)$, respectively. Similar results can be obtained for pair correlations $\varphi(r)$ with a similar tail. For example, the pair correlation for the Lennard-Jones potential with $n_b = 1$ leads to $\kappa^* = 0.205(1)r_{\rm vdW}^{-1}$ and $a_-^{(1)}/r_{\rm vdW} = -10.23(1)$.

Table 4.1: Scattering length at the three-body threshold $a_-^{(1)}$ and binding energy at unitarity $E_3 = -\frac{\hbar^2(\kappa^*)^2}{m}$ of the ground-state trimer for various potentials with $n_b = 1$. The data in the right column are taken from Ref. [192], and those in the left column are calculated with the separable potential introduced in Eqs (4.30), (4.33), and (4.40). [Table adapted from Ref. [184] with permission. Copyright © (2014) by The American Physical Society.]

Potential	Separable potential		Ref. [192]	
	$a_-^{(1)}\,[r_0]$	$E_3\left[\frac{\hbar^2}{mr_0^2}\right]$	$a_-^{(1)}\,[r_0]$	$E_3\left[\frac{\hbar^2}{mr_0^2}\right]$
Yukawa	-6.55	-0.134	-5.73	-0.172
Exponential	-11.0	-0.042	-10.7	-0.047
Gaussian	-4.47	-0.223	-4.27	-0.236
Morse ($\beta = 1$)	-12.6	-0.0299	-12.3	-0.0325
Morse ($\beta = 2$)	-16.3	-0.0166	-16.4	-0.0174
Pöschl-Teller ($\alpha = 1$)	-6.23	-0.123	-6.02	-0.135

These values are consistent with the experimentally reported value of the three-body parameter $a_-^{(1)} = -(8-10)r_{\rm vdW}$ (see Figs. 2.11 and 2.12), providing further support for our scenario shown in Sec. 4.1 as the physical origin of the universal three-body parameter.

In Table. 4.1, the scattering length at the three-body threshold $a_-^{(1)}$ and the binding energy at unitarity $E_3 = -\frac{\hbar^2(\kappa^*)^2}{m}$ of the ground-state Efimov trimer calculated with the separable potential and the original two-body potential are compared. For the latter ones, the data is taken from Ref. [192], in which the three-body Schrödinger equation has been solved numerically with a variational method. One can see that the separable potential reproduces $a_-^{(1)}$ and E_3 fairly well for various classes of two-body potentials. This can also be seen in Fig. 4.10, in which κ^* obtained with the separable potential is plotted against those obtained by solving the three-body Schrödinger equation with the original two-body potential [192]. They agree with each other within a few percents for various classes of potentials. This justifies the use of the separable potential to evaluate the three-body parameter and investigate its universality. Compared with solving the three-body Schrödinger equation, Eq. (4.37) can be solved much faster and more easily, so it is a powerful tool in investigating the three-body parameter for various classes of potentials, especially when the potential is strongly attractive. More generally, the separable potential method has a potential to be applied to study low-energy few-body systems in various kinds systems with formidable interaction potentials in a rather simple and efficient manner.

Universality classes of the three-body parameter

Now that we have established the separable potential as a quantitatively reliable method to evaluate the three-body parameter, we shall investigate the three-body parameter for various types of two-body potentials by varying their depth. Figure 4.11 shows the binding wave number of the

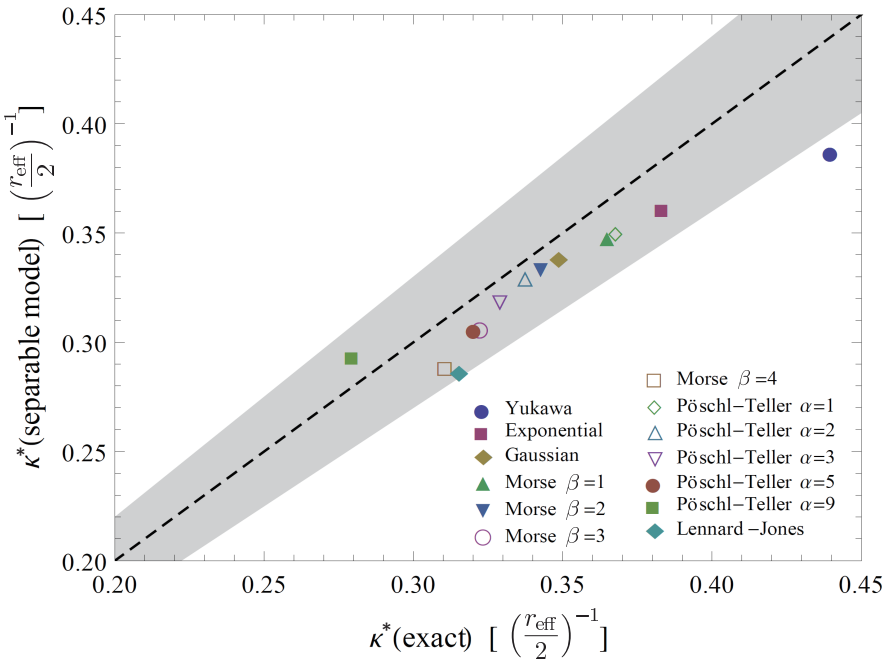

Figure 4.10: Binding wave number κ^* of the ground-state Efimov trimer at unitarity calculated with the separable potential in Eqs (4.30), (4.33), and (4.40) versus κ^* obtained by solving the three-body Schrödinger equation for the original two-body potential. The latter values are taken from Ref. [73] for the Lennard-Jones potential ($n_b = 1$) and from Ref [192] for all the other potentials ($n_b = 1$). The shaded area represents the region of 10% or less deviation. [Figure adapted from Ref. [184] with permission. Copyright © (2014) by The American Physical Society.]

ground-state Efimov trimer at unitarity for various classes of potentials: the Gaussian potential, the Pöschl-Teller potential with $\alpha = 1$ (see Eq. (4.23) for its definition), the Yukawa potential, the Morse potential with $\beta = 1$ (see Eq. (4.24) for its definition), the Lennard-Jones potential, the 8-4 potential defined in Eq. (4.20), as well as the neutron-neutron interaction potential in the ${}^1S_0$ channel [193]. For all of these potentials, the three-body parameter converges to a certain value as the depth of the potential is increased. The converged values are characterized by the effective range, and they are in the narrow window of $\kappa^* = (0.2 - 0.4)\left(\frac{r_{\rm eff}}{2}\right)^{-1}$. This is consistent with the argument presented in Sec. 4.2.1, which predicts that the three-body parameter should be characterized by the effective range for a broad class of two-body potentials.

One also finds in Fig. 4.11 that κ^* converges to the same value for all the rapidly decaying potentials (the Gaussian potential, the Pöschl-Teller potential, the Yukawa potential, the Morse potential, and the neutron-neutron potential), while κ^* for the potentials with a power-law decaying tail converges to slightly different values from them. This discrepancy can also be explained naturally with the physical mechanism presented in Sec. 4.1 by noting the difference in the behavior of the pair correlation. In Fig. 4.12, the zero-energy two-body wave functions are shown for the Pöschl-Teller potential and the Gaussian potential. If the two-body wave functions are shown in units of r_0 (see the insets), they seem to show no universal behavior. However, if they are plotted in units of the

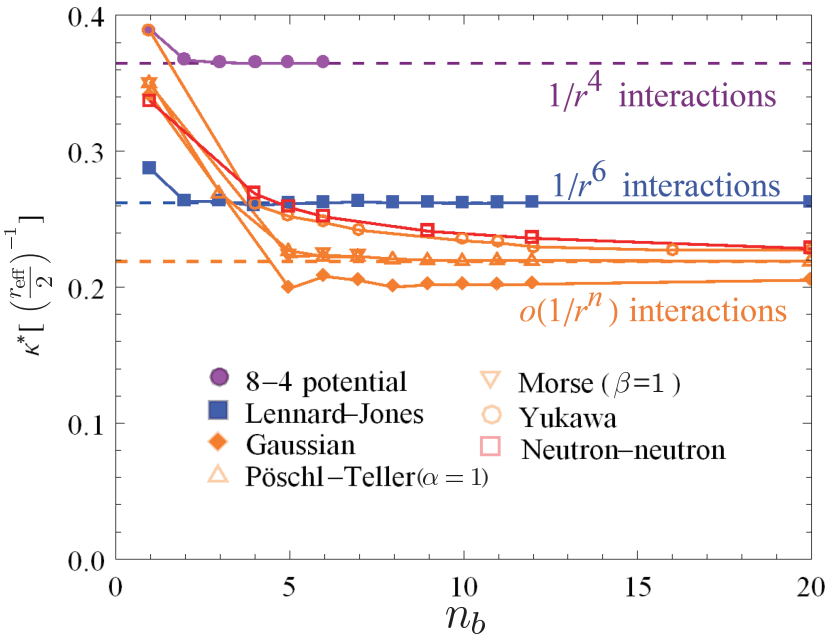

Figure 4.11: Binding wave number κ^* of the ground-state Efimov trimer at unitarity calculated with the separable potential in Eqs (4.30), (4.33), and (4.40) as a function of the depth of the potential quantified by the number of s-wave two-body bound states n_b. The two horizontal dashed lines represent the three-body parameters obtained from the universal pair correlation for the power-law class of potentials in Eq. (4.42) with $n = 4$ (purple dashed line) and $n = 6$ (blue dashed line), and the universal stepwise pair correlation in Eq. (4.41) (orange dashed line). [Figure adapted from Ref. [184] with permission. Copyright © (2014) by The American Physical Society.]

effective range (see the main panels), they converge to a stepwise pair correlation:

$$\varphi(r) = \begin{cases} 0 & (r < \frac{1}{2}r_{\rm eff}) \\ 1 & (r > \frac{1}{2}r_{\rm eff}) \end{cases} \tag{4.41}$$

This is because the effective range gets progressively larger as the depth of the potential is increased, which means that there is a sharp drop of probability in the two-body wave function near $r = \dfrac{1}{2}r_{\rm eff}$ when distances are expressed in units of $r_{\rm eff}$. It can be shown that this rescaled two-body wave function converges to the step function in the limit of strongly attractive potentials. In Fig. 4.11, the three-body parameter calculated with this universal stepwise correlation is also shown (orange dashed line). The three-body parameter for the rapidly decaying potentials slowly converges to this universal value.

On the other hand, for potentials with a power-law decaying tail, the pair correlation behaves rather differently from that of the rapidly decaying potentials. In Fig. 4.13, the zero-energy two-body wave functions are shown for potentials with $-1/r^4$ and $-1/r^6$ tails. As the depth of the potential is increased, the pair correlation converges to a smooth universal function. For potentials with a power-law tail $-1/r^n$, the zero-energy pair correlation can be derived analytically by assuming that the probability amplitude is mostly located in the tail region, which is the case if the

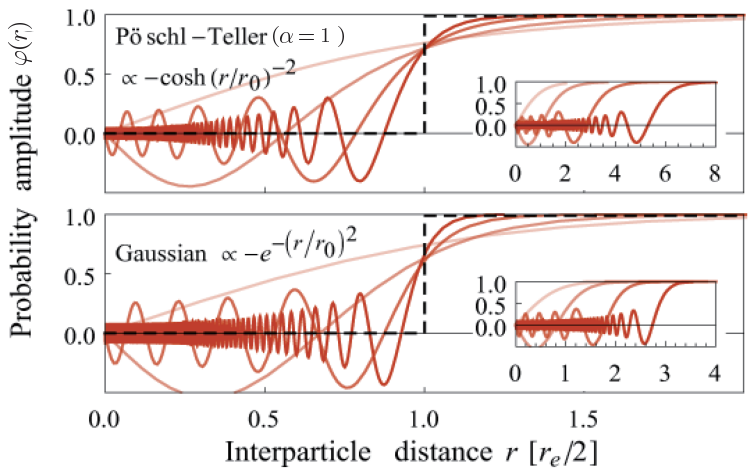

Figure 4.12: Zero-energy two-body wave function at unitarity for (a) the Pöschl-Teller potential, and (b) the Gaussian potential. In each graph, the solid curves correspond in order of opacity to potential depths supporting 1, 2, 10, and 120 s-wave bound states, respectively. The dashed curve shows the universal pair correlation limit in Eq. (4.41). The horizontal axis is scaled in units of $\frac{1}{2}r_{\rm eff}$ in the main graphs, while it is shown in units of r_0 in the insets. [Figure adapted from Ref. [184] with permission. Copyright © (2014) by The American Physical Society.]

short-distance region is strongly repulsive or attractive [194]:

$$\varphi(r) = \Gamma\left(\frac{n-1}{n-2}\right)\sqrt{x}J_{\frac{1}{n-2}}\left(2x^{-\frac{n-2}{2}}\right) - \frac{r_n}{a}\Gamma\left(\frac{n-3}{n-2}\right)\sqrt{x}J_{-\frac{1}{n-2}}\left(2x^{-\frac{n-2}{2}}\right), \tag{4.42}$$

where $r_n = \left(\frac{1}{n-2}\frac{\sqrt{mC_n}}{\hbar}\right)^{\frac{2}{n-2}}$ is the length scale characterizing the tail of the power law potential and $x = r/r_n$. When $n = 6$, r_n becomes identical to the van der Waals length $r_6 = r_{\rm vdw}$, and Eq. (4.42) becomes identical to the van der Waals pair correlation shown in Eq. (4.15). The universal pair correlation in Eq. (4.42) is shown in Fig. 4.13 as dashed curves. The pair correlation is suppressed smoothly at short distance, which is in marked contrast to the discontinuous pair correlation in Eq. (4.41). In Fig. 4.11, the three-body parameters calculated with the universal correlation in Eq. (4.42) are also shown (purple dashed line and blue dashed line). The three-body parameter for the power-law potentials converges to this universal value much more rapidly than the exponentially decaying potentials. This originates from the rapid convergence of the pair correlation shown in Fig. 4.13, while the convergence is much slower for the exponentially decaying potentials as shown in Fig. 4.12.

Universal three-body parameter described by Eq. (4.42) therefore seems rather distinct in nature from the first class characterized by Eq. (4.41), so it would be natural to classify them as two different classes of universality: those characterized by the stepwise pair correlation, and those characterized by the power-law class of smooth pair correlation. The first universality class is relevant for the Efimov states in the nuclear systems, in which the inter-neucleon potentials decays rapidly at large inter-particle separation. The second universality class is relevant for atomic sys-

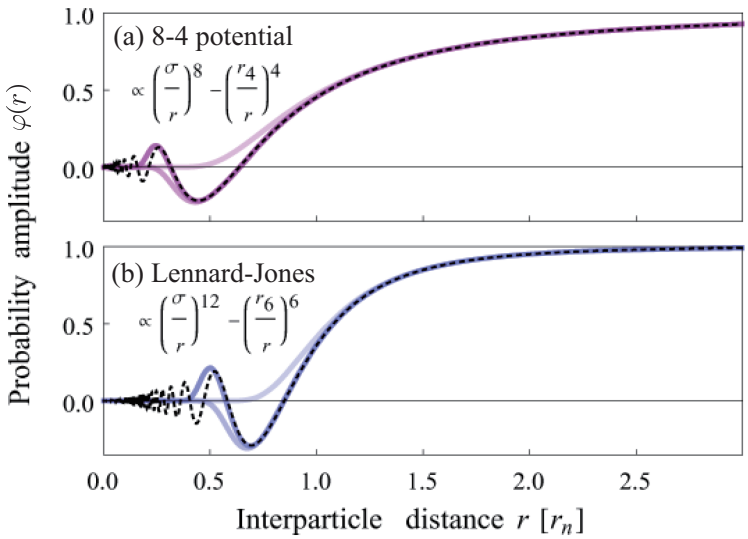

Figure 4.13: Zero-energy two-body wave function at unitarity for (a) the 8-4 potential, and (b) the Lennard-Jones potential. In each graph, the solid curves correspond in order of opacity to potential depths supporting 1, 2, and 3 *s*-wave bound states, respectively. The dashed curve represents the universal pair correlation in Eq. (4.42). [Figure adapted from Ref. [184] with permission. Copyright © (2014) by The American Physical Society.]

tems ranging from ^{4}He cluster to ultracold alkali atoms which are fine-tuned in the vicinity of a broad Feshbach resonance.

Chapter 5

Perfect screening of the inter-polaronic interaction

Recently, there has been growing interest in bridging the Efimov physics and many-body physics. For identical bosons which interact resonantly with each other, it has been demonstrated theoretically that there appear four-body bound states [77, 78, 79, 80], five-body bound states [81, 82, 83], ..., and N-body bound states associated with the Efimov states at least up to $N \approx 10 - 40$ [84, 85]. Some of these theoretical predictions have been confirmed in recent experiments in ultracold atoms. Indeed, signatures of the universal four-body bound states [26, 45, 68, 88] and five-body bound states [89] have recently been observed. Few-body physics studied for more than three particles can be regarded as an attempt to reach many-body physics in the bottom-up approach, by increasing the number of particles one by one.

There is an alternative approach to connect few-body physics and many-body physics. In some literature [94, 95, 96, 97, 98, 99, 100, 101], an interplay between few-body and many-body physics has been studied by considering a few-body problem in some many-body backgrounds. Two particles immersed in a Fermi sea has been studied in Refs. [94, 95, 96, 97], while two particles immersed in a Bose-Einstein condensate has been studied in Refs. [99, 100]. These $(N + 2)$-body systems are closely related to the few-body problems for more than three particles. Indeed, when one considers a three-body system of two particles resonantly interacting with another particle B, and starts increasing the number of the B particle, one can regard a system of two particles immersed in a many-body background as the limit where the number of B particles is large and the thermodynamic limit is taken for B particles.

Recently, it has been found that the Fermi sea tends to suppress the formation of the Efimov trimers [94, 97]. In Ref. [94], resonantly interacting $(N{+}1{+}1)$-body problem is considered with $N \gg 1$, so that one of the three components is degenerate and forms a Fermi sea. By assuming that the effect of the Fermi sea is merely to introduce a momentum cutoff in the three-body problem, just like what L. N. Cooper did in the study of superconductivity [195], they have found that the formation of the Efimov trimers is suppressed by the Fermi sea. A similar conclusion has also been obtained numerically for a system of two heavy particles immersed in a Fermi sea [97]. While these studies have demonstrated the suppression of the Efimov trimers for $(N + 2)$-body systems, one may wonder whether a similar suppression can occur for a $(N + 3)$-body system,$(N + 4)$-body

system, etc... Four-body systems of three identical particles resonantly interacting with another particle have recently been studied for both bosonic [196] and fermionic systems [90, 91, 92]. For a four-body system of three heavy bosons resonantly interacting with one light particle, it has been demonstrated that there is no four-body Efimov state, but still there exists four-body bound states associated with Efimov trimers [196]. For a four-body system of three identical fermions and one light particle, on the other hand, it has been demonstrated that four-body bound states of the Kartavtsev-Malykh character and the four-body Efimov states appear when the mass ratio between the fermions and the other particle is larger than 9.5 and 13.3, respectively [90, 92]. If the light particle is assumed to be a fermion and their number is increased in these systems, one arrives at the $(N+3)$-body problem: three heavy particles immersed in the Fermi sea of the light particles. Does the formation of the four-body bound states gets suppressed by the Fermi sea of the light particles? What about four, five, ..., and N_H heavy particles immersed in a light Fermi sea?

In this chapter, I answer this question by studying the effective interaction between N_H heavy particles immersed in a Fermi sea of light spinless (i.e., spin-polarized) fermions. With the Born-Oppenheimer method, I analytically show in Sec. 5.1 that the effective interaction between the heavy particles vanishes in the limit of high light-fermion density. To be more specific, I prove the following theorem:

Theorem. Let us consider a mixture of N_H heavy particles with mass M and spinless (i.e., spin-polarized) light degenerate fermions with mass m at zero temperature. The statistics of the heavy particles is arbitrary: they can be identical fermions, bosons, or distinguishable particles. The number of the light fermions is assumed to be so large that the Fermi sea is formed and the grand canonical ensemble can be applied to the light fermions. The interaction between the heavy particles and the light fermions is assumed to be a zero-range interaction with the s-wave scattering length a (see Eqs. (2.19) and (2.22)). The light spinless (i.e., spin-polarized) fermions do not interact with each other at low energy due to the Pauli exclusion principle. The heavy particles are assumed not to interact with each other[d]. Then, within the Born-Oppenheimer method, the effective interaction $V_{\text{eff}}(\boldsymbol{R_1}, \boldsymbol{R_2}, ..., \boldsymbol{R_{N_H}})$ between the N heavy particles positioned at $(\boldsymbol{R_1}, \boldsymbol{R_2}, ..., \boldsymbol{R_{N_H}})$ mediated by the light fermions vanishes in the limit of $k_F \to +\infty$:

$$\lim_{k_F \to +\infty} V_{\text{eff}}(\boldsymbol{R_1}, \boldsymbol{R_2}, ..., \boldsymbol{R_{N_H}}) = 0, \tag{5.1}$$

where k_F is the Fermi momentum of the light fermions.

[d]This assumption is justified when the heavy particles are identical fermions. Even when the interaction between the heavy particles is present, it merely adds to the effective interaction in the Born-Oppenheimer approximation.

Thus, the effective interaction between the heavy particles becomes vanishingly small in the dense fermionic environment. Note that the theorem is proved under a rather general condition: N_H and a can take on any value as long as $|a|, |\boldsymbol{R_i} - \boldsymbol{R_j}| \gg k_F^{-1} \to 0$ is satisfied. Therefore, it incorporate the unitarity limit $1/a = 0$. The theorem suggests that the formation of the N-body bound states associated with the Efimov effect is generally suppressed in the presence of a dense Fermi sea of light particles. In the case of two heavy particles immersed in the Fermi sea, the suppression of the

trimer formation has been numerically found in Ref. [97]. In addition to providing an analytical support for Ref. [97], our theorem generalizes it to arbitrary number of heavy particles immersed in the Fermi sea.

The theorem is closely related to polaron physics, which has been realized recently in ultracold atoms [102] and has been studied with great theoretical [96, 105, 106, 107, 108] and experimental interest [56, 102, 103, 104, 197]. In a system with large population imbalance, minority atoms interact with the surrounding majority atoms and form dressed quasi-particle states called polaron states. Our system can be regarded as N_H heavy polarons in a Fermi sea of light fermions. The theorem claims that the Born-Oppenheimer interaction between the heavy polarons gets vanishing small when the density of the surrounding fermions gets large.

We ascribe the physical origin of this vanishing effective interaction to the screening in the neutral Fermi system. While the screening is a famous phenomenon in the charged Fermi system, for a neutral Fermi system, little analytical results have been obtained, especially in the resonantly interacting regime $k_F|a| \gg 1$. The above theorem suggests that the screening phenomenon occurs for the neutral Fermi system, including the resonantly interacting regime.

This chapter is organized as follows. In Sec. 5.1, I define the effective interaction between the heavy particles within the Born-Oppenheimer method, and prove the main theorem. In Sec. 5.2, the screening phenomenon in the neutral Fermi system is discussed. I ascribe the physical origin of the vanishing interaction to the screening phenomenon in the neutral Fermi system. In Sec. 5.3, physical implications of the theorem are discussed. In Sec. 5.4, the finite temperature effects and the non-adiabatic effects beyond the Born-Oppenheimer approximation are discussed.

5.1 Theoretical description of the vanishing inter-polaronic interaction

In this section, the effective interaction between the heavy particles is studied. In Sec. 5.1.1, the effective interaction is defined with the Born-Oppenheimer approximation. In Sec. 5.1.2, I prove the main theorem.

5.1.1 Inter-polaronic interaction in the Born-Oppenheimer approximation

The effective interaction between the heavy particles $V_{\text{eff}}(\boldsymbol{R}_1, \boldsymbol{R}_2, ..., \boldsymbol{R}_{N_H})$ is defined in the same manner as in Refs. [96, 97]. With the Born-Oppenheimer approximation, one first solves the Schrödinger equation for the light fermions by regarding the heavy particles as fixed impurities, positioned at $\boldsymbol{R}_1, \boldsymbol{R}_2, ..., \boldsymbol{R}_{N_H}$. Then, the energy eigenvalue of the light particles gives an effective interaction between the heavy particles. Since the light fermions are assumed not to interact with each other, the solution of the Schrödinger equation for the light fermions is simply given by the Slater determinant $\Psi_L(\boldsymbol{r}_1, \boldsymbol{r}_2, ...) = \mathcal{A}\prod_i \psi^{(i)}_{\boldsymbol{R}}(\boldsymbol{r}_i)$, where $\mathcal{A}$ is the antisymmetrizer, $\boldsymbol{r}_i$ is the position of the i-th light fermion, and $\psi^{(i)}_{\boldsymbol{R}}$'s are the solutions of the single-particle Schrödinger equation in the presence of the impurity potentials located at $\boldsymbol{R} = (\boldsymbol{R}_1, \boldsymbol{R}_1, ..., \boldsymbol{R}_{N_H})$. The energy eigenvalue of the light particles is the sum of the single-particle eigenvalues $\varepsilon_i(\boldsymbol{R})$ corresponding to

$\psi_{\boldsymbol{R}}^{(i)}$: $E(\boldsymbol{R}) = \sum_i \varepsilon_i(\boldsymbol{R})$. The effective interaction between the heavy particles induced by the light fermions is obtained by subtracting the total energy of N independent polarons:

$$V_{\text{eff}}(\boldsymbol{R_1}, \boldsymbol{R_2}, ..., \boldsymbol{R_{N_H}}) = E(\boldsymbol{R}) - \lim_{|\boldsymbol{R_{ij}}|\to\infty} E(\boldsymbol{R}), \tag{5.2}$$

where $\lim_{|\boldsymbol{R_{ij}}|\to\infty}$ means that all the heavy particles are far apart from each other so that they may be regarded as N_H independent polarons:

$$\lim_{|\boldsymbol{R_{ij}}|\to\infty} E(\boldsymbol{R}) = E_0 - N_H\mu_0, \tag{5.3}$$

where E_0 is the total energy of non-interacting Fermi gas, and μ_0 is the energy shift induced by a single heavy particle [105]:

$$\mu_0 = \frac{\hbar^2 k_F^2}{2\pi m}\left[(1+y^2)\left(\frac{\pi}{2} + \arctan y\right) + y\right] \qquad \left(y = \frac{1}{k_F a}\right). \tag{5.4}$$

For $N_H = 2$ (i.e. two heavy particles immersed in the light Fermi sea), V_{eff} has been studied numerically in Ref. [96]. As the number of the heavy particles increases, however, it becomes impractical to calculate V_{eff} numerically, since the effective interaction cannot be written as a simple sum of two-body interactions, but rather it includes all the three-body, four-body, ..., and N-body interactions. To circumvent this difficulty, I use a formal scattering theory to evaluate V_{eff} analytically.

5.1.2 Proof of the theorem

To prove the theorem, one needs to evaluate the effective interaction in Eq. (5.2). The total energy of the light fermions $E(\boldsymbol{R})$ is the sum of the contributions from the continuum states ($\varepsilon_i \geq 0$) and the bound states ($\varepsilon_i < 0$):

$$E(\boldsymbol{R}) = \sum_{\varepsilon_i \geq 0} \varepsilon_i(\boldsymbol{R}) + \sum_{\varepsilon_i < 0} \varepsilon_i(\boldsymbol{R}). \tag{5.5}$$

To evaluate the continuum part, the scattering theory can be used by regarding the heavy particles as fixed impurity potentials located at $\boldsymbol{R_1}, \boldsymbol{R_1}, ..., \boldsymbol{R_{N_H}}$. Let us define the scattering phase shifts $\delta_n(k)$ induced by the sum of the impurity potentials as eigenvalues of the S-matrix $\mathcal{S}(k)$ [198, 199]:

$$\mathcal{S}(k)\boldsymbol{v}_n(k) = e^{2i\delta_n(k)}\boldsymbol{v}_n(k). \tag{5.6}$$

Since the heavy particles can be located rather randomly, the potential created by the heavy particles generally do not have any symmetry. Thus, the scattering phase shift and the S-matrix are those for a potential with no symmetry: non-central, parity non-conserving, etc... The scattering theory we use in the following argument is also for a non-symmetric potential.

Let us first show that the continuum part of the effective interaction can be written by the scattering phase shifts through the following lemma:

Lemma (*generalized Fumi theorem*)

$$E(\boldsymbol{R}) = E^{\mathrm{cont}}(\boldsymbol{R}) + E^{\mathrm{BS}}(\boldsymbol{R}), \tag{5.7}$$

where $E^{\mathrm{cont}}(\boldsymbol{R})$ and $E^{\mathrm{BS}}(\boldsymbol{R})$ are the continuum and bound-state contributions, respectively, which are given by

$$E^{\mathrm{cont}}(\boldsymbol{R}) = -\frac{\hbar^2}{\pi m}\sum_n \int_0^{k_F} k dk \delta_n(k) + E_0, \tag{5.8}$$

where E_0 is the total energy of non-interacting Fermi gas and

$$E^{\mathrm{BS}}(\boldsymbol{R}) = \sum_{\varepsilon_i<0} \varepsilon_i(\boldsymbol{R}). \tag{5.9}$$

In the case of a single impurity ($N_H = 1$) in the absence of bound states, this lemma reduces to the Fumi theorem [200]:

$$E(\boldsymbol{R}) - E_0 = -\frac{\hbar^2}{\pi m}\sum_n \int_0^{k_F} k dk \delta_n(k). \tag{5.10}$$

In this case, the potential created by the heavy particle is a central potential, so that the angular momentum becomes a good quantum number $n \to (\ell, m)$. In the case of two heavy particles immersed in the Fermi sea, the above theorem has been derived in Ref. [96]. In this case, the parity is a good quantum number. For $N_H \geq 3$, the configuration of the heavy particles can vary arbitrarily, and there is no good quantum number.

Proof of lemma. We use the Friedel sum rule [201, 202]:

$$N_I - N_0 = \frac{1}{\pi}\sum_n \delta_n(k_F), \tag{5.11}$$

where k_F is the Fermi momentum of the light fermions, and N_I and N_0 are the numbers of the light fermions evaluated by the grand canonical ensemble with and without the impurity potential, respectively. For a central potential, the index n represents the angular momentum quantum numbers (ℓ, m), and one recovers the original Friedel sum rule. While the Friedel sum rule was originally proved for an ideal Fermi gas interacting with a central impurity potential [201], it was subsequently generalized for an interacting system with a non-central potential [202]. The impurity potential produced by N_H heavy particles, in general, is a non-central potential, but still the Friedel sum rule remains valid.

The generalized Fumi theorem can be proved by using the Friedel sum rule. Recall that the number of the light fermions is related to the thermodynamic function Ω of the light fermions through the thermodynamic relation $\left(\frac{\partial \Omega}{\partial \mu}\right)_{T,V} = -N$. By integrating this relation with respect to the chemical potential for systems with and without the impurity potentials, and using the Friedel sum

rule, we obtain

$$\begin{aligned}\Omega_I - \Omega_0 &= -\int_{\mu\geq 0}(N_I - N_0)d\mu - \int_{\mu<0}(N_I - N_0)d\mu, \\ &= -\frac{\hbar^2}{\pi m}\sum_n \int_0^{k_F} kdk\delta_n(k) - \int_{\mu<0} N_I d\mu,\end{aligned} \tag{5.12}$$

where Ω_I and Ω_0 are the thermodynamic potentials with and without the impurity potentials, respectively. In deriving the second equality, we use the fact that there is no bound state in the absence of any potential: $N_0 = 0$ for $\mu < 0$. Since the light fermions are non-interacting, we can put $\mu_I \approx \mu_0 = \dfrac{\hbar^2 k_F^2}{2m}$ in Eq. (5.12). Indeed, the shift in the energy level induced by the impurity potential is of the order of $V^{-\frac{1}{3}}$, where V is the volume of the system, and this shift is negligible in the thermodynamic limit. Substituting $N_I = \sum_i \Theta(\mu - \varepsilon_i(\boldsymbol{R}))$, where Θ is the Heaviside step function, the second term in the second line of Eq. (5.12) can be evaluated as

$$\int_{\mu<0} N_I d\mu = -\sum_{\varepsilon_i<0}\varepsilon_i(\boldsymbol{R}). \tag{5.13}$$

Substituting this into Eq. (5.12), we arrive at the following equation

$$\Omega_I - \Omega_0 = -\frac{\hbar^2}{\pi m}\sum_n \int_0^{k_F} kdk\delta_n(k) + \sum_{\varepsilon_i<0}\varepsilon_i(\boldsymbol{R}). \tag{5.14}$$

This is equivalent to the generalized Fumi theorem in Eqs. (5.7), (5.8), and (5.9).

Proof of the main theorem. By using the generalized Fumi theorem, we can prove the main theorem. We first recall the following relation between the phase shifts $\delta_n(k)$ and the Fredholm determinant $D(k)$ [198, 199]:

$$\sum_n \delta_n(k) = -\frac{k}{4\pi}\int d\boldsymbol{x} U_{\boldsymbol{R}}(\boldsymbol{x}) + \frac{i}{2}\log\left[\frac{D(k)}{D^*(k)}\right], \tag{5.15}$$

where $U_{\boldsymbol{R}}$ is the sum of the impurity potentials produced by the heavy particles. The Fredholm determinant is defined from the kernel matrix $\mathcal{K}(k)$ of the Lippmann-Schwinger equation as $D(k) = \det[1 - \lambda\mathcal{K}(k)]_{\lambda=1}$, and has the following properties for a general short-ranged, non-central potential [198, 199]:

1. $D(k)$ is well-defined and analytic for $\mathrm{Im}k \geq 0$;
2. $\lim_{|k|\to\infty} D(k) = 1$ for $\mathrm{Im}k \geq 0$;
3. For a real k, $D^*(k) = D(-k)$;
4. The zero of $D(k = i\kappa) = 0$ in the upper-half complex k-plane has a one-to-one correspondence with a bound state with its energy $\varepsilon = -\dfrac{\hbar^2\kappa^2}{2m}$;

5. The zero of $D(k)$ can appear either on a positive imaginary plane, or at the origin $k = 0$ for a short-range potential.

Substituting Eq. (5.15) into $E^{\mathrm{cont}}(\boldsymbol{R})$ and differentiating both sides with respect to $\boldsymbol{R}_i$, we obtain

$$\begin{aligned}\nabla_{\boldsymbol{R}_i} E^{\mathrm{cont}}(\boldsymbol{R}) &= -\frac{i\hbar^2}{2\pi m}\int_0^{k_F} kdk \nabla_{\boldsymbol{R}_i} \log\left[\frac{D(k)}{D^*(k)}\right] \\ &= -\frac{i\hbar^2}{2\pi m}\int_{-k_F}^{k_F} kdk \frac{\nabla_{\boldsymbol{R}_i} D(k)}{D(k)}.\end{aligned} \tag{5.16}$$

In deriving the second equality, we have used the property 3 to transform the integration of $D^*(k)$ into that of $D(k)$ along the negative real axis. Now, let us take the limit $k_F \to +\infty$. The properties 2 and 3 ensure that there is a well-defined limit for Eq. (5.16). Furthermore, the properties 1-3 also justify the change of the integration contour into paths C_j's encircling the zeros of $D(k)$:

$$\lim_{k_F\to\infty} \nabla_{\boldsymbol{R}_i} E^{\mathrm{cont}}(\boldsymbol{R}) = -\frac{i\hbar^2}{2\pi m}\sum_j \int_{C_j} kdk \frac{\nabla_{\boldsymbol{R}_i} D(k)}{D(k)}. \tag{5.17}$$

Note that we can put $D(k) = \alpha_j(k - i\kappa_j) + O((k - i\kappa_j)^2)$ close to the zero point $k \approx i\kappa_j$ if the bound state is not degenerate [198, 199]. Substituting this into Eq. (5.17) and performing the contour integration, we obtain

$$\begin{aligned}\lim_{k_F\to\infty} \nabla_{\boldsymbol{R}_i} E^{\mathrm{cont}}(\boldsymbol{R}) &= \nabla_{\boldsymbol{R}_i} \sum_j \frac{\hbar^2\kappa_j^2}{2m} \\ &= -\nabla_{\boldsymbol{R}_i} E^{\mathrm{BS}}(\boldsymbol{R}).\end{aligned} \tag{5.18}$$

This implies that the continuum contribution exactly cancels the bound-state one, and the effective interaction vanishes:

$$\lim_{k_F\to\infty} \nabla_{\boldsymbol{R}_i} E(\boldsymbol{R}) = \lim_{k_F\to\infty} \nabla_{\boldsymbol{R}_i} V_{\mathrm{eff}}(\boldsymbol{R}_1, \boldsymbol{R}_2, ..., \boldsymbol{R}_{N_H}) = 0. \tag{5.19}$$

When the bound states are n-fold degenerate, on the other hand, $D(k)$ behaves as $D(k) \approx \alpha(k - i\kappa_j)^n + O((k - i\kappa_j)^{n+1})$ close to the zero point [198, 199]. Even with such a degeneracy, we can derive Eq. (5.18) from Eq. (5.17), and the above result remains valid.

5.2 Physical origin of the vanishing inter-polaronic interaction

As can be seen in Eq. (5.18), the effective interactions originating from the bound states and continuum states cancel exactly in the limit $k_F \to +\infty$. For $N_H = 2$, there is one bound state when $R_{12} \ll |a|$. This bound state produces an attractive inverse-square potential $E^{\mathrm{BS}}(\boldsymbol{R}) = -\dfrac{\hbar^2\Omega^2}{2mR_{12}^2}$, where $\Omega = 0.5671...$ (see Sec. 2.3.1). When there is only one light fermion, the Efimov states of the two heavy and one light particles are formed by this inverse square attraction. As the number of the light fermions is increased, the continuum part $E^{\mathrm{cont}}(\boldsymbol{R})$ starts to produce an additional repulsion,

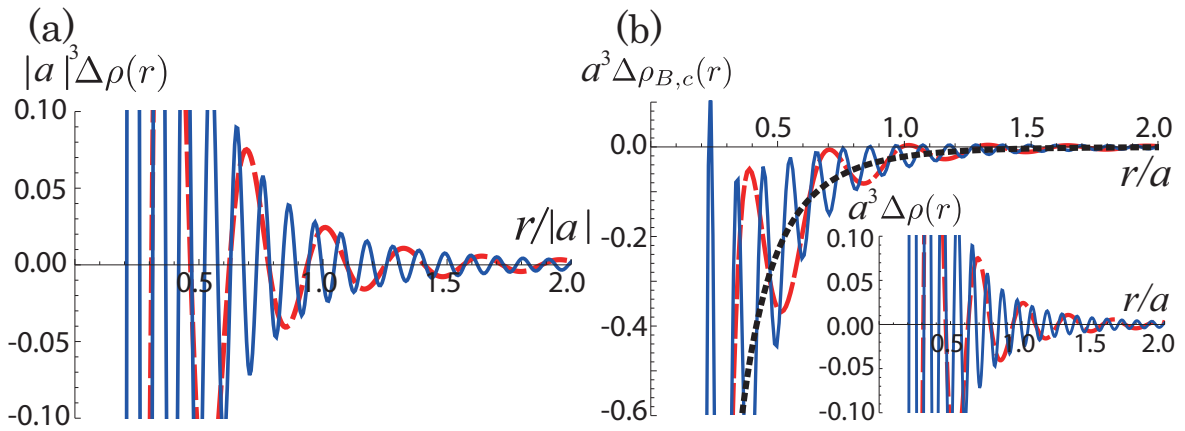

Figure 5.1: Density variations induced by a single heavy impurity for (a) $a < 0$ and (b) $a > 0$. In Fig. (a), $\Delta\rho(r)$ is shown for $k_F a = -10$ (red dashed curve) and $k_F a = -30$ (blue solid curve). In Fig. (b), $\Delta\rho_c(r)$ is shown for $k_F a = 10$ (red dashed curve) and $k_F a = 30$ (blue solid curve). The black dotted curve represents $-\Delta\rho_B(r)$. The inset in Fig. (b) shows the total density variation $\Delta\rho(r) = \Delta\rho_B(r) + \Delta\rho_c(r)$. [Figure adapted from Ref. [203] with permission. Copyright © (2014) by The American Physical Society.]

canceling the Efimov attraction and suppressing the Efimov effect. Thus, the continuum of the Fermi sea tends cancel the attraction induced by the bound state.

The cancellation of the bound-state contribution by the continuum contribution can be physically understood as originating from the screening effect. Crudely speaking, one can think that the effective interaction between the heavy particles is induced by the density variation caused by the impurities. Let us then consider the density variation of the light fermions $\Delta\rho(r)$ caused by a single impurity. The density variation can be expressed as the sum of the bound-state and continuum-state contributions $\Delta\rho(r) = \Delta\rho_B(r) + \Delta\rho_c(r)$, where

$$\begin{aligned} \Delta\rho_B(r) &= \frac{\theta(a)}{2\pi a r^2} e^{-\frac{2r}{a}}, \\ \Delta\rho_c(r) &= \frac{1}{2\pi^2 r^2} \int_0^{k_F} dk \left[\sin^2(kr + \delta_0(k)) - \sin^2 kr\right], \end{aligned} \tag{5.20}$$

and $\delta_0(k)$ is the s-wave phase shift induced by the impurity: $\tan\delta_0(k) = -ka$. In Fig. 5.1, we show $\Delta\rho(r)$'s for several values of $k_F a$. For $a < 0$ (Fig. 5.1 (a)), there is no bound state and $\Delta\rho_B(r) = 0$. The density variation reflects the Friedel oscillations characterized by k_F. As k_F increases, the oscillations become faster, but the amplitude remains the same. For $a > 0$ (Fig. 5.1 (b)), $\Delta\rho(r)$ is the sum of $\Delta\rho_B(r)$ and $\Delta\rho_c(r)$. We note that $\Delta\rho_c(r)$ follows the $-\Delta\rho_B(r)$ curve on average, so that the continuum states screen the bound-state contribution. Due to this screening effect, $\Delta\rho(r)$ undergoes fast oscillations around zero on both positive and negative sides of a. Thus, the interaction between the heavy particles mediated by this density variation should become weaker as k_F increases regardless of the value of the s-wave scattering length or the distance between the heavy particles.

The screening is closely related to the Friedel sum rule. Indeed, the Friedel sum rule suggests

$$\int d^3r\Delta\rho_B(r) + \int d^3r\Delta\rho_c(r) = \frac{1}{\pi}\delta_0(k_F). \tag{5.21}$$

In the high-fermion density limit, $\delta_0(k_F \to +\infty) \to 0$ and we obtain

$$\int d^3r\Delta\rho_B(r) + \int d^3r\Delta\rho_c(r) = 0. \tag{5.22}$$

This suggests that the density variation of the continuum is canceled by that of the bound state, as shown in Fig. 5.1.

Note that the screening in the neutral Fermi system is rather distinct from that in the charged Fermi system. In the former case, the induced interaction vanishes due to the cancellation of the bound-state contribution by the continuum one. If we add the Hamiltonian with a direct interaction between heavy particles,, the direct interaction is not screened and the effective interaction between the heavy particles remains non-vanishing. On the other hand, in the charged Fermi system, the direct interaction between the heavy particles is canceled by the induced one.

5.3 Physical implications of the theorem

Suppression of the Efimov effect

The theorem suggests that the dense Fermi sea suppresses the formation of the Efimov states and N-body bound states associated with the Efimov effect for any number of heavy particles. Indeed, the theorem claims that the heavy particles do not interact in the limit of $k_F \to +\infty$, so they cannot form any bound state in this limit. For a large but finite k_F, the theorem implies that the interaction between the heavy particles is small when $k_F^{-1} \ll |a|, \min_{i\neq j}|\boldsymbol{R_i} - \boldsymbol{R_j}|$. This can be checked for $N_H = 2$ [96] by explicit calculation of the sub-leading contribution to the effective interaction at high density. When $k_F^{-1} \ll |a|, R_{12}$, one can show that V_{eff} behaves as

$$\begin{aligned} V_{\text{eff}}(R_{12}) = &-\frac{\hbar^2}{2\pi m k_F R_{12}^3}\cos 2k_F R_{12} - \frac{\hbar^2}{4\pi m k_F^2 R_{12}^4}\sin 2k_F R_{12} + \frac{\hbar^2}{\pi m R_{12}^3 k_F^2 a}\sin 2k_F R_{12} \\ &+ \frac{\hbar^2}{m} O\left(\frac{1}{k_F^3 a R_{12}^4}, \frac{1}{k_F^3 a^3 R_{12}^2}, \frac{1}{k_F^3 a^5}, \ldots\right). \end{aligned} \tag{5.23}$$

Thus, the effective interaction is suppressed by a factor of k_F^{-1}, and becomes small as k_F increases. The range of the interaction between the heavy particles is at most of the order of k_F^{-1}. More specifically, the range of interaction between the heavy particles is $\min(|a|, k_F^{-1})$. This gives a cut-off length scale up to which the discrete scale invariance holds, so that the spatial size of the Efimov states and their associated N-body bound states cannot exceed $\min(|a|, k_F^{-1})$. One can estimate the number of the Efimov states and their associated bound states to be

$$N_B \sim \log\left[\kappa^* \min(|a|, k_F^{-1})\right], \tag{5.24}$$

where κ^* is the momentum scale characterizing the Efimov states. For the Efimov trimers, it is the three-body parameter (see Sec. 2.2.1). For the four-body Efimov state found in a system of three

identical fermions and one distinguishable particle for a mass ratio $13.3 < m_F/m_L < 13.6$ [90], κ^* is the four-body parameter. In ultracold atoms, κ^* is characterized by the van der Waals length $\kappa^* \sim r_{\rm vdw}^{-1}$. At the unitarity, Eq. (5.24) becomes

$$N_B \sim \log\left(\frac{\kappa^*}{k_F}\right). \tag{5.25}$$

While some knowledge of Eq. (5.23) has been used to derive Eq. (5.24), the estimate in Eq. (5.25) can be obtained by a dimensional analysis without using Eq. (5.23).

The estimates in Eqs. (5.24) and (5.25) also suggest that the dense Fermi sea suppresses the Efimov effect. Indeed, according to Eqs. (5.24) and (5.25), the number of the Efimov states and their associated N-body bound states decreases as k_F increases, and finally vanishes when $k_F \sim \kappa^* \sim r_{\rm vdw}^{-1}$. For two heavy particles $N_H = 2$, the suppression of the Efimov effect was numerically demonstrated in Ref. [97]. The theorem proved here and the above argument can be used to generalize what has been found in Ref. [97] for an arbitrary number of heavy particles in an analytical manner. Since the appearance of the Efimov states and their associated bound states is closely related to the loss processes in ultracold atom experiments (see Sec. 2.2.4), one can expect that the N-body losses in a resonantly interacting heavy-light mixture may be suppressed by the Fermi sea effects. This point should be studied in more detail in future studies.

Note that some prefactors of the order of unity are neglected in Eqs. (5.24) and (5.25), so they should be regarded as an order of magnitude estimates. One prefactor missing in Eqs. (5.24) and (5.25) is the number of bound states associated with each Efimov state. For a system of identical bosons, two four-body bound states exist for each Efimov trimer [78, 80]. Similar four-body bound states have also been demonstrated to exist for a hetero-nuclear bosonic system [196]. For a system of identical bosons, there also exists five-body bound states, six-body bound states associated with the Efimov trimers [81, 82, 83]. In Eqs. (5.24) and (5.25), I only count the number of the log-periodic oscillation of the Efimov effect, so one needs to multiply the number of bound states per each period for a better estimate. Another factor missing in Eqs. (5.24) and (5.25) is the parameter s appearing in the discrete scale factor $e^{\pi/s}$ of the Efimov states. This parameter characterizes the period of the log oscillation. The estimates Eqs. (5.24) and (5.25) can be improved by multiplying s/π. These possible prefactors are neglected in Eqs. (5.24) and (5.25) since we do not know some of their precise values yet for $N_H \gtrsim 3$, but from recent few-body studies [32, 78, 80, 81, 82, 83, 90, 91, 92, 196], it is natural to expect that these prefactors should be at most of the order of unity.

Note that the above argument is based on the Born-Oppenheimer approximation, and I have neglected the non-adiabatic effects discussed in Sec. 5.4. In discussing whether heavy particles can form bound states in the Fermi sea, dynamical motions of the heavy particles need to be considered. As discussed in Sec. 5.4, the non-adiabatic effects can generally affect the dynamics of the heavy particles significantly. However, one can expect that the above argument on the number of the Efimov states and their associated bound states would not be affected so much by the non-adiabatic effects because the Efimov effect is essentially a single-channel (i.e., adiabatic) effect. Indeed, for a system of two heavy and one light particles, the inverse square attraction appears in $E^{\rm BS}(\boldsymbol{R})$ and the Efimov effect can be described properly with the Born-Oppenheimer approximation. The theorem suggests that this Efimov attraction gets screened by the Fermi sea in the adiabatic channel, so one

can expect that the conclusion remains unchanged even when the channel couplings induced by the non-adiabatic effects are incorporated.

Screening of the effective interaction between heavy polarons

The system studied in this chapter is closely related to polaron physics[§]. Polaron has recently been realized in ultracold atoms by preparing a two-component Fermi system with extreme population imbalance [102]. Under such conditions, minority atoms interact with the surrounding fermions, forming dressed quasi-particle states called polarons. While the polaron state corresponds to a single particle immersed in the Fermi sea, the effective interaction between the polarons becomes relevant as the number of the minority atoms is increased. The inter-polaronic interaction is a fundamental building block in bridging the gap between the polaron state in the population imbalanced limit to many-body phases of population balanced Fermi systems [134, 135, 136, 137] and imbalanced Fermi systems [103, 204, 205].

Our system of N_H heavy particles immersed in a Fermi sea of light particles can be regarded as a system of N_H heavy polarons. The theorem implies that the effective interaction between the heavy polarons would be vanishingly small as the light fermions' density increases. Recently, the polaron state has been realized in a mass-imbalanced mixture of ^{40}K-^{6}Li atoms, and a heavy polaron has been studied [56]. This is a first step toward the investigation of the polaron physics in highly mass-imbalanced systems, such as ^{133}Cs-^{6}Li [180, 181] or ^{173}Yb-^{6}Li [57, 58]. Interestingly, in Ref. [56], the inter-polaronic interaction has been found to be irrelevant up to a rather high impurity concentration. The same feature has also been found for polarons in an equal-mass three-dimensional system [102], and in an equal-mass two-dimensional system [104]. Although the mass ratio in Ref. [56] is only $M/m = 6.64$ and therefore our analysis based on the Born-Oppenheimer approximation cannot be justified, let alone Refs. [102, 104], it is interesting to note that the theorem proved in this chapter is consistent with what have been observed in experiments. Equation (5.23) also suggests that the Born-Oppenheimer interaction between the heavy particles can be significant only when $R_{12} \lesssim k_F^{-1}$, meaning that the density of the heavy particles must be as large as that of the light particle for the inter-polaronic interaction to be significant.

The theorem suggests that the Born-Oppenheimer interaction between the heavy polarons vanishes including the unitarity limit $1/a = 0$. It is remarkable that the interaction can vanish in this strongly correlated regime. It should be noted that some behaviors similar to a non-interacting gas around the unitarity region has also been suggested in some literature. In the unitarity limit of the BEC-BCS crossover, it has been shown analytically that the thermodynamics relation is identical to that of the ideal gas $E = \frac{3}{2}P$ [138, 142, 143, 144]. Furthermore, the temperature dependence of the condensation fraction around the critical point was observed to behave in the same manner as that of the ideal Bose gas [140]. These studies have been done for a equal-mass system, and the theorem proved in this chapter is not applicable, but still it is worth noting the similarity.

As discussed in Sec. 5.4, the non-adiabatic effects can significantly affect the dynamics of the heavy particles, and therefore the theorem does not necessarily mean that heavy polarons behave as non-interacting quasi-particles. Thus, the above argument on the inter-polaronic interaction should

[§]For a review of the polaron physics in ultracold atoms, the readers may refer to Refs. [108] and [109].

be at most qualitative.

5.4 Some remarks

Finite temperature effects

Finite temperature effects can also be estimated with the Born-Oppenheimer method. At low temperature $T \ll T_F = \dfrac{\hbar^2 k_F^2}{2m}$, one can regard that all the bound state eigenstates of the light particles are occupied, so that the effective interaction between the heavy particles is modified through the thermally excited particle-hole excitations around the Fermi sea. If the number of the heavy particles is not so large $N_H \sim O(1)$, the chemical potential and the density of states at the Fermi energy do not vary significantly from those of the ideal Fermi gas. The Sommerfeld theory of the ideal Fermi gas can then be used to estimate the finite temperature effects, and one obtains

$$V_{\text{eff}}(T) - V_{\text{eff}}(T = 0) \sim \left(\frac{T}{T_F}\right)^2 T_F. \tag{5.26}$$

The finite temperature effects are therefore negligibly small at low temperature $T \ll T_F$. One can also see that it gets small as the density of the light fermions is increased while keeping the temperature. Thus, the main theorem should remain valid at finite temperature when $T \ll T_F \to +\infty$.

Non-adiabatic effects

The non-adiabatic effects beyond the Born-Oppenheimer method need to be considered in discussing the dynamics of the polarons. For systems with moderate mass imbalance, such as a ^{40}K-^{6}Li mixture [56], the Born-Oppenheimer approach fails. Even for mixtures with extreme mass imbalance recently realized, such as ^{133}Cs-^{6}Li [180, 181] or ^{173}Yb-^{6}Li [57, 58], the non-adiabatic effects may affect the dynamics significantly[§]. The dynamics of a single heavy particle in a fermionic environment has been studied in the absorption spectra of X-ray [208, 209] or the muon diffusion [210] in metals. It has been demonstrated that the motion of heavy particles can create particle-hole excitations in the Fermi sea, which leads to dissipation [211]. Indeed, in the temperature regime $\dfrac{k_F^2}{2M} \ll T \ll \dfrac{k_F^2}{2m}$, the effective action of the heavy particle is described by the Langevin type of equation with a strength of dissipation $\gamma = \dfrac{\hbar^2 k_F^2}{3\pi M} \sin^2 \delta_0$, where δ_0 is the s-wave phase shift [211, 212]. Such a dissipation cannot be taken into account with the Born-Oppenheimer method. It has also been suggested that the non-adiabatic effects can create non-trivial correlation between heavy particles [213, 214]. Our theorem only states that the adiabatic part of the interaction becomes small in the dense Fermi sea, so the effect of the non-adiabatic parts still remains

[§]Indeed, this is closely related to the Anderson orthogonality catastrophe [206, 207], which suggests that the Born-Oppenheimer approximation is inadequate in describing the dynamics of a heavy particle immersed in the Fermi sea.

unclear. Whether the interaction between the heavy particles induced by non-adiabatic effects remains significant or becomes negligibly small in the high-density limit need to be clarified in order to discuss the dynamics of the heavy particles.

Chapter 6

Conclusion and future prospects

Conclusion

In this thesis, I have theoretically studied the Efimov physics and related phenomena in ultracold atoms. In Chapters 1 and 2, I have reviewed the universality of a low-energy few-body system and the Efimov physics. I have also overviewed recent developments in theoretical and experimental studies on the Efimov physics and related phenomena in ultracold atoms. The main contributions of this thesis are presented in Chapters 3, 4, and 5.

In Chapter 3, I have studied a three-body system of two identical spinless (i.e., spin-polarized) fermions and one distinguishable particle which interact via a short-range potential with a large s-wave scattering length. In this system, two classes of universal three-body bound states have been known to appear in different regimes of the mass ratio: the Efimov trimers and the Kartavtsev-Malykh trimers, which feature the discrete and continuous scale invariance, respectively. I have found the third class of universal three-body bound states, which I call the "crossover trimers". The crossover trimers show neither discrete nor continuous scale invariance, but still they exist and behave universally close to unitarity. I have identified the regions of these three classes of trimers as a function of the mass ratio and the s-wave scattering length. I have also shown that the Kartavtsev-Malykh trimers and the Efimov trimers can continuously transform into each other via the crossover trimers as the mass ratio and the s-wave scattering length are varied. I have found that the Kartavtsev-Malykh trimers dissociate into a particle and a dimer when the s-wave scattering length is varied, owing to the presence of the crossover trimers. I have calculated the elastic particle-dimer scattering lengths in arbitrary angular-momentum channels, and shown that the particle-dimer resonances occur at the points where the trimers dissociate into a particle and a dimer. From the resonance positions, I have found accurate values of the critical mass ratios at which the Kartavtsev-Malykh trimers in the higher angular-momentum channels appear.

In Chapter 4, I have studied the three-body parameter of the Efimov states for a system of three identical bosons in the vicinity of a broad Feshbach resonance. I have elucidated the physical origin of the universality in the three-body parameter recently found in ultracold atom experiments as follows:

- For a deep two-body potential or a two-body potential with a hard-core repulsion at short distance, the probability of two particles coming close is suppressed in a universal manner.

- This universal pair correlation induces an abrupt deformation of the three-body wave function as the hyper-radius is varied.

- This abrupt deformation of the wave function results in a strong non-adiabatic repulsion $Q_{nn}(R) > 0$, which explains the appearance of the universal three-body repulsion reported in Ref. [73]. Since three particles cannot come close due to the universal three-body repulsion, three-body physics is solely determined by the long-range van der Waals part, and is insensitive to atomic species dependent short-range part.

This mechanism is verified by reproducing the universal three-body repulsion with a simple model wave function. It has also been shown that the three-body parameter becomes universal even for non-van der Waals types of two-body potentials. Two classes of two-body potentials have been identified, for which the three-body parameter has a universal value in units of their effective range. One class corresponds to short-range two-body potentials decaying as a power law, for which the universal pair correlation behaves smoothly. The other corresponds to two-body potentials decaying exponentially, for which the universal pair correlation shows a discontinuity. The former class is relevant for the Efimov states in ultracold atoms, ^{4}He cluster [8, 9, 10], and possibly polyexcitons in solids [76], while the latter class should be relevant for the Efimov states in nuclear systems [3, 4, 5]. These findings may stimulate further investigation of the three-body parameter of the Efimov physics in many fields of physics.

In Chapter 5, I have studied the induced the interaction between the heavy particles for a system of N heavy particles resonantly interacting with a Fermi sea of the light spinless (i.e., spin-polarized) fermions at zero temperature. With the Born-Oppenheimer method, I have analytically shown that the induced interaction vanishes for any N in the limit of high light-fermion density. The induced interaction vanishes even in the unitarity regime. This implies that the formation of the Efimov states and their associated N-body bound states is suppressed by the dense Fermi sea. The vanishing induced interaction has been ascribed to the screening effect in the neutral Fermi system.

In most of the above studies, I have mainly dealt with few-body systems in ultracold atoms, but they are also relevant for other physical systems, owing to the universality of a low-energy few-body system. In particular, in Chapters 3 and 5, I have used the zero-range approximation, so the results presented in Chapters 3 and 5 can be directly applied for any physical system if (i) the interaction between the particles is short-range, (ii) the energy of the system is sufficiently low, and (iii) the s-wave scattering length between the particles is resonantly large.

Future prospects

(i) Understanding the crossover physics studied in Chapter 3 in terms of the renormalization group language

In Chapter 3, I have found that the Kartavtsev-Malykh trimers continuously transform into the Efimov trimers via the crossover trimers as the mass ratio and the s-wave scattering length are varied. In other words, the continuous scale invariance of the Kartavtsev-Malykh trimers is gradually lost and then the discrete scale invariance of the Efimov trimers appear as the mass ratio

and the s-wave scattering length are varied. In the renormalization group studies, it has been shown that the Efimov states show the renormalization group limit cycle [31, 32]. It is of great interest how the crossover physics found in Chapter 3 can be understood in terms of the renormalization group: how does the limit cycle behavior change into a flow with the continuous scale invariance? This issue is currently being studied by Issei Yoshimoto in Kyushu University. For more details, the readers are referred to his Ph. D thesis [215].

(ii) Three-body parameter for hetero-nuclear (i.e., mass-imbalanced) systems

In Chapter 3, I have studied a three-body system of two heavy fermions and one light particle with the Skorniakov–Ter-Martirosian equation by imposing a momentum cutoff to introduce the three-body parameter. Throughout Chapter 3, the momentum cutoff Λ is regarded as a mere parameter, and I have expressed all the results in units of Λ. One should relate Λ with some observables such as the van der Waals length to obtain realistic energy spectra. However, the relation between Λ and physical quantities is yet to be clarified. This issue is closely related to the problem of the three-body parameter for hetero-nuclear (i.e., mass-imbalanced) systems. While the three-body parameter for a system of three identical bosons has been found to be $a_{-}^{(1)} = -8\text{-}10\, r_{\rm vdw}$, little is known for hetero-nuclear systems: to the best of the author's knowledge, there are only three pieces of work on this issue [55, 66, 168]. See Sec. 2.4 for more details. It is therefore quite desirable to study the three-body parameter for the hetero-nuclear systems, and show all the results presented in Chapter 3 in terms of realistic physical quantities. It is also desirable to understand how the results in Chapter 3 obtained with the Skorniakov–Ter-Martirosian equation can be understood in the hyper-spherical approach [216].

(iii) Universality of the N-body bound states associated with the Efimov trimers

In Chapter 4 and in Ref. [73], it has been shown for the van der Waals types of potentials that there appears universal three-body repulsion at $R \approx 2r_{\rm vdw}$, so that the three-body physics is universally characterized by the van der Waals length and the s-wave scattering length. It is natural to expect that the universal repulsion should also appear for four-body, five-body, ..., and N-body systems: when the hyper-radius of a N-body ($N \geq 4$) system gets small, either three of the N particles must come close, so that the universal three-body repulsion between the three particles gets significant and a repulsive N-body hyper-radial potential would appear at $R \sim r_{\rm vdw}$. This simple physical argument leads us to the following conjecture: for an arbitrary number of particles, N-body bound states associated with the Efimov trimers should be universally characterized by the two parameters: the van der Waals length and the s-wave scattering length.

Recently, there has been an attempt to test this conjecture. In Refs. [217, 218], a four-body problem of ^{4}He has been solved numerically with realistic ^{4}He potentials. The scattering length at which the four-body bound states dissociates into four particles has been calculated and has been found to be in excellent agreement with that for ^{133}Cs atoms observed experimentally [68] for both the ground-state and first-excited tetramers tied to the ground-state Efimov trimer[§]. This is a strong evidence that the above conjecture should be true at least for a four-body system. It would

[§]The four-body thresholds have also been observed for ^{7}Li atoms in Refs. [26, 45], but they seem to disagree with those for ^{133}Cs atoms [68] and ^{4}He atoms [217, 218]. This discrepancy may be due to the width of the Feshbach resonance: the ^{7}Li experiment has been performed for a moderately narrow Feshbach resonance $s_{\rm res} \approx 0.6$, while a broad resonance is used for the ^{133}Cs experiment.

be important to show in the future studies whether the universality of the four-body system may be explained by the appearance of the universal four-body repulsion, in a manner similar to the three-body system. It would also be of great interests to test the universality for $N \geq 5$.

Bibliography

[1] V. Efimov, Phys. Lett. B **33**, 563 (1970).

[2] V. Efimov, Sov. J. Nucl. Phys **12**, 101 (1971).

[3] D. V. Fedorov, A. S. Jensen, and K. Riisager, Phys. Rev. Lett. **73**, 2817 (1994).

[4] M. Zhukov, B. Danilin, D. Fedorov, J. Bang, I. Thompson, and J. Vaagen, Phys. Rep. **231**, 151 (1993).

[5] K. Riisager, Rev. Mod. Phys. **66**, 1105 (1994).

[6] T. Nakamura *et al.*, Phys. Rev. Lett. **96**, 252502 (2006).

[7] T. K. Lim, S. K. Duffy, and W. C. Damer, Phys. Rev. Lett. **38**, 341 (1977).

[8] T. Cornelius and W. Glöckle, J. Chem. Phys. **85**, 3906 (1986).

[9] E. Braaten and H. W. Hammer, Phys. Rev. A **67**, 042706 (2003).

[10] P. Naidon, E. Hiyama, and M. Ueda, Phys. Rev. A **86**, 012502 (2012).

[11] L. W. Bruch and I. J. McGee, J. Chem. Phys. **46**, 2959 (1967).

[12] R. A. Aziz and M. J. Slaman, J. Chem. Phys. **94**, 8047 (1991).

[13] F. Luo, G. C. McBane, G. Kim, C. F. Giese, and W. R. Gentry, J. Chem. Phys. **98**, 3564 (1993).

[14] R. E. Grisenti, W. Schöllkopf, J. P. Toennies, G. C. Hegerfeldt, T. Köhler, and M. Stoll, Phys. Rev. Lett. **85**, 2284 (2000).

[15] D. J. Wineland, R. E. Drullinger, and F. L. Walls, Phys. Rev. Lett. **40**, 1639 (1978).

[16] W. D. Phillips and H. Metcalf, Phys. Rev. Lett. **48**, 596 (1982).

[17] S. Chu, L. Hollberg, J. E. Bjorkholm, A. Cable, and A. Ashkin, Phys. Rev. Lett. **55**, 48 (1985).

[18] A. Aspect, E. Arimondo, R. Kaiser, N. Vansteenkiste, and C. Cohen-Tannoudji, Phys. Rev. Lett. **61**, 826 (1988).

[19] M. H. Anderson, J. R. Ensher, M. R. Matthews, C. E. Wieman, and E. A. Cornell, Science **269**, 198 (1995).

[20] K. B. Davis, M. O. Mewes, M. R. Andrews, N. J. van Druten, D. S. Durfee, D. M. Kurn, and W. Ketterle, Phys. Rev. Lett. **75**, 3969 (1995).

[21] S. Inouye, M. R. Andrews, J. Stenger, H. J. Miesner, D. M. Stamper-Kurn, and W. Ketterle, Nature **392**, 151 (1998).

[22] U. Fano, Phys. Rev. **124**, 1866 (1961).

[23] H. Feshbach, Ann. Phys. **5**, 357 (1958).

[24] C. Chin, R. Grimm, P. Julienne, and E. Tiesinga, Rev. Mod. Phys. **82**, 1225 (2010).

[25] S. E. Pollack, D. Dries, M. Junker, Y. P. Chen, T. A. Corcovilos, and R. G. Hulet, Phys. Rev. Lett. **102**, 090402 (2009).

[26] P. Dyke, S. E. Pollack, and R. G. Hulet, Phys. Rev. A **88**, 023625 (2013).

[27] T. Kraemer, M. Mark, P. Waldburger, J. G. Danzl, C. Chin, B. Engeser, A. D. Lange, K. Pilch, A. Jaakkola, H. C. Nägerl, and R. Grimm, Nature **440**, 315 (2006).

[28] M. Zaccanti, B. Deissler, C. D ' Errico, M. Fattori, M. Jona-Lasinio, S. Müller, G. Roati, M. Inguscio, and G. Modugno, Nature Physics **5**, 586 (2009).

[29] Y. Nishida, Y. Kato, and C. D. Batista, Nature Physics **9**, 93 (2013).

[30] Y. Nishida, Phys. Rev. B **88**, 224402 (2013).

[31] P. F. Bedaque, H. W. Hammer, and U. van Kolck, Phys. Rev. Lett. **82**, 463 (1999).

[32] E. Braaten and H. W. Hammer, Phys. Rep. **428**, 259 (2006).

[33] K. G. Wilson, Phys. Rev. B **4**, 3174 (1971).

[34] K. G. Wilson, Phys. Rev. D **3**, 1818 (1971).

[35] S. D. Głazek and K. G. Wilson, Phys. Rev. D **47**, 4657 (1993).

[36] S. D. Głazek and K. G. Wilson, Phys. Rev. Lett. **89**, 230401 (2002).

[37] D. A. Huse, Phys. Rev. B **24**, 5180 (1981).

[38] V. Efimov, Nucl. Phys. A **210**, 157 (1973).

[39] V. Efimov, JETP Letters **16**, 34 (1972).

[40] R. Amado and J. Noble, Phys. Lett. B **35**, 25 (1971).

[41] Y. Kawaguchi and M. Ueda, Phys. Rep. **520**, 253 (2012).

[42] C. Honerkamp and W. Hofstetter, Phys. Rev. Lett. **92**, 170403 (2004).

[43] V. Colussi, C. H. Greene, and J. D'Incao, arXiv:1402.2911 (2014).

[44] N. Gross, Z. Shotan, S. Kokkelmans, and L. Khaykovich, Phys. Rev. Lett. **103**, 163202 (2009).

[45] S. E. Pollack, D. Dries, and R. G. Hulet, Science **326**, 1683 (2009).

[46] N. Gross, Z. Shotan, S. Kokkelmans, and L. Khaykovich, Phys. Rev. Lett. **105**, 103203 (2010).

[47] B. S. Rem, A. T. Grier, I. Ferrier-Barbut, U. Eismann, T. Langen, N. Navon, L. Khaykovich, F. Werner, D. S. Petrov, F. Chevy, and C. Salomon, Phys. Rev. Lett. **110**, 163202 (2013).

[48] T. B. Ottenstein, T. Lompe, M. Kohnen, A. N. Wenz, and S. Jochim, Phys. Rev. Lett. **101**, 203202 (2008).

[49] T. Lompe, T. B. Ottenstein, F. Serwane, K. Viering, A. N. Wenz, G. Zürn, and S. Jochim, Phys. Rev. Lett. **105**, 103201 (2010).

[50] A. N. Wenz, T. Lompe, T. B. Ottenstein, F. Serwane, G. Zürn, and S. Jochim, Phys. Rev. A **80**, 040702 (2009).

[51] S. Nakajima, M. Horikoshi, T. Mukaiyama, P. Naidon, and M. Ueda, Phys. Rev. Lett. **106**, 143201 (2011).

[52] T. Lompe, T. B. Ottenstein, F. Serwane, A. N. Wenz, G. Zürn, and S. Jochim, Science **330**, 940 (2010).

[53] J. R. Williams, E. L. Hazlett, J. H. Huckans, R. W. Stites, Y. Zhang, and K. M. O'Hara, Phys. Rev. Lett. **103**, 130404 (2009).

[54] S. Nakajima, M. Horikoshi, T. Mukaiyama, P. Naidon, and M. Ueda, Phys. Rev. Lett. **105**, 023201 (2010).

[55] G. Barontini, C. Weber, F. Rabatti, J. Catani, G. Thalhammer, M. Inguscio, and F. Minardi, Phys. Rev. Lett. **103**, 043201 (2009).

[56] C. Kohstall, M. Zaccanti, M. Jag, A. Trenkwalder, P. Massignan, G. Bruun, F. Schreck, and R. Grimm, Nature **485**, 615 (2012).

[57] H. Hara, Y. Takasu, Y. Yamaoka, J. M. Doyle, and Y. Takahashi, Phys. Rev. Lett. **106**, 205304 (2011).

[58] A. H. Hansen, A. Khramov, W. H. Dowd, A. O. Jamison, V. V. Ivanov, and S. Gupta, Phys. Rev. A **84**, 011606 (2011).

[59] O. I. Kartavtsev and A. V. Malykh, J. Phys. B **40**, 1429 (2007).

[60] J. Levinsen, T. G. Tiecke, J. T. M. Walraven, and D. S. Petrov, Phys. Rev. Lett. **103**, 153202 (2009).

[61] O. Kartavtsev and A. Malykh, JETP Letters **86**, 625 (2008).

[62] M. Jag, M. Zaccanti, M. Cetina, R. S. Lous, F. Schreck, R. Grimm, D. S. Petrov, and J. Levinsen, Phys. Rev. Lett. **112**, 075302 (2014).

[63] S. Kato, S. Sugawa, K. Shibata, R. Yamamoto, and Y. Takahashi, Phys. Rev. Lett. **110**, 173201 (2013).

[64] M. L. González-Martínez and J. M. Hutson, Phys. Rev. A **88**, 020701 (2013).

[65] N. Gross, Z. Shotan, O. Machtey, S. Kokkelmans, and L. Khaykovich, Comptes Rendus Physique **12**, 4 (2011).

[66] S. Roy, M. Landini, A. Trenkwalder, G. Semeghini, G. Spagnolli, A. Simoni, M. Fattori, M. Inguscio, and G. Modugno, Phys. Rev. Lett. **111**, 053202 (2013).

[67] R. J. Wild, P. Makotyn, J. M. Pino, E. A. Cornell, and D. S. Jin, Phys. Rev. Lett. **108**, 145305 (2012).

[68] M. Berninger, A. Zenesini, B. Huang, W. Harm, H. C. Nägerl, F. Ferlaino, R. Grimm, P. S. Julienne, and J. M. Hutson, Phys. Rev. Lett. **107**, 120401 (2011).

[69] F. Ferlaino, A. Zenesini, M. Berninger, B. Huang, H. C. Nägerl, and R. Grimm, Few-Body Systems **51**, 113 (2011).

[70] S. Knoop, J. S. Borbely, W. Vassen, and S. J. J. M. F. Kokkelmans, Phys. Rev. A **86**, 062705 (2012).

[71] J. D'Incao, C. H. Greene, and B. Esry, J. Phys. B **42**, 044016 (2009).

[72] C. Chin, arXiv:1111.1484 (2011).

[73] J. Wang, J. P. D'Incao, B. D. Esry, and C. H. Greene, Phys. Rev. Lett. **108**, 263001 (2012).

[74] P. K. Sørensen, D. V. Fedorov, A. S. Jensen, and N. T. Zinner, Phys. Rev. A **86**, 052516 (2012).

[75] R. Schmidt, S. P. Rath, and W. Zwerger, Eur. Phys. J. B **85**, 1 (2012).

[76] J. Omachi, T. Suzuki, K. Kato, N. Naka, K. Yoshioka, and M. Kuwata-Gonokami, Phys. Rev. Lett. **111**, 026402 (2013).

[77] H. W. Hammer and L. Platter, Eur. Phys. J. A **32**, 113 (2007).

[78] J. von Stecher, J. P. D'Incao, and C. H. Greene, Nature Physics **5**, 417 (2009).

[79] M. R. Hadizadeh, M. T. Yamashita, L. Tomio, A. Delfino, and T. Frederico, Phys. Rev. Lett. **107**, 135304 (2011).

[80] A. Deltuva, Europhys. Lett. **95**, 43002 (2011).

[81] J. von Stecher, Phys. Rev. Lett. **107**, 200402 (2011).

[82] M. Gattobigio, A. Kievsky, and M. Viviani, Phys. Rev. A **84**, 052503 (2011).

[83] M. Gattobigio, A. Kievsky, and M. Viviani, Phys. Rev. A **86**, 042513 (2012).

[84] G. J. Hanna and D. Blume, Phys. Rev. A **74**, 063604 (2006).

[85] J. von Stecher, J. Phys. B **43**, 101002 (2010).

[86] M. Gattobigio, A. Kievsky, and M. Viviani, Few-Body Systems **54**, 1547 (2012).

[87] M. Gattobigio and A. Kievsky, arXiv:1309.1927 (2013).

[88] F. Ferlaino, S. Knoop, M. Berninger, W. Harm, J. P. D'Incao, H. C. Nägerl, and R. Grimm, Phys. Rev. Lett. **102**, 140401 (2009).

[89] A. Zenesini, B. Huang, M. Berninger, S. Besler, H.-C. Nägerl, F. Ferlaino, R. Grimm, C. H. Greene, and J. von Stecher, New J. Phys. **15**, 043040 (2013).

[90] Y. Castin, C. Mora, and L. Pricoupenko, Phys. Rev. Lett. **105**, 223201 (2010).

[91] N. L. Guevara, Y. Wang, and B. D. Esry, Phys. Rev. Lett. **108**, 213202 (2012).

[92] D. Blume, Phys. Rev. Lett. **109**, 230404 (2012).

[93] K. M. Daily, D. Rakshit, and D. Blume, Phys. Rev. Lett. **109**, 030401 (2012).

[94] N. Nygaard and N. Zinner, arXiv:1110.5854 (2011).

[95] C. J. M. Mathy, M. M. Parish, and D. A. Huse, Phys. Rev. Lett. **106**, 166404 (2011).

[96] Y. Nishida, Phys. Rev. A **79**, 013629 (2009).

[97] D. J. MacNeill and F. Zhou, Phys. Rev. Lett. **106**, 145301 (2011).

[98] P. Niemann and H. W. Hammer, Phys. Rev. A **86**, 013628 (2012).

[99] N. T. Zinner, Europhys. Lett. **101**, 60009 (2013).

[100] N. T. Zinner, arXiv:1312.7821 (2013).

[101] N. Zinner, arXiv:1401.0671, to be published in Few-Body Systems .

[102] A. Schirotzek, C.-H. Wu, A. Sommer, and M. W. Zwierlein, Phys. Rev. Lett. **102**, 230402 (2009).

[103] S. Nascimbène, N. Navon, K. J. Jiang, L. Tarruell, M. Teichmann, J. McKeever, F. Chevy, and C. Salomon, Phys. Rev. Lett. **103**, 170402 (2009).

[104] M. Koschorreck, D. Pertot, E. Vogt, B. Fröhlich, M. Feld, and M. Köhl, Nature **485**, 619 (2012).

[105] R. Combescot, A. Recati, C. Lobo, and F. Chevy, Phys. Rev. Lett. **98**, 180402 (2007).

[106] N. Prokof'ev and B. Svistunov, Phys. Rev. B **77**, 020408 (2008).

[107] M. Punk, P. T. Dumitrescu, and W. Zwerger, Phys. Rev. A **80**, 053605 (2009).

[108] P. Massignan, M. Zaccanti, and G. M. Bruun, arXiv:1309.0219 (2013).

[109] F. Chevy, Physics **2**, 48 (2009).

[110] F. Serwane, G. Zürn, T. Lompe, T. Ottenstein, A. Wenz, and S. Jochim, Science **332**, 336 (2011).

[111] A. Wenz, G. Zürn, S. Murmann, I. Brouzos, T. Lompe, and S. Jochim, Science **342**, 457 (2013).

[112] G. Zürn, A. N. Wenz, S. Murmann, A. Bergschneider, T. Lompe, and S. Jochim, Phys. Rev. Lett. **111**, 175302 (2013).

[113] R. J. Fletcher, A. L. Gaunt, N. Navon, R. P. Smith, and Z. Hadzibabic, Phys. Rev. Lett. **111**, 125303 (2013).

[114] P. Makotyn, C. E. Klauss, D. L. Goldberger, E. A. Cornell, and D. S. Jin, Nature Physics **10**, 116 (2014).

[115] E. Nielsen, D. Fedorov, A. Jensen, and E. Garrido, Phys. Rep. **347**, 373 (2001).

[116] F. Ferlaino and R. Grimm, Physics **3**, 9 (2010).

[117] L. H. Thomas, Phys. Rev. **47**, 903 (1935).

[118] L. D. Landau and E. M. Lifshitz, *Quantum mechanics: non-relativistic theory* (Butterworth-Heinemann, 1991).

[119] B. Gao, Phys. Rev. A **58**, 1728 (1998).

[120] B. Gao, Phys. Rev. A **58**, 4222 (1998).

[121] C. J. Pethick and H. Smith, *Bose-Einstein condensation in dilute gases* (Cambridge university press, 2002).

[122] V. V. Flambaum, G. F. Gribakin, and C. Harabati, Phys. Rev. A **59**, 1998 (1999).

[123] Y. Castin and F. Werner, The unitary gas and its symmetry properties, in *The BCS-BEC Crossover and the Unitary Fermi Gas*, pp. 127–191, Springer, 2012.

[124] J. Stuhler, A. Griesmaier, T. Koch, M. Fattori, T. Pfau, S. Giovanazzi, P. Pedri, and L. Santos, Phys. Rev. Lett. **95**, 150406 (2005).

[125] K. Aikawa, A. Frisch, M. Mark, S. Baier, A. Rietzler, R. Grimm, and F. Ferlaino, Phys. Rev. Lett. **108**, 210401 (2012).

[126] K. Aikawa, A. Frisch, M. Mark, S. Baier, R. Grimm, and F. Ferlaino, Phys. Rev. Lett. **112**, 010404 (2014).

[127] M. Lu, N. Q. Burdick, S. H. Youn, and B. L. Lev, Phys. Rev. Lett. **107**, 190401 (2011).

[128] M. Lu, N. Q. Burdick, and B. L. Lev, Phys. Rev. Lett. **108**, 215301 (2012).

[129] K. Huang and C. N. Yang, Phys. Rev. **105**, 767 (1957).

[130] H. Bethe and R. Peierls, Proc. Roy. Soc. London. A **148**, 146 (1935).

[131] E. Timmermans, P. Tommasini, M. Hussein, and A. Kerman, Phys. Rep. **315**, 199 (1999).

[132] D. S. Petrov, Phys. Rev. A **67**, 010703 (2003).

[133] D. S. Petrov, C. Salomon, and G. V. Shlyapnikov, Phys. Rev. Lett. **93**, 090404 (2004).

[134] D. Eagles, Phys. Rev. **186**, 456 (1969).

[135] A. Leggett, *Modern trends in the theory of condensed matter (Springer-Verlag Berlin 1980), pp. 13-27* .

[136] C. A. R. Sá de Melo, M. Randeria, and J. R. Engelbrecht, Phys. Rev. Lett. **71**, 3202 (1993).

[137] Y. Ohashi and A. Griffin, Phys. Rev. Lett. **89**, 130402 (2002).

[138] T. L. Ho, Phys. Rev. Lett. **92**, 090402 (2004).

[139] S. Nascimbène, N. Navon, K. Jiang, F. Chevy, and C. Salomon, Nature **463**, 1057 (2010).

[140] M. Horikoshi, S. Nakajima, M. Ueda, and T. Mukaiyama, Science **327**, 442 (2010).

[141] K. Van Houcke, F. Werner, E. Kozik, N. Prokof'ev, B. Svistunov, M. Ku, A. Sommer, L. Cheuk, A. Schirotzek, and M. Zwierlein, Nature Physics **8**, 366 (2012).

[142] S. Tan, Ann. Phys. **323**, 2952 (2008).

[143] S. Tan, Ann. Phys. **323**, 2971 (2008).

[144] S. Tan, Ann. Phys. **323**, 2987 (2008).

[145] Q. Chen, J. Stajic, S. Tan, and K. Levin, Phys. Rep. **412**, 1 (2005).

[146] W. Zwerger, editor, *The BCS-BEC Crossover and the Unitary Fermi Gas (Lecture Notes in Physics)*, 2012 ed. (Springer, 2011).

[147] P. Naidon, S. Endo, and M. Ueda, arXiv:1208.3912, submitted to Phys. Rev. A .

[148] G. A. Skorniakov and K. A. Ter-Martirosian, Sov. Phys. JETP **4**, 648 (1957).

[149] H. Suno, B. D. Esry, C. H. Greene, and J. P. Burke, Phys. Rev. A **65**, 042725 (2002).

[150] D. V. Fedorov and A. S. Jensen, Phys. Rev. Lett. **71**, 4103 (1993).

[151] A. Jensen, E. Garrido, and D. Fedorov, Few-Body Systems **22**, 193 (1997).

[152] L. Faddeev, Sov. Phys. JETP **12**, 1014 (1961).

[153] E. Braaten, H. W. Hammer, D. Kang, and L. Platter, Phys. Rev. A **78**, 043605 (2008).

[154] K. Helfrich, H. W. Hammer, and D. S. Petrov, Phys. Rev. A **81**, 042715 (2010).

[155] S. Endo, P. Naidon, and M. Ueda, Few-Body Systems **51**, 207 (2011).

[156] K. Helfrich and H. W. Hammer, J. Phys. B **44**, 215301 (2011).

[157] E. Braaten and H. W. Hammer, Phys. Rev. A **70**, 042706 (2004).

[158] B. D. Esry, C. H. Greene, and J. P. Burke, Phys. Rev. Lett. **83**, 1751 (1999).

[159] S. Knoop, F. Ferlaino, M. Mark, M. Berninger, H. Schöbel, H.-C. Nägerl, and R. Grimm, Nature Physics **5**, 227 (2009).

[160] O. Machtey, Z. Shotan, N. Gross, and L. Khaykovich, Phys. Rev. Lett. **108**, 210406 (2012).

[161] O. Kartavtsev, A. Malykh, and S. Sofianos, Sov. Phys. JETP **108**, 365 (2009).

[162] L. Pricoupenko and P. Pedri, Phys. Rev. A **82**, 033625 (2010).

[163] S. A. Vugal'ter and G. M. Zhislin, Theoretical and Mathematical Physics **55**, 357 (1983).

[164] P. Soldán, M. T. Cvitaš, and J. M. Hutson, Phys. Rev. A **67**, 054702 (2003).

[165] A. Simoni, M. Zaccanti, C. D'Errico, M. Fattori, G. Roati, M. Inguscio, and G. Modugno, Phys. Rev. A **77**, 052705 (2008).

[166] A. Derevianko, W. R. Johnson, M. S. Safronova, and J. F. Babb, Phys. Rev. Lett. **82**, 3589 (1999).

[167] E. G. M. van Kempen, S. J. J. M. F. Kokkelmans, D. J. Heinzen, and B. J. Verhaar, Phys. Rev. Lett. **88**, 093201 (2002).

[168] Y. Wang, J. Wang, J. P. D'Incao, and C. H. Greene, Phys. Rev. Lett. **109**, 243201 (2012).

[169] R. S. Bloom, M.-G. Hu, T. D. Cumby, and D. S. Jin, Phys. Rev. Lett. **111**, 105301 (2013).

[170] D. Papoular, *Manipulation des interactions dans les gaz quantiques: approche théorique*, PhD thesis, Université Paris Sud-Paris XI, 2011.

[171] D. S. Petrov, Phys. Rev. Lett. **93**, 143201 (2004).

[172] Y. Nishida, D. T. Son, and S. Tan, Phys. Rev. Lett. **100**, 090405 (2008).

[173] D. Blume and K. M. Daily, Phys. Rev. A **82**, 063612 (2010).

[174] D. Blume and K. M. Daily, Phys. Rev. Lett. **105**, 170403 (2010).

[175] I. V. Brodsky, M. Y. Kagan, A. V. Klaptsov, R. Combescot, and X. Leyronas, Phys. Rev. A **73**, 032724 (2006).

[176] S. Endo, P. Naidon, and M. Ueda, Phys. Rev. A **86**, 062703 (2012).

[177] Y. Castin and E. Tignone, Phys. Rev. A **84**, 062704 (2011).

[178] M. Iskin, Phys. Rev. A **81**, 043634 (2010).

[179] O. I. Kartavtsev and A. V. Malykh, Few-Body Systems **44**, 229 (2008).

[180] S.-K. Tung, C. Parker, J. Johansen, C. Chin, Y. Wang, and P. S. Julienne, Phys. Rev. A **87**, 010702 (2013).

[181] M. Repp, R. Pires, J. Ulmanis, R. Heck, E. D. Kuhnle, M. Weidemüller, and E. Tiemann, Phys. Rev. A **87**, 010701 (2013).

[182] D. A. Brue and J. M. Hutson, Phys. Rev. Lett. **108**, 043201 (2012).

[183] I. Bloch, Nature Physics **1**, 23 (2005).

[184] P. Naidon, S. Endo, and M. Ueda, to be published in Phys. Rev. Lett. (2014).

[185] F. Shimizu, Phys. Rev. Lett. **86**, 987 (2001).

[186] A. Bijl, Physica **7**, 869 (1940).

[187] R. Jastrow, Phys. Rev. **98**, 1479 (1955).

[188] G. Pöschl and E. Teller, Z. Phys. **83**, 143 (1933).

[189] S. Flügge, *Practical Quantum Mechanics* (Springer-Verlag, 1994).

[190] P. M. Morse, Phys. Rev. **34**, 57 (1929).

[191] Y. Yamaguchi, Phys. Rev. **95**, 1628 (1954).

[192] S. Moszkowski, S. Fleck, A. Krikeb, L. Theußl, J.-M. Richard, and K. Varga, Phys. Rev. A **62**, 032504 (2000).

[193] R. B. Wiringa, V. G. J. Stoks, and R. Schiavilla, Phys. Rev. C **51**, 38 (1995).

[194] G. F. Gribakin and V. V. Flambaum, Phys. Rev. A **48**, 546 (1993).

[195] L. N. Cooper, Phys. Rev. **104**, 1189 (1956).

[196] Y. Wang, W. B. Laing, J. von Stecher, and B. D. Esry, Phys. Rev. Lett. **108**, 073201 (2012).

[197] B. Fröhlich, M. Feld, E. Vogt, M. Koschorreck, W. Zwerger, and M. Köhl, Phys. Rev. Lett. **106**, 105301 (2011).

[198] R. Newton, J. Math. Phys. **18**, 1348 (1977).

[199] R. Newton, J. Math. Phys. **18**, 1582 (1977).

[200] J. Fumi, Phil. Mag. **46**, 1007 (1955).

[201] J. Friedel, Phil. Mag. **43**, 153 (1952).

[202] J. S. Langer and V. Ambegaokar, Phys. Rev. **121**, 1090 (1961).

[203] S. Endo and M. Ueda, arXiv:1309.7797, submitted to Phys. Rev. A .

[204] Y. Shin, M. W. Zwierlein, C. H. Schunck, A. Schirotzek, and W. Ketterle, Phys. Rev. Lett. **97**, 030401 (2006).

[205] C. Schunck, Y. Shin, A. Schirotzek, M. Zwierlein, and W. Ketterle, Science **316**, 867 (2007).

[206] P. W. Anderson, Phys. Rev. Lett. **18**, 1049 (1967).

[207] P. W. Anderson, Phys. Rev. **164**, 352 (1967).

[208] G. D. Mahan, Phys. Rev. **163**, 612 (1967).

[209] P. Nozières and C. T. De Dominicis, Phys. Rev. **178**, 1097 (1969).

[210] J. Kondo and A. Yoshimori, editors, *Fermi Surface Effects: Proceedings of the Tsukuba Institute Tsukuba Science City, Japan, August 27-29, 1987 (Springer Series in Solid-State Sciences)* (Springer-Verlag, 2011).

[211] A. Rosch, Adv. Phys. **48**, 295 (1999).

[212] M. Sassetti, E. G. d'Agliano, and F. Napoli, Physica B **154**, 359 (1989).

[213] E. G. d'Agliano, P. Kumar, W. Schaich, and H. Suhl, Phys. Rev. B **11**, 2122 (1975).

[214] O. S. Duarte and A. O. Caldeira, Phys. Rev. Lett. **97**, 250601 (2006).

[215] I. Yoshimoto, *Wilsonian renormalization group analysis of nonrelativistic three-body systems without introducing auxiliary fields*, PhD thesis, Kyushu University, 2014.

[216] A. Safavi-Naini, S. T. Rittenhouse, D. Blume, and H. R. Sadeghpour, Phys. Rev. A **87**, 032713 (2013).

[217] E. Hiyama and M. Kamimura, 原子核研究 **58**, 119 (2013).

[218] E. Hiyama and M. Kamimura, in preparation.